The role of the histone variant H3.3 and its chaperones in the response to DNA damage

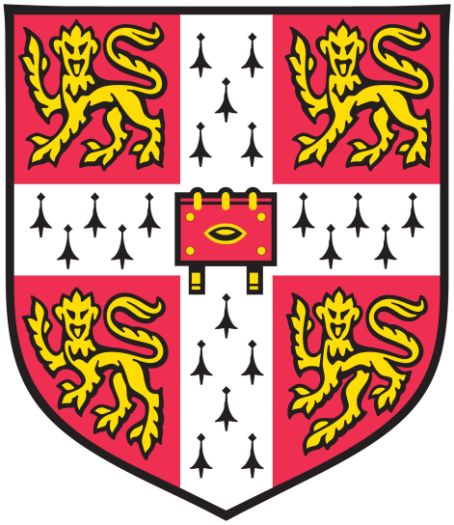

Lucy Alice Walker

University of Cambridge
Newnham College

September 2021

This thesis is submitted for the degree of Doctor of Philosophy

Declaration

This thesis is the result of my own work and includes nothing which is the outcome of work done in collaboration except as declared in the preface and specified in the text.

It is not substantially the same as any work that has already been submitted before for any degree or other qualification except as declared in the preface and specified in the text.

It does not exceed the prescribed word limit for the Biology Degree Committee.

Preface

This thesis is my own work other than the following:
C. Mellor carried out analysis of sequencing for section 6.5, as specified in the text, and generated the basis of figures 6.6 and 6.7.

Abstract

The role of the histone variant H3.3 and its chaperones in the response to DNA damage Lucy Alice Walker

H3.3 is a histone variant without a clear, single function. Unlike the canonical replication-associated H3.1 and H3.2, it is present throughout the cell cycle and can be deposited into chromatin by two distinct and specific chaperone complexes: ATRX/DAXX and HIRA. H3.3 and its chaperones have been implicated in the response to and repair of various types of DNA damage. Furthermore, a supply of H3.3 has been shown to be required to maintain replication fork progression in the transformed avian cell line DT40, despite the availability during replication of canonical H3.

In this thesis, I have examined the role of H3.3 and its chaperones in the response to UV induced DNA damage in a non-transformed, but immortalised, human cell system, the lymphoblastoid line TK6. Using CRISPR-Cas9 genome editing, I created H3.3, ATRX and HIRA knockout mutants and investigated their response to UV irradiation. *h3.3* TK6 cells are not hypersensitive to acute DNA damage but exhibit persistence of DNA damage markers. *h3.3* cells also exhibit a change in their cell cycle distribution after UV irradiation, with a G1 arrest after 24 hours. These observations support the hypothesis that there is a delay in resolving DNA damage in the absence of H3.3. The observed checkpoint activation is mediated by p53, as demonstrated by alleviation of the G1 arrest in *h3.3/p53* double knockout cells. Surprisingly, in TK6, loss of H3.3 did not result in altered fork dynamics after UV irradiation. *atrx* cells phenocopy the h3.3 cells in these responses to acute DNA damage, likewise displaying a G1 accumulation 24 hours after UV irradiation, but *hira* cells do not. This suggests that the role of H3.3 in the response to UV induced DNA damage is likely mediated by ATRX-dependent deposition rather than deposition via a HIRA-dependent pathway. To further investigate the potential pathways in which H3.3 could be involved after UV induced damage, I present the results of a proteomic screen for H3.3 interactors and a CRISPR/Cas9 screen to determine genetic interactions of H3.3. in the response to DNA damage.

Together, this work demonstrates a role for H3.3 in the response to DNA damage in non-transformed human cells and implicates deposition by its chaperone ATRX in this role.

Acknowledgements

I would like to offer special thanks to Julian Sale for his supervision, support and advice throughout my PhD. Thanks also go to members of the Sale lab, past and present, for their help and feedback. Special thanks must go to Chris Mellor for his guidance on CRISPR screens and particularly his analysis of sequencing which is included in this thesis. The LMB Flow Cytometry group have been invaluable and without them, many aspects of this project could not have happened.

My gratitude extends to the MRC for funding to allow me to undertake this PhD.

I am grateful to our collaborators Prof. Nick Brindle and Dr. Neil Bate for their enthusiasm for driving the CoronaTrap project forwards, with guidance and protocol advice.

Finally, thank you to my family for their patience and support throughout the past 4 years.

Contents

Abbreviations

6,4 PP	Pyrimidine-pyrimidine (6-4) photoproducts
ALT	Alternative Lengthening of Telomeres
bp	Base Pairs
CPD	Cyclobutane pyrimidine dimers
DSB	Double strand break
FDR	False discovery rate
G4	G quadruplex
GG-NER	Global genome nucleotide excision repair
gRNA	guide RNA
HR	Homologous recombination
MMS	Methyl methanesulphonate
MOI	Multiplicity of infection
NER	Nucleotide excision repair
NHEJ	Non-homologous end joining
NQO	4-Nitroquinoline 1-Oxide
nt	Nucleotides
RBD	Receptor binding domain
RT	Room temperature
ssDNA	Single stranded DNA
TC-NER	Transcription coupled excision repair
TLS	Translesion synthesis
TSS	Transcription Start Site
UV	Ultraviolet
WT	Wild type

Chapter 1: Introduction

1.1 Chromatin

Every human cell contains roughly $3x10^9$ base pairs of DNA which, if laid out, would be ~ 2 m long. In order to fit this large quantity of genetic information into a 10 μm cell, DNA is packaged into chromatin.

1.1.1 Nucleosome Structure

Chromatin is a complex of DNA and proteins. It is organised into repeating units, the nucleosome. The nucleosome is formed of an octamer of histone proteins with DNA wrapped around 1.65 times (approximately 150 bp), then a linker of DNA to the next nucleosome (Luger *et al.*, 1997). This forms the beads on a string structure seen by electron microscopy (Woodcock, Safer and Stanchfield, 1976). This beads on a string structure is further compacted into higher order structures (Woodcock and Ghosh, 2010).

The nucleosome octamer is made up of 2 copies each of H2A, H2B, H3 and H4. H3 and H4 assemble into a heterodimer then come together as a tetramer. H2A and H2B form 2 heterodimers to complete the octamer (Luger *et al.*, 1997). H1 can then bind at the nucleosome:linker DNA interface.

Nucleosomes are assembled and organised by histone chaperone complexes. Two of the major chaperones, CAF-1 and Asf1a/b, typically mediate assembly of nucleosomes onto newly synthesised DNA (Mello *et al.*, 2002).

As DNA is wrapped around nucleosomes, the nucleosome has a role in controlling access to the DNA. This means histones can modulate processes requiring access to DNA, such as transcription and DNA damage repair. One way chromatin function can be modulated is through the wide variety of post translational modifications which can be added to the histone (Bannister and Kouzarides, 2011). For example, histone acetylation reduces the histone's positive charge and thereby reduces the affinity of the negatively charged DNA for the histone and relaxes chromatin packing (Hong *et al.*, 1993).

Another way chromatin function can be modulated is by varying the composition of the nucleosome. All histones but H4 and H2B have variants (Franklin and Zweidler, 1977). These variants can differ in amino acid sequence to 'canonical' histones, enabling them to have different deposition and functions.

1.1.2 Histone H3 variants

H3 has 8 variants in human cells: 2 canonical, 4 replacement and 2 testes specific (Filipescu, Müller and Almouzni, 2014) (Table 1). CENPA stands out as being the least similar to all the other variants. It is important for defining centromeres (Müller and Almouzni, 2014).

Table 1 Histone 3 variants, their chaperones and functions (adapted from (Filipescu, Müller and Almouzni, 2014))

Histone variant	*Chaperones*	*Function*
H3.1	CAF-1 ASF1a/b	DNA synthesis coupled deposition
H3.2		
H3.3	HIRA complex ASF1a DAXX/ATRX	Replication independent deposition
CENPA	DAXX HJURP	Centromere localised
H3.4		Testis specific
H3.5		Testis specific
H3.Y (Wiedemann *et al.*, 2010)	HIRA	Increased deposition in response to external stress
H3.X		Potential pseudogene

H3.1, H3.2 and H3.3 are most similar to each other. H3.1 and H3.2 are the canonical H3s and make up the majority of the H3 histone pool (Hake *et al.*, 2006). They are deposited in a replication dependent manner, wrapping up new DNA as it is synthesised. H3.3 is a

replacement histone and deposited throughout the cell cycle. The other variants have minor or emerging functions.

As newly synthesised DNA requires histone deposition, the expression of H3.1 and H3,2 peaks in S phase. This is facilitated by their clustered gene structure and additionally, the stem-loop structure of their mRNA facilitates efficient translation (Gallie, Lewis and Marzluff, 1996; Marzluff *et al.*, 2002; Marzluff, Wagner and Duronio, 2008). The deposition of H3.3 is not linked to DNA synthesis and is deposited independently of replication (Tagami *et al.*, 2004). H3.3 has a different gene structure also, having a standard intron/exon structure and polyadenylated mRNAs (whereas H3.1/2 are intron-less and not polyadenylated).

The H3 variants H3.2, CENPA and H3.3 are conserved in all metazoans, with mammals having the additional canonical H3.1. The canonical (i.e. non-centromeric) H3 in *S. cerevisiae* and *S. pombe* is H3.3-like. H3.3 and canonical yeast H3 probably share a common ancestor (Elsaesser, Goldberg and Allis, 2010). H3.3 is encoded by 2 genes in humans, H3F3A and H3F3B. These have different sequences but produce identical proteins. H3F3B appears to be more similar to canonical H3 and H3.3 in distant organisms. The 2 different sequences of these genes may have arisen to have different functions. The codon usage of H3F3A resembles proliferation genes, whereas H3F3B resembles broadly expressed and differentiation induced genes, so the sequence itself could play a role in transcriptional control (Muhire, Booker and Tolstorukov, 2019).

H3.1 and H3.2 differ by only 1 residue, which seemingly does not differentiate their functions. H3.3 differs by 5 or 4 residues respectively (Figure 1.1a). These changes are in 2 regions of the nucleosome. Three of the differentiating residues are clustered on the body of the nucleosome, termed the chaperone binding patch, and one H3.3 specific residue is on the N-terminal histone tail (Figure 1.1b). These small differences are enough for H3.3 to have distinct chaperones and distribution. Its wide and varied distribution does not immediately suggest a simple, single function for H3.3.

a)

```
H3.3  1    MARTKQTARKSTGGKAPRKQLATKAARKSAPSTGGVKKPHRYRPGTVALREIRRYQKSTE  60
           MARTKQTARKSTGGKAPRKQLATKAARKSAP+TGGVKKPHRYRPGTVALREIRRYQKSTE
H3.2  1    MARTKQTARKSTGGKAPRKQLATKAARKSAPATGGVKKPHRYRPGTVALREIRRYQKSTE  60

H3.3  61   LLIRKLPFQRLVREIAQDFKTDLRFQSAAIGALQEASEAYLVGLFEDTNLCAIHAKRVTI  120
           LLIRKLPFQRLVREIAQDFKTDLRFQS+A+ ALQEASEAYLVGLFEDTNLCAIHAKRVTI
H3.2  61   LLIRKLPFQRLVREIAQDFKTDLRFQSSAVMALQEASEAYLVGLFEDTNLCAIHAKRVTI  120

H3.3  121  MPKDIQLARRIRGERA  136
           MPKDIQLARRIRGERA
H3.2  121  MPKDIQLARRIRGERA  136
```

b)

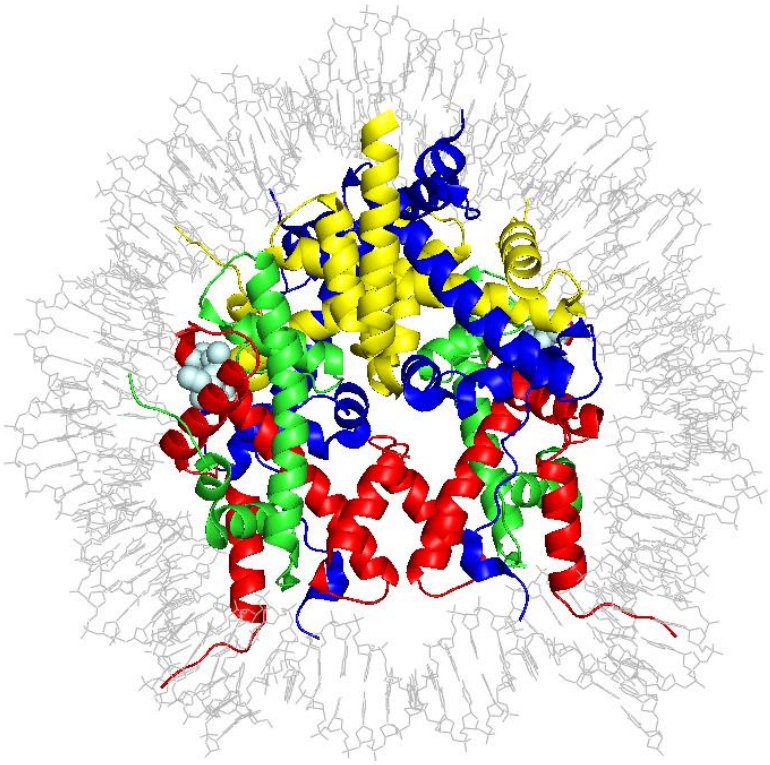

Figure 1.1 H3.3 differential residues a) Alignment of the residue sequences of the variant histone H3.3 and the canonical histone H3.2 with the 4 residue differences highlighted in yellow. b) Structure of the nucleosome/histone octamer, PDB code 3AV2. H3.3 in red, with chaperone binding patch residues expanded in light blue. The tails are unstructured and so not fully revealed.DNA in grey, H4 in green, H2A in blue, H2B in yellow.

1.1.3 The impact of H3.3 on chromatin packing

H3.3 is associated with both active genes and inactive repetitive regions (Goldberg *et al.*, 2010). This means its impact on chromatin packing is not immediately obvious.

H3.3 has been suggested to facilitate a more open chromatin structure. Areas enriched in H3.3 exhibit MNase sensitivity, suggesting greater spacing between nucleosomes, and have little higher order structure, such as chromatin intrafibre folding (Chen, Zhao and

Li, 2013). It has mutually exclusive deposition with Histone 1 (Braunschweig *et al.*, 2009), the linker histone found in transcriptionally inactive regions that enables chromatin condensation and folding into higher order structures. Across the genome, H3.3 and H1 binding sites are negatively correlated and depletion of H3.3 leads to increased H1 binding at sites where it was previously deposited. This antagonistic relationship may enable active loci to remain H1 free and therefore accessible to other proteins. H1 may interact with the tail of H3 when bound to a nucleosome (Stützer *et al.*, 2016), thereby suggesting a mechanism by which this relationship between H3.3 and H1 could be mediated. H3.3 may therefore influence chromatin packing through its relationship with other histones.

H3.3 may also impact the stability of nucleosomes of which it is part. Nucleosome core particles containing H3.3 in combination with the variant histone H2AZ (an H2A histone variant) have been found to be sensitive to disruption *in vitro* (Jin and Felsenfeld, 2007). H3.3 is enriched at the transcription start sites (TSS) of active genes in combination with H2AZ. These double variant nucleosomes could be marking the 'nucleosome free region' upstream of the TSS of active genes, acting as an easily disrupted placeholder to allow access to DNA easily when needed.

However, other reports contradict this model of H3.3 destabilising mononucleosomes. H2AZ facilitates higher order chromatin folding through its extended acidic patch and appears to enhance nucleosome stability when in nucleosomes without other variants. Incorporation of H3.3 into H2AZ containing nucleosomes has been shown to not disrupt their stability (Chen *et al.*, 2013), but can hinder chromatin intrafibre folding.

1.1.4 H3.3 Distribution

H3.3 is distributed throughout the genome. It is enriched at telomeres and centromeres, transcriptionally silent areas, as well as at genes and transcription factor binding sites (Goldberg *et al.*, 2010). (see section 1.2). H3.3 is typically replication independent, being expressed throughout the cell cycle, and not required to chromatinise newly synthesised DNA. The canonical histones are deposited in a replication dependent manner, but if CAF-1 (the H3.1 chaperone) is depleted, H3.3 can be deposited by HIRA in a replication-dependent manner to fill H3.1 gaps (Ray-Gallet et al., 2011). Other canonical H3 variants

and their chaperones, however, cannot deposit/be deposit in place of H3.3 to compensate for a lack of H3.3 (Ray-Gallet *et al.*, 2011).

1.1.5 The H3.3 specific tail residue

Histone tails protrude from the body of the nucleosome, meaning they are accessible to the nuclear environment around them. This makes them an ideal site for recognition and recruitment of factors and so are a target for post-translational modifications. These modifications can then recruit interactors to modulate chromatin function. One of the H3.3 specific residues is S31 on the N-terminal tail, making it a site of possible H3.3 specific interactors or modifications.

H3.3 has one known specific interactor which recognises H3.3 through its N-terminal tail. This is ZMYND11 (also known as BS69). This protein recognises the S31 residue and binds H3.3 in the context of H3K36 trimethylation (Guo *et al.*, 2014; Wen *et al.*, 2014). ZMYND11 interacts with components of the spliceosome, regulating intron retention. Fittingly, introns regulated by ZMYND11 are enriched for H3.3.

The N-terminal tail serine 31 is also a target for phosphorylation, further modulating H3.3 function. There is uncertainty over the kinase that creates this phosphorylation and what its function is. It is known to prevent binding of or eject bound ZMYND11 (Guo *et al.*, 2014; Armache *et al.*, 2020), demonstrating how histone modifications can regulate interactions of proteins with the nucleosome.

H3.3S31 is phosphorylated during mitosis and associated with heterochromatic regions, including telomeres (Hake *et al.*, 2005). In cells with an Alternative Lengthening of Telomeres (ALT) mechanism for replicating telomeres, H3.3S31 is phosphorylated across chromosomes during mitosis (Chang *et al.*, 2015). The ALT phenotype is associated with increased damage signalling, and in this study, it was determined that CHK1 is the kinase for H3.3S31, potentially linking H3.3 to DNA damage signalling pathways. However, these two studies were carried out using an antibody against H3.3S31P which was shown previously in the Sale lab to exhibit significant cross-reactivity with unmodified and unmodifiable H3.3 (unpublished), so the conclusions reached should be interpreted

cautiously. Other studies have use genetic approaches or different antibodies to investigate H3.3S31 phosphorylation and so may not be affected by this problem.

H3.3S31 phosphorylation has been reported to stimulate the histone acetyltransferase p300 at enhancers of genes differentially regulated during differentiation (Martire *et al.*, 2019) and promote H3.3K27 acetylation, an important modification during development (Sitbon *et al.*, 2020). It may also be phosphorylated in a stimulation dependent manner in rapidly induced genes in macrophages (Armache *et al.*, 2020). H3.3S31 phosphorylation has a link to both DNA damage signalling pathways and activation of poised or bivalent genes. It allows for further modulation of the function of histone H3.3.

1.1.6 Mutations found in cancer

Mutations in H3.3 are found in several paediatric gliomas and bone tumours (Weinberg, Allis and Lu, 2017). The mutations are somatic, heterozygous and restricted to three residues. The three residues are all found clustered on the N-terminal tail of H3.3, near the H3.3 specific S31. Of the three residues mutated in cancers (K27, G34, K36), two would usually be able to be modified (K27 and K36), but the mutations prevent this.

It has been proposed that H3.3 related cancers are driven by these alterations to histone modifications, leading to potential misregulation of proto-oncogenes, tumour suppressor genes (Bjerke *et al.*, 2013) or genes controlling embryonic differentiation (Fontebasso *et al.*, 2014). As the mutations are found in specific cell types and young children, they could occur at a developmentally early stage. In this way, the mutations could prevent proper differentiation meaning cells remain in a more stem cell like state and divide uncontrollably.

H3.3 with a K27M mutation (alongside p53 knockdown and PDGFRA overexpression) can block neural precursor cell differentiation into astrocytes and oligodendrocytes (Funato *et al.*, 2014). H3K27 would usually be post translationally modified by PRC2, but when mutated, K27M an affect PRC2 function in *cis*, causing widespread deregulation of genes controlled by PRC2 (Lewis *et al.*, 2013). The K36M mutation has been shown to interfere with chondrocyte, adipocyte and osteocyte differentiation, and again, mutations at this

residue can sequester and inhibit methyltransferases to impact regulation genome-wide (Lu *et al.*, 2016).

Mutation of K36 and G34 on the N-terminal tail have been shown to have different interactors to WT H3.3 (Lim et al., 2017). The novel interactors with mutant H3.3 are mainly related to the spliceosome and RNA processing, suggesting a change in RNA splicing and processing as a result of these mutations could contribute to the cancer phenotype.

1.2 H3.3 Chaperones

There are 2 chaperone complexes which are responsible for the deposition of H3.3: ATRX/DAXX and the HIRA complex. H3.3 is deposited in distinct regions by each of these complexes, with HIRA depositing in genic regions and ATRX at repetitive regions including telomeres and centromeric regions, as determined by chromatin immunoprecipitation and sequencing (Goldberg *et al.*, 2010).

Genome wide incorporation dynamics reveal distinct categories of turnover for H3.3, with slow turnover at telomeres and rapid turnover at promoters (Kraushaar *et al.*, 2013). This could either be a result of the different H3.3 chaperone incorporation or just a demonstration of the difference in chromatin handling between transcribed and non-transcribed regions.

1.2.1 ATRX

ATRX/DAXX is one of two H3.3 specific chaperones. ATRX is a SWI/SNF chromatin remodeller with several domains, a C-terminal ATPase, DAXX and EZH2 binding domains and an N-terminal ADD domain (Figure 1.2). The ADD domain is responsible for recognition of H3K9 and H3K9me3 (Eustermann *et al.*, 2011; Dash, Zaino and Hadden, 2018) and mutations in this domain lead to an X-linked mental retardation syndrome associated with alpha-thalassemia (Argentaro *et al.*, 2007). DAXX has varied biological functions, including modulating transcription through binding transcription factors and

its localisation to PML nuclear bodies. DAXX is the component of the complex which binds H3.3, with binding mediated by the H3.3 specific chaperone binding patch, in particular G90 (Elsässer *et al.*, 2012). ATRX then binds DAXX to mediate and direct H3.3 deposition.

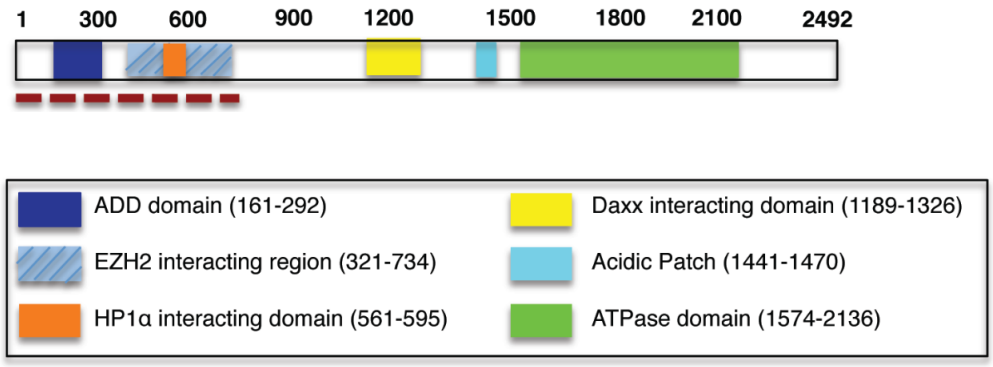

Figure 1.2 Domain structure of ATRX protein (Ratnakumar and Bernstein, 2013)

ATRX/DAXX was first identified as an H3.3 chaperone by its deposition of H3.3 at telomeres and pericentric heterochromatin in a replication independent manner (Drané *et al.*, 2010). Although DAXX is the component of the complex which binds H3.3 directly, both ATRX and DAXX are required for this deposition at telomeres and centromeric regions (Goldberg *et al.*, 2010; Wong *et al.*, 2010). Further research then showed that ATRX/DAXX is not just responsible for deposition at these 2 regions, but elsewhere throughout the genome. This includes repetitive regions such as endogenous retroviral repeats, retrotransposons and tandem repetitive elements (Elsässer *et al.*, 2015; He *et al.*, 2015; Sadic *et al.*, 2015). ATRX in these regions is associated with maintenance of the heterochromatic mark H3K9. Therefore, deposition of H3.3 by ATRX/DAXX may help maintain heterochromatin at these structures, and so help protect against aberrant transcription of repetitive regions (Voon and Wong, 2015).

DAXX has, however, been shown to have H3.3 deposition capabilities independent of ATRX. The repression of endogenous retroviral repeats is dependent on DAXX which mediates H3.3 deposition at these regions (Hoelper *et al.*, 2017). However, there is significant overlap between genes which are differentially expressed in the absence of either DAXX or ATRX, so H3.3 deposition by both chaperone partners is likely the major deposition route (Hoelper *et al.*, 2017).

1.2.1.1 ATRX in Alternative lengthening of telomeres

ATRX is key protein which is absent in cancers or immortalised cells which maintain their telomeres via alternative lengthening of telomeres (ALT) mechanism, instead of by telomerase. Telomeres are at the end of chromosomes and their DNA ends can be viewed as a double strand break, and in the case of ALT cells, this can trigger homologous recombination (HR) and break induced replication, whereby new telomere is synthesised using other telomeric sequence as a template (Sobinoff and Pickett, 2017). The absence of ATRX alone is not sufficient to cause ALT but is key to its activation (Lovejoy *et al.*, 2012; Clynes *et al.*, 2014). It is not entirely certain what role of ATRX is required to protect against ALT, but it seems likely that ATRX's role of binding G quadruplexes (G4) and depositing H3.3 at telomeres could play a part.

ATRX has been shown to bind G4s (Law *et al.*, 2010), a non-B form DNA structure formed on single stranded DNA from tracts of guanines which have undergone Hoogsteen base pairing (Gellert, Lipsett and Davies, 1962). Telomeric repeat sequences have the capacity to form these structures, which can cause obstacles to DNA processing and eventually replication stress. ATRX deficient cells have been shown to have a greater incidence of telomere fusions (Watson *et al.*, 2013), suggesting that the presence of ATRX can help processing of these difficult regions. This could be through its ability to deposit H3.3 onto sequences which can exclude nucleosomes and thereby decrease the chance of structure formation (Clynes *et al.*, 2015). However, ATRX has not been shown to unwind G4s directly (Clynes *et al.*, 2014; Teng *et al.*, 2021).

1.2.1.2 ATRX at stalled replication forks

ATRX is required at stalled replication forks. ATRX is required to resume replication after treatment with the genotoxin hydroxyurea (Leung *et al.*, 2013), although possibly not across the whole genome (Clynes *et al.*, 2014). ATRX has been shown to interact with MRE11, a component of the MRN complex. MRE11 degrades DNA and ATRX can help protect against MRE11 mediated degradation of stalled forks, facilitating replication progression. This also requires DAXX alongside ATRX, hinting at H3.3 involvement (Huh *et al.*, 2016). H3.3 has typically been characterised as a replication independent histone variant, so whether it has a specific purpose at stalled replication forks is unclear.

However, a requirement for H3.3 at replication forks has previously been reported (Frey *et al.*, 2014).

1.2.2 HIRA

HIRA binds specifically to H3.3 and deposits in a DNA synthesis independent pathway (Tagami 2004). The HIRA complex is composed of HIRA, UBN1/2, CABIN1 and works with ASF1a (Tang *et al.*, 2006) to deposit H3.3. This is mediated by binding of UBN1 to DNA and H3.3 specifically (Daniel Ricketts *et al.*, 2019). The HIRA protein acts as a scaffold (Figure 1.3), with its presence required for formation of the whole complex (Ray-Gallet *et al.*, 2018). The HIRA complex binds to H3.3 more transiently than DAXX (Zink *et al.*, 2017).

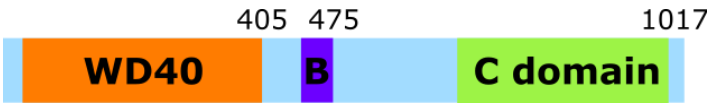

Figure 1.3 Domain structure of HIRA protein The WD40 region interacts with UBN1, the B-like domain interacts with ASF1a and the C domain interacts with CABIN1

The HIRA complex is responsible for the deposition of H3.3 to genic regions, notably enhancers and transcriptional start sites (Goldberg *et al.*, 2010; Xiong *et al.*, 2018). More recent research has identified 2 HIRA mediated H3.3 deposition pathways, with newly synthesised H3.3 dependent on the trimerisation of HIRA and UBN1 and ASF1 and HIRA required for recycling of existing H3.3 (Torné *et al.*, 2020).

1.3 DNA damage

Cells must continuously deal with DNA damage. DNA damage can arise through endogenous sources (such as reactive oxygen species), from environmental factors (such as tobacco components) and also through errors in replication. Damage must be repaired accurately and in a timely manner to ensure the processivity of replication and transcription. If DNA damage is not repaired accurately, mutations can be passed onto daughter cells and lead to cancer.

In order to cope with DNA damage, cells have mechanisms in place to detect, remove and repair lesions. Different damaging agents lead to different types of DNA lesions, which in turn are resolved by different DNA repair pathways.

1.3.1 Types of DNA damaging agents

Much of my focus in this this thesis is on the impact of UV induced DNA damage, but I also investigate the impact on the damaging agents MMS, cisplatin and NQO.

1.3.1.1 Methyl methanesulphonate (MMS)

MMS is an alkylating agent, adding an alkyl group to guanine and adenine to form 7-methylguanine (7meG) (60-80 % of products) and 3-methyladenine (3meA) (10-20 % of products) (Fu, Calvo and Samson, 2012). 7meG can lead to depurination, leaving an apurinic site which causes mismatched pairing, mutagenesis or a replication fork block (Groth *et al.*, 2010). 3meA can block the progression of polymerases. These lesions are often processed by the base excision repair pathway.

1.3.1.2 Cisplatin

Cisplatin can cause several types of DNA damage including inter-strand crosslinks, DNA protein crosslinks and mono-adducts, but the majority of lesions are intra-strand crosslinks formed between adjacent guanines and the electrophilic cisplatin product (Pinto and Lippard, 1985; Eastman, 1987). Whilst a minor component by numbers, inter-

strand crosslinks are highly cytotoxic as they prevent the two strands of DNA separating meaning polymerases cannot act on either strand.

1.3.1.3 Ultraviolet (UV) radiation

UV radiation has a range of wavelengths and is divided into 3 subsections: UV-A (320-400 nm), UV-B (295-320 nm) and UV-C (100-295 nm). Solar UV radiation is mostly made up of UV-A and UV-B (Setlow, 1974), but UV-C is used for laboratory studies. The peak emission wavelength of the UV bulb used for experiments in this thesis is 254 nm, which is close to the absorbance peak of DNA at 260 nm. Although organisms would not be exposed to UV-C in nature, the same lesions are produced with all wavelengths of UV, albeit with different efficiency (Mitchell, Jen and Cleaver, 1991).

There are 2 main types of DNA lesions produced from UV irradiation, cyclobutane pyrimidine dimers (CPDs) and pyrimidine-pyrimidine (6-4) photoproducts (6,4 PPs) (Figure 1.4). CPDs are more common, making up approximately 75% of lesions (Mitchell and Nairn, 1989). They are covalent linkages between neighbouring pyrimidines. These lesions can be accommodated in the helix structure (Wang and Taylor, 1991).

6,4 PPs also link neighbouring bases, but in such a way that there is a prominent distortion of the helix (Mizukoshi *et al.*, 2001). These lesions are usually repaired through nucleotide excision repair (NER). UV radiation can also produce small levels of other types of lesions, such as pyrimidine hydrates and thymine glycol.

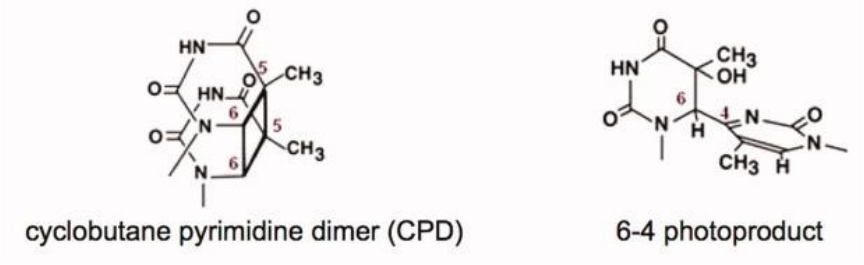

Figure 1.4 Structures of the two most common UV lesions. Adapted from (Yang, 2011)

1.3.1.4 4-Nitroquinoline 1-Oxide (NQO)

NQO causes several types of guanine and adenine adducts (Galiegue-Zouitina, Bailleul and Loucheux-Lefebvre, 1985). It is used as a UV mimetic, not because it produces

damage identical to that of UV, but because NQO damage is resolved by very similar repair pathways as 6,4 PP and CPDs (Jones, Edwards and Waters, 1989). It is useful in this context as it can be technically simpler to administer a small molecule to a large number of suspension cells than to irradiate a large volume of cells with UV.

1.3.2 DNA damage repair pathways

1.3.2.1 Base excision repair

This is the most frequently used type of DNA damage repair in nature, repairing lesions caused by alkylation, oxidation and deamination. It is also the repair pathway through which alkylated bases formed by MMS treatment are resolved.

Firstly, DNA glycosylases recognise and remove the chemically altered base by cleaving the N-glycosidic bond. There are various DNA glycosylase enzymes which recognize different types of lesion (Krokan and Bjørås, 2013). Some recognize very specific substrates, eg. mis-incorporated uracils (Lindahl, 1974), whereas others have broader specificity, eg. alkylation. The resulting abasic site is cleaved from the surrounding DNA backbone by an apurinic/apyrimidinic endonuclease, leaving a gap which needs to be filled. Incorporation of replacement nucleotides usually happens by short patch repair, whereby a single nucleotide is incorporated by Polβ (Kubota *et al.*, 1996). Long patch repair, where 2-8 nucleotides are synthesized, requires additional factors, including Pol δ or ε, PCNA and a flap endonuclease. Finally, a ligase repairs the single strand nick. Base excision repair can occur throughout the cell cycle (Branzei and Foiani, 2008) and it can be affected by chromatin packing, meaning a change in the chromatin structure could affect the efficiency of repair.

1.3.2.2 Crosslink repair

Repair of inter-strand crosslinks (such as those caused by cisplatin) requires components of multiple repair pathways (Clauson, Schärer and Niedernhofer, 2013), including nucleotide excision repair, translesion synthesis and homologous recombination. Repair mainly occurs during S phase, as replication forks stall on approaching the crosslink.

Incisions by XPF and ERCC1 lead to unhooking of the crosslink on one hand of the fork and a break on the other (Niedernhofer *et al.*, 2004). Translesion synthesis by a polymerase can progress past the crosslink, then this double strand can provide a template for HR to repair the break (Semlow and Walter, 2021). Inter-strand crosslinks distort the DNA helix, which can then be recognized by the NER machinery.

1.3.2.3 Double strand break repair

Double strand breaks can be deleterious to the cell and must be repaired to avoid genomic instability. Detection of DSBs induces DNA damage signalling, particularly ATM, and leads to phosphorylation of γH2AX on chromatin around the break. There are 2 major pathways which mediate repair of DSBs.

1.3.2.3.1 Non-homologous end joining NHEJ

Non-homologous end joining is a pathway to repair double strand breaks without the need for a DNA template, and so can happen throughout the cell cycle. DSB ends can be recognised and captured by Ku70/80. After this, the break undergoes limited end resection to remove any damaged bases and generate compatible ends. This is where errors can be introduced. DNA ligase IV and XRCC4 ligases then join the 2 ends to resolve the break (Weterings and Chen, 2008).

1.3.2.3.2 Homologous Recombination (HR)

Homologous recombination is a more accurate DSB repair pathway, with a template required for accurate repair. This requirement for a template limits HR to the S phase of the cell cycle, where a sister chromatid is present to provide a homologous repair template. A DSB can be recognised by Ku70/80, with the MRN complex also having the capability to sense DSBs (Petrini and Stracker, 2003). The DNA break ends undergo extensive resection (initiated by MRE11(Garcia et al., 2011)) to form large single stranded overhangs. This single strand then invades a section of homologous DNA to form a D-loop. DNA repair synthesis is carried out by Pol δ based on the homologous template. Finally, the Holliday junction formed by DNA crossover from strand invasion is resolved, to leave 2 stretches DNA with no break (Wright, Shah and Heyer, 2018).

1.3.2.4 Nucleotide excision repair

The nucleotide excision repair (NER) pathway resolves lesions which distort the helix, including 6,4 PP and CPDs caused by UV irradiation. This type of lesion is recognized by XPC, which binds to the damage and bends the DNA helix (Sugasawa *et al.*, 1998; Janićijević *et al.*, 2003). For UV lesions, DNA damage binding proteins 1 and 2 can bind 6,4 PPs to help recruit XPC (Sugasawa, 2010). The pre-incision complex then assembles around XPC, consisting of XPA, XPD, RPA and TFIIH. TFIIH is a helicase which opens the helix around the lesion in an ATP-dependent manner to form a bubble of 25-30 nt (Evans *et al.*, 1997), with RPA binding the opposite undamaged ssDNA strand (Lee *et al.*, 2003).

Next, the segment of DNA containing the lesion is removed. The two junction specific endonucleases ERCC1/XPF and XPG bind and cleave at the 5' and 3' ends of the bubble respectively (Harrington and Lieber, 1994; De Laat *et al.*, 1998). This releases a 24-32 nt fragment of DNA, thus removing the lesion but leaving behind a gap of ssDNA. To fill this gap, repair synthesis is carried out by Polε or Polδ (Shivji *et al.*, 1995), stimulated by PCNA. This pathway is known as global genome nucleotide excision repair (GG-NER) (Figure 1.5).

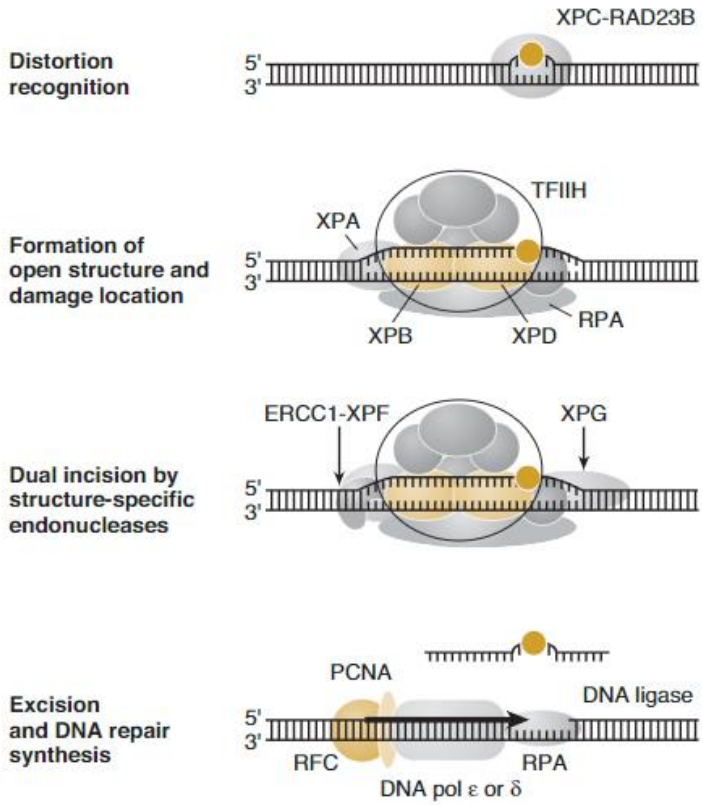

Figure 1.5 Mechanism of excision of a lesion by NER factors taken from (Friedberg *et al.*, 2005c)

There is a second pathway through which lesions enter nucleotide excision repair: transcription coupled nucleotide excision repair (TC-NER). NER is carried out at different speeds on different types of genes. NER occurs fastest on transcribed strands of active genes, slower on non-transcribed strands of active genes and slowest (via GG-NER) on transcriptionally silent regions (Mellon, Spivak and Hanawalt, 1987). TC-NER differs from GG-NER only in the initial recognition steps, with XPC not required to detect helix distortion (Laat, Jaspers and Hoeijmakers, 1999). TC-NER is specific for lesions which stall RNA polymerase II (RNAPII) (Fousteri and Mullenders, 2008), e.g. CPDs, with the stall replacing the XPC recognition step. This pathway also requires the additional factors CSA and CSB. CSB is capable of binding the stalled RNAPII and recruiting TFIIH (Tantin, 1998). CSB and its partner Rad26 may remodel the stalled polymerase, allowing access to the lesion (Friedberg *et al.*, 2005b).

1.3.2.4.1 Chromatin and nucleotide excision repair

The chromatin landscape impacts and is impacted by NER. 100bp is required for lesion excision (*in vitro*) (Huang and Sancar, 1994), but the linker between histones is only up to 80 bp. This suggests that some nucleosome reorganization is required in order for NER to take place, although larger scale disruption is not necessarily required (Thoma, 1999). NER occurs preferentially in nuclease accessible regions, but over time these same regions can become more nuclease resistant (Smerdon and Lieberman, 1978). This increased accessibility is not due to the damage caused by UV (Zolan *et al.*, 1982), showing that chromatin packing changes and loosens for NER, then resumes its tighter packing and higher order chromatin structure once the lesion is resolved (Nissen, Lan and Smerdon, 1986). These observations led to the Access/Repair/Restore model (Green, 2002; Polo and Almouzni, 2015). Nucleosomes are destabilized, disrupted or moved to allow access of nucleotide excision repair machinery to the lesion (Wang *et al.*, 2006; Zhao *et al.*, 2009; Jiang *et al.*, 2010). Chromatin remodelling is then coupled to repair (Gaillard *et al.*, 1996), with the histone chaperones CAF-1 and ASF1 working to reassemble nucleosomes (Mello *et al.*, 2002; Green and Almouzni, 2003). Nucleosome reassembly after repair of damage could be a mechanism for which H3.3 is required for DNA damage resolution.

1.3.2.5 What happens when a replication fork encounters damage

DNA lesions can present impediments to the progression of replication machinery (Zeman and Cimprich, 2014). This is due to altered bases not fitting into the active site of replicative DNA polymerases and therefore they halt or stall the replication fork (Cordeiro-Stone *et al.*, 1999; Veaute *et al.*, 2000). Whilst lesions can cause damage or mutations in one gene, if they are encountered by a replication fork and cause it to stop, larger-scale genomic instability can arise (Jackson and Bartek, 2009). There are several possibilities for what may happen if the replication fork encounters damage (Figure 1.6) and various mechanisms are in place to try to reduce the possibility of fork collapse. If a fork encounters a blockage, it may migrate backwards, forming a chicken foot structure in order to attempt to bypass a section of DNA it cannot pass (Postow *et al.*, 2001). It may also make use of translesion polymerases to pass a lesion. Translesion polymerases typically have a more spacious active site which can accommodate some types of DNA damage, and therefore replicate over the lesion. However, this process is likely to be

mutagenic as the polymerases themselves are intrinsically error-prone and the lesion itself can be non- or mis-instructional (Sale, 2013). A fork may bypass a lesion by repriming beyond the lesion, allowing replication to continue whilst leaving a gap opposite the lesion, which is filled post-replicatively. The lesion itself is then returned to duplex DNA and can then be safely excised. In vertebrates, the primase-polymerase PrimPol plays a key role in leading strand repriming (Bianchi *et al.*, 2013; García-Gómez *et al.*, 2013; Wan *et al.*, 2013). Finally, if a fork encounters a single strand break/nick, as a form of damage itself or as part of another repair pathway, it can become a double strand break (DSB) (Kuzminov, 2001). This requires DSB repair pathways to avoid genomic instability, using either the accurate homologous recombination with a sister chromatid template or the error-prone non-homologous end joining (NHEJ).

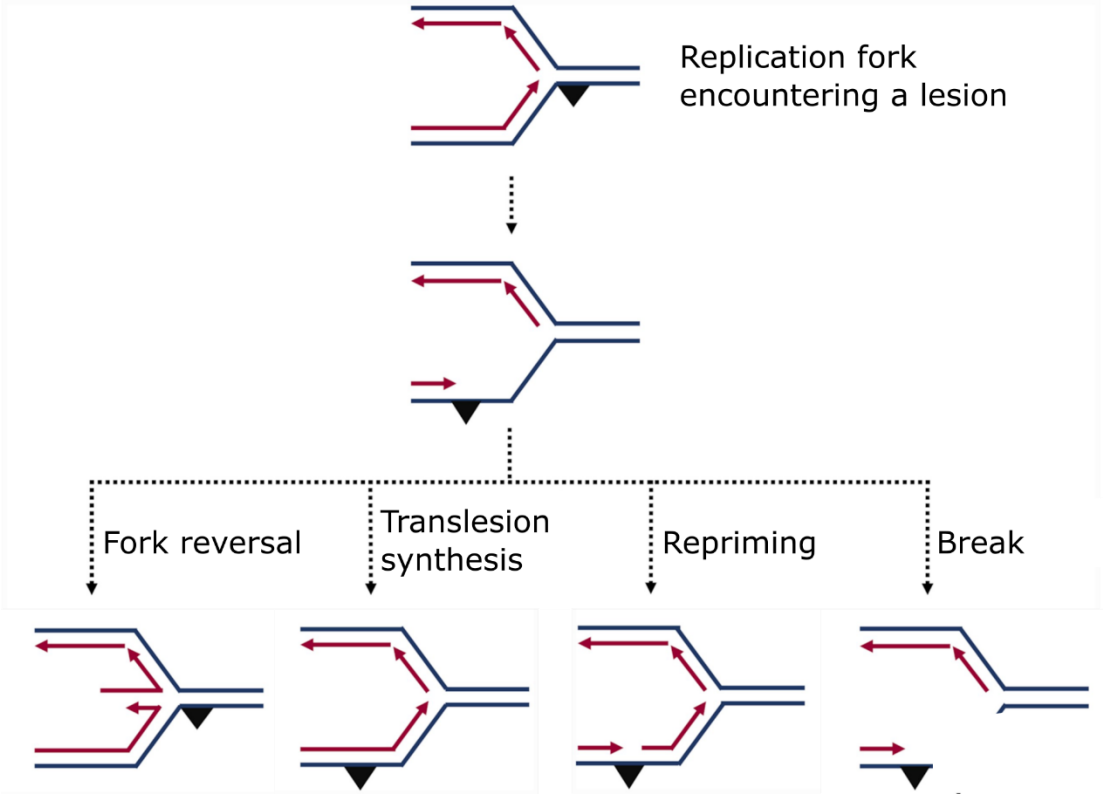

Figure 1.6 Possibilities of events following a replication fork encountering a lesion adapted from (Ashour and Mosammaparast, 2021). As a fork encounters a lesion it could: reverse, forming a chicken foot structure to avoid using damage as a template; synthesise past the lesion by using an alternative polymerase; reprime beyond the lesion to continue replication; collapse, leading to a DSB.

1.3.3 Checkpoint activation after DNA damage

One way for cells to avoid transmitting unresolved DNA damage to daughter cells (where it could lead to mutagenesis) or attempting to replicate lesions (where it could cause replication stress), is to halt the cell cycle via checkpoint activation whilst DNA damage is dealt with. This is important to avoid the possibility of mutagenesis and replication stress. Mutations can occur when lesions are repaired by error-prone mechanisms and can eventually lead to cancer. Replication stress can be defined as an event which disrupts replication fork progression, which could eventually lead to regions of the genome not being replicated.

Cells have a triad of phosphatidylinositol-3-kinase-like kinase family proteins which regulate and control large networks of DNA damage responses, including checkpoint activation. These regulators are ATM, ATR and DNA-PK. ATM and ATR and their downstream targets have key roles in both DNA damage repair and checkpoint regulation (Blackford and Jackson, 2017).

1.3.3.1 ATM damage signalling pathways

ATM is activated in response to double strand breaks, regulating and mobilising the response to these breaks. ATM is recruited to DSBs (Andegeko *et al.*, 2001) by binding to NBS1 (Falck, Coates and Jackson, 2005), a component of the DSB sensing MRN complex. Here, the activity of ATM is stimulated (Uziel *et al.*, 2003). ATM notably phosphorylates H2AX, CHK2, BRCA1 and p53 (Canman *et al.*, 1998; Matsuoka, Huang and Elledge, 1998; S. Banin *et al.*, 1998), as well as contributing to p53 stability by MDM2 phosphorylation (Cheng and Chen, 2010).

H2AX phosphorylation (forming γH2AX) happens very rapidly after a double strand break and spreads over hundreds of kilobases of DNA, recruiting DNA damage repair factors and chromatin remodellers (Meier *et al.*, 2007; Savic *et al.*, 2009). ATM further mediates this chromatin based signalling in response to DSBs by stabilizing MDC1 on chromatin as it recognises γH2AX (Stucki *et al.*, 2005; Jungmichel *et al.*, 2012).

Once activated, CHK2 acts on substrates involved in regulation of the cell cycle, apoptosis and transcription. It is very mobile throughout the nucleus, which is important for its function as a transducer (Lukas *et al.*, 2003).

1.3.3.2 ATR damage signalling pathways

ATR is activated by a wider range of genotoxic stress and phosphorylates many of the same targets as ATM, including p53 and H2AX (Ward and Chen, 2001). ATR itself can also phosphorylate ATM (Stiff *et al.*, 2006). ATR is recruited to tracts of single stranded DNA (ssDNA) coated with RPA. These are formed during uncoupling of stalled replication forks (Byun *et al.*, 2005) and processing of some types of DNA damage, possibly including UV damage in the process of being resolved by NER (Friedberg *et al.*, 2005a). A major target of ATR is CHK1 (Zhao and Piwnica-Worms, 2001), which is activated by ATR in conjunction with claspin (Chini and Chen, 2003). CHK1 can regulate key components of cell cycle regulation machinery, thereby controlling the cell cycle and checkpoints. CHK1 substrates include the cell cycle regulators Cdc25A, Cdc25C and Wee1 (Blasina *et al.*, 1998; Lee, Kumagai and Dunphy, 2001; Falck *et al.*, 2002). It also localizes at the centromere where it controls Cdk1/CyclinB and thus controls the onset of mitosis (Smith *et al.*, 2010).

CHK1 and CHK2 have both overlapping and independent targets and functions, creating a signal transduction network with redundancy and interconnections to allow a flexible response to DNA damage and genomic stress (Figure 1.7).

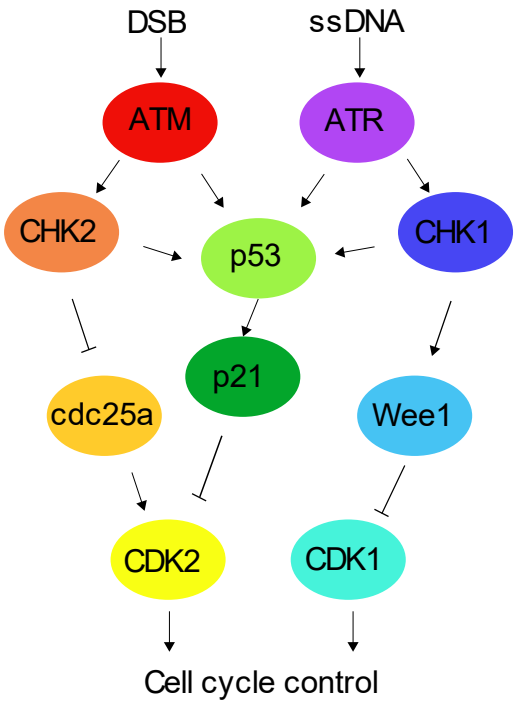

Figure 1.7 DNA damage can activate ATM and ATR signalling pathways. Activation of these pathways leads to activation of cell cycle checkpoints

1.3.3.3 p53

p53 is famous as a key tumour suppressor which is mutated in many cancers (Hollstein *et al.*, 1991). It sits at the heart of ATM/CHK2 and ATR/CHK1 regulatory networks (Figure 1.7) and has a key role in halting the cell cycle after DNA damage.

p53 is a transcriptional regulator which binds DNA as a tetramer (McLure and Lee, 1998). It is regulated post-transcriptionally, both through its interaction with MDM2 which controls its degradation (Ashcroft and Vousden, 1999), and through a wide array of post translational modifications (Bode and Dong, 2004). p53 can be activated through both ATM and ATR pathways in the response to DNA damage, eg. UV irradiation can cause induction of active p53 via ATR (Latonen, Taya and Laiho, 2001). DNA damage can lead to a G1/S cell cycle arrest through the actions of p53 (Kastan *et al.*, 1992). This is a major checkpoint at the interface between G1 and S phases of the cell cycle which can prevent cells entering the replicative segment of the cell cycle with unresolved DNA damage.

A major downstream target of p53 is p21. p21 (through the action of p53) is transcribed after DNA damage and acts as a CDK inhibitor. p21 can reduce the activity of the CDK2-

cyclinE complex (Dulić *et al.*, 1994), halting the cell cycle at the G1/S interface. It also has other substrates, including CDK1, the G2/M specific kinase (Hengst *et al.*, 1994). p21 can also inhibit the activity of DNA Pol δ and ε by sequestering PCNA (Chen *et al.*, 1995), meaning that it could have an impact on checkpoints throughout the cell cycle.

Retinoblastoma protein (pRb) is another important key cell cycle regulator involved in this pathway. During normal cell cycle progression, pRb is hyperphosphorylated by CDK4/6-cylinD and CDK2 cyclinE during the G1/S transition where it releases the transcription factor E2F (Ortega, Malumbres and Barbacid, 2002). When pRb is not phosphorylated, as a result of upstream players in this pathway regulating cyclins/CDKs, E2F is not released and cannot drive transcription of S phase transcripts.

1.3.3.3.1 p53 and NER

p53 has functions outside of checkpoint activation. Whilst p53 and its effectors can facilitate DNA damage repair, it can also directly impact DNA damage repair pathways. For example, p53 has been demonstrated to have an involvement in the NER pathway (responsible for repairing UV induced damage) (Hwang *et al.*, 1999). However, it is uncertain whether it is required in just GG-NER or both GG-NER and TC-NER (Williams and Schumacher, 2016). The role of p53 may be both direct and through its downstream effectors. p53 is a transcription factor and 2 of its targets are important for NER: DNA damage binding protein 2 and XPC (Hwang *et al.*, 1999; Adimoolam and Ford, 2002). Outside of its transcriptional action, it has been shown to modulate the activity of XPB and XPD, both helicase components of the pre-incision complex (Wang *et al.*, 1995). It can also impact chromatin remodelling during NER. p53 recruits the histone acetylase p300 to damage, where it acetylates H3 and promotes global chromatin relaxation, facilitating repair and recognition of damage (Rubbi and Milner, 2003).

1.3.3.3.2 p53 at the replication fork

p53 has been identified at the replication fork by iPOND and PLA experiments (Roy *et al.*, 2018). Here it may be able to exert some control over replication during S phase, as it can impact what happens when a replication fork stalls. After a stall, p53 promotes recombination and lesion bypass (Hampp *et al.*, 2016). p53 can potentially regulate translesion synthesis (TLS) via p21 mediated ubiquitination of PCNA (Avkin *et al.*, 2006)

and interaction with Pol ι (Ihle *et al.*, 2021), but the exact mechanism of the role of p53 in repair at the fork is still emerging.

1.4 H3.3 and its chaperones in the response to DNA damage

H3.3 and its chaperones have been implicated in various aspects of the DNA damage response.

1.4.1 H3.3 has been linked to DSB repair by NHEJ

Either side of a double strand break, nucleosome disassembly (driven by ATM) ensures histones are removed prior to repair by NHEJ (Li and Tyler, 2016). After repair is completed, histones are reassembled onto the DNA. The H3.3 chaperone HIRA in combination with ASF1a, a chaperone which passes H3.3/H4 dimers to HIRA (Tang *et al.*, 2006), are required for this chromatin reassembly (Li and Tyler, 2016). This implicates H3.3 in the recovery from a break repaired by NHEJ. However, this study (Li and Tyler, 2016), did not investigate whether H3.3 was found at the site of a repaired break. Additionally, CAF-1 (a chaperone for canonical H3s (Ridgway and Almouzni, 2000)) was shown to have an effect on chromatin reassembly, suggesting that H3.1 and H3.2 could be deposited alongside H3.3 (Li and Tyler, 2016). Since NHEJ is disfavoured during phases of the cell cycle where DNA is replicated and canonical H3s are not transcribed, one might hypothesise that H3.3 is only deposited alongside other H3s due to its availability throughout the cell cycle, rather than being deposited exclusively because it drives any specific effect on chromatin packing or recruiting specific interactors. Thus, while H3.3 is implicated in chromatin reassembly after a break, this study (Li and Tyler, 2016) did not show it to have a role in break repair itself.

Luijsterburg *et al*. showed that knocking down H3.3 in U2OS cells leads to sensitivity to ionising radiation and a reduction in break repair by NHEJ. CHD-2 is recruited to a DSB by PARP-1 upstream of H3.3 deposition. CHD-2 remodels chromatin and incorporates H3.3, allowing greater access to the damaged DNA for NHEJ factors (Luijsterburg *et al.*, 2016). CHD-2 has been demonstrated to deposit H3.3 (Harada *et al.*, 2012; Siggens *et al.*,

2015) but is not typically included as a major H3.3 specific chaperone. This study (Luijsterburg *et al.*, 2016) was carried out in U2OS cells, which do not express functional ATRX (Lovejoy *et al.*, 2012), so interpretation of chaperone function and H3.3 deposition in a cell line lacking a major H3.3 deposition pathway should be cautious.

Taken together, however, these studies both point to a role for H3.3 in chromatin remodelling after or as part of NHEJ, possibly mediated by HIRA (Li and Tyler, 2016; Luijsterburg *et al.*, 2016). NHEJ is a repair process which can take place outside the replicative phase of the cell cycle and H3.3 is the H3 variant which is expressed throughout the cell cycle (H3.1 and H3.2 are only synthesised in S phase). If any new histones are required as part of the chromatin remodelling, H3.3 is therefore likely the variant deposited and as HIRA has been demonstrated to deposit newly synthesised H3.3 (Torné *et al.*, 2020), it is a possible chaperone candidate. However, H4 is only synthesised during S phase and as an H3 forms a dimer with H4, a supply of H4 is likely needed as well as an H3 supply.

1.4.2 H3.3 is implicated in homologous recombination

Juhasz *et al.* have demonstrated through various approaches that the H3.3 chaperone complex ATRX/DAXX has a role in HR pathways. They used reporter assays in an ATRX KO cell line, whereby an inducible double strand break is placed next to a gene encoding a fluorescent reporter and the accurate or inaccurate repair of the break and subsequent fluorescence informs whether HR or NHEJ repair occurred. They determined that ATRX is needed for effective HR, but that it had no impact on NHEJ. By examining BrdU foci over time, ATRX was demonstrated to be required for extended repair synthesis. Incorporation of H3.3 at sites of damage (as determined by co-localisation of SNAP-tagged H3.3 with gH2AX and ChIP on the reporter assay locus) is dependent on RAD51, DAXX, ATRX and PCNA. This suggests that H3.3 is deposited during long tract repair synthesis as part of homologous recombination, downstream of strand invasion and D-loop formation. The authors of this study (Juhász *et al.*, 2018) propose that H3.3 is deposited on the D-loop during repair synthesis to maintain chromatin integrity and relieve torsional stress.

There is precedence for this potential role of H3.3 at sections of ssDNA. H3.3 can promote or stabilise the formation of single stranded DNA at the *IGVL* locus of DT40 avian cells, and the resulting R-loop formation (Romanello *et al.*, 2016). Additionally, the presence of H3.3 at gene regulatory regions is linked to R-loops and ssDNA. RPA binds single stranded DNA with role in replication and DNA damage repair. RPA has been demonstrated to interact with HIRA at gene regulatory regions, where deposition of newly synthesised H3.3 is facilitated (Zhang *et al.*, 2017). Here, again, H3.3 could have a role at or around tracts of ssDNA and R-loops.

The finding by Juhaz *et al.* that ATRX did not have an impact on NHEJ with the inducible break reporter assay contradicts the finding in mouse cells that ATRX is required for NHEJ (Koschmann *et al.*, 2016). These findings for a role of ATRX in NHEJ are supported by the finding that tumours with ATRX mutations are more responsive to treatment with DNA damaging agents, likely due to an inability to repair DNA damage leading to tumour cell death (Koschmann *et al.*, 2016).

ATRX has also been demonstrated to interact with the MRN complex (Leung *et al.*, 2013; Clynes *et al.*, 2014; Huh *et al.*, 2016) This is linked to its role at stalled replication forks (see section 1.2.1.2) and the recombination based ALT repair mechanism (see section 1.2.1.1). The MRN complex has been linked to the DNA damage response (Lamarche, Orazio and Weitzman, 2010), important in recognising DNA damage and repair pathway choice. This could provide a potential mechanism by which ATRX is linked to DSB repair.

1.4.3 H3.3 and its chaperones in the response to UV induced damage

The role of H3.3 in damage response could include transcriptional recovery as well as damage repair. After UV induced DNA damage, lesions block transcription and global transcription is blocked in order to prevent genomic instability and allow repair machinery to access lesions (Gregersen and Svejstrup, 2018). HIRA has been shown to be necessary as part of recovery from this transcriptional halt (Adam, Polo and Almouzni, 2013).

This study (Adam, Polo and Almouzni, 2013) also observed an enrichment of H3.3 in chromatin damaged by UV-C irradiation mediated by HIRA, although H3.1 is also found

at the damage sites. This fits into the other research that points to H3.3 deposition as a part of chromatin recovery after damage repair (Li and Tyler, 2016). Additionally, HIRA was shown to not be directly involved in damage repair itself, having no impact on the kinetics of CPD removal (over a 24-34 hr timescale).

HIRA itself is recruited to UV-C laser induced areas of damage in a transcription independent manner. It is recruited to these areas by early NER damage recognition proteins, namely Cullin 4a and DDB1/2. HIRA is released from these damage sites once DNA repair and rechromatinisation is complete (Adam, Polo and Almouzni, 2013).

This study (Adam, Polo and Almouzni, 2013) was quite focussed, with much of the work carried in U2OS (ALT positive) cells, looking at only newly synthesised H3.3 after local UV-C irradiation. Whilst this focused approach enables a deeper understanding for a role of HIRA after UV, the absence of a functional ATRX, and therefore a major H3.3 deposition pathway, should be considered when interpreting results. HIRA has been demonstrated to be able to fulfil the role of ATRX role in H3.3 deposition at telomeres in cells lacking functional ATRX (Hoang *et al.*, 2020). As there is possible redundancy in H3.3 deposition between these 2 chaperone complexes, working in a cell line with only HIRA may not give an accurate picture of what its role may be in cell lines with ATRX. Likewise, only examining H3.3 synthesised during the course of the experiment may miss some contributions from recycled H3.3.

Previous work in the Sale lab has also linked H3.3 to the response to UV induced DNA damage through NER (Frey *et al.*, 2014). Frey *et al.* found that DT40 avian cells deficient in H3.3 exhibit survival hypersensitivity to UV. Epistasis with XPA was demonstrated in a colony survival assay, implicating H3.3 in the NER repair pathway, although the XPA mutant line is extremely sensitive to UV, much more so than H3.3, so the epistasis should be interpreted with some caution.

An increased S phase population and stalled replication forks after UV was also observed in the absence of H3.3 (Frey *et al.*, 2014). H3.3 has typically been characterised as a replication independent histone variant, so this apparent role in replication was unexpected. However, the observation does echo the findings of ATRX involvement at

replication forks after DNA damage (Leung *et al.*, 2013; Clynes *et al.*, 2014; Huh *et al.*, 2016) (see section 1.2.1.2).

On further study of the H3.3 specific residues, it was found that only the chaperone binding patch is required for fork progression (not the unique tail residue, S31), but both the chaperone binding patch and the tail residue is required for survival after UV (Frey *et al.*, 2014). From this, it appears that a chaperone deposits H3.3 to enable replication fork progression, independent of the N-terminal tail which does not have a role in chaperone binding. Once H3.3 has been deposited by a chaperone, the tail residue could facilitate repair, potentially by changing chromatin packing around or recruiting factors to a lesion (Figure 1.8).

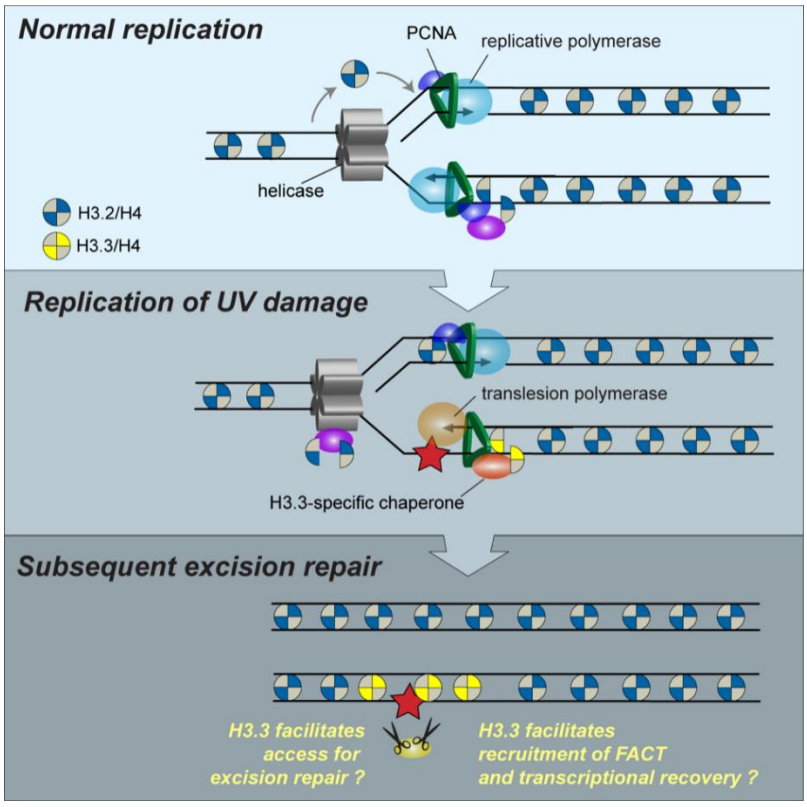

Figure 1.8 A model for the role of H3.3 during DNA damage bypass and excision repair as proposed by Frey *et al.* In normal replication, canonical H3/H4 is incorporated into nascent DNA by CAF-1 and ASF1a. When a fork encounters a lesion (denoted by a red star), the histone chaperone could switch to an H3.3 specific chaperone and incorporate H3.3 as the fork bypasses the lesion. H3.3 then facilitates repair or recovery (Frey *et al.*, 2014).

This study (Frey *et al.*, 2014) is unusual in that it focussed on H3.3 histone itself, rather than its chaperones. A H3.3 is comprised of 2 genes, complete knockout of H3.3 before the widespread use of CRISPR Cas9 was not trivial. Separating the role of the chaperone binding patch from the role of the tail residue informs us that deposition of H3.3 by a chaperone is not sufficient for full recovery from UV induced damage, and therefore that H3.3 may have other roles in the DNA damage response than simply being the only H3 variant present in the cell whilst repair occurs. However, this study did not directly investigate deposition of H3.3 in response to DNA damage.

Overall, it is clear that H3.3 and its chaperones have roles in responses to DNA damage, but a single simple function is not clear. H3.3 and its chaperones have been shown in some situations to be implicated in repair of DNA damage, but at other times required for recovery from damage after repair rather than in repair itself.

The H3.3 chaperones have roles in deposition at distinct regions of the genome (HIRA in genic regions, ATRX at repetitive regions). This spatial distinction raises the possibility that damage at different regions of the genome may have different histone chaperones involved in the damage response.

As H3.3 has a role in homologous recombination (Juhász *et al.*, 2018) and there is a separation of function between the chaperone binding patch and tail specific residue after UV irradiation (Frey *et al.*, 2014), H3.3 may have a role in DNA damage resolution outside its capacity to be deposited throughout the cell cycle.

1.5 Aims

During this thesis, I have attempted to further understand the role of H3.3 and its chaperones in the response to DNA damage. Previous work in the Sale lab in avian cells has demonstrated a role for H3.3 in survival and fork progression after UV irradiation. The chaperone binding patch was shown to be essential for H3.3's role, but the chaperone required for survival and fork progression is unknown. HIRA has been demonstrated to

play a role in recovery after NER and ATRX has a role in stalled replication forks, so either or both chaperones could have roles.

Building on this work, I have set out to confirm a role for H3.3 in the response to DNA damage in human cells, with a focus on its potential role in recovery from UV induced DNA damage. I then set out to ask the following questions:

1. Which H3.3 chaperone could mediate its action in the response to UV induced DNA damage?
2. Does H3.3 facilitate UV repair by recruiting specific interactors?

I have carried out this research in a non-transformed human cell line which expresses HIRA, ATRX and H3.3. I have removed H3.3, ATRX or HIRA and, by challenging these cells with UV-C irradiation, I have been able to confirm a role for H3.3 in the timely recovery from DNA damage. The ATRX knockout cell line phenocopies the cell cycle changes seen in the H3.3 knockout cell line after UV irradiation, making it the most likely chaperone to facilitate the involvement of H3.3 after UV induced DNA damage. Whilst I have not observed a role of H3.3 at the replication fork after damage, the cell cycle changes and raised DNA damage markers observed are likely a result of damage encountered when the cells are in S phase. I have also been able to interrogate some of the direct interactors of H3.3 after UV induced DNA damage.

Chapter 2: Materials and Methods

2.1 Restriction cloning for generation of gRNA containing plasmids

2.1.1 gRNA design

Guide RNAs were designed against the exon of interest using either the chopchop webtool or Wellcome Sanger Institute Genome Editing Tool CRISPR search. Oligos were ordered containing an overhang for ligation (see Appendix 1).

2.1.2 Digestion

10 µg of pX458 plasmid was incubated in Buffer 2.1 (NEB) with 20 U Bbs1 enzyme for 2 hrs at 37 ˚C.

2.1.3 Dephosphorylation

5µl Alkaline Phosphatase and 5 µl AP buffer (Roche) was added to the digested pX458 backbone and incubated for 1 hr at 37 ˚C. This product was loaded into a 0.7% agarose gel and run at 80 V in Ethidium Bromide buffer. Band on the gel were excised and purified using the Qiagen QIAEXII gel extraction kit according to the manufacturer's instructions. Briefly: 3 volumes of Buffer QX1 (solubilisation buffer with pH indicator) and 2 volumes of water were added to the gel slice. 30 µl QIAEXII beads were added and incubated at 50 ˚C for 10 mins until the gel slice solubilised. The mixture was centrifuged at 17900 g for 30 s and supernatant removed. The bead pellet was washed once with 500 µl Buffer QX1 and twice with 500 µl Buffer PE. The bead pellet was dried and DNA eluted by incubating for 5 mins at room temperature (RT) in 20 µl Elution Buffer. Eluate was removed from the beads after centrifugation.

2.1.4 Annealing

25 µl of each 100 µM oligo was mixed with its partner, heated to 100 ˚C for 10 mins and left to cool at RT.

2.1.5 Phosphorylation

43 µl of the annealed oligo was added to 5 µl PNK buffer, 1µl T4 PNK and 1 µl 100 µM ATP and incubated at 37 ˚C for 30 mins then 65 ˚C for 20 mins.

2.1.6 Ligation

A Roche Rapid ligation kit was used, with 10 µl 2 X T4 ligase buffer, 2 µl 2 X Dilution buffer and 6 µl H_2O added to 1 µl digested and dephosphorylated pX458, 1µl annealed and phosphorylated gRNA oligos and 1 µl T4 ligase. Incubated for 5 mins at RT.

2.1.7 Transformation

7.5 µl of the ligation product was transformed in to 50 µl DH5α competent cells by heat shock (42 ˚C for 30 s, 2 mins on ice, recovery in 450 µl LB at 37 ˚C shaking). Transformed cells were plated onto antibiotic containing plates and incubated overnight.

2.1.8 Miniprep

6 colonies per transformation were picked and cultured overnight in 2 ml LB + relevant antibiotic. Plasmids were extracted using the Qiagen QIAprep Spin Miniprep kit according to the manufacturer's instructions. Briefly: Bacteria were pelleted by centrifugation at 6800 g for 3 min and the pellet resuspended in 250 µl Buffer P1. 250 µl Buffer P2 (containing SDS) was added and mixed by inverting before 350 µl Buffer N3 (containing guanidinium and potassium acetate) was added and mixed immediately.

2.2 Cell culture

2.2.1 TK6+ cells

Cultured in RPMI 1640 + GlutaMAX (Gibco), 5 or 10 % Foetal bovine serum (FBS), 1.75 mM Sodium Pyruvate, 1 % penicillin/streptomycin. Grown at 37 ˚C, 5 % CO_2. Confluency kept below 1e6 cells/ml. Frozen in 90 % FBS, 10 % Dimethyl sulphoxide.

2.2.2 HEK293 cells

Cultured in IMDM + GlutaMAX (Gibco), 10 % FBS, 1 % penicillin/streptomycin. Grown at 37 ˚C, 5 % CO_2.

2.3 DNA extraction

2.3.1 Direct lysis of cells for PCR

96 well plate with cells spun at 500 g for 5 min and supernatant removed. Cell pellets were resuspended in 20 µl DirectPCR lysis reagent (Viagen) buffer and 0.2 mg/ml Proteinase K. Plates were incubated at 55 ˚C for 45 min then 85 ˚C for 45 min.

2.3.2 Genomic DNA extraction

DNA was extracted using the Qiagen Gentra Puregene Cell kit according to the manufacturer's instructions. Briefly: 1 million cells were spun down at 500 g for 5 min then supernatant removed. 300 µl Cell Lysis Solution (anionic detergent with DNA stabiliser) was added to the cells, which were then vortexed before 200 µl Protein Precipitation Solution was added then cells were vortexed again. This mixture was centrifuged at 16000 g for 1 min to pellet the precipitated proteins. The supernatant was poured into 300 µl isopropanol and mixed by inverting to precipitate the DNA. This mixture was spun down and supernatant discarded. The DNA pellet was washed in 300 µl 70 % ethanol before rehydration in 50 µl Millipore Water (MPW).

2.4 PCR

2.4.1 Primer design

Primers were designed using Primer3 web software (see Appendix 1).

2.4.2 PCR

PCR reactions were carried out on an Eppendorf Nexus Gradient thermocycler with the following enzymes and conditions:

2.4.2.1 Phusion

Component	Final concentration	Volume in 25 µl reaction
5X Phusion HF buffer (NEB)	1X	5
10 mM dNTPs	200 µM	0.5
10 µM Forward Primer	0.5 µM	1.25
10 µM Reverse Primer	0.5 µM	1.25
Template DNA	Variable (typically 100 ng)	
Phusion DNA polymerase (NEB)	0.5 U/ 25 µl reaction	0.25
DMSO	2 %	0.5
Millipore Water		To 25 µl

Step		Temperature/˚C	Time/s
Denaturation		98	30
Denaturation	30 cycles	98	5
Annealing		Variable (typically between 58 and 64)	15
Elongation		72	20 /kb
Extension		72	600
Hold		10	indefinitely

2.4.2.2 Q5

Component	Final concentration	Volume in 25 µl reaction
5X Q5 reaction buffer (NEB)	1X	5
10 mM dNTPs	200 µM	0.5
10 µM Forward Primer	0.5 µM	1.25
10 µM Reverse Primer	0.5 µM	1.25
Template DNA	Variable (typically 100 ng)	
Q5 DNA polymerase (NEB)	0.02 U/µl	0.25
Millipore Water		To 25 µl

Step		Temperature/˚C	Time/s
Denaturation		98	30
Denaturation	30 cycles	98	10
Annealing		Variable (typically between 58 and 64)	20
Elongation		72	30 /kb
Extension		72	120
Hold		10	indefinitely

2.4.3 PCR purification

PCR reactions were purified using the Qiagen QIAquick PCR purification kit according to the manufacturer's instructions, briefly: 5 volumes of Buffer PB (containing guanidinium and isopropanol) was added to the PCR reaction and applied to a QIAquick column. Vacuum was applied until all sample has passed through, then columns were washed with 750 µl Buffer PE (containing ethanol). Columns were then spun at 17900 g for 1 min to remove residual wash buffer. DNA was eluted into a clean tube by application of 30 µl Elution buffer (10 mM Tris/HCl, pH 8.5) and centrifugation.

2.4.4 Agarose Gel Electrophoresis

Agarose was dissolved to a concentration of 1 % in TBE by heating in a microwave. The agarose was poured into a cast and left to cool. Buffer (see below) was added and samples loaded after addition of 10 X BlueJuice loading dye alongside 1 kb ladder (Thermofisher). The gel was run at 80 V, typically for 30 mins.

2.4.5 Gel staining

2.3.5.1 SYBR Safe

1 X SYBR Safe was added to the melted agarose before pouring. The gel was run in TBE buffer and visualised on a BioRad ChemiDoc with the transilluminator on SYBR Safe settings.

2.4.5.2 Ethidium Bromide

Agarose gels were run in TBE buffer containing 50 µg/ml Ethidium Bromine. Gels were visualised on the ChemiDoc with Ethidium Bromide settings.

2.5 Western Blot

2.5.1 Protein lysis

1 e6 cells were lysed in 20 µl RIPA lysis buffer (1X RIPA, 1 X cOmplete protease inhibitor (Roche), 1 X Halt Phosphatase inhibitor (Thermo Fisher) and 0.5 U/reaction Benzonase) by rotating at 4 ˚C for 30 min then centrifugation at 16000 g at 4 ˚C for 30 min. The supernatant had 2 X Laemlli buffer added and was boiled for 10 mins at 98 C. Protein was stored at – 20 C.

2.5.2 SDS PAGE electrophoresis

For samples to be transferred by semi-dry transfer, samples were run on a NuPAGE 4-12 % Bis-Tris precast gel (ThermoFisher). 10 µl protein sample was loaded in each well, alongside 8 µl PageRuler prestained protein ladder (ThermoFisher) and the gel was run in MOPS (50 mM MOPS, 50 mM Tris, 0.1% SDS, 1mM EDTA, pH 7.7) at 120 V until the dye front reached the bottom of the gel.

For a large protein of interest (over 100 kDa) samples were run on a NuPAGE 3-8 % Tris Acetate precast gel (ThermoFisher) as above, but in Tris Acetate SDS running buffer (Novex)

2.5.2 Transfer

2.5.2.1 Semi-dry transfer

Proteins were transferred to a nitrocellulose membrane using the iBlot 2 system with iBlot transfer stacks (ThermoFisher). The gel was loaded into the stack according to the manufacturer's instructions, rolled to remove bubbles and the stack loaded into the iBlot 2 system. The gel was transferred at 7 min at 25 V for proteins of interest larger than 20 kDa or 6 mins at 25 V for smaller proteins.

2.5.2.2 Wet transfer

The gel was laid in a stack next to a nitrocellulose membrane pre-soaked in transfer buffer (1X TrisGlycine w/o SDS Running buffer (ThermoFisher), 10 % Methanol) surrounded by 4 pieces of pre-soaked Whatman paper (GE). This was placed in the cathode core surrounded by pre-soaked sponges. The anode case was added on top and wedged into the running tank. The central well was covered with transfer buffer at 4 ˚C and the outer tank was filled with water. The transfer was run at 15 V overnight at 4 ˚C or at 20 V for 4 hrs at RT.

Membranes were checked for correct transfer by Ponceau staining: 5 ml Ponceau incubated rocking for 5 min at RT and washed briefly in TBS-T (1 X TBS, 0.1 % Tween). Membranes were blocked for 1 hr at RT in either 5 % milk or 5 % BSA in TBS-T (corresponding to antibody to be used).

2.5.3 Primary antibodies used in Western blotting

Protein epitope	Catalogue/Clone no.	Manufacturer	Species
H3.3	09838	Sigma Aldrich	Rabbit
GFP	290	abcam	Rabbit
PCNA	SC-56	Santa Cruz	Mouse
ATRX	55584	Santa Cruz	Mouse
HIRA	Wc119.2H11	Active Motif	Rabbit
Tubulin	T6074	Sigma Aldrich	Mouse

2.6 Colony survival assay

1 L methylcellulose media was made up with 10 g methylcellulose, 11.9 g DMEM, 2.44 g sodium bicarbonate, 100 ml FBS, 2x Pen/Strep and water. Cells were irradiated with UV-C (265 nm) at varying doses then plated into 5 ml methylcellulose at 20000, 2000 and 200 cells/well. Plates were incubated for 2 weeks then colonies were counted.

2.7 Cell cycle analysis

2.7.1 EdU staining

1 e6 cells in 1 ml media were incubated with 25 μM EdU dissolved in DMSO for 1 hr, then collected by centrifugation at 1500 g for 4 mins. Cells were fixed immediately.

2.7.2 Fixing cells

Cell pellets were incubated for 10 mins at RT in 1 % Paraformaldehyde. They were then centrifuged at 1500 g for 4 min and the pellet resuspended in 10 % DMSO, 90 % PBS. Fixed cells were kept at -80 ˚C before staining.

2.7.3 Click-iT staining

Fixed cells were thawed and spun at 1500 g for 4 mins and supernatant removed. Cells underwent saponin-based permeabilization in 100 μl BD Perm/Wash buffer (BD Biosciences) for 15 mins. The Click-iT reaction was performed to detect EdU as per the

manufacturer's instructions, briefly: Cells were resuspended in Click-iT reaction cocktail containing CuSO4, fluorescent azide dye (either Alexa 647 or Alexa 488) and buffer additive for 30 mins at RT. Cells were spun down and resuspended in BD buffer with 1 µg DAPI to stain for DNA content and 1.5 µg RNaseA to remove contaminating RNA. After incubating for 30 mins at RT or 4 ˚C overnight, cells were taken for analysis by flow cytometry.

2.8 DNA Fibre spreading

2.8.1 DNA fibre labelling

10 e6 cells plated in 10 ml media in a 10 cm petri dish per sample. 25 µM IdU added to cells for 20 mins. At 20 mins, 25 µM CldU was added and plates immediately irradiated with UV (or sham irradiation). After a total of 40 mins, cell were stopped from further incorporation by addition of a large excess of ice cold PBS and cell spun at 4 ˚C at 500 g for 5 mins. Cells were resuspended in ice cold PBS to 1 e6 cells/ml. 3 µl of the resuspended cells were pipetted onto the top centre of a microscope slide. After waiting 5 mins for the drop to dry slightly, 7 µl spreading buffer (0.5 % SDS, 200 mM Tris/HCl, pH 6.5, 50 mM EDTA) was added from a ~ 2 cm height. After the drop had dried a little, slides were tilted to ~ 45 ˚ and the cells allowed to spread down the slides. Slides were fixed in 3:1 methanol:acetic acid.

2.8.2 Staining DNA fibres

DNA was denatured on the slides in 2.5 M Ultrapure HCl for 1 hr then dehydrated in 70 %, 90 % then 100 % EtOH. Slides were washed 3 times in cold PBS, then after drying blocked with 30 µl BlockAid (Invitrogen) under a coverslip in a humid box for 30 min at RT. All coverslips cleaned in chloroform.

All antibody solutions made up in Blockaid, incubated in a humid box at RT under coverslip cleaned with chloroform and washed 3 times for 3 mins in PBS-0.1 % Tween.

IdU/CldU detection:

1:5 anti-IdU (mouse), clone B44IgG1; 1:25 anti-CldU (rat), clone BU1/75, 45 min incubation.

1:25 anti-mouse (rabbit) 594; 1:50 anti-rat (chicken) 488, 30 min incubation.

1:25 anti-rabbit (donkey) 594; 1:50 anti-chicken (goat) 488, 30 min incubation.

DNA counterstaining:

1:25 anti –ssDNA (mouse) DSHB, 45 min incubation.

1:25 anti-mouse (rabbit) 350, 30 min incubation.

1:25 anti-rabbit (donkey) 350, 30 min incubation.

Slides were dehydrated in 70 %, 90 % then 100 % EtOH then mounted in 10 % PBS, 90 % glycerol.

2.9 GFP trap

100 e6 cells of each condition/line were spun down and washed twice in ice cold PBS. The cell pellet was lysed in 2 ml lysis buffer (50 mM Tris/HCl, pH 7.4, 150 mM NaCl, 1 % IGEPAL, 0.5 % Sodium deoxycholate, 0.1 % SDS, 2.5 mM $MgCl_2$, 75 U Benzonase, 1X cOmplete protease inhibitors, 0.7 µg/ml Pepstatin A) rotating at 4 ˚C for 30 mins. Lysate was spun at 3220 g for 30 mins at 4 C, supernatant was removed and spun again to remove any remaining precipitate. 25 µl of GFPTrap beads per sample were washed in 500 µl ice cold Wash buffer (10 mM Tris/HCl pH7.4, 150 mM NaCl, 0.5 mM EDTA, 1X cOmplete protease inhibitors) 3 times, spinning at 2.5 g for 2 mins at 4 C. The lysate was added to the beads and bound by rotating for 1 hr at 4 °C. The beads were spun down and unbound lysate removed. The beads were washed twice in Wash buffer as above then once in High Salt wash buffer (10 mM Tris/HCl pH 7.4, 0.5 M NaCl, 0.5 mM EDTA, 1x cOmplete protease inhibitors). The beads were resuspended in 50 µl 2x Laemmli Buffer and boiled for 10 mins at 95 °C. Beads were spun down and 20 µl of the supernatant was run on a 4-12 % BisTris gel in MOPS until the dye front had moved approx. 2 cm. The gel was stained in 20 ml Instant Blue for 15 mins and then washed in water. Each lane was cut into 16 fragments with sterile scalpels and each fragment put into a well of a submission plate with 25 µl water. Submitted to LMB Mass Spec facility with Farida Begum.

2.10 CRISPR Screen

2.10.1 Transfecting cells with virus (spinfection)

2.7 e6 cells/ml were plated in a 6 well plate (max 2.5 ml/well) with 4 µg/ml Polybrene (Sigma-Aldrich). Clingfilm wrapped plates were spun in a prewarmed to 37 ˚C centrifuge at 680 g for 90 mins then left to recover for 1 hr before resuspending in a larger volume of media.

2.10.2 Producing lentivirus library

HEK293 FT cells were cultured to 90% confluency in a 6 well plate in 2.5 ml media. They were then transfected with lentivirus component plasmids:

250 µl Opti-MEM Reduced Serum Media (Thermo Fisher), 1.2 µg pSPAX.2, 0.25 µg pMD2.G, 0.5 µg Yusa Library [Equimolar mix of 5 guides in: pKLV2 U6-gB2M(1-5)-puro BFP] or empty vector was added to 6 µl TransIT Lenti Transfection reagent (Mirus) vortexed and incubated for 30 min at RT. This transfection mixture applied directly to cells and media replaced. Media replaced daily and media from Days 3 and 4 (viral supernatant) snap frozen and kept at -80 ˚C.

2.10.3 Virus titration

1.2 e6 WT TK6+ cells were plated in triplicate and varying volumes of viral supernatant between 10 and 125 µl were transfected, resuspended in 5 ml media and cultured. On the third day, BFP expression was analysed by flow cytometry. To calculate the volume of virus required for an MOI of 0.3, the results were plotted on GraphPad Prism and analysed with an Asymmetric Sigmoidal Interpolation.

2.10.4 Testing cutting efficiency of Cas9 expressing cells

Library against B2M (part of MHC class 1) from Yusa library (Tzelepis *et al.*, 2016).

Cells were transfected with virus at an MOI of 0.3, cultured for 3 days before antibiotic selection added for 4 days. Cells were then stained with a conjugated antibody (anti HLA-ABC-APC, Invitrogen W6.32) for 1 hour and analysed by flow cytometry.

2.10.5 CRISPR screen

Cells were spinfected with the lentiviral library as above, then transferred to a roller bottle in RPMI with CO_2 pumped in. Cell were split every day, keeping the confluency below 1 e6 cells/ml and enough cells to maintain the required coverage. On days 3-7 puromycin selection was removed, after which the number of cells required to maintain coverage could be reduced.

2.10.6 Sample collection

200 million cells (enough for 2 library preparations) were spun down, washed twice in PBS to remove any lentivirus and vortex in a small amount of PBS to resuspend. DNA was extracted using a modified version of the Gentra Puregene DNA extraction protocol. Briefly: 14 ml cell lysis buffer added to each 100 million cells and vortexed. 300 µg RNaseA (Qiagen) added to each 100 million cells, mixed by inversion, incubated at 37 ˚C for 5 mins then cooled on ice for 30 mins. 5 ml protein precipitation solution added to each 100 million cells, vortexed then centrifuged at full speed for 5 minutes. Supernatant was removed, incubated on ice for 5 mins then centrifuged again. Supernatant added to 3 ml of isopropanol per 20 million cells and mixed by inversion. Samples were centrifuged at full speed for 15 mins. The DNA pellets were washed twice in 70 % EtOH then dried. Pellets were dissolved in EB buffer (Qiagen), 1ml per 100 million cells.

2.10.7 Library preparation

106 reactions with 5 µg gDNA per sample was required to achieve 1000X coverage. PCR mix was made up as below, 50 µl per reaction in strip tubes.

Component	Final concentration	Volume in 50 µl reaction
5X Q5 HS Master Mix (NEB)	1X	25
100 µM gRNA-HiSeq-SE50 F1	0.5 µM	0.25
100 µM gRNA-HiSeq-SE50 R1	0.5 µM	0.25
Template DNA	5 µg	Variable
Millipore Water		To 50 µl

Step		Temperature/°C	Time/s
Denaturation		98	30
Denaturation	18-22 cycles	98	10
Annealing		61	20
Elongation		72	60
Extension		72	180
Hold		10	indefinitely

PCR 1 product was concentrated using a PCR purification kit (Qiagen) and eluted in 50 µl Buffer EB per 12 reactions. Samples were incubated at 65 ˚C for 10 mins to remove ethanol.

PCR 1 products were run on a 2 % agarose gel stained with SYBR Safe. Bands were cut out and extracted using a Gel extraction kit (Qiagen). Elution in 100 µl Buffer EB.

PCR 2 added indexing primers, PCR mix made up as below. Each sample uses a different indexing primer, 8 reactions per sample

Component	Final concentration	Volume in 50 µl reaction
5X Kappa HiFi HS Master Mix (Roche)	1X	25
100 µM P5 primer	0.5 µM	0.15
100 µM P7 index primer	0.5 µM	0.15
PCR 1 product	10 ng	Variable
Millipore Water		To 50 µl

Step		Temperature/°C	Time/s
Denaturation		95	30
Denaturation	6 cycles	98	10
Annealing		60	20
Elongation		72	60
Extension		72	180
Hold		10	indefinitely

PCR 2 products concentrated using a PCR purification kit (Qiagen) eluting in 50 µl Buffer EB per 12 reactions. Samples were Incubated at 65 ˚C for 10 mins to remove ethanol. PCR 2 products were run on an 8% TBE polyacrylamide gel (ThermoFisher) at 175 V for 60 mins in TBE buffer (Novex). The gel was stained in SYBR Safe for 10 mins, then cut out bands into 2 fragments per sample.

The library was extracted from the gel using gel breaker tubes: 0.5 ml tubes with 4 holes punched into the base by a 26 G needle placed into a 1.5 ml Eppendorf tube. Gel fragments were placed in these tubes and centrifuged for 5 mins at 15000 g to shred the gel. Shredded gel was then incubated in 400 µl 0.3 M NaCl rotating for 2 hrs at RT. The mixture was resuspended and added to a Costar Spin-X filter column (Corning) and Spun at 10000 g for 2 minutes to remove gel fragments. Flowthrough was added to a LoBind DNA 1.5 ml eppendorf tube (Eppendorf). 20 µg glycogen was added, followed by 1.1 ml 100 % EtOH at -20 C. The library was precipitated overnight at -20 C. The mixture was centrifuged for 2 hrs at 4 C, 16000 g. Supernatant was removed and the DNA pellet washed twice in 70 % EtOH before air drying for 5 mins. DNA pellet was dissolved in 20 µl 10 mM Tris HCl, pH8.0. Libraries were quantified using a Qubit Fluorimiter.

Chapter 3: The response of H3.3 to UV damage

3.1 TK6 cells as a model

Whilst much of the previous work in the lab, including that on H3.3, has been carried out using DT40 chicken cells, moving to human cells offers several advantages. Antibodies tend to be raised against human antigens, so using human cells means a larger range of suitable reagents are available. The DT40 genome differs to the reference chicken genome and the annotation is still patchy, whereas the human genome is well annotated, allowing easier design of primers, gRNAs and analysis of mass spectrometry and sequencing data. Additionally, as H3.3 has been implicated in human disease, specifically a range of paediatric cancers, a human cell model has advantages in the long term if physiologically or pathologically relevant conclusions are to be drawn.

I chose to work in TK6+ cells. These are a derivative of the WIL-2 cell line (Levy, Virolainen and Defendi, 1968), a B-lymphocyte cell isolated from the spleen of a male patient with hereditary spherocytic anaemia. TK6+ were isolated from the HH4 line (in turn, derived from WIL-2) in 1978. It is heterozygous for the thymidine kinase locus which allows for selection of complete loss of thymidine kinase in consequence of a mutation on the second allele (Skopek *et al.*, 1978). The line has thus been used extensively for mutagenesis and toxicology studies (Gollapudi, White and Honma, 2019). The variant I used expressed TK allowing the *in vivo* phosphorylation of the halogenated nucleosides I used in some of my assays.

TK6+ are thus not a cancer-derived line, have a close to normal karyotype (Honma, 2005) and a functional p53 pathway. This makes them suitable for studying DNA damage repair in a more physiologically relevant context, as relevant pathways and checkpoints are intact. In addition, TK6 are genetically manipulatable by CRISPR-Cas9 and their growth characteristics fit into our existing pipelines designed for DT40 cells.

3.2 Generation of an H3.3-deficient human cell line

H3.3 protein is expressed from 2 genes: H3F3A and H3F3B. Each have a separate sequence but produce identical protein. In order to knockout all H3.3 protein production using CRISPR/Cas9-mediated gene targeting, guide RNAs (gRNAs) were designed against early exons of each gene (Figure 3.1a). These gRNA sequences were ligated into the pX458 plasmid (Ran *et al.*, 2013) (see Appendix 1) which contains the gRNA scaffold, Cas9 and GFP (Figure 3.1b). TK6 cells were transfected with 2 plasmids at a time, each with a guide against one of the two H3.3 genes. Cells which had successfully taken up the plasmid were identified by GFP expression, sorted for and plated at one cell per well to allow clonal analysis of the induced genetic changes.

I screened for mutations in each gene by fragment analysis of a fluorescently labelled PCR product spanning the gRNA target site. This shows changes in PCR product size at nucleotide resolution, with these size changes corresponding to insertion or deletion mutations.

In this first round of targeting, I used 3 combinations of H3F3A and H3F3B guides and analysed a total of 154 clones. 29 clones contained a mutation in one allele of either H3F3A or H3F3B, 7 clones had mutations in both alleles of either H3F3A or H3F3B and 2 clones had mutations in both alleles of H3F3A and one allele of H3F3B. No clones had all 4 alleles (2 from each gene) successfully targeted. (Figure 3.1c). The line 2A06 (with 2 alleles of H3F3A and 1 allele of H3F3B mutated) was taken forward for further rounds of targeting. As many clones were screened but none had all 4 alleles mutated, another round of targeting was required to completely knockout H3.3. Taking only one clone forward to the next knockout round does mean that there is the risk that any off-target effects present from the first round of targeting will be present in subsequent clones. Ideally, complementation would be the way to ensure any phenotype observed is due to a lack of H3.3

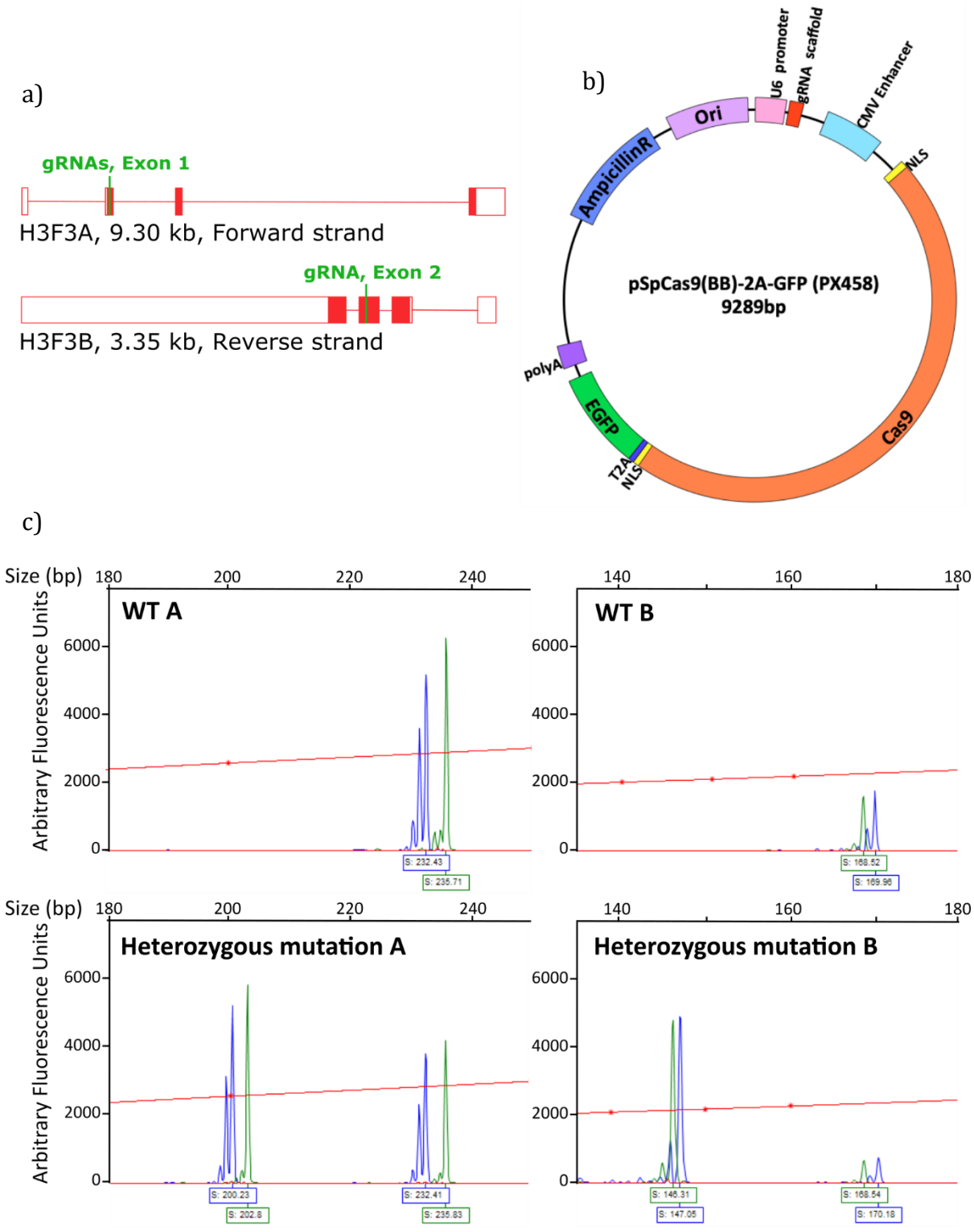

Figure 3.1 CRISPR-Cas9 targeting of H3F3A and H3F3B. a) Positions of gRNAs against both genes encoding H3.3. b) Structure of the pX458 plasmid. c) Representative fragment analysis images showing sizes of PCR products from both H3F3A and H3F3B. WT A and WT B show the PCR product size of H3F3A and H3F3B respectively from untargeted cell lines. Heterozygous A and B show the PCR product size of H3F3A and H3F3B respectively from targeted cell lines, where there is a size change in only one allele. Size ladder is shown in red.

Western blotting of this line showed these mutations reduce the levels of H3.3 compared to WT, but do not completely abrogate expression of the protein (Figure 3.2b). Therefore, as expected, both alleles of H3F3B must be mutated to completely stop H3.3 protein production.

In order to completely remove H3.3, this line underwent a second round of targeting with a single gRNA plasmid against the remaining untargeted H3F3A allele. Of a total of 89 clones screened by fragment analysis, 5 contained mutations in the final H3F3A allele, and therefore contained mutations in both alleles of both H3.3 genes. Sanger sequencing of a TOPO-cloned PCR product confirmed the mutations indicated by the fragment analysis. There was no retargeting of previously mutated alleles, as the gRNA site had been altered by the first round of targeting. Western blotting demonstrated these mutations cause complete loss of the protein (Figure 3.2b). The H3.3 KO clones used in further experiments contain identical mutations in their H3F3A gene and 1 allele of H3F3B from the first round of targeting, with mutations differing in the final H3F3B allele. (Figure 3.2a). As these clones were all generated using the same gRNAs, any guide-dependent off-target effects are likely to be the same between cell lines and since they also carry closely equivalent disruptions to the H3.3 loci, they have been used interchangeably in this chapter.

3.2.1 Basic characterisation of *h3.3* cell lines

Loss of H3.3 causes a modest reduction in doubling time compared to WT TK6 cells (Figure 3.2c), but it appears so slight that I will not alter assay timepoints for each cell line.

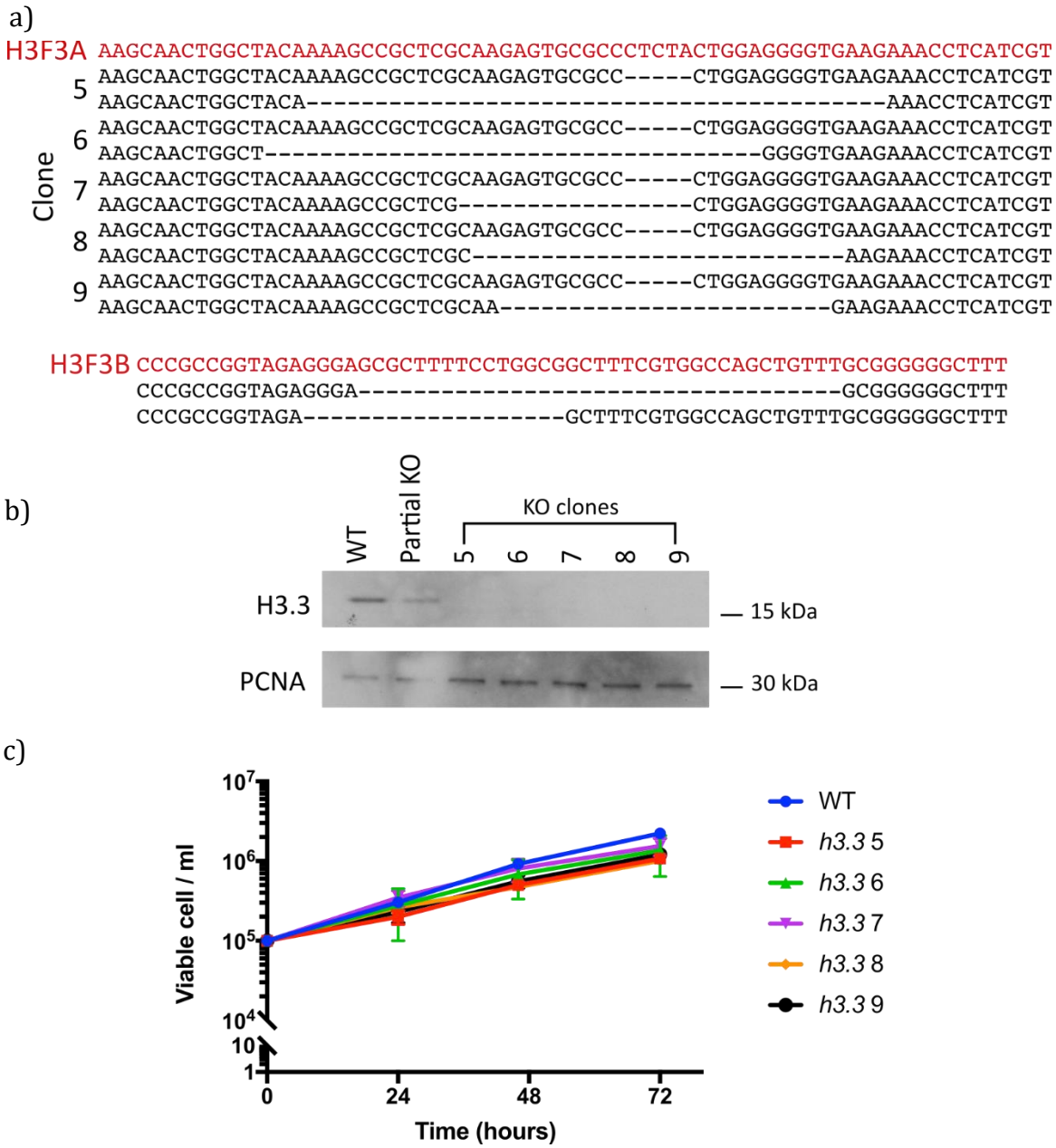

Figure 3.2 Characterisation of *h3.3* cells a) Sequence of targeted region of *h3.3* cell lines. All cell lines have the same mutations in H3F3B. b) Western blot against H3.3 in TK6+ WT, a cell line from round 1 of targeting (with 3 alleles mutated) and the *h3.3* cell lines (with mutations in all 4 alleles). c) Growth curve of WT and *h3.3* cell line. Error bars show standard deviation of 3 technical replicates

3.3 Characterisation of response of H3.3-deficient human cells to DNA damaging agents

3.3.1 H3.3-deficient TK6 do not exhibit hypersensitivity to acute genotoxin treatment

In order to determine the ability of *h3.3* cells to survive long term after DNA damage, I performed a colony survival assay with a variety of genotoxins. Varying doses of small molecules or UV irradiation were applied to the cells 1 hour before dilution and plating in methylcellulose media. This viscous medium allows assessment of a cell's ability to survive and divide to form a colony after acute genotoxin treatment. The dose range was chosen so that approximately 99 % of WT cells were killed at the highest dose. The genotoxins used were UVC irradiation, MMS and cisplatin (Figure 3.3). These genotoxins produce a variety of types of DNA damage engaging a range of pathways, allowing me to assess which damage response pathways H3.3 may be involved in (see section 1.3).

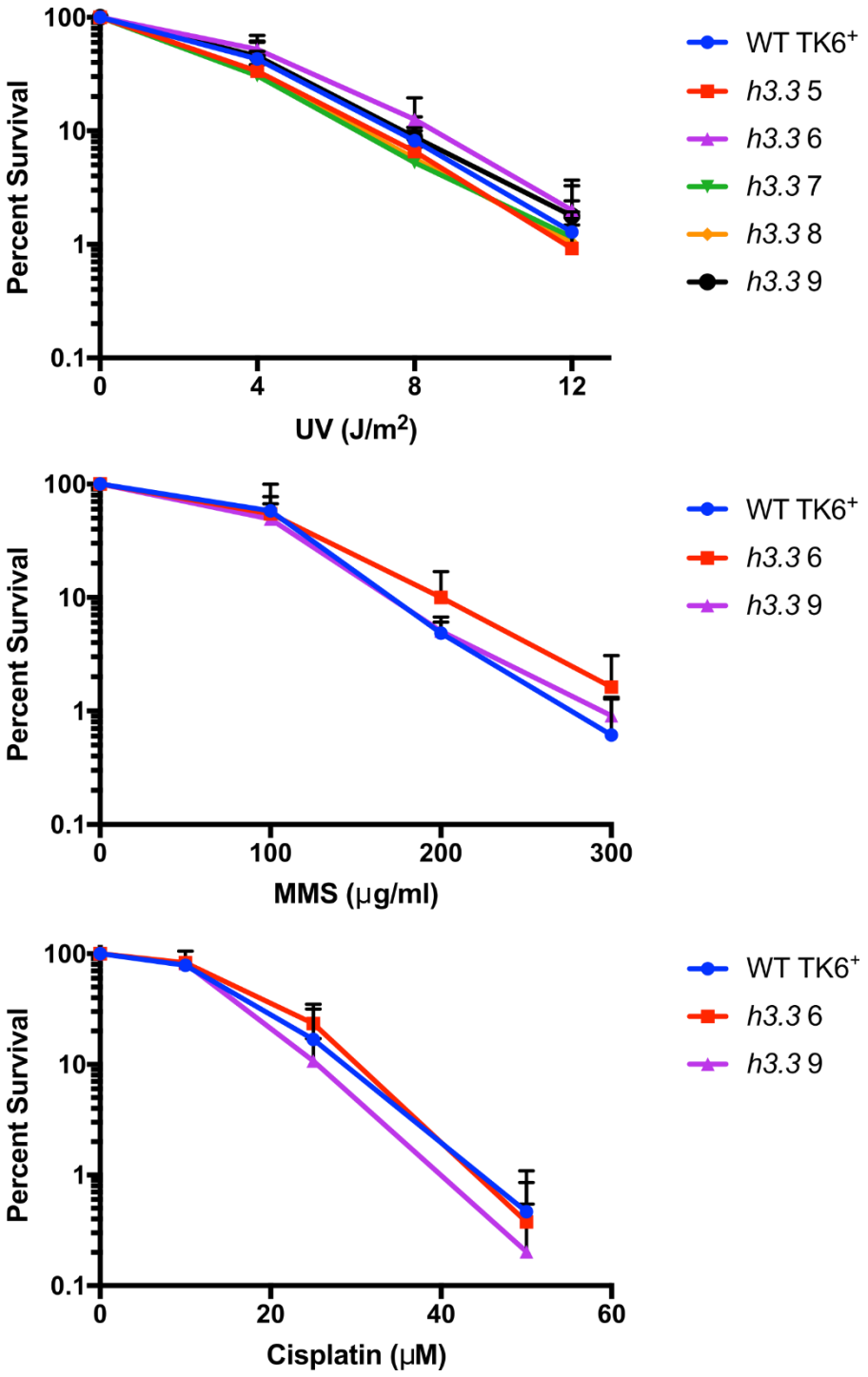

Figure 3.3 *h3.3* cells do not show hypersensitivity to UV, MMS and cisplatin. Percentage survival was calculated relative to untreated cells. 2 technical repeats per experiment, mean of 3 experiments shown. Error bars show standard deviation

In each case, *h3.3* cells did not exhibit any increased sensitivity compared to WT cells. This was unexpected, as the *h3.3* DT40 cell line showed a distinct hypersensitivity to all 3 of the genotoxins tested here. A notable difference between DT40 and TK6 cells is the presence of a functioning p53 in TK6 cells (Takao *et al.*, 1999).

Several pathways that respond to DNA damage feed into p53, where it prevents progression through the cell cycle whilst unresolved DNA damage is present. Therefore, without p53, any unresolved damage is transmitted through to the next cell cycle unrepaired, causing problems during replication which could lead to cell death. This could be one reason why DT40 are more sensitive to genotoxin treatment, but TK6 cells do survive.

3.3.2 DNA damage markers persist for longer time periods in *h3.3* cells

Lack of H3.3 in DT40 cells leads to a block in S phase after UV irradiation. This could be because, due to the lack of p53, any unresolved DNA damage is being transmitted through the G1/S checkpoint to the next S phase leading to S phase arrest. To see if TK6 cells lacking H3.3 have any change in the cell cycle response to DNA damage, I examined markers of DNA damage at timepoints after UV.

The histone variant H2AX and the damage repair protein p53 are both phosphorylated in response to damage (forming γH2AX and phospho-p53 respectively), meaning they are markers for the presence of DNA damage in a cell. A difference in the appearance and resolution of these phosphorylation events after damage between WT and *h3.3* could indicate whether there is a change in the kinetics of damage resolution as a result of a lack of H3.3.

h3.3 and WT cells were treated with a low dose of 4 J/m^2 UV irradiation. In previous work in DT40, cells were treated with 3 J/m^2. As TK6 cells appear to be slightly less sensitive to UV than DT40 (comparing colony survival assays), I chose a slightly higher dose of 4 J/m^2. I collected untreated cells at a 0 hour timepoint and treated cells at 4, 8 and 24 hour timepoints. Protein was extracted for western blotting with a γH2AX and phospho-p53 antibody (Figure 3.4).

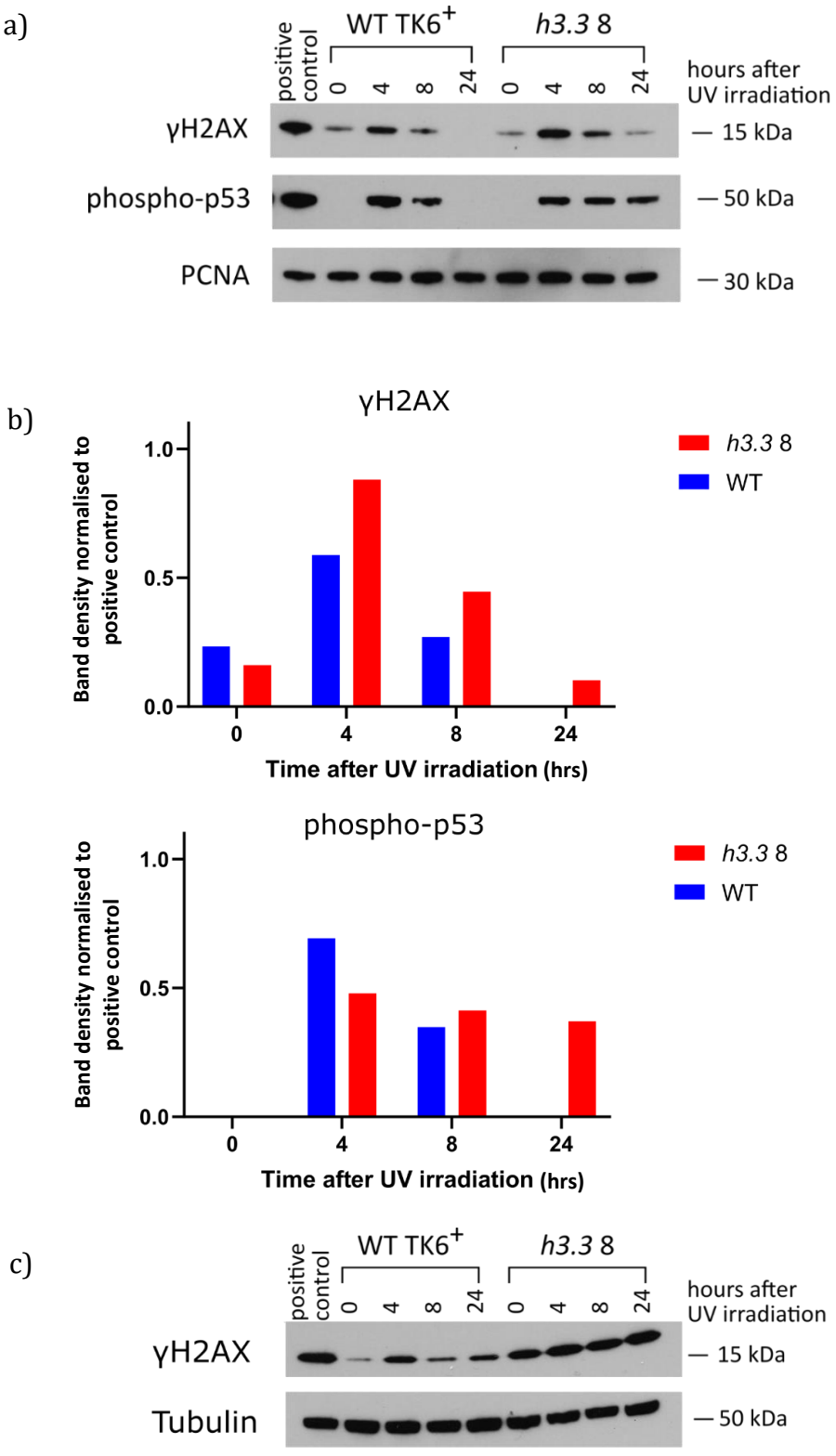

Figure 3.4 Markers of DNA damage remain elevated in *h3.3* cells a) Western blot against γH2AX and phospho-p53 in WT and *h3.3* cell lines at timepoints after irradiation with 4 J/m^2 UV. PCNA shown as a loading control. b) Quantification of a), normalised to the positive control (4hrs after 40 J/m^2 UV irradiation). c) Repeat western blot against γH2AX in WT and *h3.3* cell lines at timepoints after irradiation with 4 J/m^2 UV. Tubulin shown as a loading control

In both WT and *h3.3*, these markers are raised at 4 hrs and 8 hrs and in the WT cell line, they are no longer present at 24 hrs suggesting that the damage has been resolved. However, in the *h3.3* cell line the markers are still present at 24 hrs after UV irradiation. On repeating this experiment, γH2AX levels in *h3.3* cells remain raised above WT cells. Whilst only one *h3.3* clone was tested, cell lines generated in section 3.2 all carry disruptions of H3.3 resulting in no detectable protein expression and were generated with the same gRNAs. I would not therefore expect significant variability between lines.

This persistence of DNA damage markers in the absence of H3.3 could indicate that there is a delay in resolving DNA damage, and therefore H3.3 is required for the timely resolution of DNA damage. Alternatively, the absence of H3.3 could lead to an inability of the cells to lower these damage markers after damage resolution.

This persistence of DNA damage signalling may cause a change in the cell cycle response.

3.3.3 Phosphorylation of checkpoint activators after UV irradiation in WT and *h3.3* cells

In *h3.3* DT40 cells, UV treatment caused a block in the S phase of the cell cycle after 24 hours. To see if the persistence of DNA damage markers after UV irradiation in *h3.*3 TK6 cells is likewise coupled to an activation of S phase checkpoints, leading to an S phase arrest, I looked at the phosphorylation of checkpoint activators.

CHK1 and CHK2 are components of ATM and ATR pathways (Figure 1.7). They can be phosphorylated in response to DNA damage and signal to activate cell cycle checkpoints leading to a halt in the cell cycle during S phase.

As previously, WT and *h3.3* cells were treated with 4 J/m^2 UV and protein collected for western blotting at timepoints afterwards (Figure 3.5).

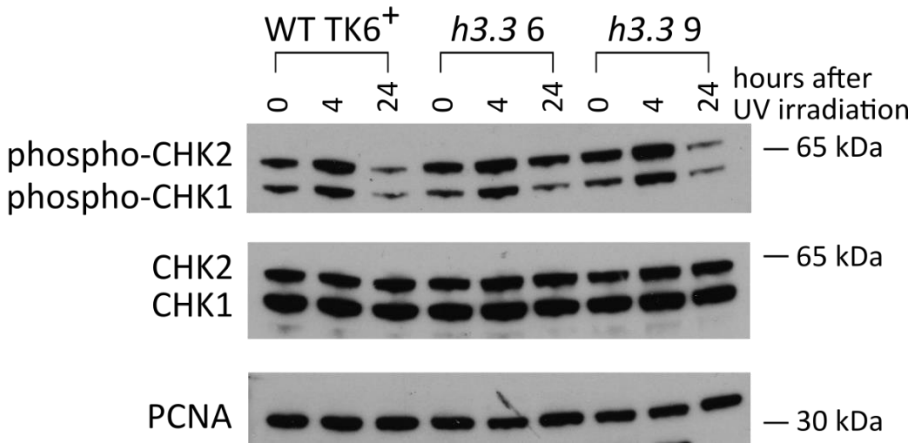

Figure 3.5 Phosphorylation of Checkpoint proteins at timepoints after UV irradiation. Western blot against phospho-CHK1 and phospho- in WT and *h3.3* cell lines at timepoints after irradiation with 4 J/m^2 UV. Unphosphorylated CHK1 and CHK2 shown as a control and PCNA shown as a loading control.

In both WT and *h3.3* cells, levels of both phospho-CHK1 and phospho-CHK2 are raised at 4 hrs after UV irradiation and reduced at 24 hrs. There is little difference between WT and *h3.3* cells.

CHK1 (part of the ATR pathway) should be phosphorylated, and thus activated, in response to UV damage and CHK2 (part of the ATM pathway) should be activated also, as raised levels of γH2AX, a DSB marker, were observed. Both CHK1 and CHK2 are phosphorylated at 4 hours, showing they are part of the normal response to UV induced DNA damage in both WT and H3.3 cells. However, their phosphorylation is not raised at the 24 hour timepoint in *h3.3* cells, the timepoint at which phospho-p53 and γH2AX remain elevated. Either, CHK1 and CHK2 signalling has been switched off whilst their downstream effectors remain active or the persistent damage is activating a different signalling pathway. Potentially, p53 could be detecting persistent damage directly (section 1.3.3.3.1) explaining the raised p53 at 24 hours in *h3.3* cells, without phosphorylation of upstream effectors of ATM and ATR pathways.

I next asked whether the persistently raised DNA damage markers in *h3.3* cells was reflected in a change in the cell cycle profile after UV exposure.

3.3.4 Changes in cell cycle progression after UV irradiation

Changes in DNA damage resolution or persistence of DNA damage signalling in *h3.3* cells should impact how the cells progress through the cell cycle. Changes in how cells progress through the cell cycle could inform how cells are responding to and dealing with DNA damage, so I therefore analysed the cell cycle of WT and *h3.*3 cells in the presence and absence of UV induced DNA damage.

To examine the cell cycle response to UV irradiation in WT and *h3.3* cells, I performed 2D cell cycle analysis. In this assay the nucleotide analogue EdU is added to cells to show which are actively incorporating nucleotides, so replicating their DNA. A fluorophore can then be conjugated to the incorporated EdU via a Click-iT reaction. DAPI staining is also carried out to determine the DNA content of the cells. In combination, this staining can show which stage of the cell cycle each cell is in.

Cells were irradiated with 4 J/m^2 UV and collected at 4, 8 and 24 hours after this treatment, or without any UV irradiation. Live and single cells were gated and divided into different phases of the cell cycle (Figure 3.6a). The proportion of cells in each phase of the cell cycle was calculated and compared (Figure 3.6b and c).

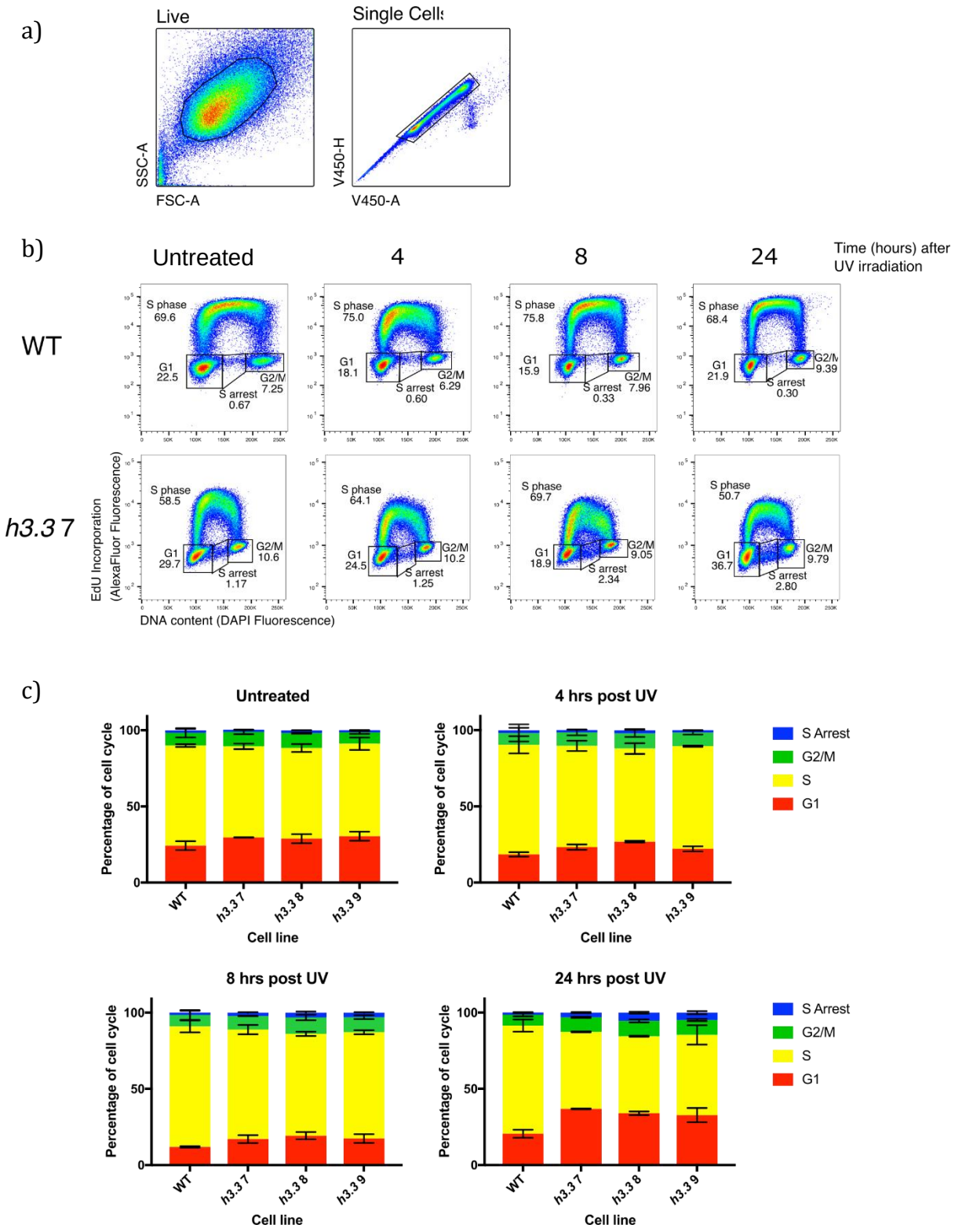

Figure 3.6 Cell cycle changes in WT and *h3.3* cells after UV irradiation. a) Gating strategy for live and single cells used in all cell cycle analysis. b) Representative cell cycle dotplots of WT and *h3.3* cells at timepoints after 4 J/m^2 UV irradiation, displaying gating strategy for cell cycle phases. c) Cell cycle proportions without UV and at timepoints after 4 J/m^2 UV. Error bars show standard deviation of the mean. Data from 2 biological replicates shown

In WT TK6 cells, there are changes in cell cycle proportions at intermediate timepoints after UV irradiation. Particularly, the proportion of cells in S phase slightly increased at 4 and 8 hours but the proportions return to be similar to untreated again by 24 hours.

h3.3 cells also change cell cycle proportions after UV. The distribution of cells within S phase is noticeably different at intermediate timepoints and they still have an altered cell cycle compared to untreated at 24 hours. There is a pronounced G1 block at 24 hours, with the G2/M and S arrest populations also increasing.

This difference in cell cycle proportions at 24 hrs between WT and *h3.3* cells indicates that after UV damage, the G1 checkpoint prevents *h3.3* cells from entering S phase for longer than in WT cells. This fits with the previously observed persistently raised phospho-p53 in *h3.3* cells, as p53 can activate the G1/S checkpoint (Figure 1.7). Taken together, this could suggest that in the absence of H3.3, UV induced DNA damage is not repaired in a timely manner and p53 remains active. p53 can then activate the G1/S checkpoint in cells with unresolved damage in order to prevent re-entry into S phase. Cells with unresolved damage which escape this G1 arrest could pass into S phase, where the damage could cause a problem to replication and explain the increased proportion of cells in the S arrest gate. Cells in this S arrest population are likely to be cells which started replication, but failed to continue and complete replication and so have an intermediate DNA content and are not incorporating nucleotides.

I initially found this assay produced inconsistent results. My main issue was that the WT untreated cells sometimes had an unusually large G1 population of around 40 % in untreated cells, higher than the UV treated *h3.3* cells. Leaving cells to grow overconfluent, instead of adding more media at 8 hours after UV, did not resolve this large G1 population. Irradiating the cells in PBS (as opposed to media) also did not make any difference. However, changing the media recipe for culturing TK6 cells from 5 % FBS to 10 % FBS increased viability counts during regular culturing, and also lead to consistent, more expected G1 populations in WT untreated cells. This indicates that the culturing conditions for TK6 cells of 5 % FBS may not be optimal for their unperturbed growth. Serum starvation can lead to G1 arrest in many cell types (Chen *et al.*, 2012). Additionally, small differences in viability of the cells can lead to changes in cell cycle, disrupting the

results of 2D cell cycle analysis and demonstrating how sensitive the G1 checkpoint can be. Moving forward, only experiments with an untreated G1 population of under 35 % were included in analysis.

3.3.5 Cells respond to UV in a dose dependent manner

To ensure that the phenotype seen is directly as a result of UV and not just down to a growth difference in the cell lines, I looked at the impact on cell cycle changes of increasing doses of UV (Figure 3.7).

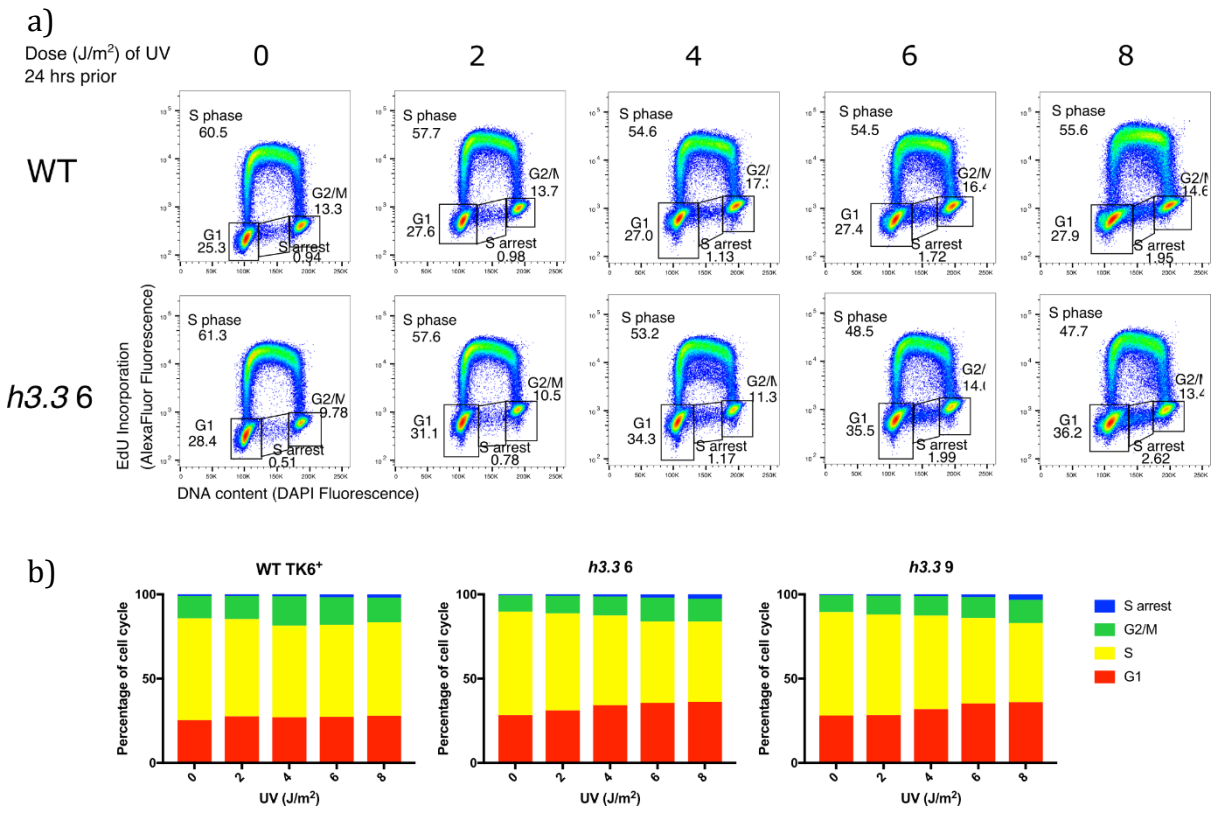

Figure 3.7 Changes in cell cycle 24 hours after irradiation with increasing doses of UV irradiation a) Representative cell cycle dotplots of WT and *h3.3* at 24 hours after varying doses of UV irradiation, displaying gating strategy for cell cycle phases. b) Cell cycle proportions of WT and *h3.3* cell lines 24 hours after varying doses of UV irradiation.

In WT TK6+ cells, there is little difference between irradiated and untreated cells. However, in *h3.3* cells, as the UV dose increases, the proportion of cells in G1 increases.

As the increasing UV dose has little impact on the cell cycle of WT cells and the G1 block in *h3.*3 cells is more pronounced as UV dose increases, it indicates that the G1 block phenotype is linked to UV irradiation.

3.4 Complementation of *h3.3* cells with a GFP-tagged H3.3

In order to ensure that any phenotype seen in the *h3.3* cells is due to loss of H3.3 and not off-target effects caused by CRISPR-Cas9 targeting, a GFP-tagged H3.3 was reintroduced to the cells to complement the deletion. Previous work in DT40 cells showed that GFP-tagged H3.3 is capable of rescuing *h3.3* phenotypes, indicating that the GFP does not interfere with integration into chromatin (Frey *et al.*, 2014).

2 of the *h3.3* clones were transfected with a plasmid containing H3.3 tagged at the C-terminal with GFP and a neomycin resistance gene. These transfected cells were plated in G418 (neomycin) and single colonies picked. These populations were screened for GFP expression by flow cytometry (Figure 3.8).

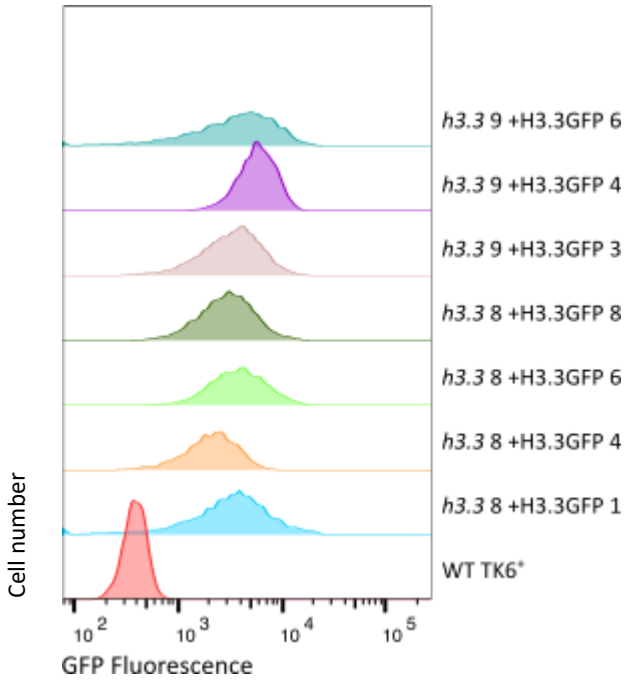

Figure 3.8 *h3.3* cells complemented with H3.3 GFP. Flow cytometry plot showing fluorescence of *h3.3* cell lines transfected with H3.3 GFP compared to an untransfected WT cell line

There are varying levels of GFP expression between the different populations, possibly due to the plasmid integrating into the genome a different number of times or at different sites. Populations with similar GFP expression levels were selected for further study.

3.4.1 Cell cycle analysis of *h3.3* cells complemented with a GFP-tagged H3.3

Cell cycle analysis was carried out as previously, with 4 J/m^2 UV irradiation applied to cells which were then collected at 4, 8 and 24 hour timepoints or without treatment (Figure 3.9).

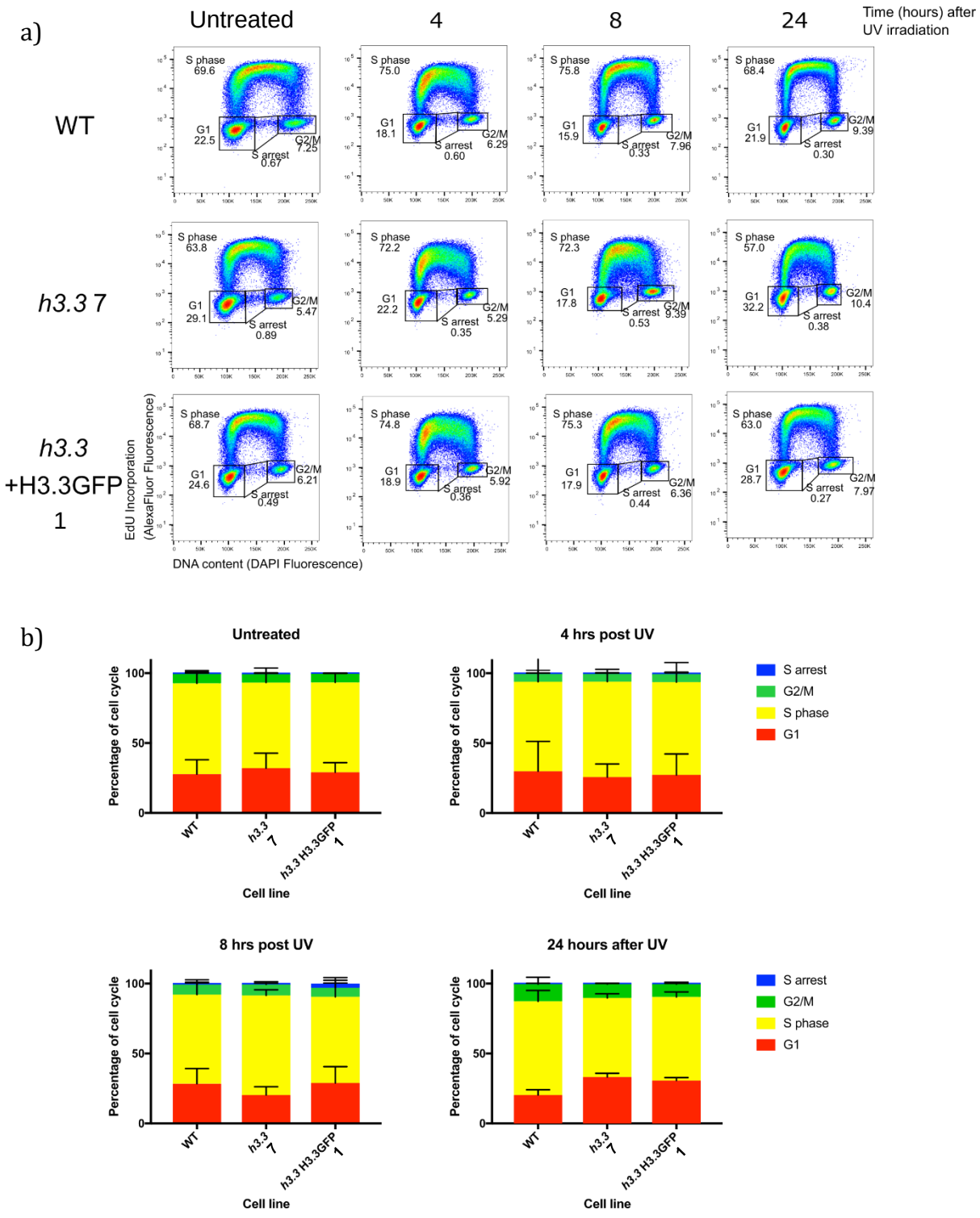

Figure 3.9 Cell cycle changes in WT, *h3.3* and *h3.3*+H3.3GFP cells after UV irradiation a) Representative cell cycle dotplots of WT, *h3.3* and *h3.3*+H3.3GFP cells at timepoints after 4 J/m^2 UV irradiation, displaying gating strategy for cell cycle phases. b) Cell cycle proportions without UV and at timepoints after 4 J/m^2 UV. Error bars show standard deviation of the mean. Data from 2 biological replicates shown

The proportion of cells in G1 at 24 hours after UV irradiation in the complemented *h3.3*+H3.3GFP line is greater than in the untreated condition. This is more similar to the results seen in *h3.3* lines than WT TK6. However, on close examination of the dotplots, the S phase population at 24 hours after UV irradiation is clustered above G1 in *h3.3* cells, but further across towards G2/M in WT and *h3.3*+H3.3GFP cells. This could indicate that the change in cell cycle proportions seen in *h3.3* cells is either due to an off-target effect of the CRISPR gene editing consistent across multiple clones, or because H3.3GFP is not able to be sufficiently incorporated into chromatin and so cannot entirely compensate for the lack of endogenous H3.3.

Tagging H3.3 with GFP could interrupt its function. The GFP could interfere with chaperone binding or incorporation into the nucleosome. In DT40 cells, H3.3GFP was shown to be able to compensate for the absence of endogenous H3.3, suggesting that the GFP fusion can function. Therefore, potentially the introduced H3.3GFP is expressed at low levels in TK6 cells. As the shape of the cell cycle dotplots in the compensated line is more similar to WT than to *h3.3*, particularly in S phase, I expect that the H3.3GFP is not being incorporated into chromatin in high enough levels to fully compensate for the loss of endogenous H3.3.

3.5 H3.3 has no impact on replication fork progression after UV

The increased S arrest population seen in *h3.3* cells could indicate a problem with replication progression after UV in the absence of H3.3. To determine if there is a change in progression of the replication fork after UV irradiation, I examined stretched DNA fibres. Making use of two nucleotide analogues, new DNA synthesis can be visualised after staining these fibres and difference in incorporation before and after UV can be measured (Figure 3.10a).

This DNA fibre assay was carried out in DT40 (Frey *et al.*, 2014) and *h3.3* cells were unexpectedly found to have a fork progression defect after UV, leading to the model being put forward that as a replication for encounters DNA damage, H3.3 could be incorporated and aid repair.

Nucleotide analogues were added to cells before (IdU) and after (CldU) an acute high dose (40 J/m^2) of UV irradiation. Cells were lysed and the DNA fibres spread on a microscope slide. The nucleotide analogues incorporated into the spread DNA fibres are stained differentially, allowing visualisation of tracts of incorporation before and after UV. These incorporation lengths before and after UV are measured, and the ratio between the two can show any change in the rate of nucleotide incorporation after UV (Figure 3.10b and c).

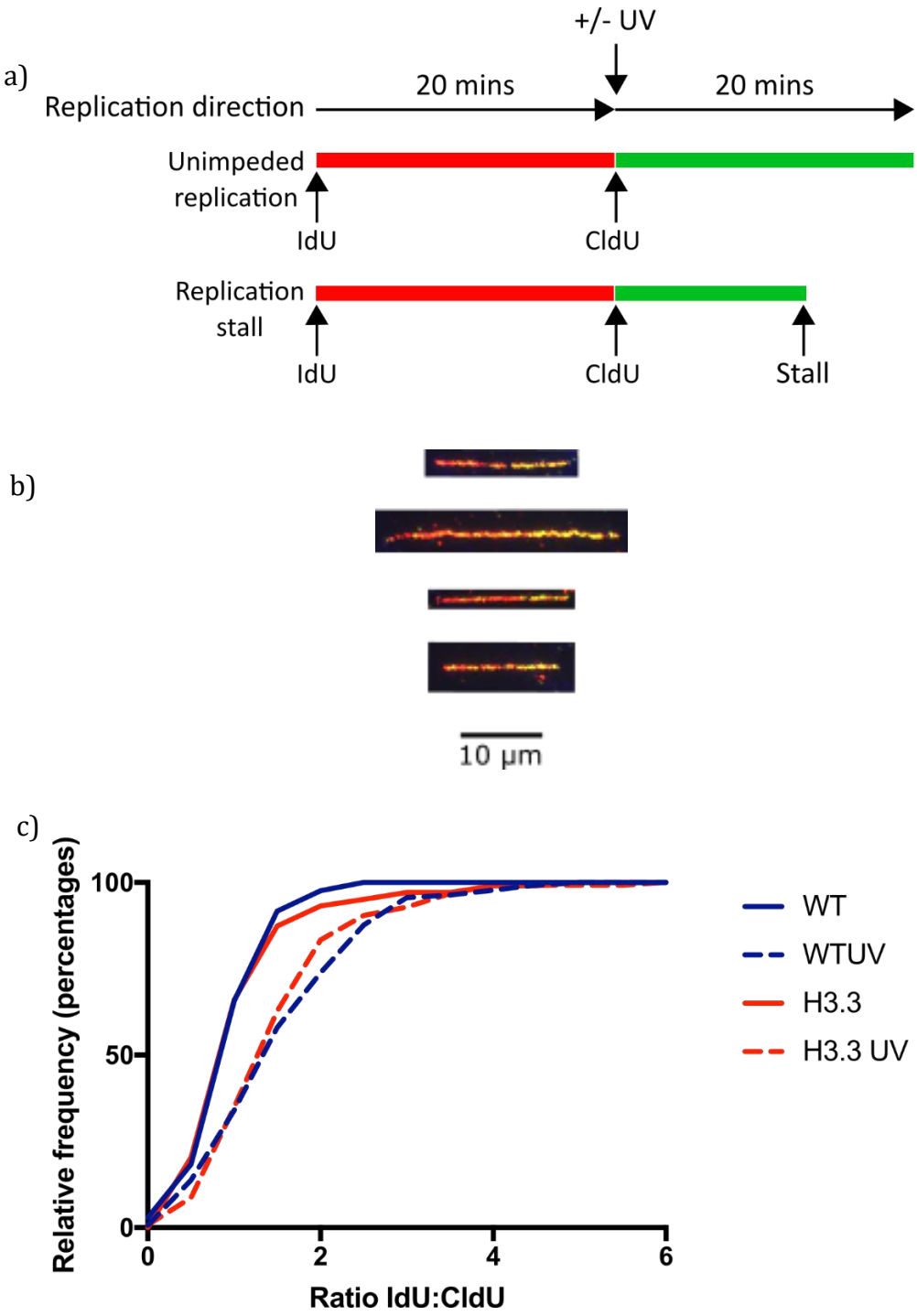

Figure 3.10 Replication fork progression with and without UV irradiation in WT and *h3.3* cells. a) Schematic of fibre labelling in DNA fibre assay. b) Representative fibre images, with IdU in red, CldU in green. From WT cells c) The ratio of the length of the second labelled fibre to the first is displayed as a cumulative percentage of forks at each IdU:CldU ratio. At least 100 fibres were measured for each condition. The p-value that the cumulative distribution of *h3.3* is different from WT (with UV) is 0.1773/not significant by two-sample Kolmogorov-Smirnov test.

From this, we see that fork progression is reduced after UV in both WT and *h3.3* cells, but there is not any increased sensitivity in *h3.3* cells.

In TK6 cells, H3.3 does not seem to be required for replication fork progression after UV irradiation.

This result was surprising, as some impact on replication was expected. The increased S arrest population in *h3.3* cells suggests UV damage in *h3.3* cells causes problems with replication progression. However, this increased S arrest population appears at a much later timepoint after UV than this DNA fibre assay examines. The S arrest population at 24 hours after UV could be due to a delay in resolving damage. Some *h3.3* cells with unresolved damage may escape the G1 block then enter replication, where UV lesion could be converted to a break and disrupt replication.

Again, p53 could be responsible for the different phenotypes observed in TK6 vs in DT40 *h3.3* cells. p53 can play a role at the replication fork during DNA damage, promoting translesion synthesis. TK6 cells may therefore they be more competent than DT40 cells at translesion synthesis and use this more frequently to bypass lesions. This could allow TK6 cells to maintain replication fork progression more effectively, even when lesions are encountered, or repair factors are absent.

3.6 The impact of p53 on the response of H3.3 to damage

TK6 expresses functional p53, a potential reason why my results have looked different to results from previous work in DT40 cells. p53 is a key player in the DNA damage response and is involved in many different pathways. This includes coordinating the G1/S checkpoint, activation of which is seen in the TK6 *h3.3* cells. If there were to be a problem with a branch of a damage repair pathway (potentially caused by a lack of H3.3), activation of p53 could ensure other, redundant, repair pathways are activated and so damage can be repaired by alternative mechanisms. If p53 were to be absent, there may be less cross-talk between repair pathways. Then, if there were a problem with one

branch, alternative repair mechanisms may not be activated without p53 at the centre of repair networks. Therefore, removing p53 could reveal an underlying damage sensitivity of *h3.3* TK6 cells. Additionally, p53 can activate the G1 cell cycle checkpoint (see section 1.3.3.3) and could therefore mediate the increased G1 population observed.

I therefore decided to knockout p53 in *h3.3* cells to determine if disrupting a key member of damage repair networks could reveal an underlying sensitivity of *h3.3* cells to UV compared to wild type cells lacking p53.

To remove p53, I used a different approach to the one taken to remove H3.3. I created WT TK6 and *h3.3* cell lines stably expressing Cas9 then caused mutations in p53 by adding relevant gRNAs. Reagents to remove p53 by this method already existed in the lab, created by C. Mellor, and creating cell lines with stably integrated Cas9 would be useful for future studies, such as creating other gene knockout cell lines and CRISPR screening (see Chapter 6).

3.6.1 Creating and validating p53 deficient cell lines in WT and *h3.3* backgrounds

Once I had generated cell lines stably expressing Cas9 in both WT and *h3.3* backgrounds (see Chapter 6), I needed to remove p53. To do this I transfected the cell lines with 4 plasmids with different gRNAs both upstream and downstream of the p53 gene (designed and created by C. Mellor) (Figure 3.11a). This strategy aims to generate multiple breaks in the gene at the same time and thereby remove the entire gene, as p53 has many splice isoforms (Joruiz and Bourdon, 2016) and so a single gRNA may not be sufficient.

The infected cells were sorted for RFP expression (for successful transfection) and clones which grew were screened. To screen for loss of p53, I carried out a PCR using primers designed within the targeted region (Figure 3.11b). By carrying out a PCR with primers internal to the gRNA sites, a product would only be generated if the targeting was unsuccessful and there is no large deletion between the 2 gRNA sites. Therefore, any clones which generate a PCR product using these internal primers do not have the large deletion in TP53 and are not taken forward. Clones with no PCR product from these internal primers may have a large deletion in TP53 and so were taken forward for further validation (Figure 3.11c).

Western blotting to determine the presence of p53 protein showed that 9 of 11 of these clones where successful p53 knockouts, showing no p53 protein (Figure 3.11d).

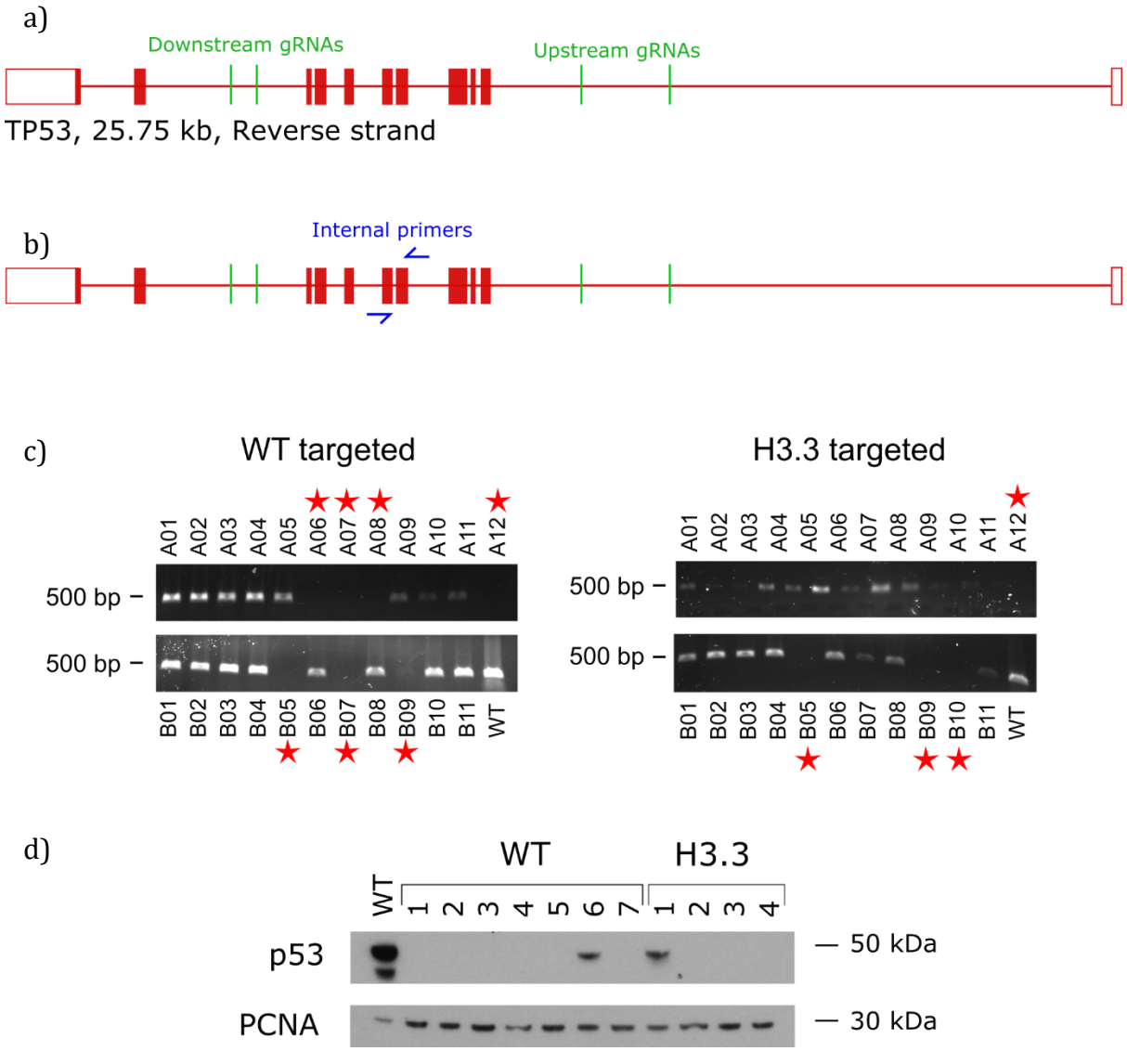

Figure 3.11 Generation of p53 null cell lines a) Map of TP53 gene and positions of targeting gRNAs. b) Map of TP53 with positions of screening PCR primers. c) Gel electrophoresis of PCR products from potential knockout clones using internal primers (Expected size: 485 bp). Red stars indicate clones to be taken forward for further validation. d) Western blot of potential knockout clones. PCNA shown as a loading control

3.7 The response of response of p53 null cells to DNA damaging agents

Without p53, TK6 cells may not be able to recover from DNA damage as effectively as with p53. While p53 is present, there was no difference between WT and *h3.3* long term survival, as shown by the colony survival assay, but there was a difference in cell cycle progression and the presence of DNA damage markers.

Without p53, cells lacking H3.3 may not be able to activate the G1 checkpoint effectively. This could allow cells with unresolved DNA damage to continue through the cell cycle, leading to damage entering the next S phase where it could cause replication catastrophe and cell death.

3.7.1 Cell cycle distribution of *p53* and *h3.3/p53* cell lines after UV irradiation

p53 and *h3.3/p53* cell lines underwent cell cycle analysis as described previously alongside their WT and *h3.3* counterparts (Figure 3.12).

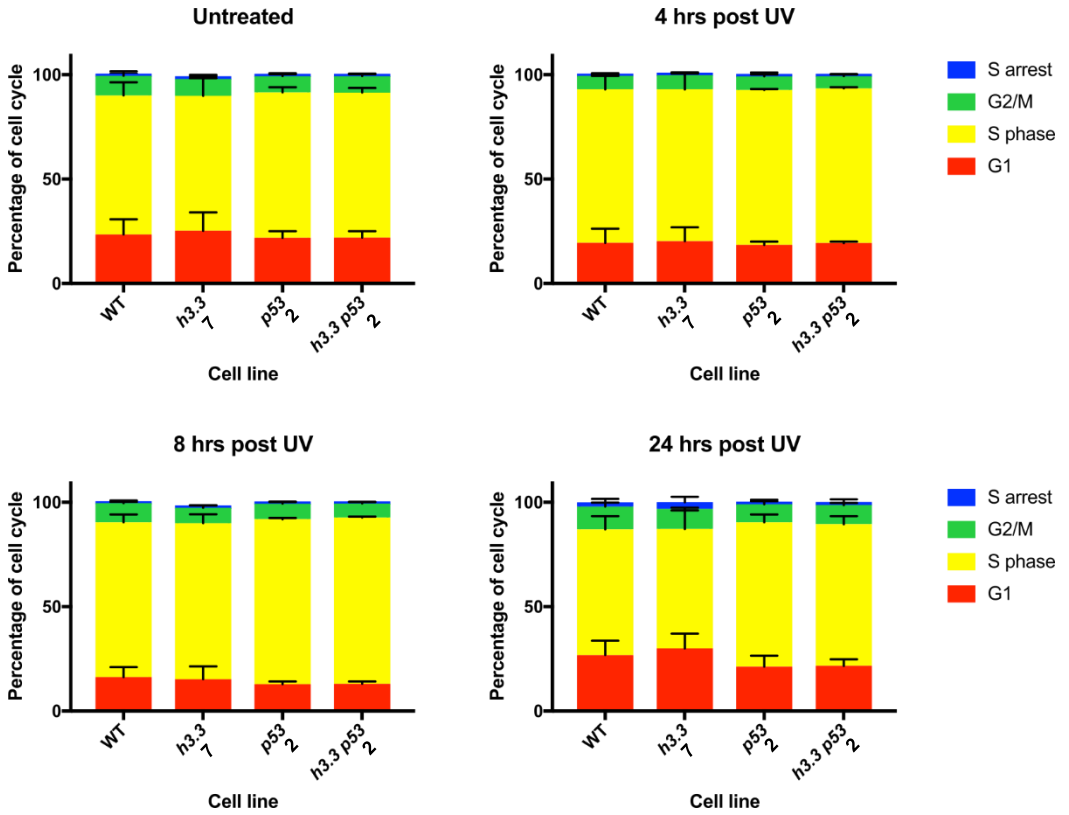

Figure 3.12 Cell cycle changes in p53 null cell lines after UV irradiation Cell cycle proportions without UV and at timepoints after 4 J/m^2 UV. Error bars show standard deviation of the mean. Data from 3 biological replicates shown

p53 deficient cells have no G1 block 24 hrs after UV irradiation, regardless of the presence or absence of H3.3. There are no other major changes in the cell cycle proportions.
As I had found in some instances previously, this assay can produce inconsistent results with cell viability having an impact on results. This could be a reason for why there is little difference between WT and *h3.3* cell lines in these experiments.

This lack of G1 block is expected, as p53 is key in establishing the G1/S cell cycle arrest in response to DNA damage. However, removing p53 did not lead to an S phase block, as seen in DT40 cells. If H3.3 causes a delay in resolving UV induced DNA damage and a lack of p53 enables cells to continue cycling, unresolved damage could pass into the replicative phase of the cell cycle, where it may cause replication fork collapse or activation of S phase checkpoints, and therefore I might expect an increased S phase or S arrest population.

As the *p53/h3.3* cell line does not have a change in cell cycle proportions after UV, damage may be passing through the cell cycle and causing problems to the cells on a longer timescale. I therefore examined the survival of the p53 deficient cell lines after UV.

3.7.2 No change in long term survival of *p53* cells after acute genotoxin treatment

Cells were treated with varying doses of either UV irradiation or MMS before being plated in methylcellulose medium. Once grown, colony numbers were counted and compared to untreated control to determine the percentage of cell which survived and continued dividing after the acute genotoxin treatment (Figure 3.13).

Between this experiment and the previous colony survival experiment on *h3.3* cells, the UV bulb was changed in the UV box used to irradiate cells. The calibration of this new bulb appears to be slightly different to previously, as higher doses of UV were required to obtain the same survival rates of WT cells as in previous work.

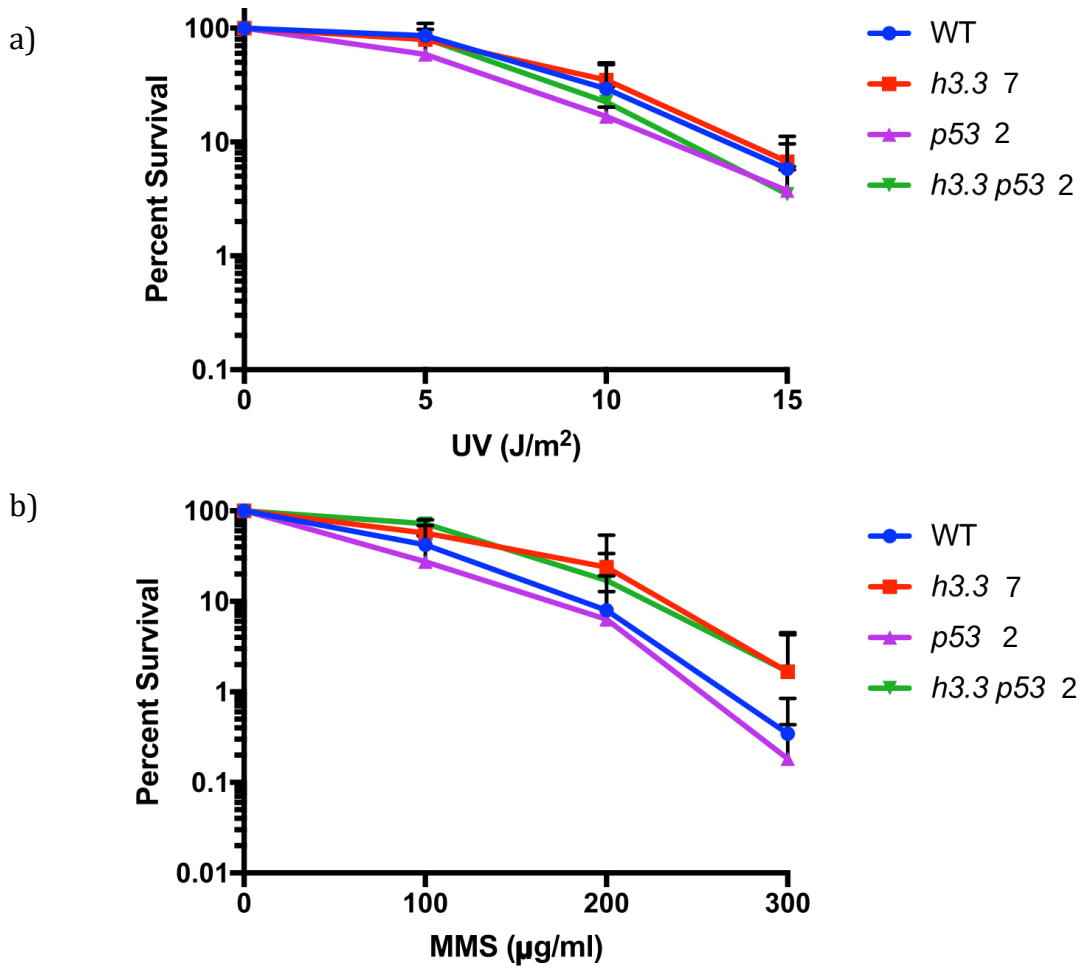

Figure 3.13 *p53* cells do not show hypersensitivity to a) UV or b) MMS. Percentage survival was calculated relative to untreated cells. 2 technical repeats per experiment, mean of 3 experiments shown here. Error bars show standard deviation. At 300 ug/ml MMS, there is no significant difference between either WT and *p53* or *h3.3* and *h3.3 p53* by unpaired t-test

There is no increased sensitivity in p53 deficient cells lines compared to p53 proficient cell lines. Although there seems to be a difference between cell lines with and without H3.3 after MMS treatment, this difference is not significant and would require further replicates to verify.

I had expected to see an increased sensitivity to genotoxins in cells lacking p53, as p53 is a key component of many damage signalling and repair pathways. It is also an important difference between TK6 and DT40 cells, so removing p53 could have given results similar to those obtained in the DT40 cells. As there is no increased sensitivity, TK6 cells must be proficient for cell survival and DNA damage repair, even in the absence of p53.

As TK6 cells are not a cancer cell line, but a non-transformed immortalised cell line, they potentially have intact and competent repair pathways, meaning they can survive DNA damage and small alterations to repair processes. A colony survival assay will not, however, reveal whether there is an impact on the cells other than a change in survival or division, for example, if there is a greater mutational burden in *h3.3* or *h3.3/p53* cells.

Chapter 4: The response of H3.3 chaperones to UV damage

H3.3 appears to have a role in the response to UV induced DNA damage, and this is likely to be mediated by one of its two chaperones. Both ATRX/DAXX and the HIRA complex have been implicated in the response to DNA damage and so I investigated which of these chaperones might be involved with H3.3 in the response to UV damage. To study whether the role of H3.3 in the response to UV damage is involved with either or both ATRX/DAXX and the HIRA complex, I created knockout cell lines of ATRX and HIRA.

4.1 Does ATRX have a role after UV damage?

ATRX is one of the two H3.3 chaperones, partnering with DAXX to deposit H3.3 onto repetitive regions of the genome, including telomeres. It is reported to have roles in double strand break repair and at stalled forks (section 1.4).

In order to study the possible involvement of ATRX in H3.3's response to UV induced DNA damage, I created an ATRX knockout cell line. I chose to remove ATRX rather than DAXX. H3.3 is bound by DAXX rather than ATRX, and whilst DAXX has ATRX independent functions (namely repressing endogenous retroviruses) (Hoelper *et al.*, 2017), ATRX has been shown to be required for deposition of H3.3 onto chromatin (Watson *et al.*, 2013).

4.1.1 Generation of an ATRX deficient human cell line

To remove ATRX from TK6 cells, I used a similar approach to the H3.3 knockout creation, using a single gRNA designed against an early exon (Figure 4.1a). This exon is upstream of any defined functional domains in the ATRX protein. As ATRX is a large gene/protein, it was important that the targeted exon is common to as many isoforms to try to completely remove the protein.

I cloned the ATRX gRNA into the pX458 plasmid and transfected this into TK6+ cells. After sorting for GFP expression, clones which grew successfully were screened for change in size of the PCR product spanning the target site by fragment analysis (as with the H3.3

cell lines). Of the 90 clones screened, 11 clones had size changes and 3 were taken forward for full characterisation.

The 3 selected clones had the PCR product spanning the targeted site TOPO cloned into a plasmid then Sanger sequenced to see the precise sequence of the mutation (Figure 4.1b). These 3 clones all had exactly the same 32 bp deletion (only in one allele as ATRX is X linked and the TK6 cell line is male). A 32 bp deletion would be likely to cause a frameshift mutation, as it is not divisible by 3, and therefore mRNA from this mutated gene would undergo nonsense mediated degradation or a premature stop codon may result. There are several possible explanations for why only one type of mutation was found. A cell with this mutation could have divided before plating as single cells, so the mutation only arose once and they are all clones. TK6 cells could favour a repair with a deletion of this size from this gRNA placement due to the repair mechanism used or the chromatin environment of this region. Finally, the primers are positioned to give a fairly short (249 bp) PCR product, so any large deletions may not be amplified and recovered.

Western blotting with an antibody against ATRX shows that the protein is depleted in these targeted lines (Figure 4.1c). There is a faint band in these lines, which could be due to some continuing ATRX expression. The antibody used binds to a C-terminal epitope, far from the region targeted by my gRNA, so detection of protein could be due to some alternative splicing allowing skipping of the targeted exon. The antibody is also reported to produce non-specific bands at a lower weight, so any possibility of splice variants which can leave functional protein of a lower weight is difficult to determine. However, I did not observe any changes in lower weight bands between WT and knockout lines. Even if these lines do not have a complete absence of ATRX, the depletion is enough to observe an effect. These ATRX depleted cell lines will be noted as *atrx* cells. A further experiment which could be carried out to determine if these are ATRX knockout clones would be to compare to U2OS cells, which are known to have no functional ATRX protein (Lovejoy *et al.*, 2012).

Depletion of ATRX has little effect on doubling time compared to WT TK6+ cells (Figure 4.1d)

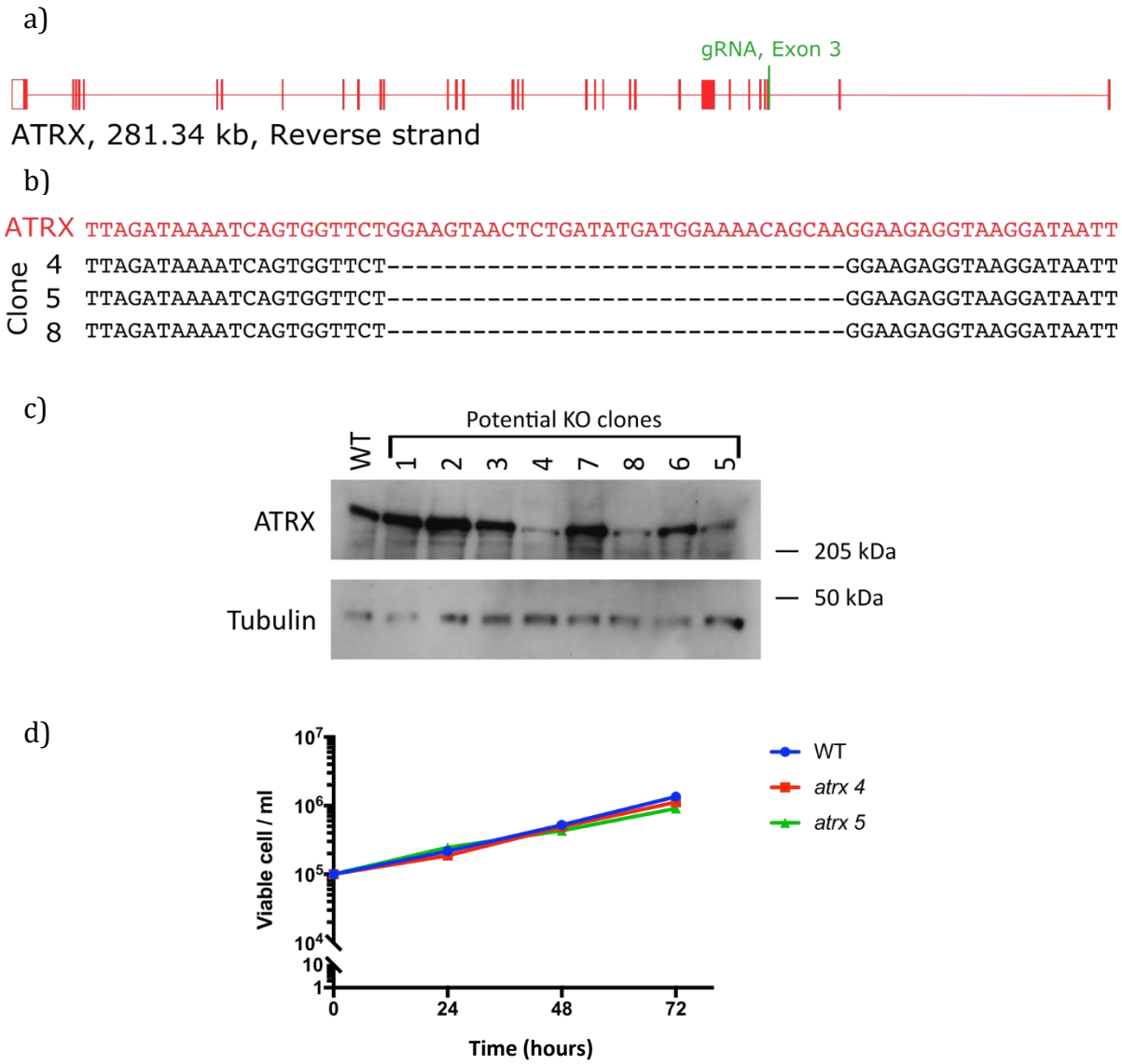

Figure 4.1 CRISPR-Cas9 targeting of ATRX a) Map of ATRX showing position of gRNA b) Sequence of targeted region in successfully targeted *atrx* clones c) Western blot of potential *atrx* clones. Tubulin shown as a loading control d) Growth curve of WT and *atrx* cell lines. Error bars show standard deviation of 3 technical replicates.

4.2 Does HIRA have a role after UV damage?

The HIRA complex is the other of the two H3.3 chaperones, responsible for depositing H3.3 in genic regions (Goldberg *et al.*, 2010). It is comprised of CABIN1, UBN1, ASF1a and HIRA. I decided to target HIRA as it acts as a scaffold to the complex and removal of HIRA has been demonstrated to destabilise the whole complex and prevent its formation (Ray-

Gallet *et al.*, 2018). HIRA has also been implicated in the response to DNA damage, specifically in the transcriptional recovery after UV irradiation (Adam, Polo and Almouzni, 2013).

4.2.1 Generation of a HIRA deficient human cell line

Initially, I took the same single guides against an early exon approach to remove HIRA, as I had carried out with H3.3 and ATRX. However, after several attempts at transfection, sorting and screening by fragment analysis, there were no clones with mutations in both alleles. I decided to take a different approach, designing gRNAs against both ends of the gene in an attempt to remove a large portion of the gene (Figure 4.2a).

To screen for mutations, I designed PCR primers to amplify between the 2 gRNAs, ie. in the region I expect to remove (Figure 4.2b). Clones which gave no PCR product from these primers (Figure 4.2c), were screened for the presence of HIRA protein by western blot Figure 4.2d). Several clones appeared to have no HIRA protein, but on longer exposure, it was possible to see a faint band, suggesting HIRA had not been eliminated in all but 1 clone. This single HIRA knockout cell line (clone 4) was taken forward for further experiments.

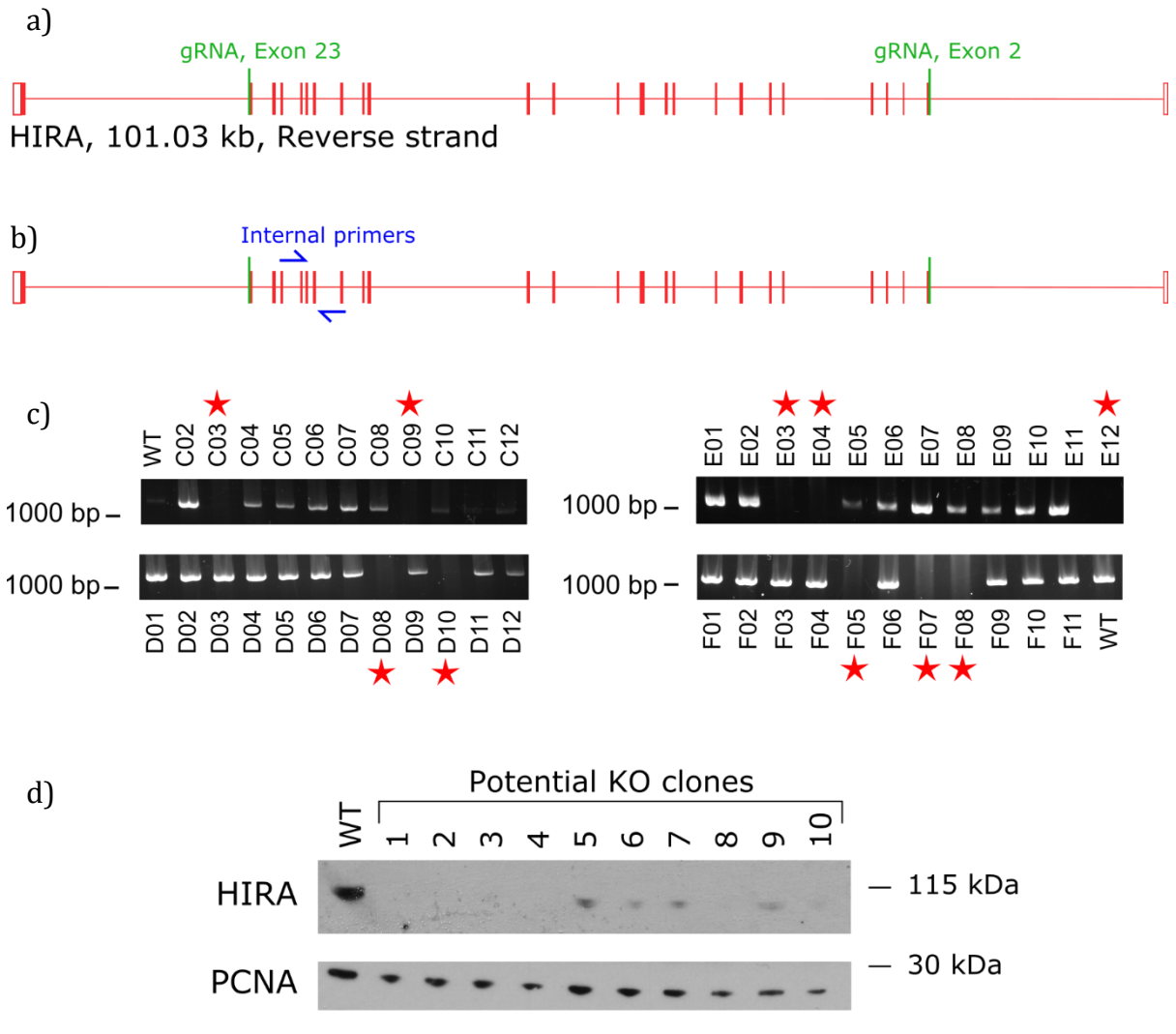

Figure 4.2 CRISPR-Cas9 targeting of HIRA a) Map of HIRA showing position of gRNAs b) Position of PCR primers between gRNAs against HIRA c) Gel electrophoresis of PCR products from potential knockout clones using internal primers. Red stars indicate clones to be taken forward for further validation. d) Western blot of potential *hira* clones with short exposure. PCNA shown as a loading control

HIRA was unexpectedly difficult to knockout by CRISPR targeting. Complete abrogation of HIRA, or any component of the HIRA complex, causes gastrulation defects and is embryonic lethal in mice (Roberts *et al.*, 2002). This could indicate important roles in cell function, and thereby explain the difficulty in removing HIRA. The one clone (*hira* 4) which I am confident has no HIRA protein could have changes other than HIRA mutation to allow it to survive HIRA depletion. Ideally, complementation would be the way to ensure any phenotype observed is due to a lack of HIRA. The several clones which display reduced HIRA protein levels, as demonstrated in the western blots, may either have

mutations in 1 of 2 alleles or partial HIRA expression through only a single gRNA causing mutations and alternative splicing allowing some HIRA expression.

4.3 The response of H3.3 chaperone deficient cell lines to UV irradiation

H3.3 is incorporated into chromatin by two chaperone complexes. H3.3's role in the response to UV induced DNA damage is likely mediated by deposition of H3.3 by one or both of these chaperones. Removing each of these chaperones will help inform which chaperone may be involved in the UV response, as the chaperone(s) involved are likely to phenocopy the *h3.*3 cells. Understanding which (or both) chaperone mediates the H3.3 UV response could help inform us further on what situations or regions of the genome H3.3 is needed for resolving UV induced DNA damage.

4.3.1 *atrx* and *hira* cell lines do not exhibit hypersensitivity to UV irradiation in a long-term survival assay

Both *atrx* and *hira* cell lines were treated with varying doses of UV irradiation, plated in methylcellulose medium and colonies were allowed to form and grow for approximately 2 weeks. A higher number of colonies demonstrates a larger proportion of cells were able to survive and continue dividing after the initial genotoxin treatment (Figure 4.3).

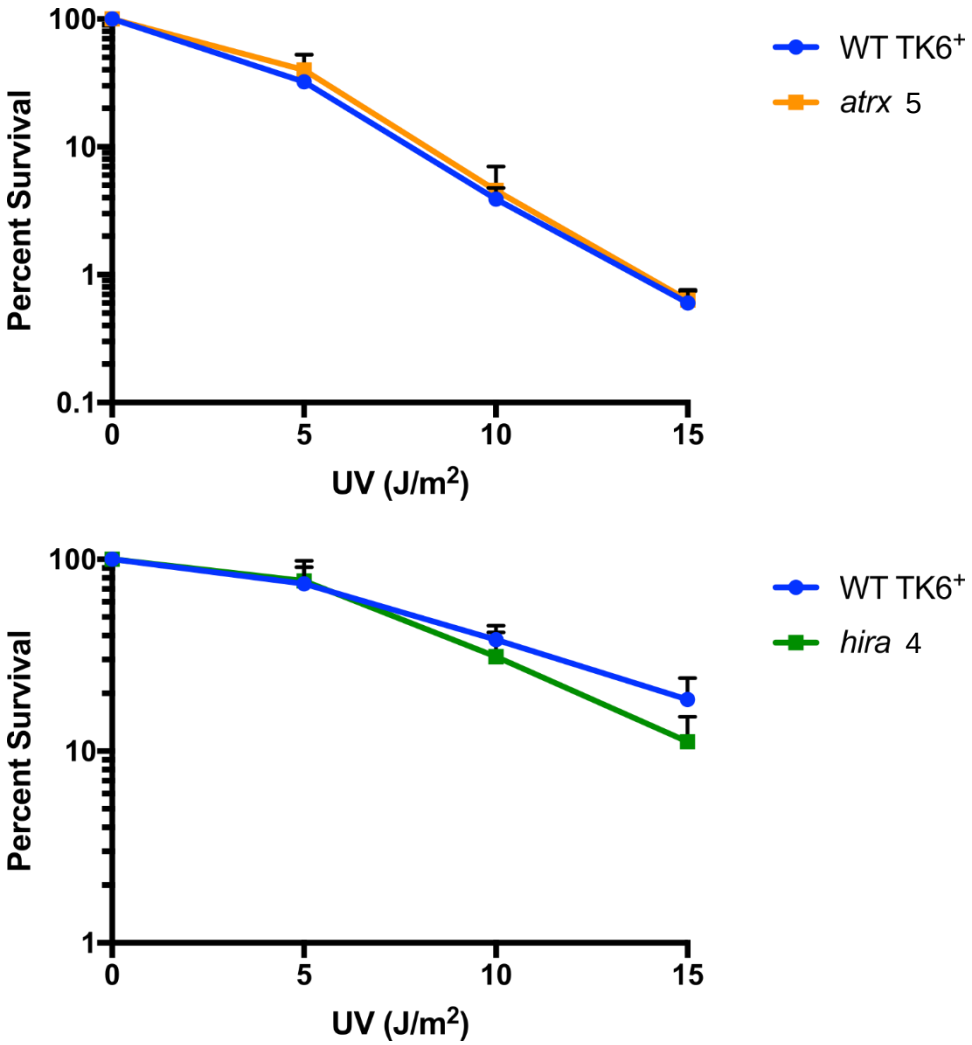

Figure 4.3 *atrx and hira* cells do not show hypersensitivity to UV. Percentage survival was calculated relative to untreated cells. 2 technical repeats per experiment, mean of 3 experiments shown here. Error bars show standard deviation. At 15 J/m2, *hira* is not significantly different to WT by unpaired t-test.

Neither the *atrx* nor the *hira* cell lines showed an increased sensitivity to UV irradiation compared to the WT TK6. Additionally, the difference in WT percentage survival between the 2 experiments (which were carried out 18 months apart) demonstrates the variability of the UV bulb.

This matches the results seen in *h3.3* cells and so indicates that ATRX and HIRA do not have an H3.3 independent role in the response to UV induced DNA damage.

4.3.2 Changes to cell cycle progression in *atrx* and *hira* cell lines after UV irradiation

The H3.3 response to UV damage is most prominent in TK6 cells in the cell cycle changes after irradiation. To determine if the role of H3.3 in the response to UV is mediated by either or both of its chaperones, I carried out 2D cell cycle analysis in the *atrx* and *hira* cell lines at timepoints after UV irradiation (Figures 4.4 and 4.5).

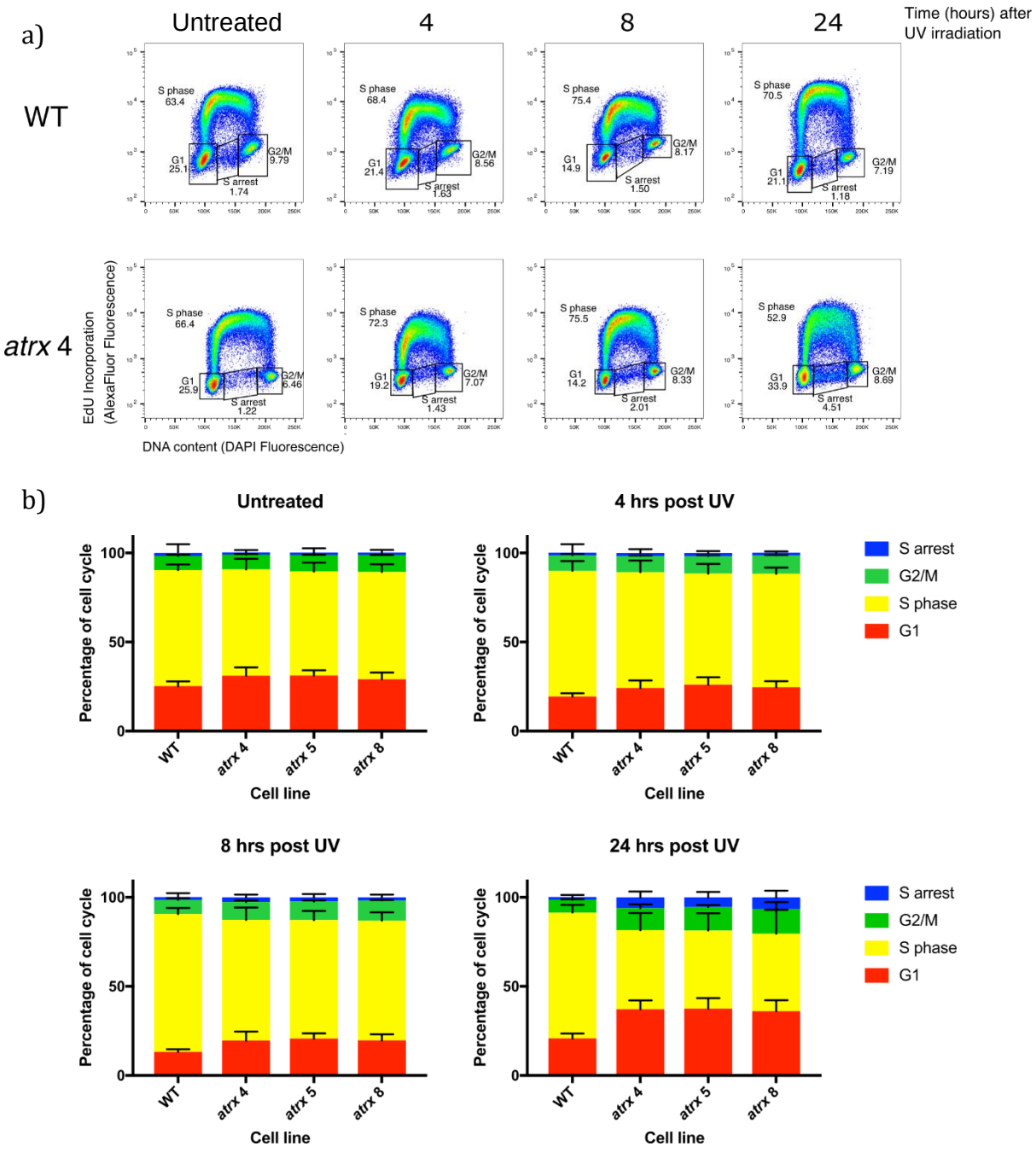

Figure 4.4 Cell cycle changes in WT and *atrx* cells after UV irradiation a) Representative cell cycle dotplots of WT and *atrx* cells at timepoints after 4 J/m^2 UV irradiation, displaying gating strategy for cell cycle phases. b) Cell cycle proportions without UV and at timepoints after 4 J/m^2 UV. Error bars show standard deviation of the mean. Data from 3 biological replicates shown

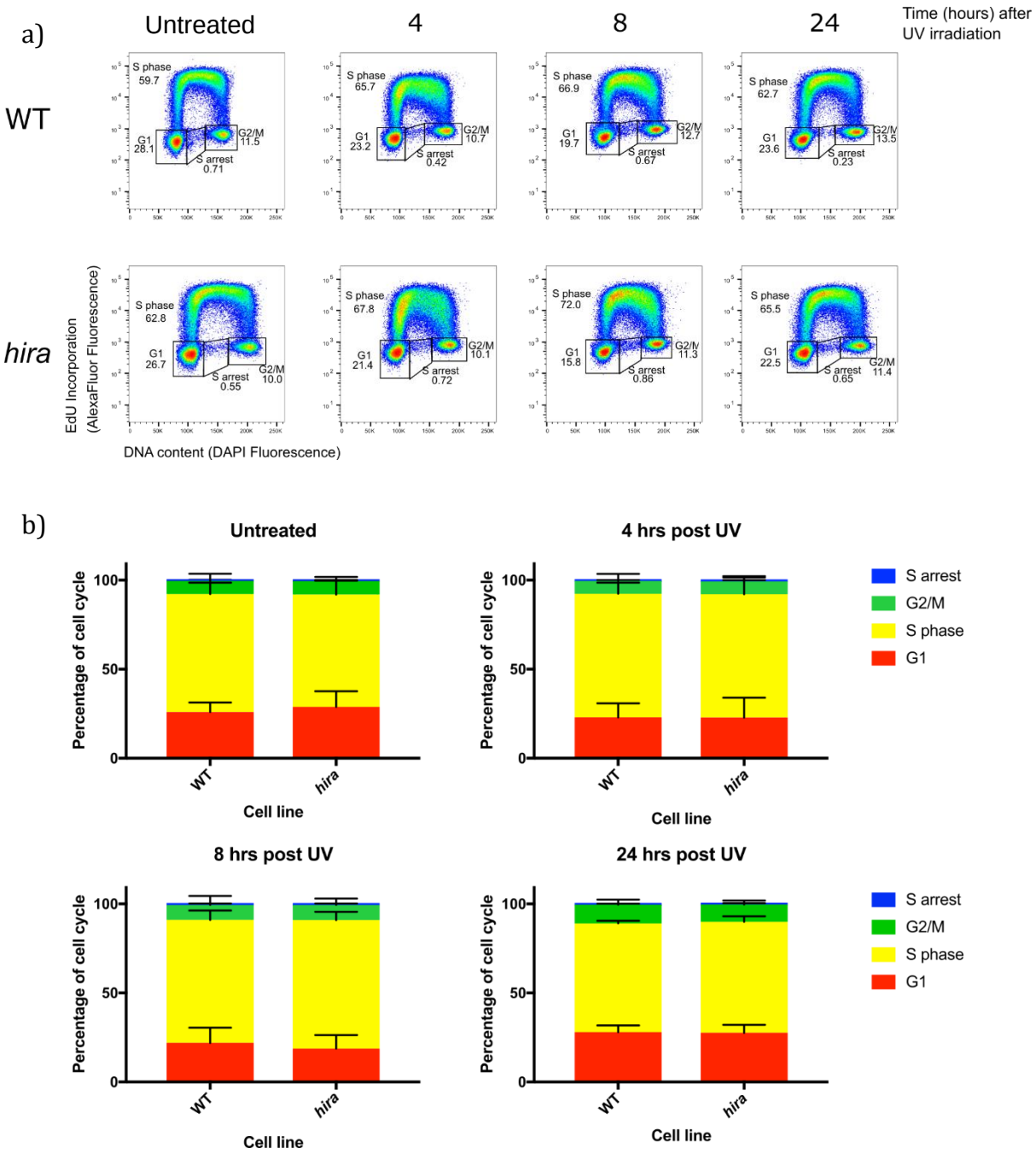

Figure 4.5 Cell cycle changes in WT and *hira* cells after UV irradiation a) Representative cell cycle dotplots of WT and *hira* cells at timepoints after 4 J/m^2 UV irradiation, displaying gating strategy for cell cycle phases. b) Cell cycle proportions without UV and at timepoints after 4 J/m^2 UV. Error bars show standard deviation of the mean. Data from 3 biological replicates shown

The *atrx* cells have a very pronounced G1 block at 24 hrs after UV, as well as an increased G2/M and S arrest population.

To determine if this response of *atrx* cells to UV is more pronounced than the *h3.3* cells, I carried out the cell cycle analysis on both cell lines on the same day to ensure the UV dose is exactly the same (Figure 4.6).

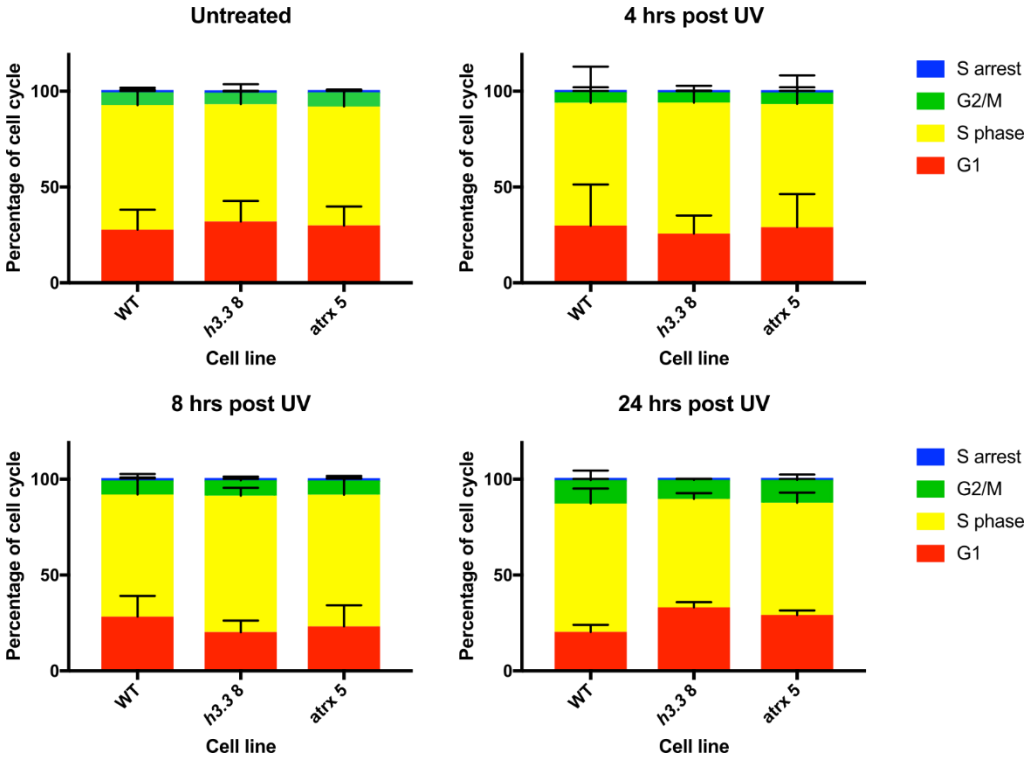

Figure 4.6 Cell cycle changes in WT, *h3.3* and *atrx* cells after UV irradiation Cell cycle proportions without UV and at timepoints after 4 J/m^2 UV. Error bars show standard deviation of the mean. Data from 3 biological replicates shown

This demonstrated that the impact of UV on cell cycle changes in H3.3 and ATRX deficient cell lines is similar.

Overall, this shows ATRX is involved in the response to UV. As these cell cycle results mirror the change in cell cycle proportions seen in the *h3.3* cell lines, ATRX could be responsible for mediating H3.3's role in the response to UV induced damage. A double mutant lacking both H3.3 and ATRX would be required to establish if there is epistasis in the response to UV damage confirm this.

However, changes in the *hira* cell line cell cycle after UV are minimal and are very similar to the WT cells. HIRA seemingly has no effect on the cell cycle after UV irradiation, suggesting it is unlikely to mediate role of H3.3 in the response to UV damage.

Together, these results point towards ATRX being the chaperone which is involved in the response to UV damage in TK6 cells, linked to the role of H3.3. Further work involving ATRX mutants would be required to determine whether ATRX deposits H3.3 in response to UV.

4.3.3 Replication fork progression after UV in *atrx* and *hira* cell lines

Although my earlier results did not indicate a role for H3.3 in replication fork progression, ATRX has previously been implicated in fork progression after damage (Leung *et al.*, 2013; Clynes *et al.*, 2014; Huh *et al.*, 2016). I therefore decided to examine DNA synthesis after UV irradiation in both the *atrx* and *hira* cell lines to determine if there are roles for the H3.3 chaperones independent of H3.3 in the response to UV (Figure 4.7).

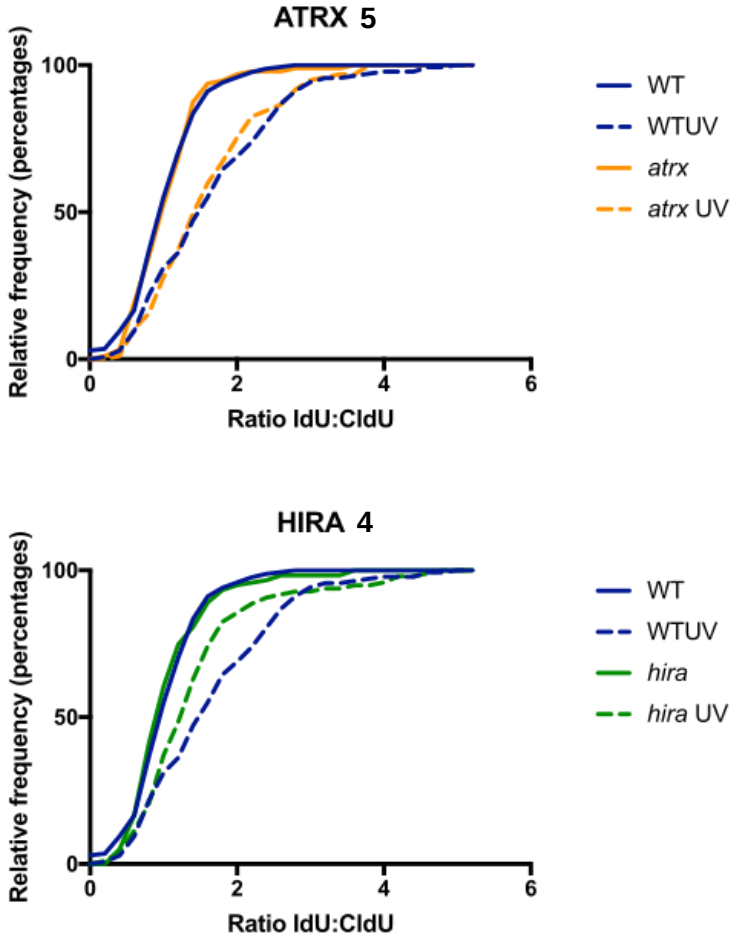

Figure 4.7 Replication fork progression with and without UV irradiation in WT, ATRX deficient and *hira* cells Cells were irradiated with a high, acute does of 40 J/m^2 UV. The ratio of the length of the second labelled fibre to the first is displayed as a cumulative percentage of forks at each IdU:CldU ratio. a) The p-value that the cumulative distribution of *atrx* is different from WT (with UV) is 0.7099/not significant by two-sample Kolmogorov-Smirnov test b). The p-value that the cumulative distribution of *hira* is different from WT (with UV) is 0.0302 - significant by two-sample Kolmogorov-Smirnov test.

atrx cells showed no change in replication fork progression after UV irradiation compared to WT cells. Unexpectedly, when treated with UV, *hira* cells showed a significant difference compared to WT cells. Replication forks appear to progress faster after UV in the absence of HIRA.

The absence of any effect of ATRX on replication fork progression after UV was not entirely expected, as stalled replication forks can be protected by ATRX (Leung *et al.*,

2013; Huh *et al.*, 2016). These studies, however, induced fork stalling by HU, which disrupts the supply of nucleotides, rather than through DNA lesions. The 40 J/m^2 of UV used in this experiment would be expected to introduce lesions at least every 10 kbs (Edmunds, Simpson and Sale, 2008), so I would expect a large proportion of forks to encounter a lesion during the course of the experiment. TK6 cells may deal with damage encountered by replication forks in a way that minimises fork stalling, e.g. through lesion bypass mechanisms, and so ATRX may not be required. The observed absence for a role at the fork could also suggest that any ATRX mediated role of H3.3 in response to UV induced DNA damage may be at sites other than the replication fork.

A double H3.3/ATRX knockout cell line would be a way to investigate the ATRX requirement in the H3.3 response to DNA damage. This would allow demonstration of epistasis, but would not demonstrate ATRX mediated H3.3 deposition.

HIRA has not been reported to have a role at the replication fork. HIRA has been implicated in the response to UV damage, localising to damaged chromatin regions and 'priming' regions for transcriptional recovery (Adam, Polo and Almouzni, 2013).

If there is less transcription after UV due to a lack of HIRA, there could be fewer collisions between transcription and replication machinery, allowing replication forks to progress with fewer impediments and therefore appear to move faster than in WT cells.

Chapter 5: The protein interactome of H3.3 after UV irradiation

The H3.3 specific residue on its N-terminal tail offers the possibility of specific interactors, as demonstrated by the H3.3 specific interactor ZMYND11 which recognises the H3.3 N-terminal tail specific S31 residue. To test the hypothesis that H3.3 may facilitate DNA damage repair by recruitment of specific factors, I examined proteins interacting with H3.3 after UV irradiation.

5.1 GFP Trap

To investigate whether H3.3 has specific interactions induced by UV irradiation, I used GFP trap and proteomic analysis. GFP Trap utilises anti-GFP nanobodies immobilised on agarose beads which can bind a GFP-tagged protein of interest and pull it down, alongside its interactors. GFP trap involves lysis of cells containing GFP-tagged H3.3, binding of lysate to GFP Trap beads, then gel electrophoresis to separate the proteins pulled down and mass spectrometry to identify protein interactors.

TK6 WT cells were transfected with H3.3-GFP, selected for with neomycin and assessed for successful transfection by flow cytometry. Clones containing H3.3GFP were taken forward for use with GFP Trap.

To confirm that GFP Trap beads are successfully binding and pulling down GFP tagged H3.3, I carried out the binding assay and a western blot on the input, unbound and bound fractions (Figure 5.1).

Cell lysis included Benzonase treatment to digest DNA, as proteins linked by a section of DNA could appear as interactor. Digesting DNA is important to ensure only protein-protein interactors are found. Lysate was allowed to bind to GFP Trap beads for 1 hr at 4 °C, as recommended by the manufacturers. Beads were washed to remove non-specific interactors, including a high salt wash. The whole process was carried out in the presence of protease inhibitors to minimise any degradation of interacting proteins.

This confirmed the pull down is working as expected. H3.3GFP is present in the input fraction, but not in the unbound fraction. There is more H3.3GFP present in the bound fraction than in the input, demonstrating enrichment.

H3.3GFP is also visible on a gel, without the need for western blotting (Figure 5.1b).

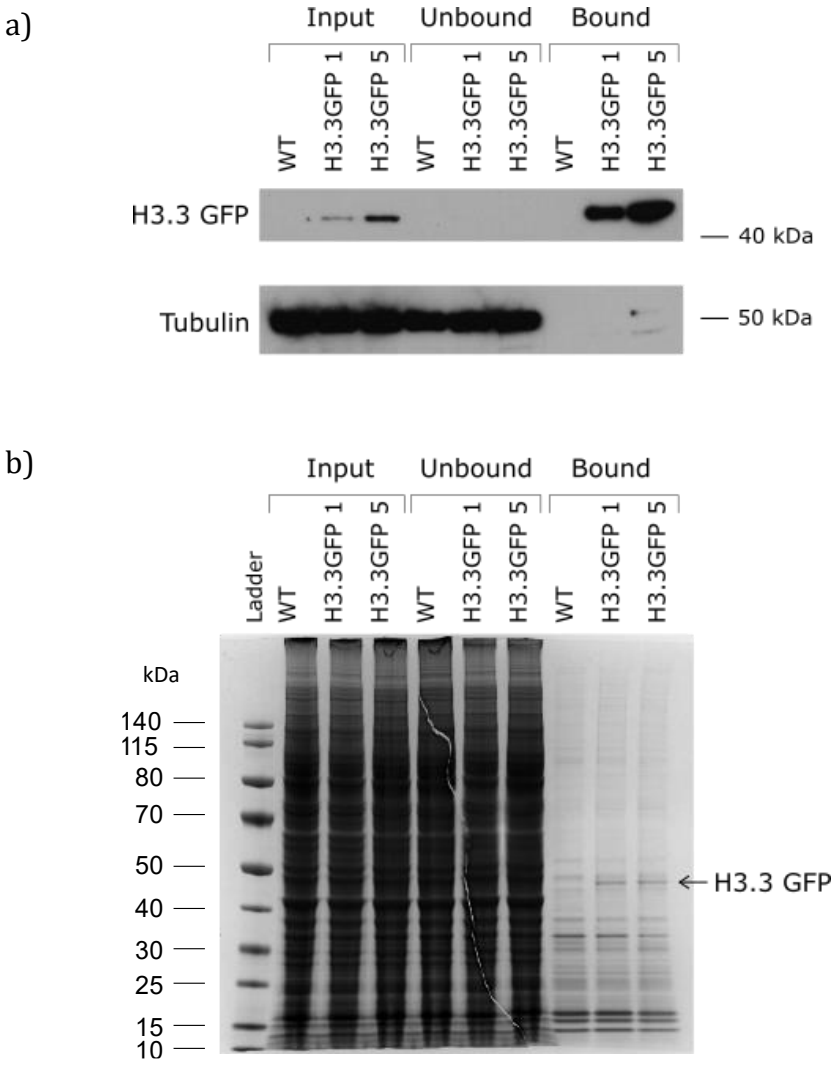

Figure 5.1 Confirmation of GFP Trap pulldown a) Western blot against GFP of input, unbound and bound fractions of pulldown, tubulin shown as a loading control. b) Gel of input, unbound and bound fractions Coomassie stained to visualise protein.

To compare proteins associated with H3.3 before and after UV, I irradiated cells with 8 J/m^2 UV and collected 30 mins later. These underwent GFP trap binding alongside cells

not treated with irradiation and gel electrophoresis before submission for mass spectrometry.

5.2 H3.3 interactors

The top 500 results (by percentage of total spectrum) were examined and a protein was considered enriched if there were 4 or more unique peptides between the control (WT/untransfected cells, no GFP expression) and both H3.3-GFP-expressing cell lines (Appendix 3). Requiring a threshold of several unique peptides can increase the certainty that the interactors are specific, and comparing to the WT control, which contain no GFP-tagged protein, will eliminate any proteins which interact with the GFP nanobody or agarose beads, rather than the H3.3.

As an internal control, I looked for DAXX in the H3.3 interactors. DAXX binds H3.3 specifically and is found in the interactome of H3.3 in other pulldown studies (Lewis *et al.*, 2010; Zink *et al.*, 2017; Sitbon *et al.*, 2020). I would therefore expect DAXX to appear as an interactor. Although I carried out 3 repeats, DAXX was only enriched in both clones in one of the repeats, so I focussed my analysis on this dataset as I have taken the presence of DAXX as an indicator that the pulldown has been successful. The other repeats (repeats 2 and 3) contained at least 1 H3.3 GFP sample with an emPAI score of less than 0.1, and so DAXX is not considered enriched (Table 2)

Table 2 emPAI scores of DAXX in each of the 3 replicates with and without UV

	without UV			with UV		
Cell line	**WT**	**H3.3 GFP 1**	**H3.3 GFP 2**	**WT**	**H3.3 GFP 1**	**H3.3 GFP 2**
Repeat 1	0	0.28256	0.75947	0	0.75896	0.20971
Repeat 2	0	0.082457	0	0	0.20068	0
Repeat 3	0	0.33027	0.11381	0	0.28012	0.083949

In proteins pulled down as H3.3 specific interactors both with and without UV (Appendix 3), DAXX and other chromatin remodellers were recovered. This confirms that histone interactors are present. Other H3.3 specific interactors (ZMYND11 and members of the

HIRA complex) were not observed. They may have more transient interactions with H3.3 or only interact under certain circumstances, not tested here.

I do see other histone proteins at the top of the interactors list by percentage of total spectrum, as would be expected, but they also appear in the WT sample, so are not listed as enriched. Histones are very abundant proteins, which could be why they appear non-specifically.

Amongst the proteins enriched in H3.3 binding after UV (Table 3), two DNA damage associated proteins appear: MSH6 and MDC1.

Table 3 H3.3 interactors enriched after UV damage in order of decreasing percentage of total spectra

Protein	*Protein name*	*Brief description of function*	*Cellular localisation*
MDC1	Mediator of DNA damage checkpoint protein 1	Activates the S and G2/M phase cell cycle checkpoints in response to DNA damage. Interacts with H2AX to recruit repair proteins to DNA damage foci.	Nucleus
BRWD1	Bromodomain and WD repeat-containing protein 1	May be involved in transcriptional activation and chromatin remodelling.	Nucleus
MSH6	DNA mismatch repair protein Msh6	Dimerises with MSH2 to form MutS which detects mismatched DNA and initiates mismatch repair.	Nucleus
DHX15	DEAH-box helicase 15	Putative ATP-dependent RNA helicase implicated in pre-mRNA splicing	Nucleus
PRPF8	Pre-mRNA-processing-splicing factor 8	Scaffolds U2, U5 and U6 snRNAs at splice sites on pre-mRNAs	Nucleus
UTP20	Small subunit processome component 20 homolog	Component of U3 snoRNA and involved in 18S rRNA processing	Nucleus
RRP1B	Ribosomal RNA processing protein 1 homolog B	60S ribosomal RNA processing. Potentially modulates chromatin structure	Nucleus

RRP5	Protein RRP5 homolog	Involved in biogenesis of rRNA	Nucleus
SPB1	pre-rRNA processing protein FTSJ3	Methyltransferase involved in pre-rRNA processing	Nucleus
IF4G1	Eukaryotic translation initiation factor 4 gamma 1	Part of the complex which recruits mRNA to the ribosome.	Cytosol
IMDH2	Inosine-5'-monophosphate dehydrogenase 2	Enzyme in de novo guanine biosynthesis pathway	Cytosol
PDCD61P	Programmed cell death 6-interacting protein	Functions in the abscission stage of cytokinesis	Cytoskeleton, cytosol, extracellular
MACF1	Microtubule-actin cross linking factor 1	Facilitates actin-microtubule interactions	Cytoskeleton
SPTAN1	Spectrin alpha chain, non-erythrocytic 1	Filamentous cytoskeletal protein. Implicated in cell cycle regulation and DNA repair.	Cytoskeleton
PTCD3	Pentatricopeptide repeat domain-containing protein 3	Mitochondrial translation protein	Mitochondria

MSH6 is part of the mismatch repair pathway, a form of excision repair. MSH6 acts with MSH2 as a heterodimer to recognise mismatched DNA. Mismatch repair can play a role in the response to UV damage, with cells lacking mismatch repair bearing a higher mutation load after UV (Borgdorff *et al.*, 2006). MSH6 has been reported to interact with H3K36me3 (Vermeulen *et al.*, 2010), which immediately suggests a possibility for H3.3 interaction.

MDC1 is involved early on in the response to DNA damage, acting as a scaffold to recruit DNA signalling and repair factors. MDC1 has many interactors important to DNA damage signalling, including components of the MRN complex, γH2AX, ATM and p53 (Coster and Goldberg, 2010). It has not previously been linked to H3.3.

MDC1interacts with and MSH6 co-localises with γH2AX (Vermeulen *et al.*, 2010; Shahi *et al.*, 2011), a DNA damage marker I have observed to be raised in *h3.3* cells after UV. H3.3 has not been reported to be enriched in nucleosomes containing H2AX, so it seems

unlikely that their interaction with H3.3 is mediated by H2AX in a double variant nucleosome.

Both MDC1 and γH2AX tend to be associated with DSBs. The high dose of UV used prior to GFP Trap pulldown could potentially lead to double strand breaks. TK6 cells spend approximately 65 % of their cell cycle in S phase. If UV lesions are encountered by a replication fork, it could be converted to a DSB. I may therefore be examining interactors involved in double strand break repair, rather than nucleotide excision repair.

These interactions would need to be validated further, but both these proteins provide interesting possibilities for a role of H3.3 after UV damage, with both DNA damage repair and signalling pathways remaining a possibility. MSH6 could be interesting to follow up, as it has been shown to bind H3, but H3.3 has not been implicated in mis-match repair previously.

There are also several H3.3 interactors after UV which are involved with splicing. It is possible that H3.3 is implicated in splicing, as the H3.3 specific interactor ZMYND11 plays a part in intron retention.

The conclusions which can be drawn from this list of interactors remains limited, as a canonical H3-GFP control was not used. These interactors may therefore not be specific to H3.3 but associated with chromatin more generally after UV damage.

Additionally, Figure 3.9 shows that H3.3GFP does not seem to fully rescue the H3.3 knockout phenotype, with insufficient incorporation into chromatin being a possible explanation. If there is limited incorporation of H3.3GFP into chromatin, interactors recovered from the GFP-Trap may not be binding to chromatin.

To take this experiment forward, MSH6 and MDC1 would need to be validated as H3.3 specific interactors, for example by western blotting after immunoprecipitation. An H3.2-GFP expressing cell line could be used as a control to determine H3.3 specific binding or an H3.3S31A-GFP expressing cell line could determine if the interactors bind to the H3.3 specific N-terminal tail. Cellular fractionation before proteomic analysis could help

eliminate proteins outside the nucleus and unlikely to be involved in DNA damage response.

Chapter 6: Genetic interactors of H3.3

Genetic interactors of H3.3 have not previously been studied. Whilst proteomic approaches can inform us of protein-protein interactions specific to H3.3, and in particular after UV, genetic interactions could inform us of relationships between genes and pathways. To probe genetic interactions, I used a CRISPR screen. By using an H3.3 deficient cell line, a CRISPR screen can ask which genes, when removed, change the viability of *h3.3* cells.

A dropout CRISPR Cas9 knockout screen works by systematically disrupting every gene in the genome. Usually, there are multiple guides to each gene to provide for redundancy and increase the power of the downstream statistical analysis. The guide RNAs and Cas9, if the enzyme is not already expressed in the cells, are delivered by lentiviral vectors and cells with a gene targeted that is essential for survival in the genetic background in question will die or become less fit. The infecting viral titre is set so that, on average, cells take up one or no guides. This will result, in time, in guides that reduce fitness being lost from the pool of cells. This is assessed by recovering the guides from cells population after a given period that allows editing and for cells to drop out of the population. This will reveal guides that target genes that are both intrinsically essential and those that are essential only in the genetic condition under test, in this case H3.3 deficiency. It is also possible to stress the cells, and in this case I also carried out the screen in the presence of the DNA damaging agent 4-nitroquinoline-1-oxide (4-NQO) (Galiegue-Zouitina, Bailleul and Loucheux-Lefebvre, 1985).

6.1 Creating and validating stably expressing Cas9 cell lines

Since vectors carrying both Cas9 and guides are large, reducing the efficiency with which they are taken up into cells, I opted to integrate Cas9 into the known safe harbour locus AAVS1. I transfected 2 plasmids into each cell line. One contained a gRNA against the AAVS1 locus (pX330sgAAVS1) (gifted from the Patel lab) and the other Cas9 with homology arms matching the AAVS1 locus (pBSAAVS1Cas9-YFP-bsd) (created by C. Mellor and S. Šviković). Colonies were picked after antibiotic selection with blasticidin and screened by flow cytometry for YFP expression (Figure 6.1a). Most of the populations

have very similar levels of YFP expression, suggesting the Cas9YFP has integrated the same number of times. To obtain monoclonal populations, the YFP positive lines were plated at a limiting dilution before undergoing flow cytometry again. Lines with matched levels of YFP expression were taken forward (Figure 6.1b).

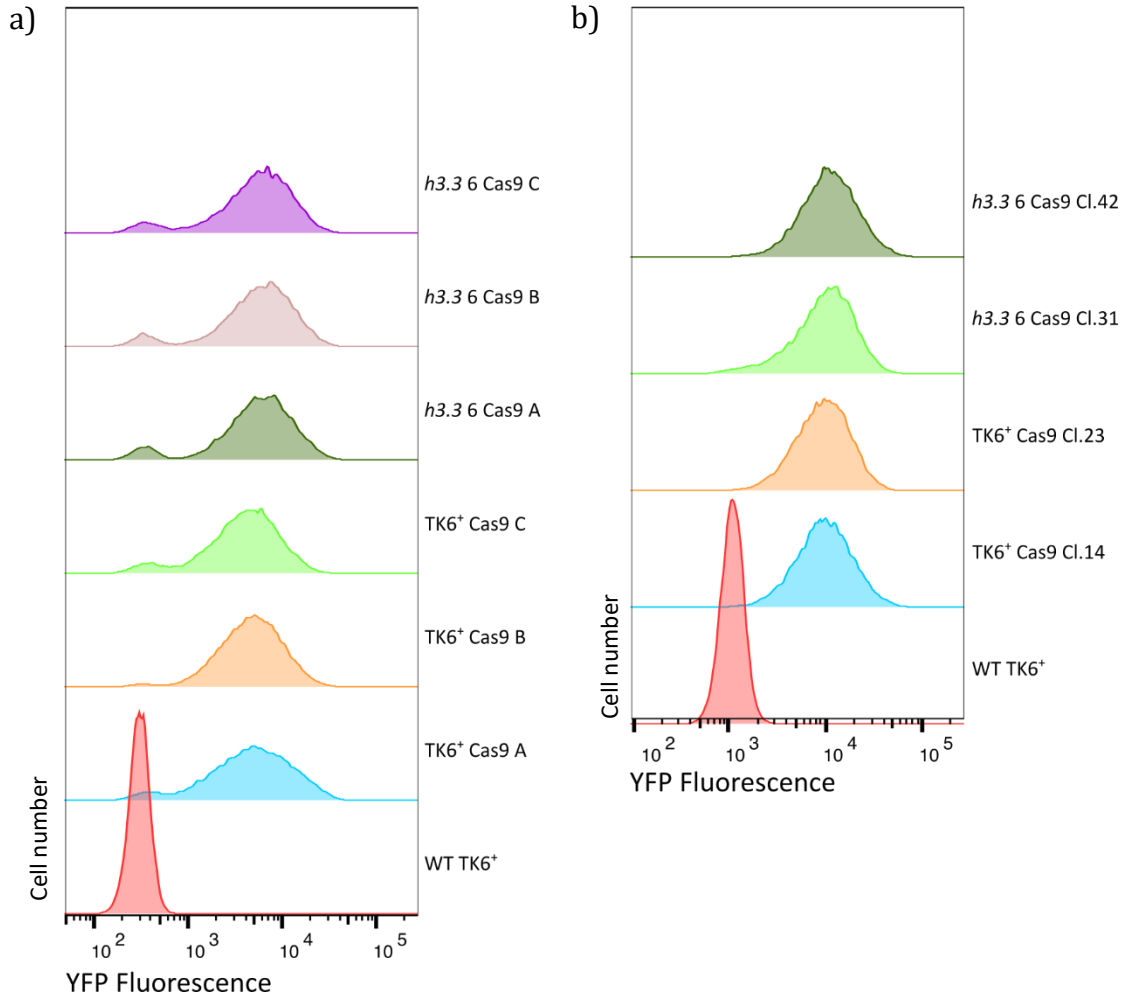

Figure 6.1 Creating cell lines with stably integrated Cas9. a) Fluorescence of Cas9 integrated bulk populations. b) Fluorescence of Cas9 integrated clonal populations.

In order to assess the cutting efficiency of the Cas9 expressing cell lines, I used a system previously established in the lab by C. Mellor, targeting a surface expressed marker, MHC Class I, and staining and assessing the percentage of cells that had lost surface expression. To do this, I produced a lentivirus library containing 5 guides against beta-2-microglobulin (B2M), a component of the MHC class 1 complex, and essential for it to be expressed on the cell surface (Figure 6.2a).

To determine the amount of virus needed for an MOI of 0.3, which by the Poisson formula creates the desired condition of the majority of cells taking up one or no guide-containing virus, TK6 Cas9 cells were infected with varying volumes of empty or B2M lentiviral library. Flow cytometry was carried out to determine levels of infection of by gRNA-containing virus by monitoring BFP fluorescence, which was driven from the same virus. This allowed me to calculate the multiplicity of infection to ensure that the quantity of virus used will lead to no more than 1 viral particle per cell using the Poisson formula (Figure 6.2b).

Once the titre of virus for an MOI of 0.3 had been established (35 µl/ml), cells with and without Cas9 were infected with the empty or B2M mini-library at an MOI of 0.3 to determine the activity of the integrated Cas9. After infection and selection cells were collected and stained for MHC. The proportion of MHC negative (and therefore successfully targeted) cells was assessed by flow cytometry (Figure 6.2c). This shows the integrated Cas9 is active in both WT Cas9 and *h3.3* Cas9 cell lines.

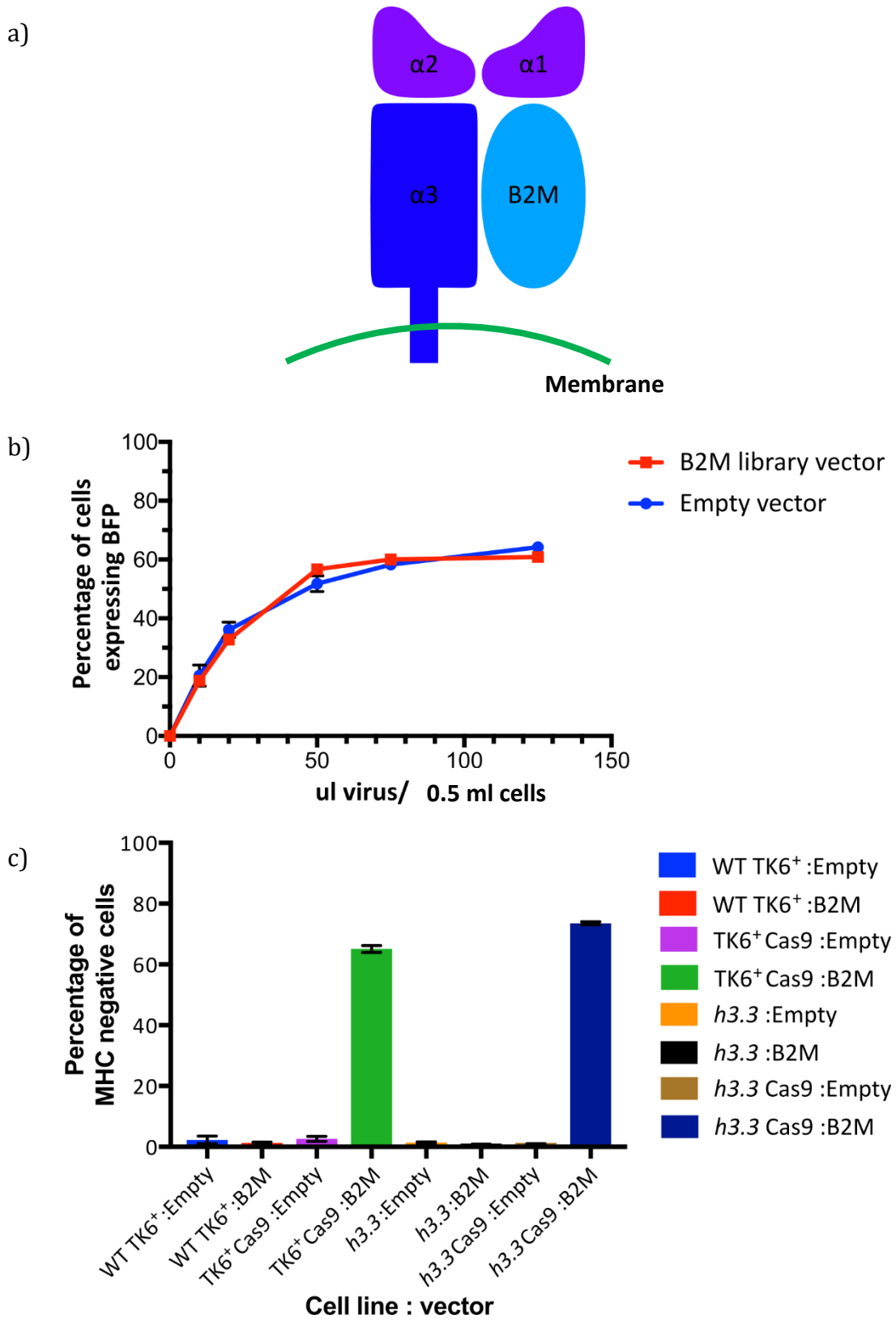

Figure 6.2 Validating Cas9 activity in integrated cell lines a) Schematic of MHC Class I, showing the targeted B2M unit. B) Percentage of live, single cells expressing BFP. Mean of 3 technical replicates shown, error bars show standard deviation c) Percentage of live, single cells negative for MHC staining. Mean of 3 technical replicates shown, error bars show standard deviation. One-way ANOVA determined samples TK6+ Cas9:B2M and *h3.3* Cas9:B2M statistically significant

There is little difference in doubling times between WT Cas9 and *h3.3* Cas9 cell lines (Figure 6.3), so CRISPR screen timescales do not need to be adjusted for each cell line.

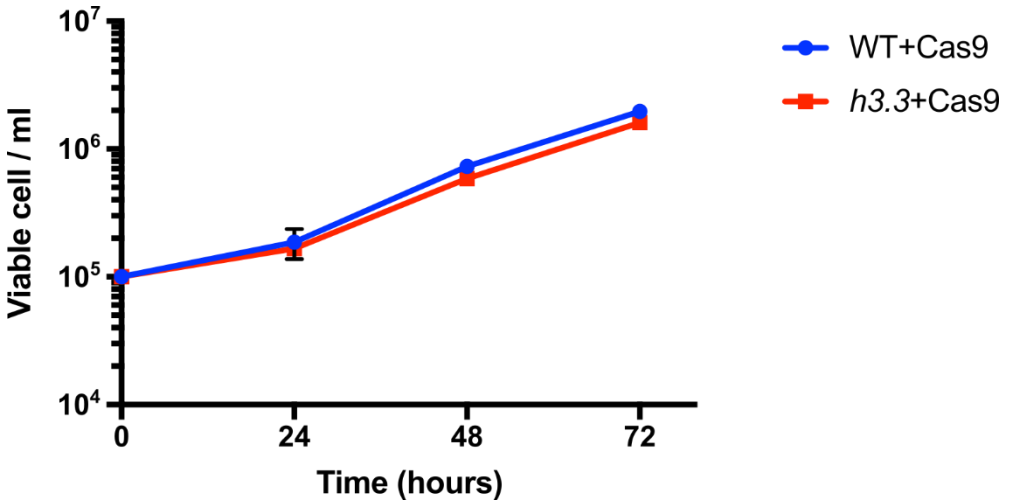

Figure 6.3 Growth curve of WT + Cas9 and *h3.3* + Cas9 cell lines. Error bars show standard deviation of 3 technical replicates

6.2 Determining NQO dosage

UV irradiation is not practical to use on large volumes of cells, as the bulb available in our lab only targets 10 cm^2. A large depth of media can mean some cells are shielded by overlapping cells, and the UV is attenuated by medium and the proteins it contains. Thus, the irradiation received by the cells is not constant or controllable. In order to induce damage in the large volume of cells required in a CRISPR screen, I used the small molecule 4-Nitroquinoline 1-Oxide (NQO). NQO has been described as a UV mimetic, but this is based on similar cellular responses and genetic requirements for tolerance as for UV. It does not produce the same DNA lesions as UV. However, the adducts it creates are repaired by NER, like UV lesions (Jones, Edwards and Waters, 1989).

To determine concentration of NQO to use to induce damage during the CRISPR screen, I carried out a colony survival assay of TK6 cells with acute NQO treatment (Figure 6.4).

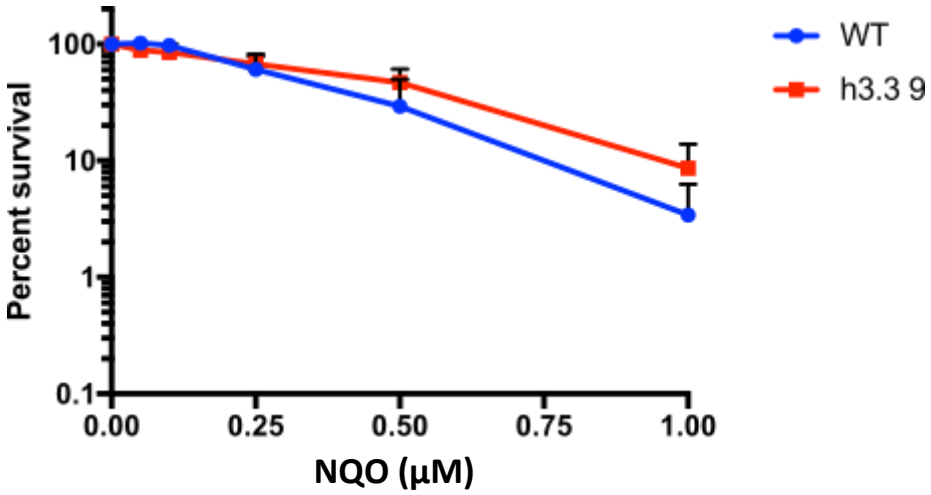

Figure 6.4 Survival after acute NQO treatment Percentage survival was calculated relative to untreated cells. 2 technical repeats per experiment, mean of 3 experiments shown here. Error bars show standard deviation. At 1 µM NQO, the difference between *h3.3* 9 and WT is not significant by unpaired t-test.

From this, I could determine that the dose of NQO which give an equivalent survival to the 4 J/m^2 used in other experiments is around 0.5 µM. However, the colony survival assay uses acute genotoxic treatment, whereas the CRISPR screen uses chronic treatment. Therefore, I used a lower dose of 0.1 µM NQO in the CRISPR screen.

6.3 Carrying out the CRISPR screen

Cas 9 expressing WT and *h3.3* cell lines were spinfected (see section 2.10.1) with a lentiviral library, at a multiplicity of infection of 0.3 to ensure only one lentivirus/gRNA per cell on average. The library used, known as the Yusa library (Tzelepis *et al.*, 2016), uses 5 gRNAs per gene in the whole genome, totalling 90,709 gRNAs against 18,010 genes. Using 5 guides against each gene ensures that even if some guides target less effectively, redundancy ensures each gene is likely to be targeted.

Enough cells were transfected and maintained throughout passaging to ensure 1000x coverage. 4 screens were carried out, WT and *h3.3* untreated and WT and *h3.3* with NQO. Cells were screened by flow cytometry to ensure the multiplicity of infection was not above 0.3, to be confident that each cell only contains no more than 1 gRNA. Cells were then selected with puromycin. At this 7-day timepoint, selection was removed and NQO added to a WT and a *h3.3* screen. NQO was topped up in fresh media every day for 7 days, whilst the untreated screen continued passaging alongside. NQO was then removed from

and both screens were passaged for another 7 days. This final untreated phase was demonstrated by C. Mellor in a similar screen increase the confidence with which differential hits could be identified. Cells were then collected and genomic DNA harvested.

6.4 Library preparation and sequencing

Libraries for next generation sequencing were prepared from the genomic DNA of each screen (see section 2.10.7). First, PCR primers either side of the inserted gRNA sequenced were used to amplify the gRNAs present in the screened population. A second round of PCR was then carried out on the amplified gRNAs to add a barcode for sequencing, in order to differentiate each sample once pooled for sequencing (Figure 6.5).

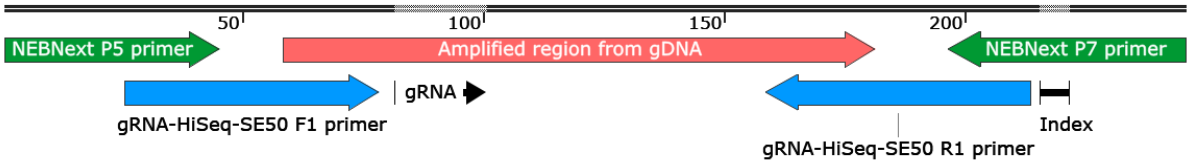

Figure 6.5 Map of library for sequencing Amplification primers in blue, indexing primers in green, genomic DNA in red

Sequencing was carried out on a NovaSeq, using a 150 bp paired end run. The protocol had been designed (by S. Šviković) for use with a custom primer to maximise the read length of the guide that could be obtained with 50 bp single end sequencing, but the custom primer was not compatible with the NovaSeq run, and so a longer read length was required.

6.5 Sequencing analysis

C. Mellor kindly carried out analysis of this sequencing. Reads were aligned to the gRNA sequences of the Yusa Library using MAGeCK 0.5.

Unfortunately, no reads aligned from the WT + NQO screen library preparation, suggesting that the library preparation had failed. Therefore, the *h3.3* + NQO screen has no control, so H3.3 specific hits after damage could not be determined. In the other 3

samples, whilst 85 % of the reads aligned, there were only enough reads to provide around 100 X coverage, rather than the 500-1000 X coverage hoped for. This means not all relevant hits may be discovered.

As an internal control to determine the screen has worked as expected, fitness genes were compared to existing datasets. Fitness genes were defined as genes whose guides were depleted from the untreated WT cells compared to the starting Yusa guide library, with a False Discovery Rate (FDR) < 0.05. This gave a list of around 1700 genes, which were compared to fitness genes found by C. Mellor from a similar screen and core fitness genes shared across 5 cell lines by Hart *et al.*, 2015. (Figure 6.6). This demonstrated that the majority of the fitness genes identified in my screen have been identified as fitness genes elsewhere, despite different approaches, and so suggested that the screen was working as expected.

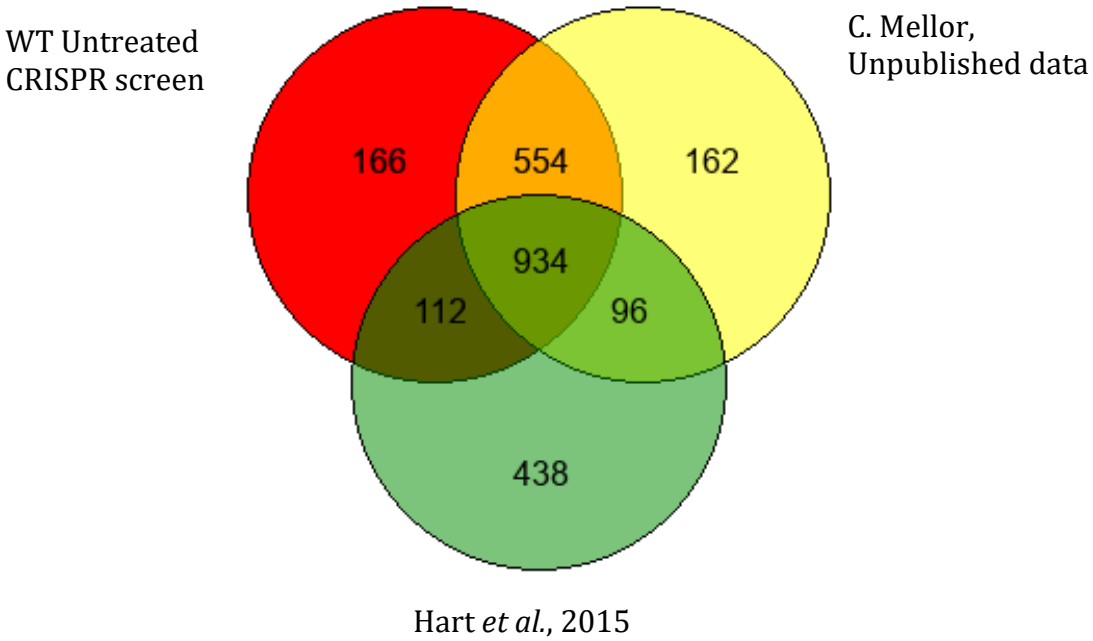

Figure 6.6 Overlap in 'fitness' genes in three databases. Number of fitness genes overlapping between 3 screens. WT Untreated and C. Mellor data is both for TK6 cells and using the Yusa library.

Despite the failure of the DNA damage exposed experiment, I was able to look for genetic interactions with H3.3 that affected fitness in unperturbed conditions. Guide abundance was compared between the 2 screens, and the log fold change in enrichment or depletion in the H3.3 comparted to WT sample were plotted against MAGeCK derived p-values to generate a 'volcano' plot. A 'hit' was determined as a point with an FDR of < 0.1 (Figure 6.7 and Tables 4 and 5)

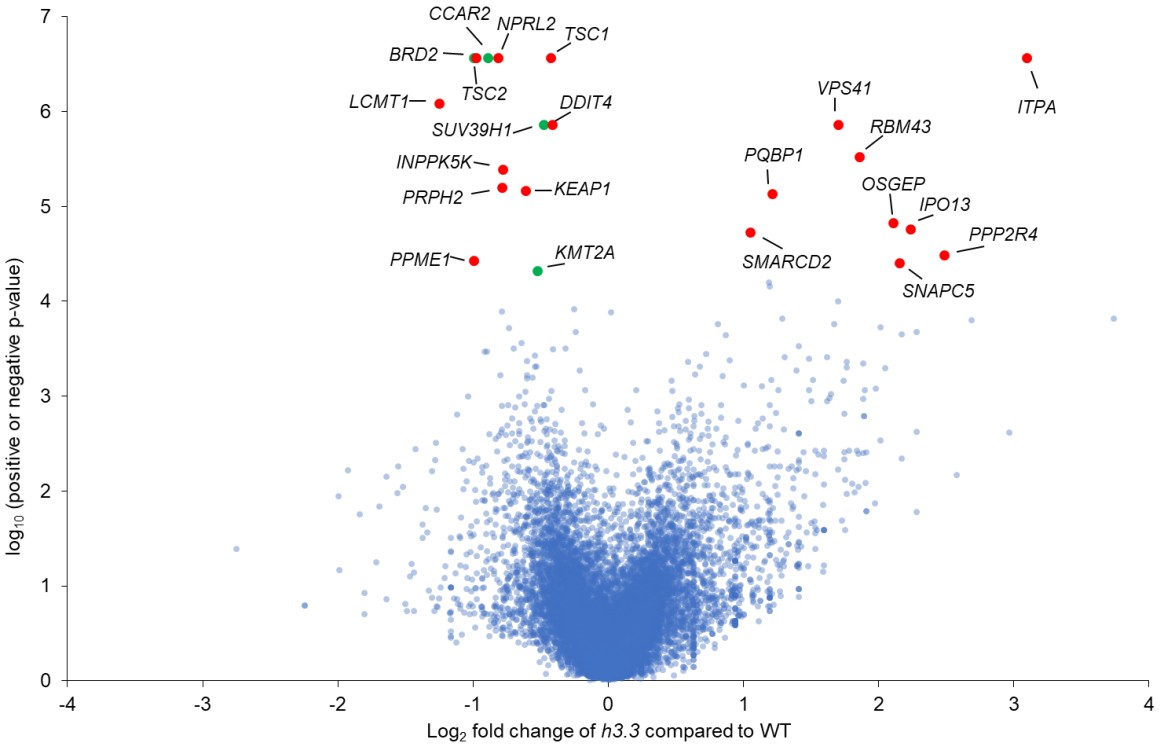

Figure 6.7 Volcano plot of CRISPR Screen results. Volcano plot of MAGeCK derived p-values of gRNAs. Log fold change plotted on the x axis against the log p-value – negative p- value when log fold change is < 0 and positive p-value when log fold change is > 0. Hits with a false discovery rate of <0.1 denoted in red, hits discussed in relation of H3.3 in green.

Hits with a positive p-value are enriched in the *h3.3* screen compared to WT, and therefore their loss improves the survival of cells lacking H3.3 (Table 4).

Table 4 Hits enriched in *h3.3* screen in order of decreasing $\log_{10}$ (positive p-value)

Protein	*Protein name*	*Brief description of function*	*Cellular localisation*
ITPA	Inosine Triphosphatase	An Inosine Triphosphate Pyrophosphohydrolase	Cytosol
VPS41	Vacuolar Protein Sorting-Associated Protein 41 Homolog	Involved in formation and fusion of transport vesicles	Cytosol, Lysosome
RBM43	RNA binding protein 43	Modulates cyclin B1 expression	Nucleus
PQBP1	Polyglutamine binding protein 1	Involved with transcriptional activation	Nucleus
SMARCD2	SWI/SNF Related, Matrix Associated, Actin Dependent Regulator of Chromatin, Subfamily D, Member 2	Chromatin remodeller	Nucleus
OSGEP	O-Sialoglycoprotein Endopeptidase	Acyl transferase activity	Plasma membrane, nucleus
IPO13	Importin 13	Nuclear transport protein	Nucleus
PPP2R4	Protein Phosphatase 2 Phosphatase Activator	Ser/Thr phosphatase	Nucleus
SNAPC5	Small Nuclear RNA Activating Complex Polypeptide 5	Transcription of snRNA genes	Nucleus

Hits with a negative p-value are depleted in the *h3.3* screen compared to WT, and therefore cells lacking H3.3 and this 'hit' gene cannot survive.

Of the 13 hits depleted in the absence of H3.3 (Table 5) i.e. genes whose removal results in synthetic sickness when H3.3 is absent, 4 have obvious possible links to H3.3. SUV39H1 has H3K9 methyltransferase activity, KMT2A has H3K4 methyltransferase activity, BRD2 can bind H4ac and CCAR2 acts as a tumour suppressor.

Table 5 Hits depleted in *h3.3* screen in order of decreasing $\log_{10}$ (negative p-value)

Protein	*Protein name*	*Brief description of function*	*Cellular localisation*
BRD2	Bromodomain Containing 2	H4K12ac interactor	Nucleus
TSC2	TSC Complex Subunit 2	Tumour suppressor which negatively regulates mTORC1 signalling	Cytosol
CCAR2	Cell cycle and apoptosis regulator 2 (also known as DBC1)	Alternative splicing and p53 stabilisation	Nucleus
NPRL2	Nitrogen Permease Regulator 2-Like Protein	A component of GATOR1 complex, inhibiting mTORC1 signalling	Lysosome, Cytosol
TSC1	TSC Complex Subunit 1	Tumour suppressor which negatively regulates mTORC1 signalling	Cytosol, Plasma membrane
LCMT1	Leucine Carboxyl Methyltransferase 1	Methylates K309 of PP2A	Nucleus, Cytosol
SUV39H1	Suppression of Variegation 3-9 Homolog 1	H3K9 methyltransferase	Nucleus
DDIT4	DNA Damage Inducible Transcript 4	Regulates p53-mediated apoptosis by inhibition of mTORC1	Cytosol, Mitochondria
INPP5K	Inositol Polyphosphate-5-Phosphatase K	5-phosphatase activity towards polyphosphate inositol	Plasma membrane, Nucleus, Cytosol
PRPH2	Peripherin 2	Cell surface glycoprotein in rod and cone photoreceptor cells	Plasma membrane
KEAP1	Kelch Like ECH Associated Protein 1	Sensor of oxidative and electrophilic stress	Cytoskeleton, Nucleus, Cytosol
PPME1	Protein Phosphatase Methylesterase 1	Demethylates PP2A	Nucleus
KMT2A	Lysine methyltransferase 2A	H3K4 Methyltransferase	Nucleus, Cytosol

BRD2 binds a nucleosome via H4K12ac (Filippakopoulos *et al.*, 2012) and has potential roles in DNA repair. BRD2 is recruited to DSBs, where it promotes spreading of H4Kac either side of the break and is required for repair (Gursoy-Yuzugullu, Carman and Price, 2017). H3.3 could be involved in chromatin rearrangements around sites of lesions

(Soria, Polo and Almouzni, 2012), so the relationship between H3.3 and BRD2 could be worth further investigation.

CCAR2 have several roles which could be interesting to investigate further in relation to H3.3. CCAR2 is a member of the DBIRD complex which acts at the interface between RNAPII and pre-mRNA to regulate splicing (Close *et al.*, 2012). H3.3 could have role in alternative splicing through its interactor ZMYND11, which interacts with components of the spliceosome and regulates intron retention.

CCAR2 also acts as a tumour suppressor, interacting with MDM2 to stabilise p53 (Qin *et al.*, 2015). Additionally, it has roles after DNA damage. CCAR2 can be recruited to double strand breaks an influence choice of repair pathway (López-Saavedra *et al.*, 2016), favouring NHEJ as it protects against end resection. This could have possibilities for the role of H3.3 in NHEJ (Li and Tyler, 2016).

CCAR2 interacts with another hit, SUV39H1 to inhibit its H3K9 methyltransferase activity (Li *et al.*, 2009). These several possible roles in splicing, DNA damage repair and interaction with a H3 methyltransferase offers potential for pathways involving H3.3.

The activity of SUV39H1 could easily apply to H3.3, as H3.3 can be modified like the canonical H3 as it shares most of the same residues. It seems very likely that SUV39H1 acts on H3.3, as SUV39H1 is recruited to promote heterochromatin by ATRX/DAXX, which also deposits H3.3 (He *et al.*, 2015).

KMT2A is another methyltransferase, methylating H3K4 which is associated with active genomic regions (Rao and Dou, 2015). This finding of methyltransferases associated with both euchromatin and heterochromatin related to H3.3 is consistent with the duality of H3.3 existing both at telomeres and active transcriptional start sites.

The library preparation and sequencing would ideally need to be repeated to find DNA damage specific H3.3 genetic interactors, as the untreated screens are intended as a control to separate out damage related hits.

Chapter 7: Discussion

7.1 Summary

Previous work in DT40 showed H3.3 is required for fork progression and cell survival after UV damage. The sensitivity of H3.3-deficient cells to UV was epistatic with loss of the NER factor XPA ,but not with the key translesion synthesis factor REV1 (Frey *et al.*, 2014), suggesting a model in which H3.3 incorporation during the replication of UV damage may somehow facilitate its subsequent repair. Other studies have also reported role for H3.3 and its two chaperones, ATRX and HIRA, in various DNA damage repair and recovery pathways (see section 1.4). To further investigate the role of H3.3 and its chaperones, I created mutated cell lines, removing H3.3 and HIRA and depleting ATRX in the non-transformed human cell line TK6. *h3.3* cells show no survival defect in response to UV, but the damage markers γH2AX and phospho-p53 remain raised longer than in WT cells, pointing to a delay in damage resolution in the absence of H3.3. Cell cycle analysis reveals a G1 block in *h3.3* cells, supporting the idea that damage is not being resolved in a timely manner. Removing p53 demonstrates this G1 arrest is mediated by p53. The ATRX deficient cell line mirrored this accumulation in G1 after UV, but HIRA did not. This shows ATRX likely mediates the role of H3.3 in the cell cycle changes after UV damage, rather than HIRA. The GFP Trap pulldown after UV demonstrated the possibility that H3.3 could interact with members of DNA damage repair and signalling pathways.

In this section I will discuss the possibilities of H3.3 involvement in repair of and recovery from DNA damage and address the questions:
How, when and where is H3.3 deposited?
What function does H3.3 have once deposited after damage?
How do my findings fit into the current knowledge of H3.3 and its chaperones after DNA damage?
How does research in different systems or use of different methodologies impact interpretation of my and others findings?

7.2 H3.3 deposition after UV induced damage

7.2.1 Is H3.3 deposited after damage at the replication fork?

In DT40 cells, H3.3 is required for survival and fork progression after UV irradiation with the chaperone binding patch essential to both (Frey *et al.*, 2014). Their model proposed that this requirement could be due to H3.3 deposition at the fork as it encounters DNA damage. As ATRX has previously been implicated at stalled replication forks (Leung *et al.*, 2013; Clynes *et al.*, 2014; Huh *et al.*, 2016), if H3.3 is deposited at replication forks, ATRX/DAXX seems the most likely candidate as chaperone.

In TK6 cells, I do not find a requirement for H3.3 in either survival or fork progression after UV, but my results show the H3.3 chaperone ATRX plays a role in the response to UV damage, with deposition of H3.3 a likely function. As I do not find a role in replication fork progression after UV for either H3.3 or ATRX, the possibility remains that ATRX could deposit H3.3 outside S phase in the response to UV damage. However, whilst H3.3 has been implicated in DNA damage repair types which occur outside S phase (Adam, Polo and Almouzni, 2013; Frey *et al.*, 2014; Li and Tyler, 2016), ATRX only has reported roles in homologous recombination (Juhász *et al.*, 2018), which occurs during S phase.

7.2.2 Is H3.3 deposited after damage outside S phase?

A major difference between H3.3 and the canonical H3.1 and H3.2 histones is the presence of H3.3 throughout the cell cycle. The canonical histones are only expressed during S phase, so as to provide a supply of new histones to wrap newly synthesised DNA, whereas H3.3 is expressed in all phases of the cell cycle. This means that if deposition of new histones is required outside of S phase, H3.3 is likely the histone variant deposited. Newly synthesised H3.3 has been shown to have roles in various types of DNA damage response (Adam, Polo and Almouzni, 2013; Juhász *et al.*, 2018), some of which occur outside S phase, by studies using the SNAP-tag system of labelling H3.3 synthesised during the experiment.

However, the histone H4 (which has no variants) which H3.3 pairs with to be incorporated into a nucleosome is only synthesised during S phase (Mitra *et al.*, 2003).

Therefore, if H3.3 is to be incorporated outside S phase, there must be a supply of recycled H4.

If a repair pathway requires new histones to resolve a lesion outside S phase, it would require H3.3, and therefore a lack of H3.3 could lead to a delay in resolving DNA damage. UV lesions are often repaired by nucleotide excision repair, and Frey et al. demonstrated epistasis between H3.3 and XPA, a member of the NER pathway. Nucleotide Excision Repair requires some rearrangement of nucleosomes (Luijsterburg *et al.*, 2012) in order to access and repair and repair a lesion. After the repair is completed, chromatin is again remodelled (Polo and Almouzni, 2015) (see section 1.3.2.3.1). Potentially, this remodelling could be an opportunity for replication independent incorporation of H3.3 as part of recovery from DNA damage.

HIRA has been reported to have a role in H3.3 after UV induced DNA damage (Adam, Polo and Almouzni, 2013). They did not observe sensitivity of cells lacking HIRA to UV, and in my results I also found no role for HIRA in survival after UV damage, nor in cell cycle changes. This absence of role for HIRA after UV in the assays I have tested, where a role for ATRX was observed, could be due to the difference between damage resolution and chromatin rearrangements after damage repair.

Whilst my results implicate ATRX after UV induced damage, ATRX has not previously been linked to NER and has only been demonstrated to have a role in HR. It could be possible that UV lesions are leading to other types of damage, which are resolved by pathways other than NER and that is why I see a role for ATRX.

7.3 H3.3 incorporation/presence could affect repair factor access or recruitment to lesion

Which property of H3.3 is needed for its function in DNA damage resolution is still unclear. The expression of H3.3 throughout the cell cycle could play a part in its role, but H3.3 also has the potential to alter chromatin packing or signal to other factors which could aid repair.

7.3.1 Does H3.3 change chromatin packing to facilitate repair?

H3.3 has been shown to have an impact on chromatin packing, being implicated in a looser chromatin structure, with areas enriched in H3.3 exhibiting MNase sensitivity, suggesting greater spacing between nucleosomes (Chen *et al.*, 2013). Additionally, cells with reduced H3.3 have increased H1, which could lead to an increased nucleosome repeat length, whereby a greater proportion of DNA is bound to a nucleosome (Braunschweig *et al.*, 2009). This ability of H3.3 to change chromatin packing could explain its role in the response to DNA damage. If H3.3 were to be deposited at or around sites of DNA damage, the resulting loosening of chromatin packing could allow greater access of signalling and repair factors to the lesion and therefore facilitate repair.

7.3.2 Could H3.3's impact on chromatin packing affect the damage load received?

This impact of H3.3 on chromatin packing could have an impact on the load of DNA damage received by a cell lacking H3.3. If a cell without H3.3 received a greater load of UV lesions, this could be a reason why DNA damage could take longer to resolve and have a greater impact on the cell cycle – there is simply more damage to resolve. This would suggest that H3.3 is not needed for the resolution of damage, rather the damage received by a cell is a function of the presence or absence of H3.3 and the resulting chromatin packing.

However, I do not think this is sufficient to explain the impact of UV on *h3.3* cells. Cells lacking H3.3 could be expected to have a more tightly packed chromatin structure. It has been demonstrated that damage is less likely to occur on DNA which is wrapped around a nucleosome (Gonzalez-Perez, Sabarinathan and Lopez-Bigas, 2019), therefore I would not expect *h3.3* to receive a greater damage load then their WT counterparts. Additionally, challenging WT with higher doses of UV irradiation did not lead to the same phenotype as seen in *h3.3* cells with lower UV doses, which I would expect to happen if a change in damage load received is the only cause of the differences between the *h3.3* and WT cell lines. Therefore, I believe H3.3 does have an impact on the resolution of UV induced DNA damage and any contribution of an altered load of lesions due to a change in chromatin packing in the absence of H3.3 is not a major factor.

7.3.3 Does H3.3 recruit factors to facilitate repair?

The H3.3 specific residue S31 on the N terminal tail provides intriguing possibilities for the function of H3.3. As the N terminal tail protrudes from the body of the nucleosome, it is accessible to the environment around it and would be an ideal site for modification and/or signalling. The S31 tail residue has been demonstrated to be able to have a specific reader, eg. ZMYND11 binds H3.3 via S31 in the context of H3K6me3 (Guo *et al.*, 2014; Wen *et al.*, 2014). Additionally, the S31 residue can be phosphorylated (Sitbon *et al.*, 2020), adding more modulation of possible signalling.

In the context of DNA repair, this specific N-terminal tail offers the possibility for H3.3 containing nucleosomes near a lesion to signal and recruit factors to sites of DNA damage, thereby facilitating repair, essentially 'labelling' the site of repair. The GFP Trap results demonstrating MDC1 as a potential H3.3 interactor after UV could place H3.3 into DNA damage signalling pathways. This possibility could be investigated further.

7.3.4 Does H3.3 directly impact DNA damage signalling?

H3.3 could have impacts on signalling other than 'labelling' sites of lesions. DNA damage markers (γH2AX and phospho-p53) remain raised in cells lacking H3.3 after UV damage, which could either be down to a persistence of DNA damage or an inability for cells lacking H3.3 to downregulate DNA damage signalling. H3.3 could directly impact DNA damage signalling.

H3.3 could be required as part of chromatin reassembly after DNA damage repair has occurred (Adam, Polo and Almouzni, 2013; Li and Tyler, 2016). H3.3 in these studies has been determined to not be involved in repair of the lesion itself, but required for cellular recovery after repair of the lesion has occurred, particularly as part of rechromatinisation. H3.3 could therefore be incorporated at sites of lesions after the damage has been repaired as part of chromatin reassembly. H3.3 deposition at the site of a repaired lesion could act as a signal that repair and recovery from DNA damage is complete. This 'completion' signal could be detected by an H3.3 interactor and lead to downregulation of DNA damage signalling pathways, such as ATM/ATR pathways. If H3.3 deposition at the site of a repaired lesion acts as a signal that repair and recovery is complete, the absence of H3.3 would interrupt this signal and could lead to a persistence

of DNA damage markers remaining raised, even if the damage itself is resolved, as the cell has not fully completed recovery from the damage.

7.4 Chaperones

7.4.1 ATRX in DNA damage repair

Other studies which examine ATRX at replication forks have examined replication stress induced by HU (which interrupts the supply of nucleotides), as opposed to DNA damage as I have done. Whilst they find ATRX is required at stalled forks and for fork restart (Leung *et al.*, 2013), one study found that ATRX only affected a subset of forks, increasing the frequency of very slow replicating forks (Clynes *et al.*, 2014). This indicates that ATRX may only be required for a subset of forks, and so if ATRX and H3.3 do have a role at the fork after DNA damage (as observed in DT40 cells, but not in TK6), then it is possible it is only at a subset of forks, for example, only in certain regions of the genome. The global approach on asynchronous cells I have taken may not be sensitive enough to observe a subtle effect. I do observe an increase in the S arrest population during cell cycle analysis in *h3.3* and *atrx* lines. This could be due to a small subset of replication forks requiring H3.3 and ATRX for progression after damage, and failure for forks to progress would leave cells with an intermediate DNA content but not incorporating nucleotides, and therefore part of the 'S arrest' population. However, this increased S arrest population does not become apparent until later timepoints (24 hrs), so I believe it more likely to be a result of fork collapse due to persistent, unresolved DNA damage.

ATRX has been implicated in DNA damage repair, in NHEJ (Koschmann *et al.*, 2016) and in homologous recombination (Juhász *et al.*, 2018), which fits with its potential role in ALT (Sobinoff and Pickett, 2017). My results show a role for ATRX after UV induced damage (which is typically repaired by NER). If ATRX has a role in damage repair which occurs outside of S phase, eg. NER, it could be due to a requirement for new histone deposition. As H3.3 is produced throughout the cell cycle it is available for incorporation and ATRX could mediate this. However, ATRX has a role in HR (Juhász *et al.*, 2018), which occurs during S phase, where it deposits H3.3. As ATRX can deposit H3.3 in response to

damage when other histones are available, the possibility remains that a biochemical property of H3.3 or ATRX (other than its presence throughout the cell cycle) is required for UV damage repair via NER. It could be the impact of H3.3 on chromatin packing or signalling potential which ATRX deposition mediates to explain the requirement of ATRX after damage. ATRX must be able to be recruited to sites of damage in order to deposit H3.3. If the damage is being repaired during S phase, it is possible that ATRX could encounter a lesion by associating with a fork which has stalled on encountering the lesion. If damage repair occurs outside S phase, ATRX may interact with damage signalling factors in order to deposit H3.3 in response to damage.

7.4.2 HIRA in DNA damage repair

HIRA has been shown to have roles after damage repair as part of recovery from DNA damage in both NHEJ and NER (Adam, Polo and Almouzni, 2013; Li and Tyler, 2016). Survival hypersensitivity to UV was not observed in the case of HIRA absence in U2OS cells, but this study did not determine if there is a survival hypersensitivity in the absence of H3.3 is these cells, which would be needed to confirm if HIRA is required for survival of DNA damage (Adam, Polo and Almouzni, 2013). I do not see an impact of HIRA on cell cycle progression after UV, as I did for H3.3 and ATRX, suggesting that HIRA does not have a role in resolving lesions. It remains possible that HIRA has functions in recovery after DNA damage which I have not seen in the cellular assays from this thesis.

I did find HIRA has an impact on fork progression after UV irradiation, although the absence of HIRA appears to allow faster fork progression than in WT cells after UV irradiation. After UV, HIRA has been reported to localise to damaged chromatin regions and 'prime' regions for transcriptional recovery (Adam, Polo and Almouzni, 2013). If HIRA is absent, transcriptional recovery after repair is impaired. Collisions between transcriptional and replication polymerases can cause a halt to replication fork progression (García-Muse and Aguilera, 2016). If, in the absence of HIRA, there is less transcription after damage repair, there could be fewer collisions between transcription and replication machineries. Fewer impediments could allow replication forks to appear to progress faster than in WT cells.

7.4.3 Chaperones at distinct regions of the genome

H3.3 chaperones are reported to have distinct deposition regions (Goldberg *et al.*, 2010). The requirement of them for DNA damage response may be related to their zones of action. ATRX is required for H3.3 deposition at telomeres and HIRA for H3.3 deposition in genic regions. Potentially, DNA damage at telomeres could require ATRX for repair and damage in genic regions could require HIRA for repair. Global approaches to administering and studying the role of H3.3 and its chaperones in the response to DNA damage could miss a subtlety of requirements at only certain regions. The requirement of H3.3 and HIRA has also been demonstrated across the nucleus (Adam, Polo and Almouzni, 2013), but as HIRA and H3.3 are found across genic regions, we could expect a requirement across much of the genome. Although ATRX has been shown to have a role in DSBs at telomeres (Lovejoy *et al.*, 2020), it has also been demonstrated to act across the nucleus (Juhász *et al.*, 2018). This points towards a role in regions outside telomeres and centromeres, where ATRX has typically been characterised to deposit H3.3, which does not support the idea that H3.3 chaperones have roles in damage at the sites of deposition.

7.4.4 Redundancy between chaperones

Much of the research into the two H3.3 chaperones shows their functions in cellular processes and H3.3 related roles as distinct and separate. Whilst investigating each chaperone separately can be helpful to understand their function, any redundancy between HIRA and ATRX in their H3.3 related functions is not clear. H3.3 cannot be chaperoned by canonical chaperones, but can be deposited by HIRA in place of H3.1 (Ray-Gallet *et al.*, 2011), demonstrating the possibility of a wider range of function possible for HIRA. A redundancy in the H3.3 related functions of the two chaperones could both emphasise the importance of H3.3 and conceal the impact of H3.3 in experimental studies investigating only one chaperone.

7.5 The impact of experimental systems on result interpretation

7.5.1 Differences between DT40 and TK6 cell lines

In DT40 H3.3 is required for normal survival after DNA damage, but TK6 cells do not need H3.3 to survive and continue dividing after UV irradiation. A notable difference between the TK6 and DT40 systems is the presence of p53. As p53 is at the centre of repair signalling networks it might be expected that it could aid cells in rerouting repair down alternative pathways if there is a defect in one mechanism.

In DT40, a loss of H3.3 leads to an S phase block after UV, whereas TK6 *h3.3* cells have a p53 mediated G1 block. In TK6 cells lacking both H3.3 and p53, the G1 block is alleviated, but rather than a S phase block as seen in the DT40, there is an increased S arrest population. Without a G1 block, DNA damage is transmitted through to S phase where it could cause catastrophe at the replication fork. This possibility of damage causing problems during replication is hinted at in TK6 cells where there is an increased S arrest population after UV in the absence of H3.3. Possibly, some *h3.3* cells with unresolved damage after escape the G1 block and go into S phase, where their unresolved damage causes problems at the replication fork. However, the loss of p53 does not result in decreased long-term survival after UV, showing the fundamental difference between DT40 and TK6 cells is greater than just the presence of a functional p53.

Additionally, p53 can impact how damage encountered by a replication fork is dealt with (see section 1.3.3.3.2). TK6 contains p53, which can promote translesion synthesis (Hampp *et al.*, 2016), whereas DT40 may rely more on other mechanisms for dealing with damage at the fork, such as fork reversal. This could impact the apparent fork speed observed.

Both DT40 and TK6 cells are derived from cells in the same blood cell lineage (B lymphocyte and lymphoblastoid cells respectively), although at different stages of differentiation. However, DT40 are derived from a cancerous tumour with a viral promoter upstream of c-myc, whereas TK6 are derived from 'normal' cells (Skopek *et al.*, 1978; Baba, Giroir and Humphries, 1985). A hallmark of cancer is mutation and genome instability (Hanahan and Weinberg, 2011). This can often be a result of defective DNA

repair mechanisms, which in turn results in increased rates of mutagenesis. It is therefore possible that DT40 does not have entirely intact DNA damage repair pathways. There may be less redundancy in its repair pathways, so removing one component (e.g. H3.3) could eliminate an entire pathway and, with reduced redundancy could lead to defective DNA repair in the cell and severe consequences, i.e. cell death. As TK6 cells are not a cancer line they may be more likely to be able to cope with DNA damage due to redundancy in DNA damage signalling and repair pathways. This may be a factor in why I do not see the same results in TK6 as in DT40, even when p53 is removed from p53 cells.

Additionally, I was unable to fully rescue the H3.3 phenotype in TK6 cells by expression of H3.3GFP, whereas H3.3GFP expression in DT40 cells was able to rescue the phenotypes. Whilst this could be a result of off-target effects in TK6 from the CRISPR approach used to generate the knockout, it could also be a result of inadequate expression or incorporation of the tagged H3.3 in the TK6 cells. This needs further investigation.

7.5.2 Mutagenesis

It is possible that whilst I observe only small effects on cellular responses to UV in TK6 cells in the absence of H3.3, there may be other impacts which I have not examined. If acute damage is persisting in the absence of H3.3, it must be ultimately repaired, as cells survive long term after UV damage without H3.3. However, it is possible that damage persistence could lead to increased mutagenesis in cells lacking H3.3, particularly in the absence of p53. Whilst a role for H3.3 an oncogenesis linked to its involvement in damage repair pathways has not been proven (H3.3 tail mutations found in cancers lead to epigenetic changes and this is currently proposed to be the primary mechanism driving cellular transformation), it is possible the absence of H3.3 and the resulting alterations to DNA repair would be able to play a part in mutagenesis leading to cancer. Sequencing would be required to determine if this were the case in *h3.3* cells after genotoxin treatment.

7.5.3 What type of damage am I studying?

Lesions which are passed through the replicative phase of the cell cycle and encountered by forks can lead to replication fork collapse and double strand break formation. TK6 cells spend around 65 % of their cell cycle in S phase, so the likelihood of a fork encountering

a UV lesion is high. In my cell cycle analysis of *h3.3* cells after UV, the raised G1 population does not appear until 24 hours after irradiation, with intermediate timepoints displaying an altered S phase. As the G1 block does not appear immediately, it seems unlikely that cells in G1 which receive damage fail to progress through the cell cycle. It seems more likely that cells in S phase which receive damage and fail to resolve lesions continue to progress through the cell cycle until they reach G1, where the cell cycle is then arrested. It is therefore possible that as forks encounter UV lesions in S phase, they are converted to DSBs. As I see a persistence of raised γH2AX, a marker typically found at DSBs, after UV irradiation in *h3.3* cells, it is possible that the involvement of H3.3 and ATRX I see after UV irradiation is to do with the response to DSBs, rather than an involvement in NER pathways.

7.6 Interpreting results from different experimental systems

siRNA removes protein from a system by disrupting mRNA and preventing new protein production. It is therefore most suitable to study proteins with a short half-life to ensure they are absent from the cell after siRNA treatment. Some studies use siRNA approaches to studying H3.3 and its chaperones. HIRA is reported to be a long lived protein, with a half-life of 12 hours (De Lucia *et al.*, 2001). Nucleosomes have varying turnover rates dependent on modifications and position in actively transcribed regions of the genome, but often length of cell cycle has impact on turnover of histones (Zee *et al.*, 2010). Therefore, it is possible that H3.3 could persist in the cell in nucleosomes, particularly in heterochromatic regions, such as telomeres. This possibility of some targeted protein remaining should be considered when interpreting results from siRNA experiments.

On the other hand, if the property of H3.3 being studied is its availability throughout the cell cycle, meaning newly synthesised H3.3 is important, siRNA would abolish new synthesis, even if existing H3.3 persists. Several approaches use tagged H3.3 synthesised throughout the course of the experiment to study H3.3 directly, but again this only captures the action of newly synthesised H3.3. H3.3 is 2 genes, so more difficult to remove than many other proteins encoded by only one gene.

Some studies on the roles of H3.3 and HIRA have been carried out in U2OS cells (Adam, Polo and Almouzni, 2013; Luijsterburg *et al.*, 2016). These have an ALT phenotype, meaning they do not express a functional ATRX. HIRA has been demonstrated to be able to perform ATRX's H3.3 deposition function, depositing H3.3 at telomeres in cells with an ALT phenotype (Hoang *et al.*, 2020). Interpretation of results obtained in a system missing one of the key chaperone components should be cautious, particularly as there is redundancy in deposition systems, as it could complicate delineation between the functions of HIRA, ATRX and H3.3.

7.7 Future study

Studies into H3.3 and DNA damage have told us much about which types of repair H3.3 is implicated in and which chaperone could mediate its functions. However, why H3.3 is required could be elucidated further.

Further investigating H3.3 interactors after UV could help understand if its role after DNA damage is in recruiting repair factors or not. In particular, finding if the H3.3 specific N-terminal tail S31 residue is capable of recruiting repair factors (with or without phosphorylation).

An ATRX/H3.3 double knockout could help further confirm that the role of H3.3 I observe in TK6 cells after UV is mediated by ATRX. Complementation with mutant ATRX could possibly confirm if H3.3 is deposited by ATRX after damage. Additionally, further double knockout lines with H3.3 and key members of repair pathways could be used for epistatic analysis. This could indicate which repair pathway H3.3 is involved in, which could be particularly informative as UV damage in dividing TK6 cells could lead to different types of lesions.

Chapter 8:
CoronaTrap: *in vitro* evolution of a SARs-CoV2 ligand trap

8.1 Introduction

8.1.1 Coronavirus

The pandemic caused by Severe Acute Respiratory Syndrome Corona Virus 2 interrupted scientific progress in 2020, but also inspired research. Alongside studying the coronavirus itself, research has been tackling how to treat and protect against this pathogen.

SARS-CoV2 is an enveloped virus with a single strand of RNA. Its lipid membrane contains envelope and spike proteins. Spike is a transmembrane glycoprotein which forms a trimer on the surface of the viron (Ke, *et al.*, 2020) (Figure 8.1). Spike is responsible for binding the SARS-CoV2 target of Angiotensin Converting Enzyme 2 (ACE2) and mediating viral uptake into human cells (Walls *et al.*, 2020).

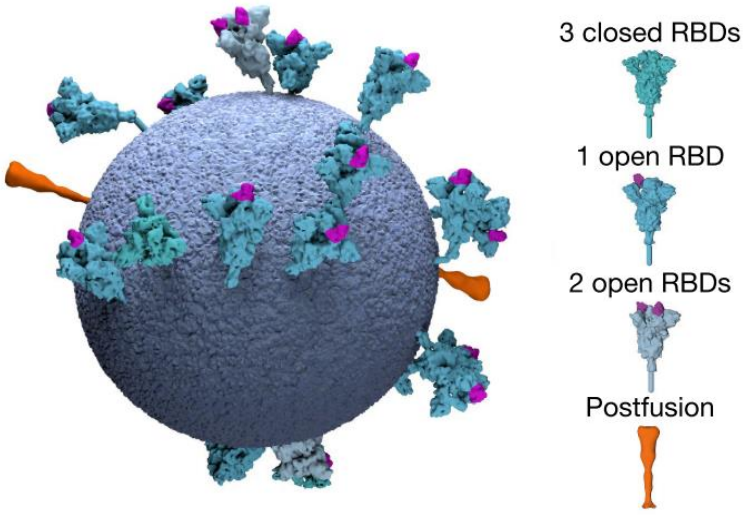

Figure 8.1 Structure of Spike on the surface of a viron (Ke, *et al.*, 2020)

The spike trimer exists in 2 unbound conformations, open and closed, with the receptor binding domain (RBD) of the spike protein hidden in the closed conformation and sitting exposed atop the trimer in the open confirmation (Wrapp *et al.*, 2020; Xiong *et al.*, 2020). Upon binding its ACE2 target, spike protein undergoes proteolytic cleavage to form a post

fusion conformation and fuse lipid membrane with the infected cell (Cai *et al.*, 2020; Hoffmann *et al.*, 2020).

8.1.2 Therapies against SARS-CoV2

As spike is prominent on the surface of the virus and specific to SARS-CoV2, it is a target for developing treatments against Covid-19 infection and is the target of current vaccines (Izda, Jeffries and Sawalha, 2021). However, there may be other approaches to prevent Covid-19 illness. Preventing infection by the virus could be achieved by blocking spike binding to ACE2 on human cells. By treating with a molecule that has a higher binding affinity for spike than ACE-2, the coronavirus could be blocked from binding ACE2 and therefore infecting a cell.

There are 2 possible approaches to take if trying to formulate a molecule with a higher binding for spike than its target ACE2. The first is a rational design. Detailed structures of spike in its various conformations (Hoffmann *et al.*, 2020; Ke, *et al.*, 2020) were elucidated fairly early during the pandemic, allowing design of a molecule to fit the RBD (Cao *et al.*, 2020). The second is an evolutionary approach. By harnessing the power of antibody diversification systems, a molecule which binds RBD can be produced. One example of this is antibody production against RBD to bind spike and block it from infecting via ACE2 (Tuccori *et al.*, 2020). However, there is another possible approach which has parallels with antibody production: the development of a ligand trap.

8.1.3 Somatic hypermutation in the DT40 cell line

The DT40 cell line is a chicken B cell line which is notable for its antibody evolution capacities. This line, when recombination is prevented by insertion of a non-homologous template (Sale *et al.*, 2001), diversifies its Ig loci by somatic hypermutation. Somatic hypermutation is a process by which point mutations are introduced into the antibody genes to generate variation. The enzyme responsible for this is Activation Induced Deaminase (AID). AID is a cytosine deaminase which acts on single stranded DNA preferentially at the Ig locus (Bransteitter *et al.*, 2003; Dickerson *et al.*, 2003; Di Noia and Neuberger, 2007). The uracil generated as a result of cytosine deamination can be processed as DNA damage by various mechanisms, some of which can lead to mutations (Figure 8.2).

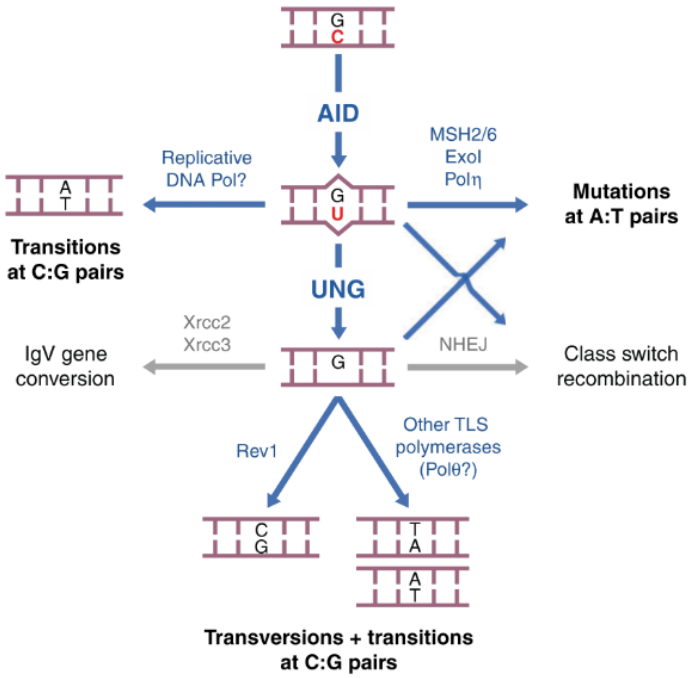

Figure 8.2 Mechanisms of AID induced somatic hypermutation (adapted from (Di Noia and Neuberger, 2007))

The DT40 cell line can be used for its mutation capacities. By replacing the antibody encoding locus in the genome with the sequence of a target protein, said target could acquire mutations through AID activity during somatic hypermutation (Arakawa *et al.*, 2008). By rounds of selection, the sequence of a target-like protein with higher binding capacity that the original target can be generated.

8.1.4 Using DT40 to develop disease treatments

This approach has precedence for producing therapeutic molecules. In 2013 the Sale and Brindle labs collaborated to create an Angiopoetin-2 ligand trap (Brindle *et al.*, 2013). Using the DT40 cell line, the sequence of Tie2 (angiopoetin 2's binding partner) was inserted into the IgG. Due to its insertion in this locus, the mutated Tie2 was also expressed on the surface of DT40 cells, allowing rounds of selection of a Tie2 mutant protein which did not bind Angiopoetin 1 (another Tie2 binding partner) and had a high binding affinity for Angiopoetin 2. 8 rounds of selection against Ang 1 binding and for Ang 2 binding resulted in 3 common mutations in Tie2. These mutations altered the binding specificity from that of the endogenous Tie2. This demonstrated the power of an

evolutionary approach to create ligands from the sequence of an endogenous binding partner.

8.1.5 Aim

During the pandemic, the two labs collaborated again to use this approach to try to produce an ACE2 like protein to act as a 'decoy', to prevent SARS-CoV2 spike protein binding endogenous ACE2 and infecting cells.

8.2 Materials and Methods

8.2.1 DT40 cell culture

Cultured in RPMI 1640 + GlutaMAX (Gibco), 3.3 % Chicken serum, 6.7 % Foetal bovine serum (FBS), 1 % penicillin/streptomycin. Grown at 39 ˚C, 10 % CO_2. Confluency kept below 1e6 cells/ml and at least 1e6 kept between splits. Frozen in 90 % FBS, 10 % Dimethyl sulphoxide.

8.2.2 Binding assay and staining

Cells were spun down and washed in PBS. Cells were then resuspended in PBSF (90 % PBS, 10 % FBS) and RBD and incubated at RT for 30 mins. Cells were washed in PBSF and resuspended in PBSF and antibodies. Cells were incubated on ice for 20 mins before washing in PBSF. Stained cells were resuspended in PBSF and taken for flow cytometry or sorting.

8.2.2.1 With dimeric RBD

For sorting: 40 e6 cells per sample, incubated with RBD in 12 ml PBSF, incubated with antibodies in 500 µl PBSF and 5 µl of antibody/s, resuspended in 1 ml PBSF for sorting.
For flow cytometry: 2 e6 cells per sample, incubated with RBD in 50 µl PBSF, incubated with antibodies in 50 µl PBSF and 0.5 µl of antibody/s, resuspended in 400 µl PBSF for flow cytometry.

8.2.2.2 With monomeric RBD

For sorting: 40 e6 cells per sample, incubated with RBD in 160 ml PBSF, incubated with antibodies in 500 µl PBSF and 5 µl of antibody/s, resuspended in 1 ml PBSF for sorting.
For flow cytometry: 2 e6 cells per sample, incubated with RBD in 40 ml PBSF, incubated with antibodies in 50 µl PBSF and 0.5 µl of antibody/s, resuspended in 400 µl PBSF for flow cytometry.

8.2.3 Antibodies

Anti-chicken IgM (Mouse) PE, Southern Biotech, 8310-09

Anti-FLAG APC, Miltenyi Biotech, Clone REA216

Anti-human IgG (goat) PE, Abcam, 98596

Anti-His PE, Miltenyi Biotech, Clone GG11-8F35.1

8.2.4 Sequencing primers (designed by M. Wang)

Forward: CTGTTTATGCCCATGGGGTCTCT

Reverse: CACCTACTCAGACAATGCGATGC

Methods as main thesis:

Genomic DNA extraction

PCR with Q5 polymerase

Gel electrophoresis

Gel extraction

8.3 Results

8.3.1 Integration of ACE2 into the Ig locus of DT40 cells

Constructs for targeting ACE2 into the DT40 Ig light chain locus (*IGVL*) were created by S. Šviković from templates by D. Peris and G. Williams (Figure 8.3). These were transfected into DT40 cells and clones selected for by S. Šviković.

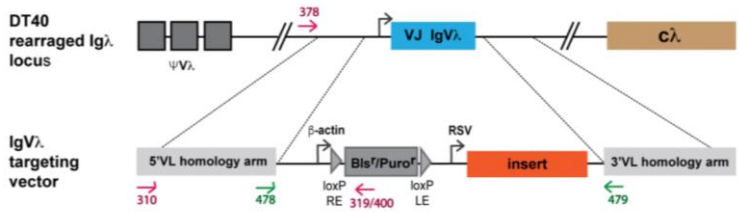

Figure 8.3 Schematic of ACE2 Integration into the DT40 Ig locus From D. Peris

Firstly, correct integration of the ACE2 construct into *IGVL* of DT40 was needed. The ACE2 construct included a FLAG tag, the presence of which on the surface of cells would demonstrate insertion of ACE2 into the genome. If correctly inserted into *IGVL*, IgM would not be expressed, as it would be interrupted by correct ACE2 insertion. To find clones positive for FLAG and negative for IgM, clones were stained with antibodies against FLAG and IgM (Figure 8.4). 48 clones were screened, of which 24 clones were positive for FLAG and negative for IgM (Appendix 4), and therefore contained correctly inserted ACE2.

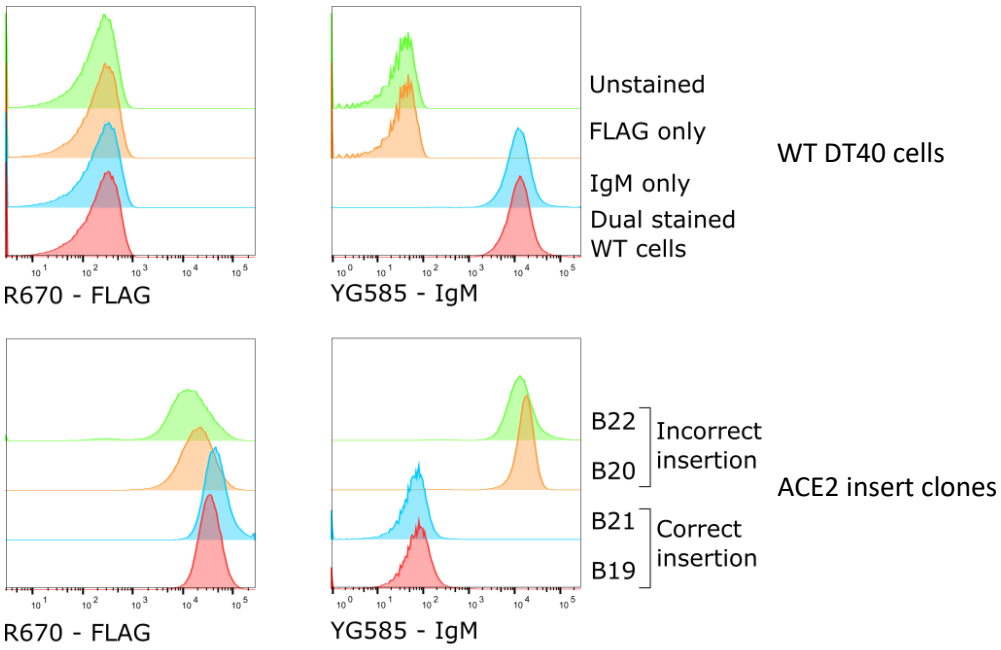

Figure 8.4 Integration of ACE2 into the Ig locus a) Staining controls on WT DT40 cells b) examples of clones with incorrect ACE2 insertion and correct ACE2 insertion.

Multiple cell lines were taken forward for experimentation. 2 single clones were taken forward (Clone A and Clone B), and in an attempt to maintain as much diversity as possible, 2 pools of clones were created. 7 clones with similar FLAG expression were pooled to create Pool A and 5 clones were pooled to create Pool B.

Next, I determined whether the ACE2 expressed on the surface of the DT40 cells was capable of binding an element of SARS CoV2. The cells were incubated with a fragment of the spike protein of SARS CoV2 corresponding to the receptor binding domain. This protein was produced by N. Bate in Leicester. It exists as a dimeric form of the RBD, as two elements of the trimeric spike (as exists on the surface of the virus) can act at once on ACE2 (Ke *et al.*, 2020). The RBD also contains an Fc and His tag, allowing for antibody staining and visualisation by flow cytometry. Cells were incubated with RBD, excess unbound RDB washed off then cells were stained for bound RBD.

8.3.2 Determination of RBD concentration for binding assay

In order to determine the concentration of RBD to use in future sorting experiments, I performed a titration of varying concentrations of RBD to observe the effect on RBD binding. 0.6 ug/million cells was suggested as a starting point based on experiments completed by N. Bate. A 1:2 serial dilution was carried out from this starting point, then cells were incubated then washed and stained as previously (Figure 8.5).

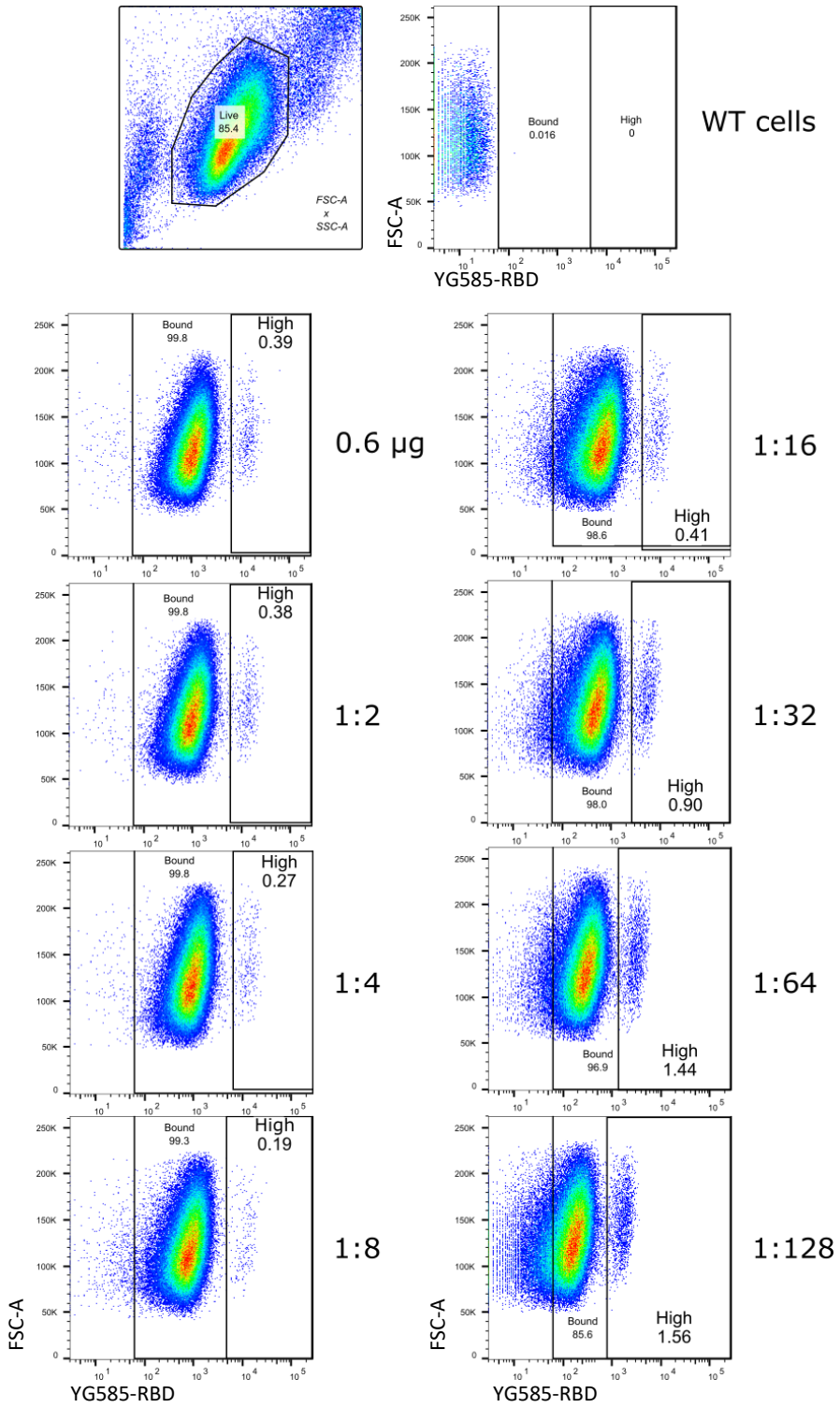

Figure 8.5 Titration of RBD a) Gating strategy for live cells carried out on all samples b) WT cells as a control, demonstrating no binding c) Dotplots of cells with bound RBD, gated for RBD bound and High binding populations.

With every concentration of RBD, nearly all cells have bound RBD (and so are stained positively for Fc). There is also a distinct population of cells with a higher fluorescence. A higher fluorescence could be a result of more RBD bound to a cell, possibly because it is

bound more tightly and has not dissociated during the wash step. This is therefore a population I am interested in for the evolution of tighter binding ACE2. As the concentration of RBD applied to cells increases, the proportion of cells part of this distinct 'high' binding population increases. As RBD molecules become scarcer, possibly cells with a greater binding capacity capture RBD more effectively, so 'high' binders are revealed. Additionally, as the concentration of RBD decreases, the brightness of all the bound cells decreases. This shift may be because there is less RBD available, so the number of RBD molecules bound per cell is less, leading to reduced fluorescence.

In order to maximise this 'high' binding population, the lowest concentration of RBD was used in further experiments.

8.3.3 Sorting for higher binding cells

In order to obtain cells expressing an ACE2 with higher binding capacity for RBD than endogenous, cells were sorted based on bound RBD staining. These cells were then kept growing and sorted again for higher binding to RBD, in the hope that mutations which increase affinity for RBD are being introduced. Cells were cultured at 39 °C, as at this temperature their cell cycle is reduced from ~ 11 hrs (observed at 37 ˚C) to ~ 8 hrs. The greater the number of divisions, the greater the likelihood for mutations to arise and spread through a population.

Cells were incubated with 3.9 pM RBD, washed then stained as previously. The brightest fluorescing cells, approximately the top 1 %, were sorted. These cells then underwent the same binding assay alongside unsorted cells (Figure 8.6).

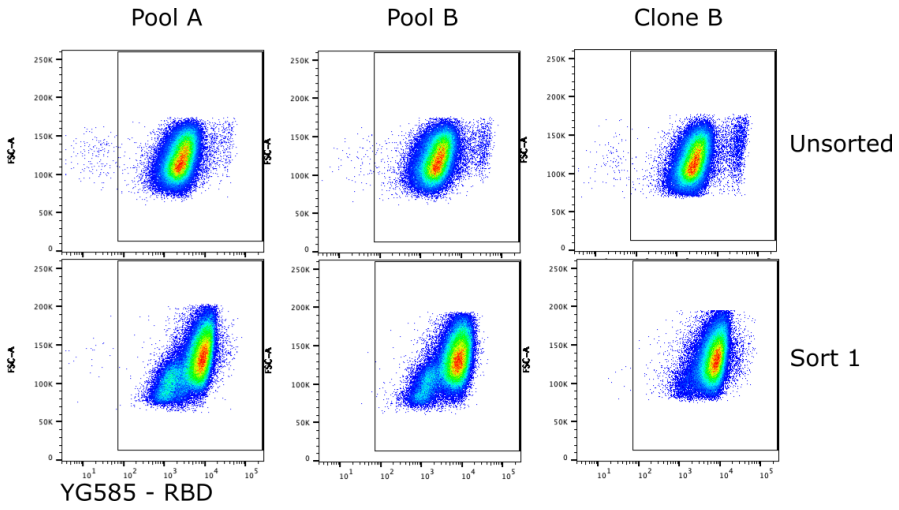

Figure 8.6 Sort 1 vs unsorted cells a) Staining for RBD binding in 2 samples comparing unsorted and sorted cells

There is a marked increase in fluorescence between unsorted and sorted cells. However, it may not be quite as high as the 'high' binding population in the unsorted samples, and there remains some 'lower' bound cells in the sorted population.

These sorted cells were cultured for approximately 36 cell divisions then sorted again, using the same procedure as previously and selecting the top ~1 % highest fluorescing cells (Figure 8.7).

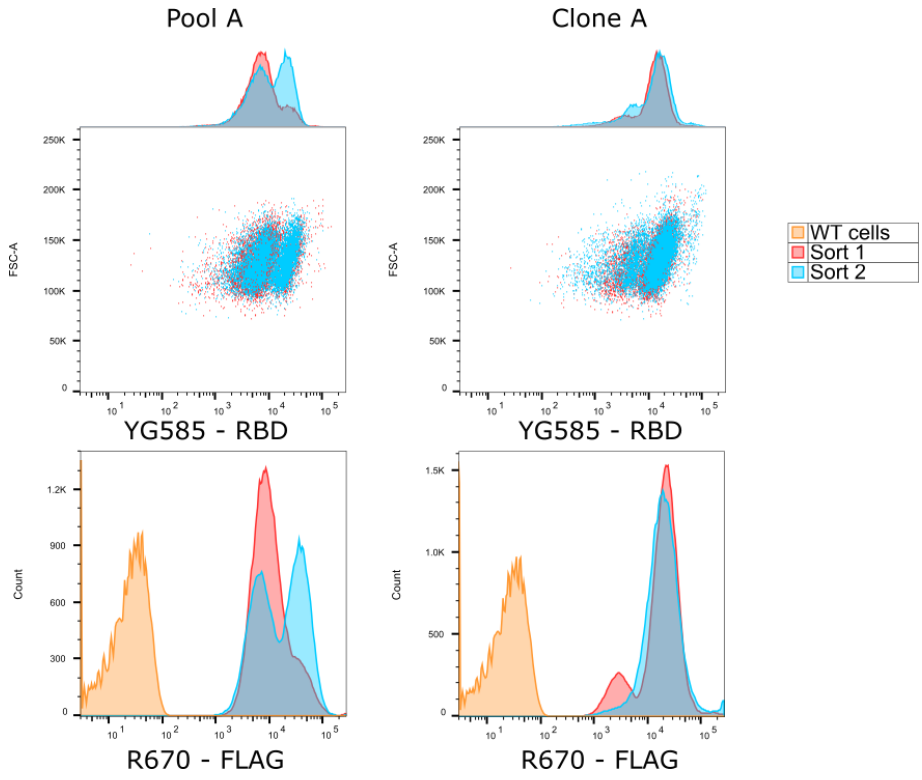

Figure 8.7 Sort 1 vs Sort 2 a) Staining for RBD binding in 2 samples comparing first and second sorts. b) Staining for ACE2 expression in 2 samples comparing first and second sorts

In this second sort, some samples increased the proportion of cells with higher RBD fluorescence/binding, whereas in other samples there was a smaller shift towards higher fluorescence.

In these early experiments, the antibodies for FLAG and Fc were not compatible as they cross-react, and so cells were sorted on only Fc fluorescence/RBD binding, not FLAG fluorescence/ACE2 expression. On staining the sorted populations for ACE2 expression, it became clear that there were several ACE2 expression levels within the population of cells.

If cells express more ACE2 molecules, they could be capable of binding more RBD molecules, which could increase fluorescence on staining. Therefore, by only sorting on Fc fluorescence, I may have selected for high ACE2 expression, rather than for cells containing ACE2 mutations which allow tighter binding.

Alternative antibodies were obtained to allow for dual staining, to determine the effect of ACE2 expression on RBD binding levels in a population (Figure 8.8).

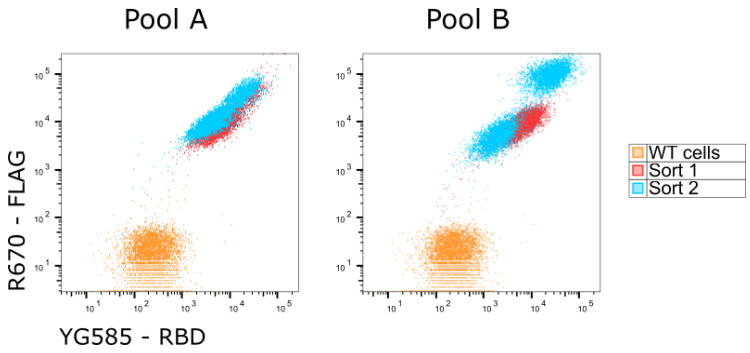

Figure 8.8 Dual staining of ACE2 expression and RBD binding. Dotplots of cells stained against both ACE2 (FLAG) and RBD binding (His). 2 population lineages shown and 2 sorts compared to each other and WT cells.

The multiple ACE2 expression levels can impact the RBD binding levels of a population. As clearly visible in pool B, sort 2, the cells with highest RBD binding also have high ACE2 expression, indicating that high ACE2 expression can lead to high RBD binding. Therefore, sorting on RBD binding alone is not sufficient to obtain tight binding ACE2 varieties. Moving forward, sorting was carried out on dual stained cells, allowing selection of cells with tight binding and 'medium' ACE2 expression levels.

The cells from sort 2 were cultured for approximately 60 cell divisions then sorted again, but this time with dual staining. Cells underwent the binding assay alongside cells from the previous sort, sort 2 (Figure 8.9).

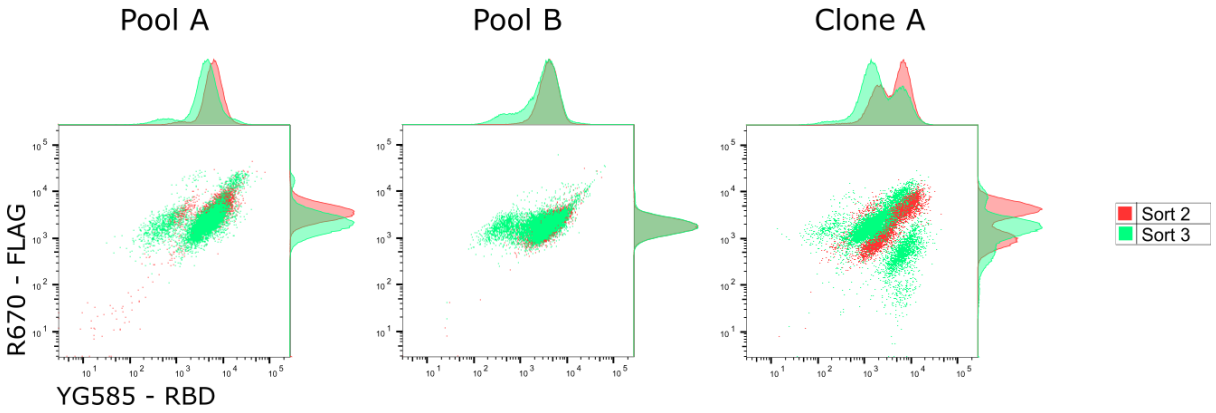

Figure 8.9 Sort 3 vs Sort 2 Dotplots of cells stained against both ACE2 (FLAG) and RBD binding (His). 3 population lineages shown and 2 sorts compared to each other.

There are several populations in the sort 3 samples with varying RBD binding and ACE2 expression levels, particularly in clone A, sort 3 where there are at least 5 distinct populations. A gradual increase in the proportion of cells with higher RBD binding or a shift towards higher RBD fluorescence in the whole population was expected. Possibly the sorting gates were too stringent and instead of selecting tight binders, abnormal cells were selected, causing unwanted divergence of populations.

8.3.4 Competition binding assay

An aspect of choosing tighter binding ACE2 could be to select for a slower off-rate of bound RBD. A way to achieve this is through a competition assay. Cells were incubated with RBD, washed and stained as in previous experiments, but then an excess of RBD added before flow cytometry. Cells containing ACE2 which binds more weakly to RBD and have a fast off rate may lose the stained RBD for the later added RBD, and therefore not fluoresce. Cells expressing an ACE2 which binds tightly and has a slow off-rate will remain bound to the stained RBD and fluoresce. This could give an additional level of selection.

Pool B, sort 2 cells were incubated with an either 5- or 10-fold excess of RBD (compared to initial concentration) for either 5, 10, 30 or 60 minutes (Figure 8.10).

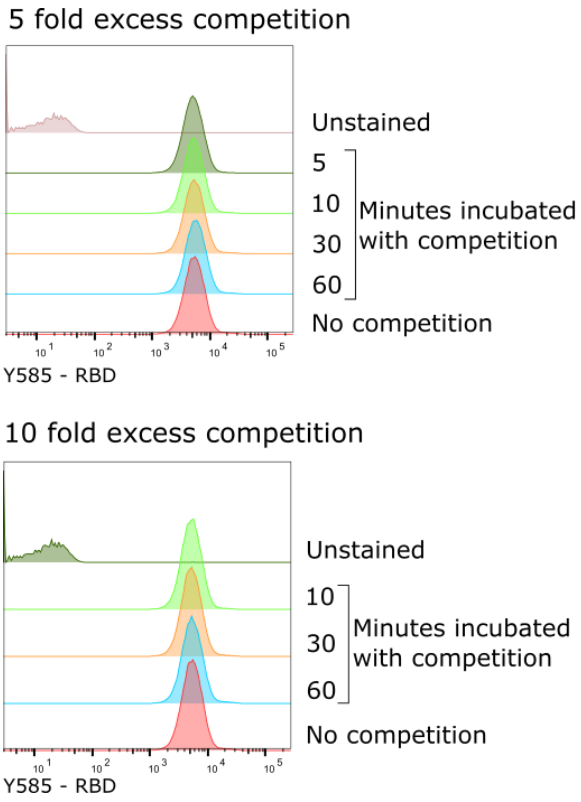

Figure 8.10 Competition assay Histogram of binding fluorescence after competition assay with varying excess and incubation time

There is no change in RBD fluorescence/binding after the competition assay compared to cells stained without competition.

A larger excess or a longer second incubation time could lead to a change in fluorescence. Ideally, the competition RBD would have a different label to allow visualisation of any ACE2 which has released and then rebound RBD and therefore has a fast off rate and is unwanted. This assay also relies on the anti-His tag antibody which binds RBD having a slower off-rate than RBD. If the anti-His antibody releases from His tagged RBD quickly, RBD could also release from ACE2, rebind and be stained again by free anti-His. This assay was not taken forward.

8.3.5 Sorting with monomeric RBD protein

A dimeric form of the RBD is a useful starting point for evolution of a tighter binding ACE2. However, a monomeric form of the RBD is useful for increasing the affinity of the RBD for ACE2-like protein further, as it reduces avidity.

Sorting was carried out as previously, this time using 0.8 µg monomeric RBD/million cells. The cell lines sorted were Pool A and Clone B (unsorted) and Pool A sort 2 and Clone B sort 2.

During the first 2 sorts (with approximately 30 cell divisions between each sort, sorting for increased His fluorescence and constant FLAG fluorescence), there was very little shift in fluorescence. However, the 3rd sort resulted in a definite increased His/binding fluorescence in 3 of the 4 cells lines (Figure 8.11)

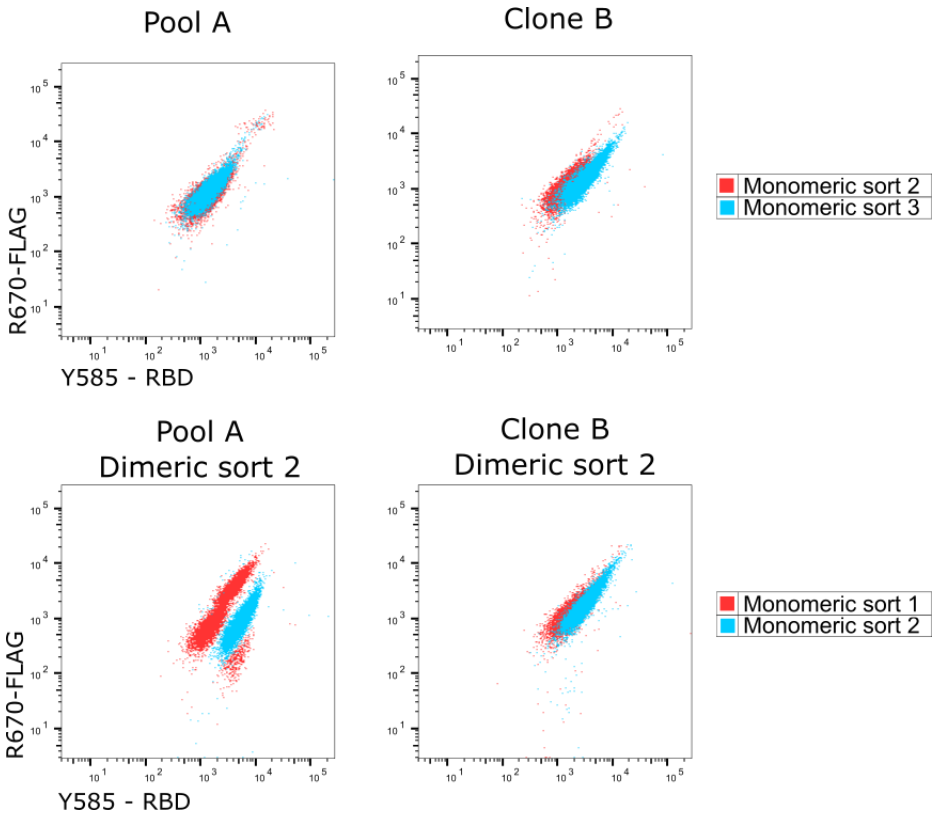

Figure 8.11 Sorts with monomeric RBD Dotplots of cells stained against both ACE2 (FLAG) and RBD binding (His).

The 4th sort using monomeric RBD again produced little shift in fluorescence due to increased binding (data not shown). As seen with then final sort using dimeric protein, the 5th sort with monomeric RBD generated several populations with varied FLAG and His/binding fluorescence. Again, I think this is due to stringent sorting selecting for abnormal cells, and therefore these population were not analysed by sequencing.

When comparing unsorted cells to cells which have undergone many cell divisions since ACE2 insertion and several rounds of sorting for RBD binding, it is clear that the binding capacity of these populations of cells has increased (Figure 8.12).

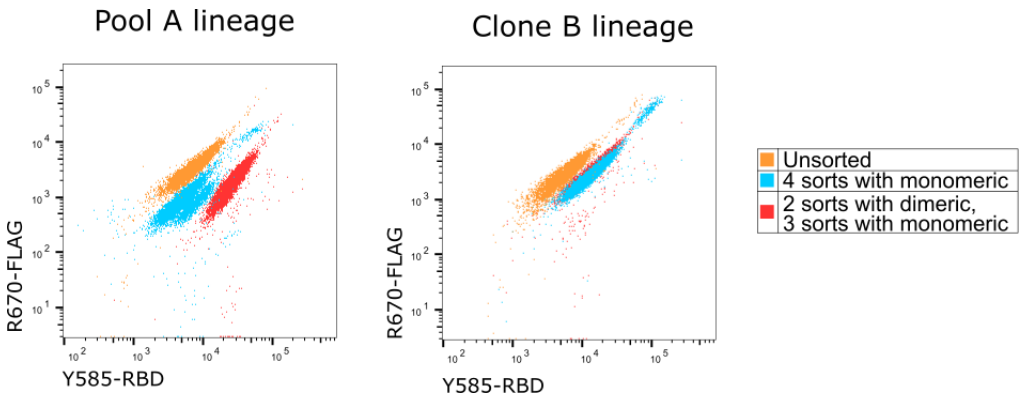

Figure 8.12 Comparing unsorted and sorted RBD binding levels Dotplots of cells stained against both ACE2 (FLAG) and RBD binding (His).

8.3.6 Sequencing mutations

In order to determine if the changes in RBD binding are due to a change in sequence in the inserted ACE2, I carried out Sanger sequencing. Ideally, sequencing of each individual cell would provide most information on the range of ACE2 mutations present in a population, but this can be time consuming and costly. I therefore used PCR and Sanger sequencing of ACE2 within the bulk population to find any popular mutations. If a particular mutation is present in a large proportion of a population of sorted cells, it may be a key mutation for increasing ACE2 binding to RBD.

M. Wang designed primers against the first half of the inserted ACE2 and I carried out PCR on genomic DNA extracted from sorted populations. We expect AID to act closest to the promoter (Di Noia and Neuberger, 2007), so sequencing this region should allow any mutations to be visualised. The PCR product was sent for Sanger sequencing (Genewiz) and traces aligned and analysed (Figure 8.13).

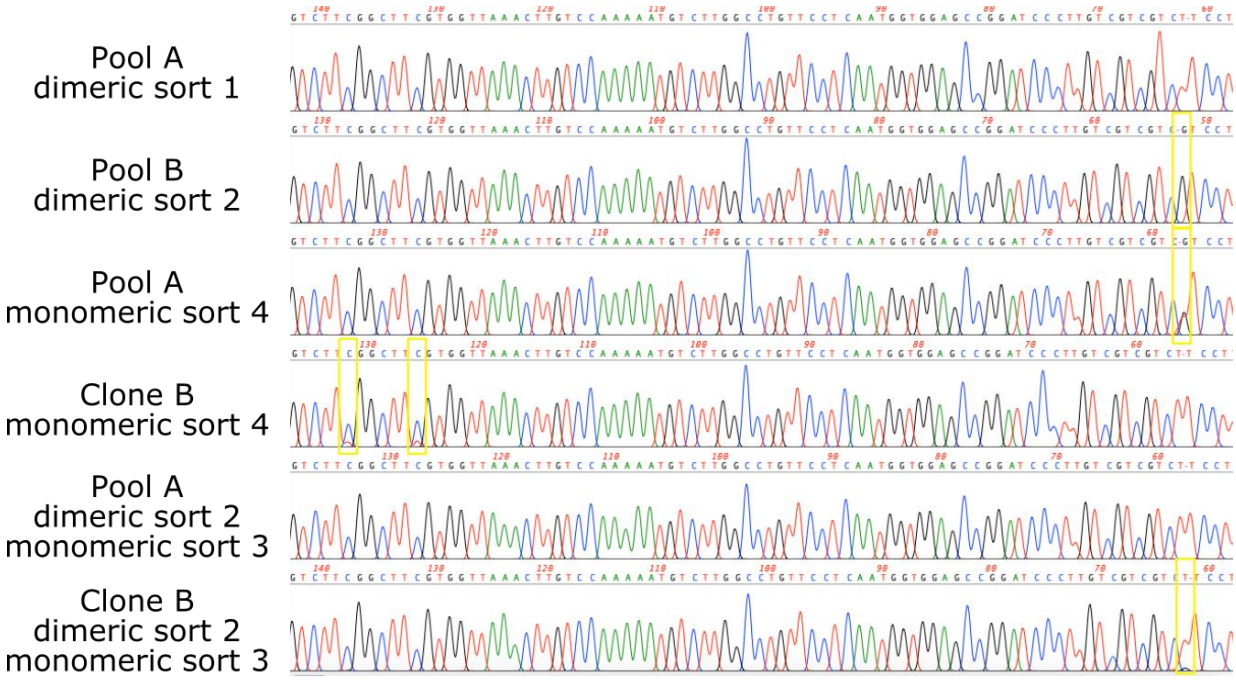

Figure 8.13 Sanger Sequencing trace a representative region of the sequencing trace from PCR of various populations at different rounds of sorting. Yellow boxes indicate mutations.

On the trace, some positions have more than one peak visible, indicating a mutation present in some of the population. The quality of the sequencing is high enough to be able to see small peaks beneath the main peak, and so visualising mutations present in a small proportion of the bulk population is possible.

These mutations which could lead to residue changes were positioned on a structure of ACE2 to show where mutations which are common in populations with increased ACE2 binding are positioned (Figure 8.14).

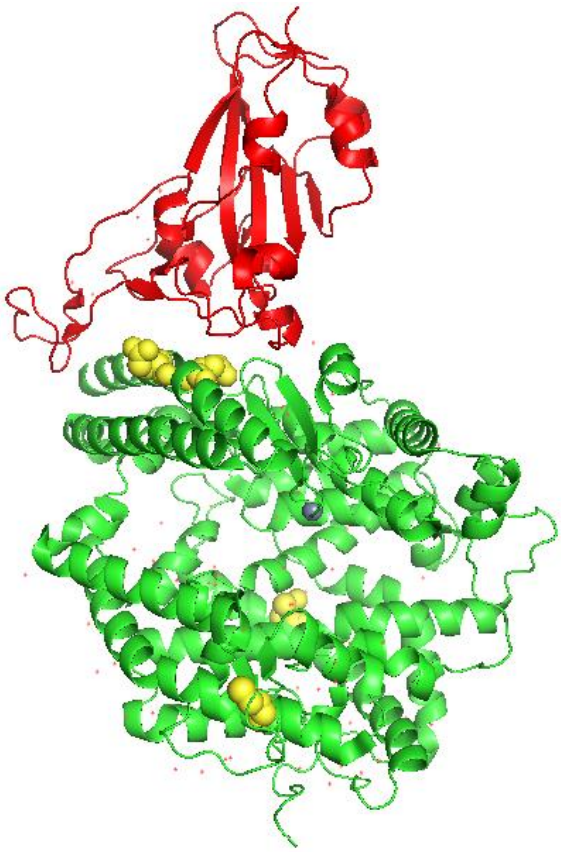

Figure 8.14 Structure of ACE2 binding RBD with potential mutations ACE2 in green, RBD in red, sites of residue changes due to mutations in yellow

In the sample from 1 round of sorting (Pool A dimeric sort 1), no mutations were visible. This is not surprising, as although there may be mutations within the population, they may not be at a high enough proportion to be visible during bulk sequencing as they have not been selected for yet.

In figure 8.12, it appears that the greatest shift in His fluorescence from unsorted is in Pool A dimeric sort 2 monomeric sort 3. However, this sample does not have the most mutations (visible by this approach), with only 1 mutation found which does not result in an amino acid change.

This mutation which does not result in an amino acid change was found in 3 of the 7 samples sequenced, which are all from separate lineages at varying numbers of sorts. This mutation could confer an advantage and so is selected for by the sorting. However, as seen in figure 8.13, there are trinucleotide repeats immediately adjacent, so a polymerase

either in the DT40 cells or in the PCR reaction could mis-incorporate a base, causing this particular mutation. As it does not lead to an amino acid change, it may arise regardless of selection applied and be allowed to persist as it does not impact the selection.

The sample with most mutations is Clone B monomeric sort 4. 2 of its mutations cause amino acid changes at the RBD binding interface of ACE2. These could alter the binding capacity of ACE2 for RBD. As this sequencing is of a bulk population, I cannot know if these mutations occur in the same cell. Sequencing of individual cells to determine this would be required. The other mutation in this population leads to an amino acid change on the body of ACE2, away from the RBD binding site. This change could make alterations to the shape of the ACE2 protein and alter RBD binding in this way. A different mutation in the Pool B dimeric sort 2 population also alters an amino acid on the body of ACE2, confirming that alterations away from the RBD binding site could impact the binding capacity of ACE2.

3 populations contain mutations early in the inserted ACE2 sequence, upstream of the protein coding regions. AID is expected to have high activity near the Ig locus promoter, so mutations here are expected (Di Noia and Neuberger, 2007). It is not clear, however, how these upstream mutations become prevalent in a sorted population as they presumably do not affect the structure of ACE2, and any impact on expression levels should be controlled for due to selection based on FLAG levels. Potentially, these could be passenger mutations which occur in the same cell as a selected for mutation. However, in 1 of the clones with these upstream mutations I do not observe any other mutations. This emphasises the need for sequencing of each cell individually to find out what mutations are present.

8.4 Discussion

Overall, this approach of inserting ACE2 in a locus prone to mutations selection by rounds of sequential sorting can increase the binding capacity of ACE2 for RBD through mutations. However, to determine the future of using this approach to create a therapy against Covid-19 infection would require quantification of the relative binding strength of our evolved ACE2 for RBD compared to the endogenous ACE2.

With the benefit of hindsight, there are aspects of this project which I may have carried out differently. Combinations of mutations which ultimately lead to tighter ACE2 binding of RBD may arise singly, with only a modest increase in binding capacity. By using a very stringent sorting criteria, mutations that only cause a modest increase in binding singly may not be selected for and therefore lost. Therefore, in early rounds of sorting, a wider selection criteria could have been used to capture a wider variety of potentially useful mutations.

A competition assay would have been a useful tool to further increase strong binding ACE2. My attempt at a competition assay was not successful using the same RBD as competition, an RBD protein with a different or no label as competition could be more successful. Once mutations which can increase binding have been established, putting additional pressure on the system by a competition assay would help select for greater affinity.

Sequencing for mutations was carried out after rounds of sorting. However, if bulk populations had undergone sequencing alongside sorting, populations with a variety of mutations present could have been chosen to take forward to focus efforts and make best use of limited sorting time available. Sequencing the same lineages throughout the rounds of sorting would allow me to follow when mutations arise and when they become prevalent in the population. Sequencing cells individually could also give valuable information on the variety of mutations present in a population and what combinations are present in a single cell.

An additional complication has become clear as the pandemic has progressed. As Covid-19 has spread around the world through millions of people, the virus has had many opportunities to mutate, giving rise to variants (Boehm *et al.*, 2021). Some of these variants have mutations in their spike protein, including in the RBD region, and can therefore alter the affinity of RBD for ACE2 (Luan, Wang and Huynh, 2021; Nelson *et al.*, 2021; Ramanathan *et al.*, 2021). As different variants become prevalent due to their increased transmissibility or ability to evade immunity acquired against earlier variants, the approach taken here would also need to change. Developing a tighter binding ACE2 against a variant which is no longer a major component in the pandemic will not be a useful therapy. Any mutations in ACE2 which lead to tighter binding of one RBD variant, may not lead to tighter binding in another RBD variant. Mutations in both ACE2 and RBD are both are likely to be at the RBD/ACE2 binding interface, and therefore using the most relevant RBD variant in this approach is important. Additionally, these SARS-CoV 2 variants can have increased affinity for ACE2, as this can increase transmissibility. Any decoy we could develop would therefore need an even higher affinity for RBD than first anticipated in order to compete against endogenous binding and be an effective treatment.

Due to their potential to mutate, viral targets are difficult to develop treatments against. On this small scale, generating mutations and selecting for them can be time consuming, and during this time, the SARS-CoV 2 it could protect against may have mutated. Approaches to successfully solving the Covid-19 pandemic will have to overcome this issue. The approach used here does have the potential to rapidly respond to viral mutations, but a much larger scale approach to keep up with the continually changing SARS-CoV2 would be required.

Bibliography

Adam, S., Polo, S. E. and Almouzni, G. (2013) 'Transcription Recovery after DNA Damage Requires Chromatin Priming by the H3.3 Histone Chaperone HIRA', *Cell*, 155(4), p. 963. doi: 10.1016/j.cell.2013.10.039.

Adimoolam, S. and Ford, J. M. (2002) 'p53 and DNA damage-inducible expression of the xeroderma pigmentosum group C gene', *Proceedings of the National Academy of Sciences of the United States of America*, 99(20), pp. 12985–12990. doi: 10.1073/pnas.202485699.

Andegeko, Y. *et al.* (2001) 'Nuclear Retention of ATM at Sites of DNA Double Strand Breaks *', *Journal of Biological Chemistry*. Â© 2001 ASBMB. Currently published by Elsevier Inc; originally published by American Society for Biochemistry and Molecular Biology., 276(41), pp. 38224–38230. doi: 10.1074/jbc.M102986200.

Arakawa, H. *et al.* (2008) 'Protein evolution by hypermutation and selection in the B cell line DT40', *Nucleic Acids Research*, 36(1), pp. 1–11. doi: 10.1093/nar/gkm616.

Argentaro, A. *et al.* (2007) 'Structural consequences of disease-causing mutations in the ATRX-DNMT3-DNMT3L (ADD) domain of the chromatin-associated protein ATRX', *Proceedings of the National Academy of Sciences of the United States of America*, 104(29), pp. 11939–11944. doi: 10.1073/pnas.0704057104.

Armache, A. *et al.* (2020) 'Histone H3.3 phosphorylation amplifies stimulation-induced transcription', *Nature*. doi: 10.1038/s41586-020-2533-0.

Ashcroft, M. and Vousden, K. H. (1999) 'Regulation of p53 stability', *Oncogene*, 18(53), pp. 7637–7643. doi: 10.1038/sj.onc.1203012.

Ashour, M. E. and Mosammaparast, N. (2021) 'Mechanisms of damage tolerance and repair during DNA replication', *Nucleic Acids Research*. Oxford University Press, 49(6), pp. 3033–3047. doi: 10.1093/nar/gkab101.

Avkin, S. *et al.* (2006) 'p53 and p21 Regulate Error-Prone DNA Repair to Yield a Lower Mutation Load', *Molecular Cell*, 22(3), pp. 407–413. doi: 10.1016/j.molcel.2006.03.022.

Baba, T. W., Giroir, B. P. and Humphries, E. H. (1985) 'Cell lines derived from avian lymphomas exhibit two distinct phenotypes', *Virology*, 144(1), pp. 139–151. doi: 10.1016/0042-6822(85)90312-5.

Bannister, A. J. and Kouzarides, T. (2011) 'Regulation of chromatin by histone modifications', *Cell Research*. Nature Publishing Group, 21(3), pp. 381–395. doi: 10.1038/cr.2011.22.

Bianchi, J. *et al.* (2013) 'Primpol bypasses UV photoproducts during eukaryotic chromosomal DNA replication', *Molecular Cell*. Elsevier Inc., 52(4), pp. 566–573. doi: 10.1016/j.molcel.2013.10.035.

Bjerke, L. *et al.* (2013) 'Histone H3.3 mutations drive pediatric glioblastoma through upregulation of MYCN', *Cancer Discovery*, 3(5), pp. 512–519. doi: 10.1158/2159-8290.CD-12-0426.

Blackford, A. N. and Jackson, S. P. (2017) 'ATM, ATR, and DNA-PK: The Trinity at the Heart of the DNA Damage Response', *Molecular Cell*. Elsevier Inc., 66(6), pp. 801–817. doi: 10.1016/j.molcel.2017.05.015.

Blasina, A. *et al.* (1998) 'A human homologue of the checkpoint kinase Cds1 directly inhibits Cdc25 phosphatase', pp. 1–10.

Bode, A. M. and Dong, Z. (2004) 'Post-translational modification of p53 in tumorigenesis', *Nature Reviews Cancer*, 4(10), pp. 793–805. doi: 10.1038/nrc1455.

Boehm, E. *et al.* (2021) 'Novel SARS-CoV-2 variants: the pandemics within the

pandemic', *Clinical Microbiology and Infection*. Elsevier Ltd, 27(8), pp. 1109–1117. doi: 10.1016/j.cmi.2021.05.022.
Borgdorff, V. *et al.* (2006) 'DNA mismatch repair mediates protection from mutagenesis induced by short-wave ultraviolet light', *DNA Repair*, 5(11), pp. 1364–1372. doi: 10.1016/j.dnarep.2006.06.005.
Bransteitter, R. *et al.* (2003) 'Activation-Induced Cytidine Deaminase Deaminates Deoxycytidine on Single-Stranded DNA But Requires the Action of RNase', *Proc. Nadl. Acad. Sci. USA*, 100, pp. 4102–4107.
Branzei, D. and Foiani, M. (2008) 'Regulation of DNA repair throughout the cell cycle', *Nature Reviews Molecular Cell Biology*, 9(4), pp. 297–308. doi: 10.1038/nrm2351.
Braunschweig, U. *et al.* (2009) 'Histone H1 binding is inhibited by histone variant H3.3', *EMBO Journal*. Nature Publishing Group, 28(23), pp. 3635–3645. doi: 10.1038/emboj.2009.301.
Brindle, N. P. J. *et al.* (2013) 'Directed evolution of an angiopoietin-2 ligand trap by somatic hypermutation and cell surface display', *Journal of Biological Chemistry*. Â© 2013 ASBMB. Currently published by Elsevier Inc; originally published by American Society for Biochemistry and Molecular Biology., 288(46), pp. 33205–33212. doi: 10.1074/jbc.M113.510578.
Byun, T. S. *et al.* (2005) 'Functional uncoupling of MCM helicase and DNA polymerase activities activates the ATR-dependent checkpoint', pp. 1040–1052. doi: 10.1101/gad.1301205.well.
Cai, Y. *et al.* (2020) *Distinct conformational states of SARS-CoV-2 spike protein*. Available at: http://science.sciencemag.org/.
Canman, C. E. *et al.* (1998) 'Activation of the ATM Kinase by Ionizing Radiation and Phosphorylation of p53', 281(September), pp. 1996–1999.
Cao, L. *et al.* (2020) 'De novo design of picomolar SARS-CoV-2 miniprotein inhibitors', *Science*, 370(6515), pp. 426–431. doi: 10.1126/science.abd9909.
Chang, F. T. M. *et al.* (2015) 'CHK1-driven histone H3.3 serine 31 phosphorylation is important for chromatin maintenance and cell survival in human ALT cancer cells', *Nucleic Acids Research*, 43(5), pp. 2603–2614. doi: 10.1093/nar/gkv104.
Chen, J. *et al.* (1995) 'Separate domains of p21 involved in the inhibition of Cdk kinase and PCNA Junjle', 374(March), pp. 386–388.
Chen, M. *et al.* (2012) 'Serum starvation induced cell cycle synchronization facilitates human somatic cells reprogramming', *PLoS ONE*, 7(4). doi: 10.1371/journal.pone.0028203.
Chen, P. *et al.* (2013) 'H3.3 actively marks enhancers and primes gene transcription via opening higher-ordered chromatin', *Genes and Development*, 27(19), pp. 2109–2124. doi: 10.1101/gad.222174.113.
Chen, P., Zhao, J. and Li, G. (2013) 'Histone variants in development and diseases', *Journal of Genetics and Genomics*. Elsevier Limited and Science Press, 40(7), pp. 355–365. doi: 10.1016/j.jgg.2013.05.001.
Cheng, Q. and Chen, J. (2010) 'Mechanism of p53 stabilization by ATM after DNA damage Mechanism of p53 stabilization by ATM after DNA damage', 4101. doi: 10.4161/cc.9.3.10556.
Chini, C. C. S. and Chen, J. (2003) 'Human Claspin Is Required for Replication Checkpoint Control', *Journal of Biological Chemistry*. Â© 2003 ASBMB. Currently published by Elsevier Inc; originally published by American Society for Biochemistry and Molecular Biology., 278(32), pp. 30057–30062. doi: 10.1074/jbc.M301136200.
Clauson, C., Schärer, O. D. and Niedernhofer, L. (2013) 'Advances in understanding the

complex mechanisms of DNA inter strand cross-link repair', *Cold Spring Harbor Perspectives in Medicine*, 3(10). doi: 10.1101/cshperspect.a012732.
Close, P. *et al.* (2012) 'DBIRD complex integrates alternative mRNA splicing with RNA polymerase II transcript elongation', *Nature*, 484(7394), pp. 386–389. doi: 10.1038/nature10925.
Clynes, D. *et al.* (2014) 'ATRX dysfunction induces replication defects in primary mouse cells', *PLoS ONE*, 9(3). doi: 10.1371/journal.pone.0092915.
Clynes, D. *et al.* (2015) 'Suppression of the alternative lengthening of telomere pathway by the chromatin remodelling factor ATRX', *Nature Communications*. Nature Publishing Group, 6(May). doi: 10.1038/ncomms8538.
Cordeiro-Stone, M. *et al.* (1999) 'Analysis of DNA Replication Forks Encountering a Pyrimidine Dimer in the Template to the Leading Strand'.
Coster, G. and Goldberg, M. (2010) 'The cellular response to dna damage: A focus on MDC1 and its interacting proteins', *Nucleus*, 1(2). doi: 10.4161/nucl.11176.
Daniel Ricketts, M. *et al.* (2019) 'The HIRA histone chaperone complex subunit UBN1 harbors H3/H4- And DNA-binding activity', *Journal of Biological Chemistry*. Â© THE AUTHORS. Currently published by Elsevier Inc; originally published by American Society for Biochemistry and Molecular Biology., 294(23), pp. 9239–9259. doi: 10.1074/jbc.RA119.007480.
Dash, R. C., Zaino, A. M. and Hadden, M. K. (2018) 'A metadynamic approach to understand the recognition mechanism of the histone H3 tail with the ATRX ADD domain', *Biochimica et Biophysica Acta - Gene Regulatory Mechanisms*. Elsevier, 1861(6), pp. 594–602. doi: 10.1016/j.bbagrm.2018.05.001.
Dickerson, S. K. *et al.* (2003) 'AID mediates hypermutation by deaminating single stranded DNA', *Journal of Experimental Medicine*, 197(10), pp. 1291–1296. doi: 10.1084/jem.20030481.
Drané, P. *et al.* (2010) 'The death-associated protein DAXX is a novel histone chaperone involved in the replication-independent deposition of H3.3', *Genes and Development*, 24(12), pp. 1253–1265. doi: 10.1101/gad.566910.
Dulić, V. *et al.* (1994) 'p53-dependent inhibition of cyclin-dependent kinase activities in human fibroblasts during radiation-induced G1 arrest', *Cell*, 76(6), pp. 1013–1023. doi: 10.1016/0092-8674(94)90379-4.
Eastman, A. (1987) 'The formation, isolation and characterization of DNA adducts produced by anticancer platinum complexes', *Pharmacology and Therapeutics*, 34(2), pp. 155–166. doi: 10.1016/0163-7258(87)90009-X.
Edmunds, C. E., Simpson, L. J. and Sale, J. E. (2008) 'PCNA Ubiquitination and REV1 Define Temporally Distinct Mechanisms for Controlling Translesion Synthesis in the Avian Cell Line DT40', *Molecular Cell*, 30(4), pp. 519–529. doi: 10.1016/j.molcel.2008.03.024.
Elsaesser, S. J., Goldberg, A. D. and Allis, C. D. (2010) 'New functions for an old variant: No substitute for histone H3.3', *Current Opinion in Genetics and Development*. Elsevier Ltd, 20(2), pp. 110–117. doi: 10.1016/j.gde.2010.01.003.
Elsässer, S. J. *et al.* (2012) 'DAXX envelops a histone H3.3–H4 dimer for H3.3-specific recognition', *Nature*, 491(7425), pp. 560–565. doi: 10.1038/nature11608.
Elsässer, S. J. *et al.* (2015) 'Histone H3.3 is required for endogenous retroviral element silencing in embryonic stem cells', *Nature*, 522(7555), pp. 240–244. doi: 10.1038/nature14345.
Eustermann, S. *et al.* (2011) 'Combinatorial readout of histone H3 modifications specifies localization of ATRX to heterochromatin', *Nature Structural and Molecular*

Biology. Nature Publishing Group, 18(7), pp. 777–782. doi: 10.1038/nsmb.2070.
Evans, E. *et al.* (1997) 'Mechanism of open complex and dual incision formation by human nucleotide excision repair factors', *EMBO Journal*, 16(21), pp. 6559–6573. doi: 10.1093/emboj/16.21.6559.
Falck, J. *et al.* (2002) 'The DNA damage-dependent intra – S phase checkpoint is regulated by parallel pathways', 30(February), pp. 290–294. doi: 10.1038/ng845.
Falck, J., Coates, J. and Jackson, S. P. (2005) 'Conserved modes of recruitment of ATM , ATR and DNA-PKcs to sites of DNA damage', 434(March).
Filipescu, D., Müller, S. and Almouzni, G. (2014) 'Histone H3 Variants and Their Chaperones During Development and Disease: Contributing to Epigenetic Control', *Annual Review of Cell and Developmental Biology*, 30(1), pp. 615–646. doi: 10.1146/annurev-cellbio-100913-013311.
Filippakopoulos, P. *et al.* (2012) 'Histone recognition and large-scale structural analysis of the human bromodomain family', *Cell*, 149(1), pp. 214–231. doi: 10.1016/j.cell.2012.02.013.
Fontebasso, A. M. *et al.* (2014) 'Epigenetic dysregulation: a novel pathway of oncogenesis in pediatric brain tumors', *Acta Neuropathologica*, 128(5), pp. 615–627. doi: 10.1007/s00401-014-1325-8.
Fousteri, M. and Mullenders, L. H. F. (2008) 'Transcription-coupled nucleotide excision repair in mammalian cells: Molecular mechanisms and biological effects', *Cell Research*, 18(1), pp. 73–84. doi: 10.1038/cr.2008.6.
Franklin, S. G. and Zweidler, A. (1977) 'Non-allelic variants of histones 2a , 2b and 3 in mammals', 266(March), pp. 1975–1977.
Frey, A. *et al.* (2014) 'Histone H3.3 is required to maintain replication fork progression after UV damage', *Current Biology*, 24(18), pp. 2195–2201. doi: 10.1016/j.cub.2014.07.077.
Friedberg, E. C. *et al.* (2005a) 'Cell Cycle Checkpoints: Signal Transmission and Effector Targets', *DNA Repair and Mutagenesis*. (Wiley Online Books), pp. 779–815. doi: https://doi.org/10.1128/9781555816704.ch21.
Friedberg, E. C. *et al.* (2005b) 'Heterogeneity of Nucleotide Excision Repair in Eukaryotic Genomes', *DNA Repair and Mutagenesis*. (Wiley Online Books), pp. 351–377. doi: https://doi.org/10.1128/9781555816704.ch10.
Friedberg, E. C. *et al.* (2005c) 'Mechanism of Nucleotide Excision Repair in Eukaryotes', *DNA Repair and Mutagenesis*. (Wiley Online Books), pp. 317–350. doi: https://doi.org/10.1128/9781555816704.ch9.
Fu, D., Calvo, J. A. and Samson, L. D. (2012) 'Balancing repair and tolerance of DNA damage caused by alkylating agents', *Nature Reviews Cancer*, 12(2), pp. 104–120. doi: 10.1038/nrc3185.
Funato, K. *et al.* (2014) 'Use of human embryonic stem cells to model pediatric gliomas with H3.3K27M histone mutation', *Science*, 346(6216), pp. 1529–1533. doi: 10.1126/science.1253799.
Gaillard, P. L. *et al.* (1996) 'Chromatin Assembly Coupled to DNA Repair : A New Role for Chromatin Assembly Factor I', 86, pp. 887–896.
Galiegue-Zouitina, S., Bailleul, B. and Loucheux-Lefebvre, M. H. (1985) 'Adducts from in Vivo Action of the Carcinogen 4-Hydroxyaminoquinoline 1-Oxide in Rats and from in Vitro Reaction of 4-Acetoxyaminoquinoline 1-Oxide with DNA and Polynucleotides', *Cancer Research*, 45(2), pp. 520–525.
Gallie, D. R., Lewis, N. J. and Marzluff, W. F. (1996) *The histone 3′-terminal stem-loop is necessary for translation in Chinese hamster ovary cells*, *Nucleic Acids Research*. Oxford

University Press.
García-Gómez, S. *et al.* (2013) 'PrimPol, an Archaic Primase/Polymerase Operating in Human Cells', *Molecular Cell*, 52(4), pp. 541–553. doi: 10.1016/J.MOLCEL.2013.09.025.
García-Muse, T. and Aguilera, A. (2016) 'Transcription-replication conflicts: How they occur and how they are resolved', *Nature Reviews Molecular Cell Biology*. Nature Publishing Group, 17(9), pp. 553–563. doi: 10.1038/nrm.2016.88.
Gellert, M., Lipsett, M. N. and Davies, D. R. (1962) 'Helix formation by guanylic acid', *Proceedings of the National Academy of Sciences of the United States of America*, 48, pp. 2013–2018. doi: 10.1073/pnas.48.12.2013.
Goldberg, A. D. *et al.* (2010) 'Distinct Factors Control Histone Variant H3.3 Localization at Specific Genomic Regions', *Cell*. Elsevier Ltd, 140(5), pp. 678–691. doi: 10.1016/j.cell.2010.01.003.
Gollapudi, B. B., White, P. A. and Honma, M. (2019) 'The IWGT in vitro Mammalian Cell Gene Mutation (MCGM) assays working group—Introductory remarks & consensus statements', *Mutation Research - Genetic Toxicology and Environmental Mutagenesis*. Elsevier, 848(March), p. 403061. doi: 10.1016/j.mrgentox.2019.05.017.
Gonzalez-Perez, A., Sabarinathan, R. and Lopez-Bigas, N. (2019) 'Local Determinants of the Mutational Landscape of the Human Genome', *Cell*. Elsevier Inc., 177(1), pp. 101–114. doi: 10.1016/j.cell.2019.02.051.
Green, C. M. (2002) 'When repair meets chromatin First in series on chromatin dynamics', 3(1), pp. 28–33.
Green, C. M. and Almouzni, G. (2003) 'Local action of the chromatin assembly factor CAF-1 at sites of nucleotide excision repair in vivo', *EMBO Journal*, 22(19), pp. 5163–5174. doi: 10.1093/emboj/cdg478.
Gregersen, L. H. and Svejstrup, J. Q. (2018) 'The Cellular Response to Transcription-Blocking DNA Damage', *Trends in Biochemical Sciences*. Elsevier Ltd, 43(5), pp. 327–341. doi: 10.1016/j.tibs.2018.02.010.
Groth, P. *et al.* (2010) 'Methylated DNA Causes a Physical Block to Replication Forks Independently of Damage Signalling, O6-Methylguanine or DNA Single-Strand Breaks and Results in DNA Damage', *Journal of Molecular Biology*. Elsevier Ltd, 402(1), pp. 70–82. doi: 10.1016/j.jmb.2010.07.010.
Guo, R. *et al.* (2014) 'BS69/ZMYND11 reads and connects histone H3.3 lysine 36 trimethylation-decorated chromatin to regulated pre-mRNA processing', *Molecular Cell*. Elsevier Inc., 56(2), pp. 298–310. doi: 10.1016/j.molcel.2014.08.022.
Gursoy-Yuzugullu, O., Carman, C. and Price, B. D. (2017) 'Spatially restricted loading of BRD2 at DNA double-strand breaks protects H4 acetylation domains and promotes DNA repair', *Scientific Reports*. Springer US, 7(1), pp. 1–13. doi: 10.1038/s41598-017-13036-5.
Hake, S. B. *et al.* (2005) 'Serine 31 phosphorylation of histone variant H3.3 is specific to regions bordering centromeres in metaphase chromosomes', *Proceedings of the National Academy of Sciences of the United States of America*, 102(18), pp. 6344–6349. doi: 10.1073/pnas.0502413102.
Hake, S. B. *et al.* (2006) 'Expression patterns and post-translational modifications associated with mammalian histone H3 variants', *Journal of Biological Chemistry*, 281(1), pp. 559–568. doi: 10.1074/jbc.M509266200.
Hampp, S. *et al.* (2016) 'DNA damage tolerance pathway involving DNA polymerase ι and the tumor suppressor p53 regulates DNA replication fork progression', *Proceedings of the National Academy of Sciences of the United States of America*, 113(30), pp. E4311–E4319. doi: 10.1073/pnas.1605828113.

Hanahan, D. and Weinberg, R. A. (2011) 'Hallmarks of cancer: The next generation', *Cell*. Elsevier Inc., 144(5), pp. 646–674. doi: 10.1016/j.cell.2011.02.013.
Harada, A. *et al.* (2012) 'Chd2 interacts with H3.3 to determine myogenic cell fate', *EMBO Journal*. Nature Publishing Group, 31(13), pp. 2994–3007. doi: 10.1038/emboj.2012.136.
Harrington, J. J. and Lieber, M. R. (1994) 'Functional domains within FEN-1 and RAD2 define a family of structure- p ecific endonucleases: implications or nucleotide excision repair', pp. 1344–1355.
Hart, T. *et al.* (2015) 'High-Resolution CRISPR Screens Reveal Fitness Genes and Genotype-Specific Cancer Liabilities', *Cell*. Elsevier Inc., 163(6), pp. 1515–1526. doi: 10.1016/j.cell.2015.11.015.
He, Q. *et al.* (2015) 'The Daxx/Atrx Complex Protects Tandem Repetitive Elements during DNA Hypomethylation by Promoting H3K9 Trimethylation', *Cell Stem Cell*. Elsevier, 17(3), pp. 273–286. doi: 10.1016/j.stem.2015.07.022.
Hengst, L. *et al.* (1994) 'A cell cycle-regulated inhibitor of cyclin-dependent kinases', *Proceedings of the National Academy of Sciences of the United States of America*, 91(12), pp. 5291–5295. doi: 10.1073/pnas.91.12.5291.
Hoang, S. M. *et al.* (2020) 'Regulation of ALT-associated homology-directed repair by polyADP-ribosylation', *Nature Structural and Molecular Biology*. Springer US, 27(12), pp. 1152–1164. doi: 10.1038/s41594-020-0512-7.
Hoelper, D. *et al.* (2017) 'Structural and mechanistic insights into ATRX-dependent and -independent functions of the histone chaperone DAXX', *Nature Communications*. Springer US, 8(1). doi: 10.1038/s41467-017-01206-y.
Hoffmann, M. *et al.* (2020) 'SARS-CoV-2 Cell Entry Depends on ACE2 and TMPRSS2 and Is Blocked by a Clinically Proven Protease Inhibitor', *Cell*, 181(2), pp. 271-280.e8. doi: 10.1016/j.cell.2020.02.052.
Hollstein, M. *et al.* (1991) 'p53 Mutations in Human Cancers', (July), pp. 49–54.
Hong, L. *et al.* (1993) 'Studies of the DNA binding properties of histone H4 amino terminus. Thermal denaturation studies reveal that acetylation markedly reduces the binding constant of the H4 "tail" to DNA', *Journal of Biological Chemistry*, 268(1), pp. 305–314. doi: 10.1016/s0021-9258(18)54150-8.
Honma, M. (2005) 'Generation of loss of heterozygosity and its dependency on p53 status in human lymphoblastoid cells', *Environmental and Molecular Mutagenesis*, 45(2–3), pp. 162–176. doi: 10.1002/em.20113.
Huang, J. C. and Sancar, A. (1994) 'Determination of minimum substrate size for human excinuclease', *Journal of Biological Chemistry*. Â© 1994 ASBMB. Currently published by Elsevier Inc; originally published by American Society for Biochemistry and Molecular Biology., 269(29), pp. 19034–19040. doi: 10.1016/s0021-9258(17)32270-6.
Huh, M. S. *et al.* (2016) 'Stalled replication forks within heterochromatin require ATRX for protection', *Cell Death and Disease*. Nature Publishing Group, 7(5), pp. e2220-12. doi: 10.1038/cddis.2016.121.
Hwang, B. J. *et al.* (1999) 'Expression of the p48 xeroderma pigmentosum gene is p53-dependent and is involved in global genomic repair', *Proceedings of the National Academy of Sciences of the United States of America*, 96(2), pp. 424–428. doi: 10.1073/pnas.96.2.424.
Ihle, M. *et al.* (2021) 'Impact of the interplay between stemness features, p53 and pol iota on replication pathway choices', *Nucleic Acids Research*, 49(13), pp. 7457–7475. doi: 10.1093/nar/gkab526.
Izda, V., Jeffries, M. A. and Sawalha, A. H. (2021) 'COVID-19: A review of therapeutic

strategies and vaccine candidates', *Clinical Immunology*. Elsevier Inc., 222(November 2020), p. 108634. doi: 10.1016/j.clim.2020.108634.
Jackson, S. P. and Bartek, J. (2009) 'The DNA-damage response in human biology and disease'. Nature Publishing Group, 461(October), pp. 1071–1078. doi: 10.1038/nature08467.
Janićijević, A. *et al.* (2003) 'DNA bending by the human damage recognition complex XPC-HR23B', *DNA Repair*, 2(3), pp. 325–336. doi: 10.1016/S1568-7864(02)00222-7.
Jiang, Y. *et al.* (2010) 'INO80 chromatin remodeling complex promotes the removal of UV lesions by the nucleotide excision repair pathway', pp. 2–7. doi: 10.1073/pnas.1008388107/-/DCSupplemental.www.pnas.org/cgi/doi/10.1073/pnas.1008388107.
Jin, C. and Felsenfeld, G. (2007) 'Nucleosome stability mediated by histone variants H3.3 and H2A.Z', *Genes and Development*, 21(12), pp. 1519–1529. doi: 10.1101/gad.1547707.
Jones, C. J., Edwards, S. M. and Waters, R. (1989) 'The repair of identified large DNA adducts induced by 4-nitroquinoline-1-oxide in normal or xeroderma pigmentosum group a human fibroblasts, and the role of DNA polymerases α or δ', *Carcinogenesis*, 10(7), pp. 1197–1201. doi: 10.1093/carcin/10.7.1197.
Joruiz, S. M. and Bourdon, J. C. (2016) 'P53 isoforms: Key regulators of the cell fate decision', *Cold Spring Harbor Perspectives in Medicine*, 6(8), pp. 1–21. doi: 10.1101/cshperspect.a026039.
Juhász, S. *et al.* (2018) 'ATRX Promotes DNA Repair Synthesis and Sister Chromatid Exchange during Homologous Recombination', *Molecular Cell*, pp. 1–14. doi: 10.1016/j.molcel.2018.05.014.
Jungmichel, S. *et al.* (2012) 'The molecular basis of ATM-dependent dimerization of the Mdc1 DNA damage checkpoint mediator', 40(9), pp. 3913–3928. doi: 10.1093/nar/gkr1300.
Kastan, M. B. *et al.* (1992) 'A mammalian cell cycle checkpoint pathway utilizing p53 and GADD45 is defective in ataxia-telangiectasia', *Cell*, 71(4), pp. 587–597. doi: 10.1016/0092-8674(92)90593-2.
Ke, Z., Oton, J., Qu, K., Cortese, M., Zila, V., McKeane, L., Nakane, T., Zivanov, J., Neufeldt, Christopher J., *et al.* (2020) 'Structures and distributions of SARS-CoV-2 spike proteins on intact virions', *Nature*. Nature Research, 588(7838), pp. 498–502. doi: 10.1038/S41586-020-2665-2.
Ke, Z., Oton, J., Qu, K., Cortese, M., Zila, V., McKeane, L., Nakane, T., Zivanov, J., Neufeldt, Christopher J, *et al.* (2020) 'Structures and distributions of SARS-CoV-2 spike proteins on intact virions', *Nature*, 588(7838), pp. 498–502. doi: 10.1038/s41586-020-2665-2.
Koschmann, Carl; *et al.* (2016) 'ATRX loss promotes tumor growth and impairs nonhomologous end joining DNA repair in glioma', *Science Translational Medicine*, 8(328). doi: 10.1126/scitranslmed.aac8228.
Kraushaar, D. C. *et al.* (2013) 'Genome-wide incorporation dynamics reveal distinct categories of turnover for the histone variant H3.3', *Genome Biology*, 14(10). doi: 10.1186/gb-2013-14-10-r121.
Krokan, H. E. and Bjørås, M. (2013) 'Base excision repair', *Cold Spring Harb Perspect Biol.* doi: 10.1142/9789812706782_0002.
Kubota, Y. *et al.* (1996) 'Reconstitution of DNA base excision-repair with purified human proteins: Interaction between DNA polymerase β and the XRCC1 protein', *EMBO Journal*, 15(23), pp. 6662–6670. doi: 10.1002/j.1460-2075.1996.tb01056.x.
Kuzminov, A. (2001) 'Single-strand interruptions in replicating chromosomes cause double-strand breaks', *Proceedings of the National Academy of Sciences of the United*

States of America, 98(15), pp. 8241–8246. doi: 10.1073/pnas.131009198.
De Laat, W. L. *et al.* (1998) 'DNA structural elements required for ERCC1-XPF endonuclease activity', *Journal of Biological Chemistry*. Â© 1998 ASBMB. Currently published by Elsevier Inc; originally published by American Society for Biochemistry and Molecular Biology., 273(14), pp. 7835–7842. doi: 10.1074/jbc.273.14.7835.
Laat, W. L. de, Jaspers, N. G. J. and Hoeijmakers, J. H. J. (1999) 'Molecular mechanism of global genome nucleotide excision repair', *Genes and Development*. doi: 10.32607/20758251-2014-6-1-23-34.
Lamarche, B. J., Orazio, N. I. and Weitzman, M. D. (2010) 'The MRN complex in double-strand break repair and telomere maintenance', *FEBS Letters*, 584(17), pp. 3682–3695. doi: 10.1016/j.febslet.2010.07.029.
Latonen, L., Taya, Y. and Laiho, M. (2001) 'UV-radiation induces dose-dependent regulation of p53 response and modulates p53-HDM2 interaction in human fibroblasts', *Oncogene*, 20(46), pp. 6784–6793. doi: 10.1038/sj.onc.1204883.
Law, M. J. *et al.* (2010) 'ATR-X syndrome protein targets tandem repeats and influences allele-specific expression in a size-dependent manner', *Cell*. Elsevier Ltd, 143(3), pp. 367–378. doi: 10.1016/j.cell.2010.09.023.
Lee, J. H. *et al.* (2003) 'NMR study on the interaction between RPA and DNA decamer containing cis-syn cyclobutane pyrimidine dimer in the presence of XPA: Implication for damage verification and strand-specific dual incision in nucleotide excision repair', *Nucleic Acids Research*, 31(16), pp. 4747–4754. doi: 10.1093/nar/gkg683.
Lee, J., Kumagai, A. and Dunphy, W. G. (2001) 'Positive Regulation of Wee1 by Chk1 and 14-3-3 Proteins', 12(March), pp. 551–563.
Leung, J. W. C. *et al.* (2013) 'Alpha thalassemia/mental retardation syndrome X-linked gene product ATRX is required for proper replication restart and cellular resistance to replication stress', *Journal of Biological Chemistry*, 288(9), pp. 6342–6350. doi: 10.1074/jbc.M112.411603.
Levy, J. A., Virolainen, M. and Defendi, V. (1968) 'Human lymphoblastoid lines from lymph node and spleen', *Cancer*, 22(3):517-.
Lewis, P. W. *et al.* (2010) 'Daxx is an H3.3-specific histone chaperone and cooperates with ATRX in replication-independent chromatin assembly at telomeres', *Proceedings of the National Academy of Sciences of the United States of America*, 107(32), pp. 14075–14080. doi: 10.1073/pnas.1008850107.
Lewis, P. W. *et al.* (2013) 'Inhibition of PRC2 Activity by a Gain-of-FunctionH3 Mutation Found in Pediatric Glioblastoma', *Science*, 340(May), pp. 857–861. doi: 10.1126/science.1232245.
Li, X. and Tyler, J. K. (2016) 'Nucleosome disassembly during human non-homologous end joining followed by concerted HIRA- and CAF-1-dependent reassembly', *eLife*, 5(JUN2016), pp. 1–18. doi: 10.7554/eLife.15129.
Li, Z. *et al.* (2009) 'Inhibition of SUV39H1 methyltransferase activity by DBC1', *Journal of Biological Chemistry*. Â© 2009 ASBMB. Currently published by Elsevier Inc; originally published by American Society for Biochemistry and Molecular Biology., 284(16), pp. 10361–10366. doi: 10.1074/jbc.M900956200.
Lindahl, T. (1974) 'An N glycosidase from Escherichia coli that releases free uracil from DNA containing deaminated cytosine residues', *Proceedings of the National Academy of Sciences of the United States of America*, 71(9), pp. 3649–3653. doi: 10.1073/pnas.71.9.3649.
López-Saavedra, A. *et al.* (2016) 'A genome-wide screening uncovers the role of CCAR2 as an antagonist of DNA end resection', *Nature Communications*, 7. doi:

10.1038/ncomms12364.
Lovejoy, C. A. *et al.* (2012) 'Loss of ATRX, genome instability, and an altered DNA damage response are hallmarks of the alternative lengthening of Telomeres pathway', *PLoS Genetics*, 8(7), pp. 12–15. doi: 10.1371/journal.pgen.1002772.
Lovejoy, C. A. *et al.* (2020) 'ATRX affects the repair of telomeric DSBs by promoting cohesion and a DAXX-dependent activity', *PLoS biology*, 18(1), p. e3000594. doi: 10.1371/journal.pbio.3000594.
Lu, C. *et al.* (2016) 'Histone H3K36 mutations promote sarcomagenesis through altered histone methylation landscape', *Science*, 352(6287), pp. 844–849. doi: 10.1126/science.aac7272.
Luan, B., Wang, H. and Huynh, T. (2021) 'Enhanced binding of the N501Y-mutated SARS-CoV-2 spike protein to the human ACE2 receptor: insights from molecular dynamics simulations', *FEBS Letters*, 595(10), pp. 1454–1461. doi: 10.1002/1873-3468.14076.
De Lucia, F. *et al.* (2001) 'Subnuclear localization and mitotic phosphorylation of HIRA, the human homologue of Saccharomyces cerevisiae transcriptional regulators Hir1p/Hir2p', *Biochemical Journal*, 358(2), pp. 447–455. doi: 10.1042/0264-6021:3580447.
Luger, K. *et al.* (1997) 'Crystal structure of the nucleosome core particle at 2.8 Å resolution', *Nature*, 389(6648), pp. 251–260. doi: 10.1038/38444.
Luijsterburg, M. S. *et al.* (2012) 'DDB2 promotes chromatin decondensation at UV-induced DNA damage', *Journal of Cell Biology*, 197(2), pp. 267–281. doi: 10.1083/jcb.201106074.
Luijsterburg, M. S. *et al.* (2016) 'PARP1 Links CHD2-Mediated Chromatin Expansion and H3.3 Deposition to DNA Repair by Non-homologous End-Joining', *Molecular Cell*. The Authors, 61(4), pp. 547–562. doi: 10.1016/j.molcel.2016.01.019.
Lukas, C. *et al.* (2003) 'Distinct spatiotemporal dynamics of mammalian checkpoint regulators induced by DNA damage', 5(March). doi: 10.1038/ncb945.
Martire, S. *et al.* (2019) 'Phosphorylation of histone H3.3 at serine 31 promotes p300 activity and enhancer acetylation', *Nature Genetics*. Springer US, 51(6), pp. 941–946. doi: 10.1038/s41588-019-0428-5.
Marzluff, W. F. *et al.* (2002) 'The Human and Mouse Replication-Dependent Histone Genes', 80(5), pp. 487–498. doi: 10.1006/geno.2002.6850.
Marzluff, W. F., Wagner, E. J. and Duronio, R. J. (2008) 'Metabolism and regulation of canonical histone mRNAs: Life without a poly(A) tail', *Nature Reviews Genetics*, 9(11), pp. 843–854. doi: 10.1038/NRG2438.
Matsuoka, S., Huang, M. and Elledge, S. J. (1998) 'Linkage of ATM to Cell Cycle Regulation by the Chk2 Protein Kinase', 282(December), pp. 1893–1898.
McLure, K. G. and Lee, P. W. K. (1998) 'How p53 binds DNA as a tetramer', *EMBO Journal*, 17(12), pp. 3342–3350. doi: 10.1093/emboj/17.12.3342.
Meier, A. *et al.* (2007) 'Spreading of mammalian DNA-damage response factors studied by ChIP-chip at damaged telomeres', 26(11), pp. 2707–2718. doi: 10.1038/sj.emboj.7601719.
Mello, J. A. *et al.* (2002) 'Human Asf1 and CAF-1 interact and synergize in a repair-coupled nucleosome assembly pathway', 3(4), pp. 329–334.
Mellon, I., Spivak, G. and Hanawalt, P. C. (1987) 'Selective removal of transcription-blocking DNA damage from the transcribed strand of the mammalian DHFR gene', *Cell*, 51(2), pp. 241–249. doi: 10.1016/0092-8674(87)90151-6.
Mitchell, D. L., Jen, J. and Cleaver, J. E. (1991) 'RELATIVE INDUCTION OF CYCLOBUTANE DIMERS and CYTOSINE PHOTOHYDRATES IN DNA IRRADIATED in vitro and in vivo

WITH ULTRAVIOLET-C and ULTRAVIOLET-B LIGHT', *Photochemistry and Photobiology*, 54(5), pp. 741–746. doi: https://doi.org/10.1111/j.1751-1097.1991.tb02084.x.
Mitchell, D. and Nairn, R. (1989) 'THE BIOLOGY OF THE (6–4) PHOTOPRODUCT', *Photochemistry and Photobiology*, 49(6), pp. 805–819. doi: https://doi.org/10.1111/j.1751-1097.1989.tb05578.x.
Mitra, P. *et al.* (2003) 'Identification of HiNF-P, a Key Activator of Cell Cycle-Controlled Histone H4 Genes at the Onset of S Phase', *Molecular and Cellular Biology*, 23(22), pp. 8110–8123. doi: 10.1128/mcb.23.22.8110-8123.2003.
Mizukoshi, T. *et al.* (2001) 'Structural study of DNA duplexes containing the (6-4) photoproduct by fluorescence resonance energy transfer', *Nucleic Acids Research*, 29(24), pp. 4948–4954. doi: 10.1093/nar/29.24.4948.
Muhire, B. M., Booker, M. A. and Tolstorukov, M. Y. (2019) 'Non-neutral evolution of H3.3-encoding genes occurs without alterations in protein sequence', *Scientific Reports*, 9(1), pp. 1–11. doi: 10.1038/s41598-019-44800-4.
Müller, S. and Almouzni, G. (2014) 'A network of players in H3 histone variant deposition and maintenance at centromeres', *BBA - Gene Regulatory Mechanisms*. Elsevier B.V., 1839(3), pp. 241–250. doi: 10.1016/j.bbagrm.2013.11.008.
Nelson, G. *et al.* (2021) 'Molecular dynamic simulation reveals E484K mutation enhances spike RBD-ACE2 affinity and the 1 combination of E484K, K417N and N501Y mutations (501Y.V2 variant) induces conformational change greater than N501Y mutant alone, potentially resulting in an esc', *bioRxiv*, p. 2021.01.13.426558. Available at: https://doi.org/10.1101/2021.01.13.426558.
Niedernhofer, L. J. *et al.* (2004) 'The Structure-Specific Endonuclease Ercc1-Xpf Is Required To Resolve DNA Interstrand Cross-Link-Induced Double-Strand Breaks', *Molecular and Cellular Biology*, 24(13), pp. 5776–5787. doi: 10.1128/mcb.24.13.5776-5787.2004.
Nissen, K. A., Lan, S. Y. and Smerdon, M. J. (1986) 'Stability of nucleosome placement in newly repaired regions of DNA.', *Journal of Biological Chemistry*. Â© 1986 ASBMB. Currently published by Elsevier Inc; originally published by American Society for Biochemistry and Molecular Biology., 261(19), pp. 8585–8588. doi: 10.1016/S0021-9258(19)84417-4.
Di Noia, J. M. and Neuberger, M. S. (2007) 'Molecular mechanisms of antibody somatic hypermutation', *Annual Review of Biochemistry*, 76, pp. 1–22. doi: 10.1146/annurev.biochem.76.061705.090740.
Ortega, S., Malumbres, M. and Barbacid, M. (2002) 'Cyclin D-dependent kinases, INK4 inhibitors and cancer', *Biochimica et Biophysica Acta - Reviews on Cancer*, 1602(1), pp. 73–87. doi: 10.1016/S0304-419X(02)00037-9.
Pinto, A. L. and Lippard, S. J. (1985) 'BINDING OF THE ANTITUMOR DRUG c/s-DIAMMINEDICHLOROPLATINUM(II) (CISPLATIN) TO DNA', *Biochimica etBiophysicaActa*, 780, pp. 167–180.
Polo, S. E. and Almouzni, G. (2015) 'Chromatin dynamics after DNA damage : The legacy of the access – repair – restore model'. Elsevier B.V., 36, pp. 114–121.
Postow, L. *et al.* (2001) 'Positive Torsional Strain Causes the Formation of a Four-way Junction at Replication Forks', *Journal of Biological Chemistry*. © 2001 ASBMB. Currently published by Elsevier Inc; originally published by American Society for Biochemistry and Molecular Biology., 276(4), pp. 2790–2796. doi: 10.1074/jbc.M006736200.
Qin, B. *et al.* (2015) 'DBC1 functions as a tumor suppressor by regulating p53 stability', *Cell Reports*. The Authors, 10(8), pp. 1324–1334. doi: 10.1016/j.celrep.2015.01.066.
Ramanathan, M. *et al.* (2021) 'SARS-CoV-2 B.1.1.7 and B.1.351 spike variants bind

human ACE2 with increased affinity', *The Lancet Infectious Diseases*. Elsevier Ltd, 21(8), p. 1070. doi: 10.1016/S1473-3099(21)00262-0.
Ran, F. A. *et al.* (2013) 'Genome engineering using the CRISPR-Cas9 system', *Nature Protocols*, 8(11), pp. 2281–2308. doi: 10.1038/nprot.2013.143.
Rao, R. C. and Dou, Y. (2015) 'Hijacked in cancer: The KMT2 (MLL) family of methyltransferases', *Nature Reviews Cancer*. Nature Publishing Group, 15(6), pp. 334–346. doi: 10.1038/nrc3929.
Ratnakumar, K. and Bernstein, E. (2013) 'ATRX: The case of a peculiar chromatin remodeler', *Epigenetics*, 8(1), pp. 3–9. doi: 10.4161/epi.23271.
Ray-Gallet, D. *et al.* (2011) 'Dynamics of Histone H3 Deposition In Vivo Reveal a Nucleosome Gap-Filling Mechanism for H3.3 to Maintain Chromatin Integrity', *Molecular Cell*, 44(6), pp. 928–941. doi: 10.1016/j.molcel.2011.12.006.
Ray-Gallet, D. *et al.* (2018) 'Functional activity of the H3.3 histone chaperone complex HIRA requires trimerization of the HIRA subunit', *Nature Communications*. Springer US, 9(1). doi: 10.1038/s41467-018-05581-y.
Ridgway, P. and Almouzni, G. (2000) 'CAF-1 and the inheritance of chromatin states: at the crossroads of DNA replication and repair.', *Journal of cell science*, 113 (Pt 1, pp. 2647–58. Available at: http://www.ncbi.nlm.nih.gov/pubmed/10893180.
Roberts, C. *et al.* (2002) ' Targeted Mutagenesis of the Hira Gene Results in Gastrulation Defects and Patterning Abnormalities of Mesoendodermal Derivatives Prior to Early Embryonic Lethality ', *Molecular and Cellular Biology*, 22(7), pp. 2318–2328. doi: 10.1128/mcb.22.7.2318-2328.2002.
Romanello, M. *et al.* (2016) 'Histone H3.3 promotes IgV gene diversification by enhancing formation of <scp>AID</scp> -accessible single-stranded <scp>DNA</scp>', *The EMBO Journal*, 35(13), pp. 1452–1464. doi: 10.15252/embj.201693958.
Roy, S. *et al.* (2018) 'p53 orchestrates DNA replication restart homeostasis by suppressing mutagenic RAD52 and POLθ pathways', *eLife*, 7, pp. 1–23. doi: 10.7554/eLife.31723.
Rubbi, C. P. and Milner, J. (2003) 'p53 is a chromatin accessibility factor for nucleotide excision repair of DNA damage', *EMBO Journal*, 22(4), pp. 975–986. doi: 10.1093/emboj/cdg082.
S. Banin, L. *et al.* (1998) 'Enhanced Phosphorylation of p53 by ATM in Response to DNA Damage', 281(September), pp. 1674–1678.
Sadic, D. *et al.* (2015) 'Atrx promotes heterochromatin formation at retrotransposons', *EMBO reports*, 16(7), pp. 836–850. doi: 10.15252/embr.201439937.
Sale, J. E. *et al.* (2001) 'Ablation of XRCC2/3 transforms immunoglobulin V gene conversion into somatic hypermutation [4]', *Nature*, 412(6850), pp. 921–926. doi: 10.1038/35091100.
Sale, J. E. (2013) 'Translesion DNA synthesis and mutagenesis in prokaryotes', *Cold Spring Harbor Perspectives in Biology*, 5(12). doi: 10.1101/cshperspect.a012682.
Savic, V. *et al.* (2009) 'Article Formation of Dynamic g -H2AX Domains along Broken DNA Strands Is Distinctly Regulated by ATM and MDC1 and Dependent upon H2AX Densities in Chromatin', *Molecular Cell*. Elsevier Ltd, 34(3), pp. 298–310. doi: 10.1016/j.molcel.2009.04.012.
Semlow, D. R. and Walter, J. C. (2021) 'Mechanisms of Vertebrate DNA Interstrand Cross-Link Repair', *Annual Review of Biochemistry*, 90, pp. 107–135. doi: 10.1146/annurev-biochem-080320-112510.
Setlow, R. B. (1974) 'The wavelengths in sunlight effective in producing skin cancer: A theoretical analysis', *Proceedings of the National Academy of Sciences of the United States*

of America, 71(9), pp. 3363–3366. doi: 10.1073/pnas.71.9.3363.
Shahi, A. *et al.* (2011) 'Mismatch-repair protein MSH6 is associated with Ku70 and regulates DNA double-strand break repair', *Nucleic Acids Research*, 39(6), pp. 2130–2143. doi: 10.1093/nar/gkq1095.
Shivji, M. K. K. *et al.* (1995) 'Nucleotide Excision Repair DNA Synthesis by DNA Polymerase ∈ in the Presence of PCNA, RFC, and RPA', *Biochemistry*, 34(15), pp. 5011–5017. doi: 10.1021/bi00015a012.
Siggens, L. *et al.* (2015) 'Transcription-coupled recruitment of human CHD1 and CHD2 influences chromatin accessibility and histone H3 and H3.3 occupancy at active chromatin regions', *Epigenetics and Chromatin*, 8(1), pp. 1–14. doi: 10.1186/1756-8935-8-4.
Sitbon, D. *et al.* (2020) 'Histone variant H3.3 residue S31 is essential for Xenopus gastrulation regardless of the deposition pathway', *Nature Communications*. Springer US, 11(1). doi: 10.1038/s41467-020-15084-4.
Skopek, T. R. *et al.* (1978) 'Isolation of a human lymphoblastoid line heterozygous at the thymidine kinase locus: Possibility for a rapid human cell mutation assay', *Biochemical and Biophysical Research Communications*, 84(2), pp. 411–416. doi: 10.1016/0006-291X(78)90185-7.
Smerdon, M. J. and Lieberman, M. W. (1978) 'Nucleosome rearrangement in human chromatin during UV-induced DNA repair synthesis', 75(9), pp. 4238–4241.
Smith, J. *et al.* (2010) 'The ATM–Chk2 and ATR–Chk1 Pathways in DNA Damage Signaling and Cancer', in Vande Woude, G. F. and Klein, G. B. T.-A. in C. R. (eds) *Advances in Cancer Research*. Academic Press, pp. 73–112. doi: https://doi.org/10.1016/B978-0-12-380888-2.00003-0.
Sobinoff, A. P. and Pickett, H. A. (2017) 'Alternative Lengthening of Telomeres: DNA Repair Pathways Converge', *Trends in Genetics*. Elsevier Ltd, 33(12), pp. 921–932. doi: 10.1016/j.tig.2017.09.003.
Soria, G., Polo, S. E. and Almouzni, G. (2012) 'Prime, Repair, Restore: The Active Role of Chromatin in the DNA Damage Response', *Molecular Cell*, 46(6), pp. 722–734. doi: 10.1016/j.molcel.2012.06.002.
Stiff, T. *et al.* (2006) 'ATR-dependent phosphorylation and activation of ATM in response to UV treatment or replication fork stalling', 25(24), pp. 5775–5782. doi: 10.1038/sj.emboj.7601446.
Stucki, M. *et al.* (2005) 'MDC1 Directly Binds Phosphorylated Histone H2AX to Regulate Cellular Responses to DNA Double-Strand Breaks', pp. 1213–1226. doi: 10.1016/j.cell.2005.09.038.
Stützer, A. *et al.* (2016) 'Modulations of DNA Contacts by Linker Histones and Post-translational Modifications Determine the Mobility and Modifiability of Nucleosomal H3 Tails', *Molecular Cell*, 61(2), pp. 247–259. doi: 10.1016/j.molcel.2015.12.015.
Sugasawa, K. *et al.* (1998) 'Xeroderma pigmentosum group C protein complex is the initiator of global genome nucleotide excision repair', *Molecular Cell*, 2(2), pp. 223–232. doi: 10.1016/S1097-2765(00)80132-X.
Sugasawa, K. (2010) 'Regulation of damage recognition in mammalian global genomic nucleotide excision repair', *Mutation Research - Fundamental and Molecular Mechanisms of Mutagenesis*, 685(1–2), pp. 29–37. doi: 10.1016/j.mrfmmm.2009.08.004.
Tagami, H. *et al.* (2004) 'Histone H3.1 and H3.3 Complexes Mediate Nucleosome Assembly Pathways Dependent or Independent of DNA Synthesis', *Assembly*, 116(1), pp. 51–61. doi: http://dx.doi.org/10.1016/S0092-8674(03)01064-X.
Takao, N. *et al.* (1999) 'Disruption of ATM in p53-null cells causes multiple functional

abnormalities in cellular response to ionizing radiation', *Oncogene*, 18(50), pp. 7002–7009. doi: 10.1038/sj.onc.1203172.
Tang, Y. *et al.* (2006) 'Structure of a human ASF1a-HIRA complex and insights into specificity of histone chaperone complex assembly', *Nature Structural and Molecular Biology*, 13(10), pp. 921–929. doi: 10.1038/nsmb1147.
Tantin, D. (1998) 'RNA polymerase II elongation complexes containing the cockayne syndrome group B protein interact with a molecular complex containing the transcription factor IIH components xeroderma pigmentosum B and p62', *Journal of Biological Chemistry*. Â© 1998 ASBMB. Currently published by Elsevier Inc; originally published by American Society for Biochemistry and Molecular Biology., 273(43), pp. 27794–27799. doi: 10.1074/jbc.273.43.27794.
Teng, Y. C. *et al.* (2021) 'ATRX promotes heterochromatin formation to protect cells from G-quadruplex DNA-mediated stress', *Nature Communications*. Springer US, 12(1). doi: 10.1038/s41467-021-24206-5.
Thoma, F. (1999) 'Light and dark in chromatin repair : repair of UV- induced DNA lesions by photolyase and nucleotide', *EMBO Journal*, 18(23), pp. 6585–6598. Available at: http://dx.doi.org/10.1093/emboj/18.23.6585.
Torné, J. *et al.* (2020) 'Two HIRA-dependent pathways mediate H3.3 de novo deposition and recycling during transcription', *Nature Structural and Molecular Biology*. Springer US, 27(11), pp. 1057–1068. doi: 10.1038/s41594-020-0492-7.
Tuccori, M. *et al.* (2020) 'Anti-SARS-CoV-2 neutralizing monoclonal antibodies: clinical pipeline', *mAbs*. Taylor & Francis, 12(1). doi: 10.1080/19420862.2020.1854149.
Tzelepis, K. *et al.* (2016) 'A CRISPR Dropout Screen Identifies Genetic Vulnerabilities and Therapeutic Targets in Acute Myeloid Leukemia', *Cell Reports*. ElsevierCompany., 17(4), pp. 1193–1205. doi: 10.1016/j.celrep.2016.09.079.
Uziel, T. *et al.* (2003) 'Requirement of the MRN complex for ATM activation by DNA damage', 22(20).
Veaute, X. *et al.* (2000) 'UV lesions located on the leading strand inhibit DNA replication but do not inhibit SV40 T-antigen helicase activity', pp. 19–28.
Vermeulen, M. *et al.* (2010) 'Quantitative Interaction Proteomics and Genome-wide Profiling of Epigenetic Histone Marks and Their Readers', *Cell*. Elsevier Inc., 142(6), pp. 967–980. doi: 10.1016/j.cell.2010.08.020.
Voon, H. P. J. and Wong, L. H. (2015) 'New players in heterochromatin silencing: Histone variant H3.3 and the ATRX/DAXX chaperone', *Nucleic Acids Research*, 44(4), pp. 1496–1501. doi: 10.1093/nar/gkw012.
Walls, A. C. *et al.* (2020) 'Structure, Function, and Antigenicity of the SARS-CoV-2 Spike Glycoprotein', *Cell*. Elsevier, 181(2), pp. 281-292.e6. doi: 10.1016/j.cell.2020.02.058.
Wan, L. *et al.* (2013) 'HPrimpol1/CCDC111 is a human DNA primase-polymerase required for the maintenance of genome integrity', *EMBO Reports*. Nature Publishing Group, 14(12), pp. 1104–1112. doi: 10.1038/embor.2013.159.
Wang, C. and Taylor, J. (1991) 'Site-specific effect of thymine dimer formation on dA.dT. tract bending and its biological implications', *Proc. Nadl. Acad. Sci. USA*, 88(October), pp. 9072–9076.
Wang, H. *et al.* (2006) 'Histone H3 and H4 Ubiquitylation by the CUL4-DDB-ROC1 Ubiquitin Ligase Facilitates Cellular Response to DNA Damage', pp. 383–394. doi: 10.1016/j.molcel.2006.03.035.
Wang, X. W. *et al.* (1995) 'p53 modulation of TFIIH- associated nucleotide excision repair activity', 10(june).
Ward, I. M. and Chen, J. (2001) 'Histone H2AX Is Phosphorylated in an ATR-dependent

Manner in Response to Replicational Stress *', *Journal of Biological Chemistry*. Â© 2001 ASBMB. Currently published by Elsevier Inc; originally published by American Society for Biochemistry and Molecular Biology., 276(51), pp. 47759–47762. doi: 10.1074/jbc.C100569200.
Watson, L. A. *et al.* (2013) 'ATRX deficiency induces telomere dysfunction, endocrine defects and reduced life span', 123(5), pp. 2049–2063. doi: 10.1172/JCI65634.ic.
Weinberg, D. N., Allis, C. D. and Lu, C. (2017) 'Oncogenic mechanisms of histone H3 mutations', *Cold Spring Harbor Perspectives in Medicine*, 7(1), pp. 1–14. doi: 10.1101/cshperspect.a026443.
Wen, H. *et al.* (2014) 'ZMYND11 links histone H3.3K36me3 to transcription elongation and tumour suppression', *Nature*. Nature Publishing Group, 508(7495), pp. 263–268. doi: 10.1038/nature13045.
Wiedemann, S. M. *et al.* (2010) 'Identification and characterization of two novel primate-specific histone H3 variants, H3.X and H3.Y', *Journal of Cell Biology*, 190(5), pp. 777–791. doi: 10.1083/jcb.201002043.
Williams, A. B. and Schumacher, B. (2016) 'p53 in the DNA-damage-repair process', *Cold Spring Harbor Perspectives in Medicine*, 6(5), pp. 1–16. doi: 10.1101/cshperspect.a026070.
Wong, L. H. *et al.* (2010) 'ATRX interacts with H3.3 in maintaining telomere structural integrity in pluripotent embryonic stem cells', *Genome Research*, 20(3), pp. 351–360. doi: 10.1101/gr.101477.109.
Woodcock, C. L. F., Safer, J. P. and Stanchfield, J. E. (1976) 'STRUCTURAL REPEATING UNITS IN CHROMATIN I . Evidence for their General Occurrence It has recently been shown that under cer- tain preparative conditions , chromatin fibers exhibit a distinctive particulate sub- structure [l-3]. This is in contrast to th', 97(1975).
Woodcock, C. L. and Ghosh, R. P. (2010) 'Chromatin Higher-order Structure and Dynamics'.
Wrapp, D. *et al.* (2020) 'Cryo-EM structure of the 2019-nCoV spike in the prefusion conformation', *Science*, 367(6483), pp. 1260–1263. doi: 10.1126/science.aax0902.
Xiong, C. *et al.* (2018) 'UBN1/2 of HIRA complex is responsible for recognition and deposition of H3.3 at cis-regulatory elements of genes in mouse ES cells', *BMC Biology*. BMC Biology, 16(1), pp. 1–18. doi: 10.1186/s12915-018-0573-9.
Xiong, X. *et al.* (2020) 'A thermostable, closed SARS-CoV-2 spike protein trimer', *Nature Structural & Molecular Biology*. doi: 10.1038/s41594-020-0478-5.
Yang, W. (2011) 'Surviving the sun: Repair and bypass of DNA UV lesions', *Protein Science*, 20(11), pp. 1781–1789. doi: 10.1002/pro.723.
Zee, B. M. *et al.* (2010) 'Global turnover of histone post-translational modifications and variants in human cells', *Epigenetics and Chromatin*, 3(1), pp. 1–11. doi: 10.1186/1756-8935-3-22.
Zeman, M. K. and Cimprich, K. A. (2014) 'Causes and consequences of replication stress', *Nature Cell Biology*, 16(1), pp. 2–9. doi: 10.1038/ncb2897.
Zhang, H. *et al.* (2017) 'RPA Interacts with HIRA and Regulates H3.3 Deposition at Gene Regulatory Elements in Mammalian Cells', *Molecular Cell*. Elsevier Inc., 65(2), pp. 272–284. doi: 10.1016/j.molcel.2016.11.030.
Zhao, H. and Piwnica-Worms, H. (2001) 'ATR-Mediated Checkpoint Pathways Regulate Phosphorylation and Activation of Human Chk1', 21(13), pp. 4129–4139. doi: 10.1128/MCB.21.13.4129.
Zhao, Q. *et al.* (2009) 'Modulation of Nucleotide Excision Repair by Mammalian SWI / SNF Chromatin-remodeling Complex', *Journal of Biological Chemistry*. Â© 2009 ASBMB.

Currently published by Elsevier Inc; originally published by American Society for Biochemistry and Molecular Biology., 284(44), pp. 30424–30432. doi: 10.1074/jbc.M109.044982.
Zink, L. M. *et al.* (2017) 'H3.Y discriminates between HIRA and DAXX chaperone complexes and reveals unexpected insights into human DAXX-H3.3-H4 binding and deposition requirements', *Nucleic Acids Research*, 45(10), pp. 5691–5706. doi: 10.1093/nar/gkx131.
Zolan, M. E. *et al.* (1982) 'Rearrangement of mammalian chromatin structure following excision repair', 299(September), pp. 462–464.

Appendix 1: List of Oligonucleotides used in this thesis

PCR and sequencing primers used for knockout screening or genotyping

Primer name	*Forward*	*Reverse*
H3F3A genotyping	GTCTCTGTACCATGGCT	AAACGAAAAAGTTTTCCT
H3F3B genotyping	CGCCCGACCTACCTGTA	TCTTCGGGGCGTCTTTCT
p53 screening (internal)	TCTCGATCTCCCAACCTCG	GATAGCGATGGTGAGCAGC
ATRX genotyping	GGTATCAGTAGCCTTCG	AATGGGTTTGTGGAGTTA
HIRA screening (internal)	CACCAGGCTTTTGTCACCTC	CCCAATCCACCTTCCCTTCT
M13F: topo cloning - provided by Genewiz	GTAAAACGACGGCCAG	

Oligonucleotides for insertion of gRNAs into pX458 plasmid

gRNA name	*Top Oligo*	*Bottom Oligo*
H3F3A gRNA1	CACCGTTTCTTCACCCCTCCAGTAG	AAACCTACTGGAGGGGTGAAGAAAC
H3F3A gRNA2	CACCGCAGACTGCCCGCAAATCGAC	AAACGTCGATTTGCGGGCAGTCTGC
H3F3B	CACCGAGAGGGAGCGCTTTTCCTGG	AAACCCAGGAAAAGCGCTCCCTCTC
ATRX	CACCGTGGAAGTAACTCTGATATGA	AAACTCATATCAGAGTTACTTCCAC
HIRA gRNA1	CACCGGCACGGTACCTCGTAAACGA	AAACTCGTTTACGAGGTACCGTGCC
HIRA gRNA2	CACCGGACGGGACCAAGTTCGCAAC	AAACGTTGCGAACTTGGTCCCGTCC
p53 gRNA1	CACCGCCGAGACGGGCCATTCGTGA	AAACTCACGAATGGCCCGTCTCGGC
p53 gRNA2	CACCGAATGGAGCCGTGTATCAGGT	AAACACCTGATACACGGCTCCATTC
p53 gRNA3	CACCGAACACGTTTCAAGTAGGCTA	AAACTAGCCTACTTGAAACGTGTTC
p53 gRNA4	CACCGATAGCTCATTATACCCTCCT	AAACAGGAGGGTATAATGAGCTATC

Primers for generation of CRISPR screen library

Primer name	*Sequence*
gRNA-HiSeq-SE50 F1	ACACTCTTTCCCTACACGACGCTCTTCCGATCTCTTGTGGAAAGGACGAAACA
gRNA-HiSeq-SE50 R1	GACTGGAGTTCAGACGTGTGCTCTTCCGATCTCCGACTCGGTGCCACTTTTTCAA
P5	AATGATACGGCGACCACCGAGATCTACACTCTTTCCCTACACGAC
P7 Index 2	CAAGCAGAAGACGGCATACGAGATACATCGGTGACTGGAGTTCAGACGT
P7 Index 4	CAAGCAGAAGACGGCATACGAGATTGGTCAGTGACTGGAGTTCAGACGT
P7 Index 5	CAAGCAGAAGACGGCATACGAGATCACTGTGTGACTGGAGTTCAGACGT
P7 Index 6	CAAGCAGAAGACGGCATACGAGATATTGGCGTGACTGGAGTTCAGACGT
P7 Index 7	CAAGCAGAAGACGGCATACGAGATGATCTGGTGACTGGAGTTCAGACGT
P7 Index 12	CAAGCAGAAGACGGCATACGAGATTACAAGGTGACTGGAGTTCAGACGT

Appendix 2: Full 2D cell cycle analysis plots

H3.3 knockout clones (section 3.3.4)

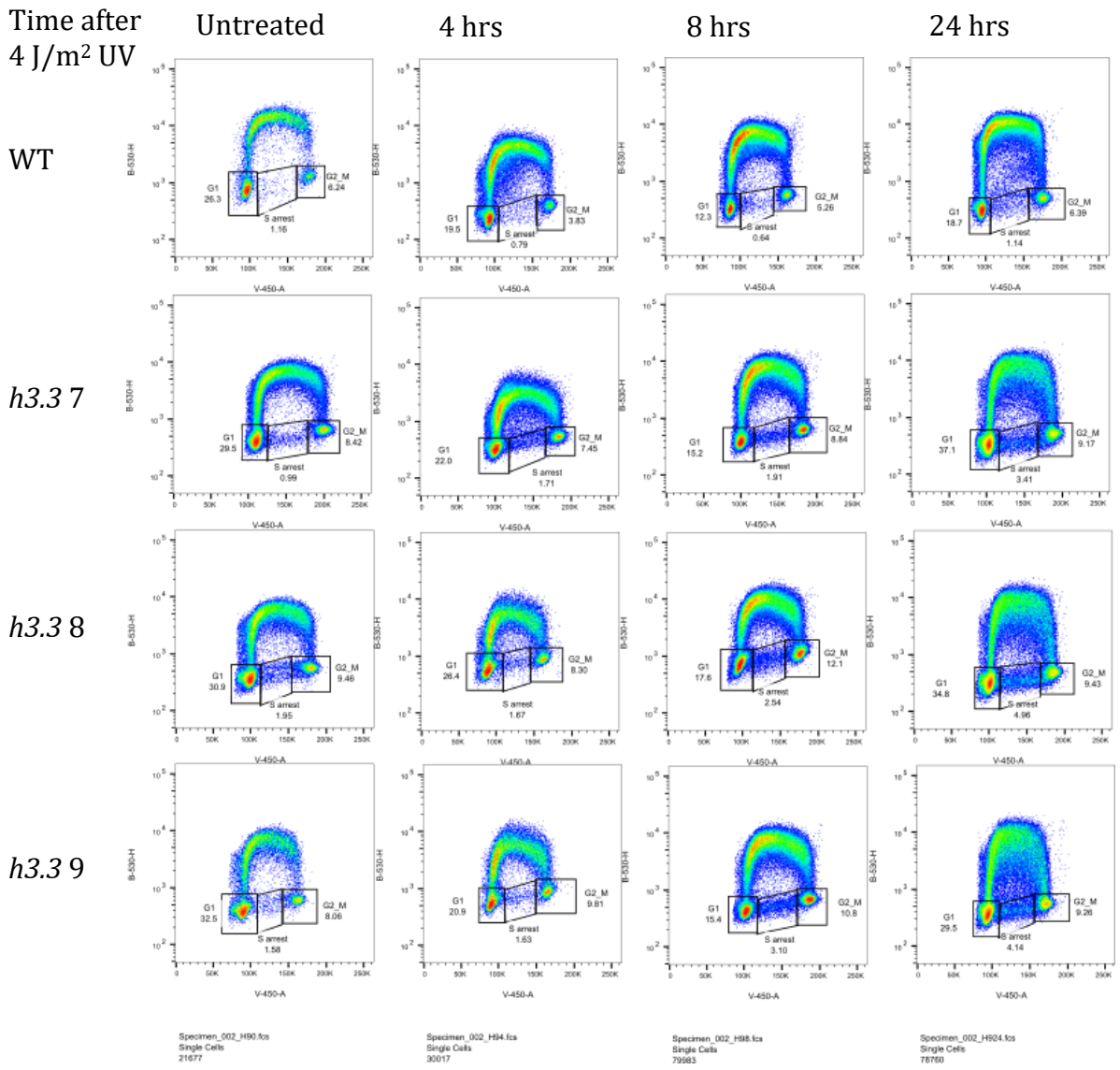

Time after 4 J/m² UV	Untreated	4 hrs	8 hrs	24 hrs
WT	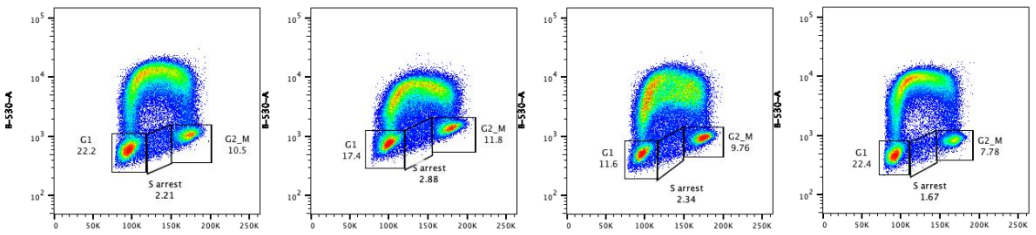			
h3.3 7	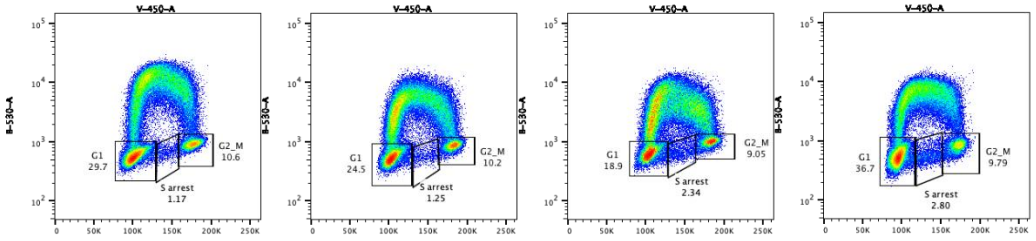			
h3.3 8	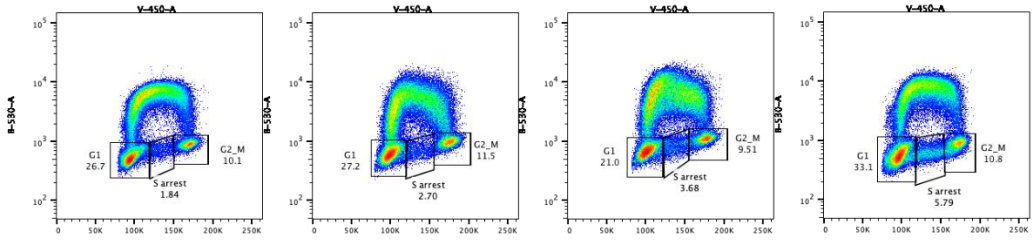			
h3.3 9	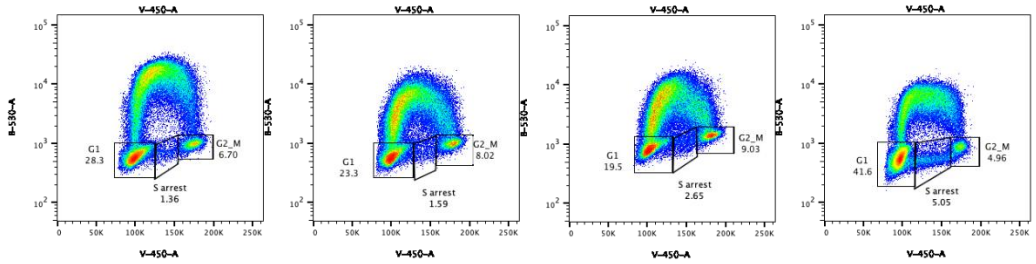			

H3.3 complemented (section 3.4.1)

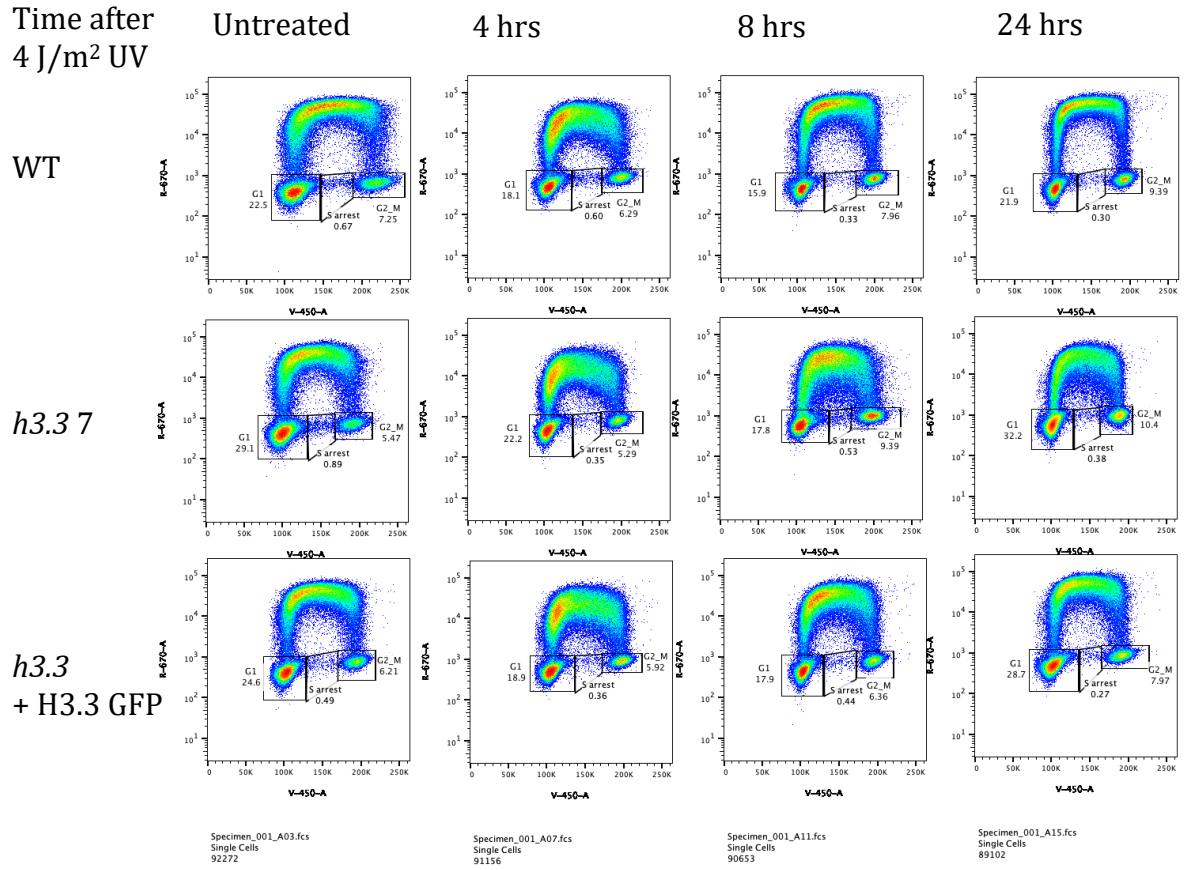

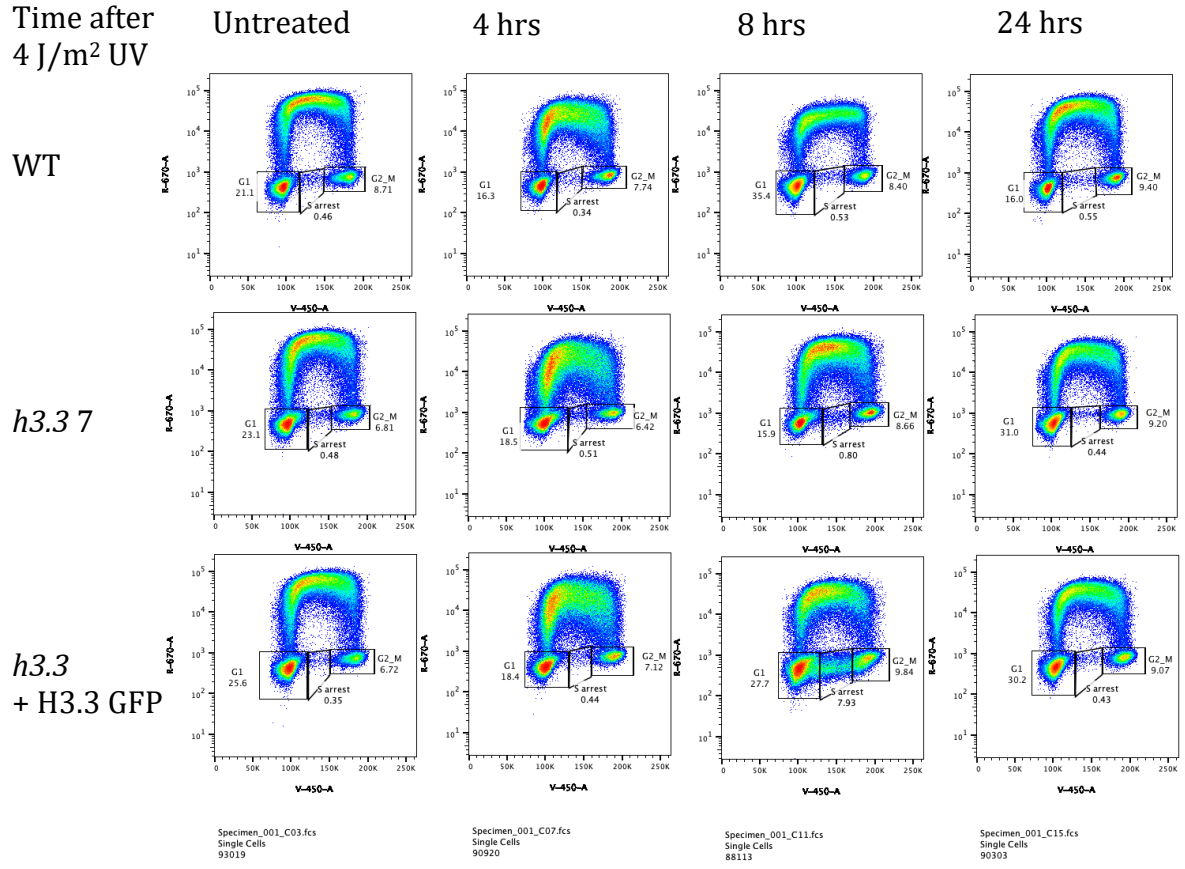

ATRX knockout clones (section 4.3.2)

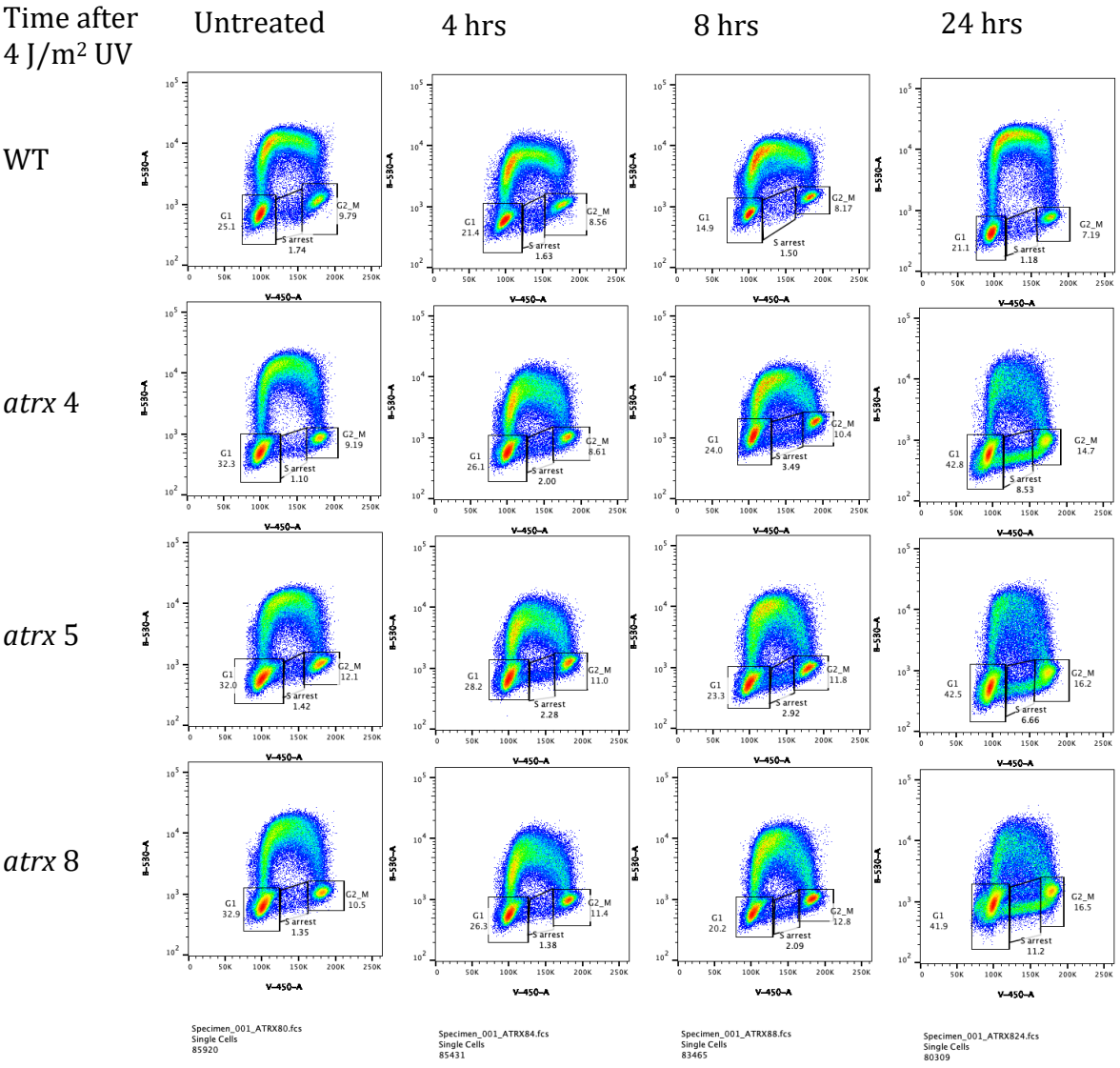

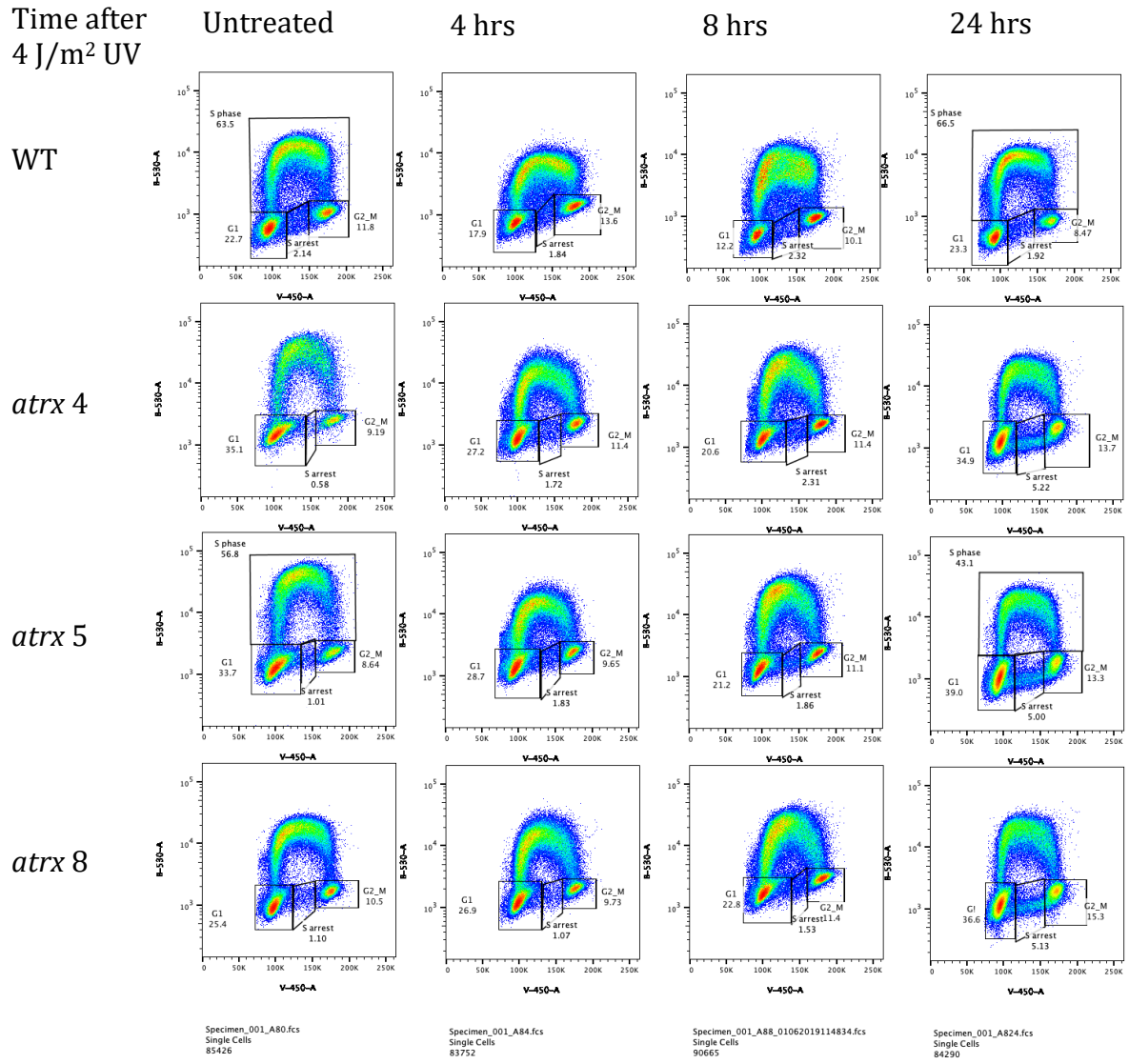
Time after 4 J/m² UV
Untreated
4 hrs
8 hrs
24 hrs
WT
atrx 4
atrx 5
atrx 8
S phase 63.5
G1 22.7
S arrest 2.14
G2_M 11.8
G1 17.9
S arrest 1.84
G2_M 13.6
G1 12.2
S arrest 2.32
G2_M 10.1
S phase 66.5
G1 23.3
S arrest 1.92
G2_M 8.47
G1 35.1
S arrest 0.58
G2_M 9.19
G1 27.2
S arrest 1.72
G2_M 11.4
G1 20.6
S arrest 2.31
G2_M 11.4
G1 34.9
S arrest 5.22
G2_M 13.7
S phase 56.8
G1 33.7
S arrest 1.01
G2_M 8.64
G1 28.7
S arrest 1.83
G2_M 9.65
G1 21.2
S arrest 1.86
G2_M 11.1
S phase 43.1
G1 39.0
S arrest 5.00
G2_M 13.3
G1 25.4
S arrest 1.10
G2_M 10.5
G1 26.9
S arrest 1.07
G2_M 9.73
G1 22.8
S arrest 1.53
G2_M 11.4
G1 36.6
S arrest 5.13
G2_M 15.3
B-530-A
V-450-A
Specimen_001_A80.fcs
Single Cells
85426
Specimen_001_A84.fcs
Single Cells
83752
Specimen_001_A88_01062019114834.fcs
Single Cells
90665
Specimen_001_A824.fcs
Single Cells
84290

Time after 4 J/m² UV	Untreated	4 hrs	8 hrs	24 hrs
WT	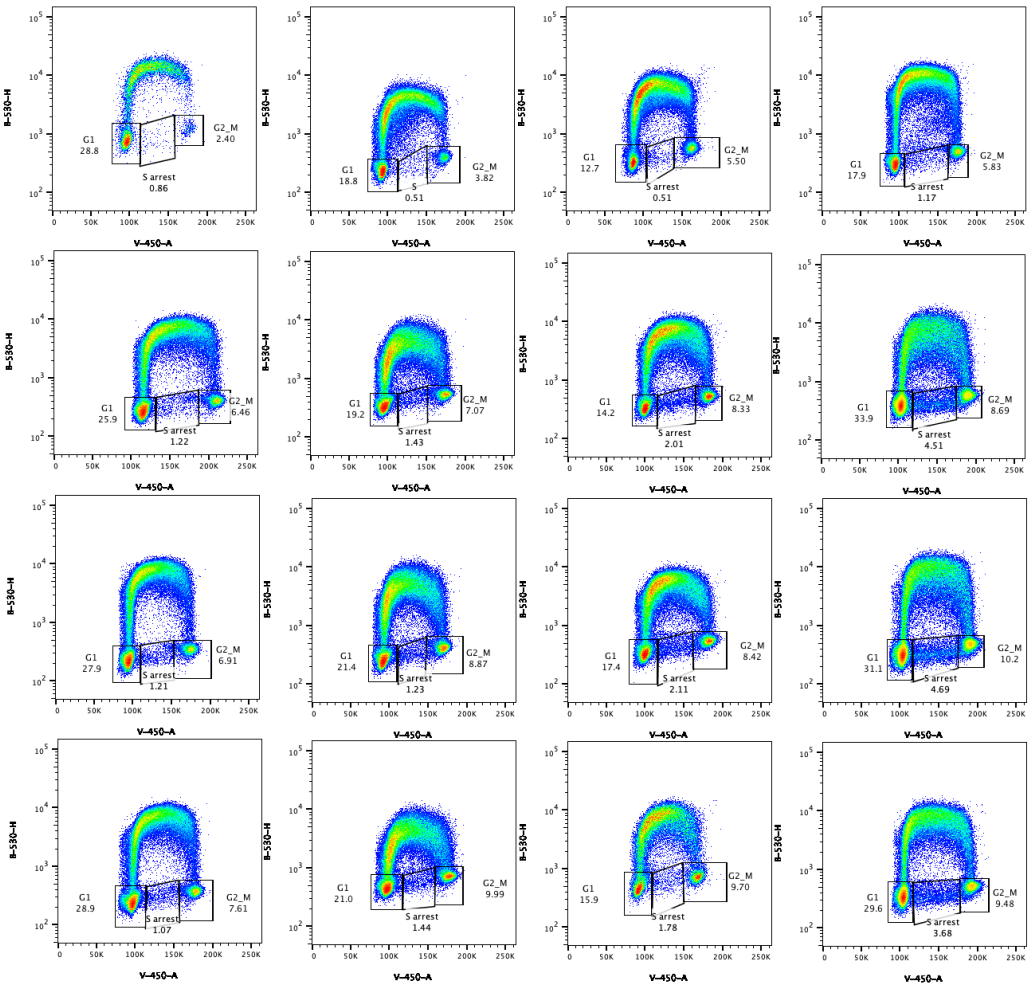			
atrx 4				
atrx 5				
atrx 8				

HIRA knockout cell line (section 4.3.2)

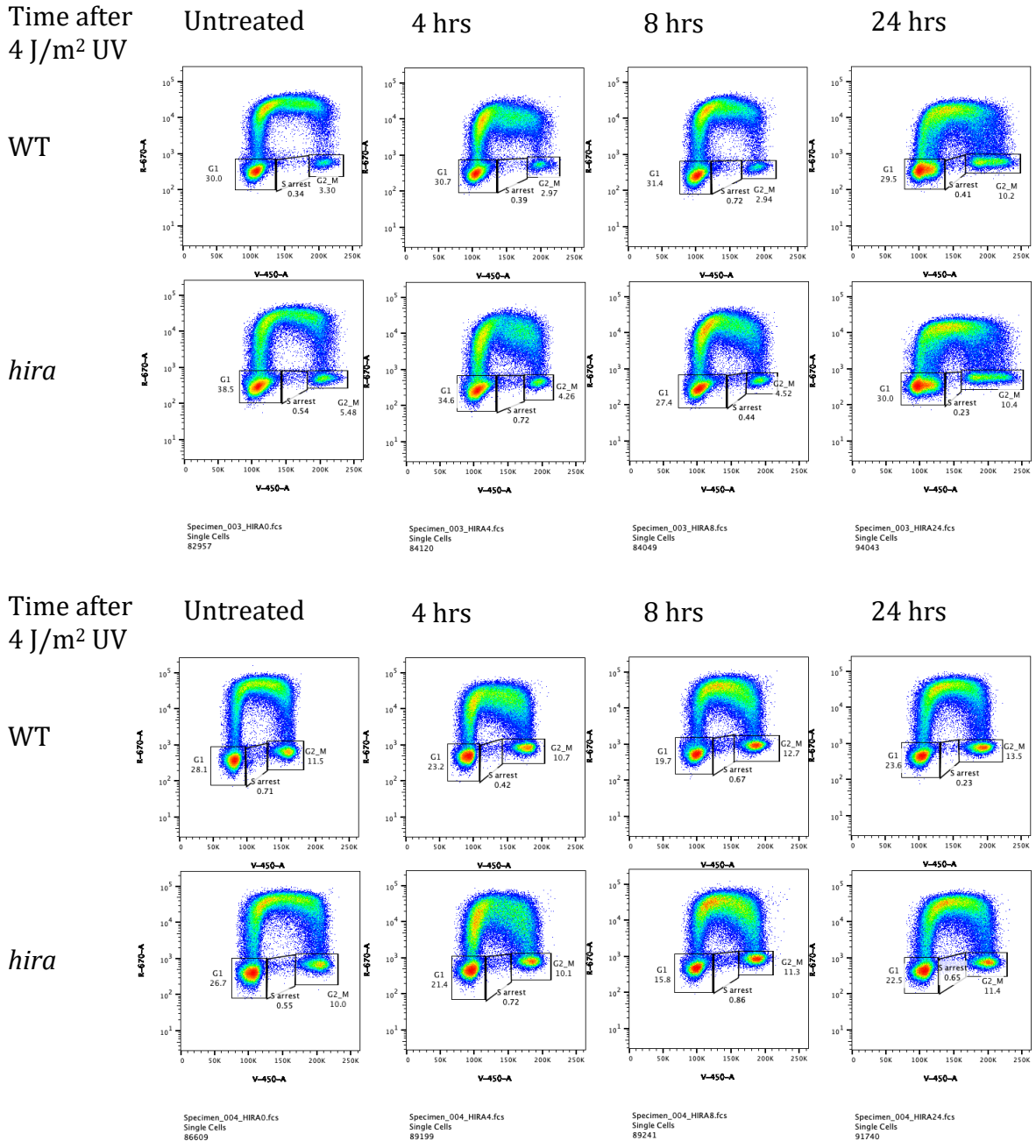

Time after 4 J/m² UV	Untreated	4 hrs	8 hrs	24 hrs
WT	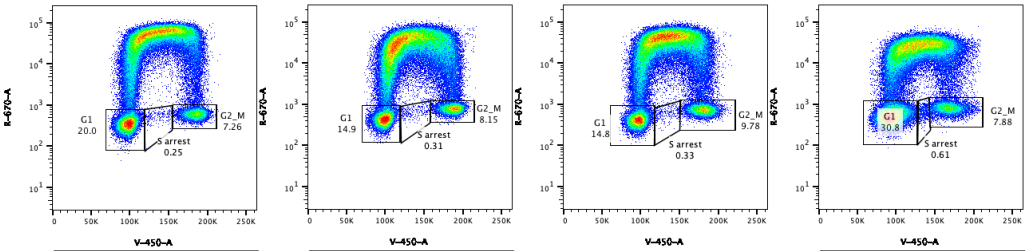			
hira	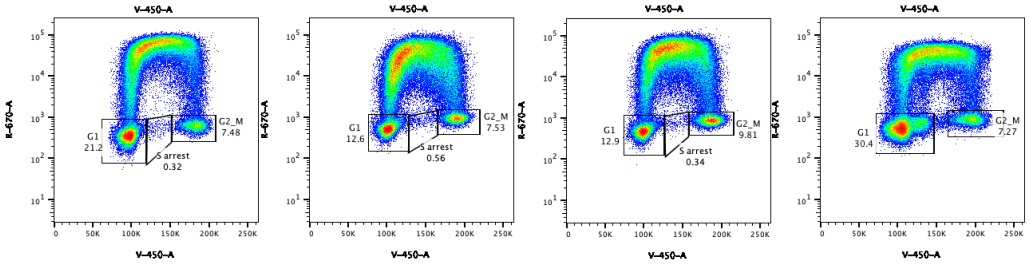			

Specimen_005_HIRA0.fcs
Single Cells
91024

Specimen_005_HIRA4.fcs
Single Cells
91826

Specimen_005_HIRA8.fcs
Single Cells
91128

Specimen_005_HIRA24.fcs
Single Cells
95690

Appendix 3: Proteins found by mass spectrometry and GFP-trap

Enriched both with and without UV, in the top 500 by percentage of total spectrum	*Enriched after UV only, in the top 500 by percentage of total spectrum*	*Enriched both with and without UV, outside the top 500 by percentage of total spectrum*	*Enriched without UV only, in the top 500 by percentage of total spectrum*
CHD1	BRWD1	BAZ1B	1433S
CHD1L	DHX15	COPA	ADT2
CHD4	IF4G1	DYNC1H1	ATD2B
DAXX	MACF1	GCN1	ATD3A
FLNA	MDC1	HUWE1	CAND1
RPB1	MSH6	IQGA1	CKAP4
RPB2	PDC6I	PRKDC	CNN2
RSF1	PRPF8	SMCA2	CYFP2
UBR7	PTCD3	SON	DOCK8
	RRP1B	SPTBN1	FAS
	RRP5	TPR	GEMI4
	SPB1	UBR4	HNRPM
	SPTAN1		HS90B
	UTP20		MUC7
			NOC3L
			NU155
			NUMA1
			P66A
			PUR2
			PYR1
			RBBP4
			SMCA5
			SMHD1
			SYEP
			SYFB
			SYQ
			TCPQ
			UBA6
			XRCC5

Enriched both with and without UV, in the top 500 by percentage of total spectrum

Protein	*Protein name*	*Brief description of function*	*Cellular localisation*
CHD1	Chromodomain-helicase-DNA-binding protein 1	Chromatin remodelling factor	Nucleus
CHD1L	Chromodomain-helicase-DNA-binding protein 1-like	DNA helicase which remodels chromatin after DNA damage	Nucleus
CHD4	Chromodomain-helicase-DNA-binding protein 4	Helicase part of nucleosome remodelling and deacetylase complexes	Nucleus and cytoskeleton
DAXX	Death domain-associated protein 6	Transcription repressor. H3.3 chaperone. May regulate apoptosis	Nucleus and cytosol
FLNA	Filamin A	Crosslinks actin filaments	Nucleus, cytoskeleton, cytosol, extracellular
RPB1	DNA-directed RNA polymerase II subunit RPB1	Transcribes DNA into RNA. Largest subunit that forms part of the core element	Nucleus
RPB2	DNA-directed RNA polymerase II subunit RPB2	Transcribes DNA into RNA. Second largest component that forms part of the core element	Nucleus
RSF1	Remodelling and spacing factor 1	Assembles regular nucleosome arrays	Nucleus
UBR7	Putative E3 ubiquitin-protein ligase	E3 ubiquitin ligase	Nucleus

Enriched after UV only, in the top 500 by percentage of total spectrum

Protein	*Protein name*	*Brief description of function*	*Cellular localisation*
BAZ1B	Bromodomain adjacent to zinc finger domain 1B	Phosphorylates H2AX after DNA damage. Also a transcription regulator and chromatin remodeller	Nucleus
COPA	Coatamer subunit alpha	Part of the coatamer complex required for budding from golgi membrane	Cytosol, golgi, and extracellular
DYNC1H1	Cytoplasmic dynein 1 heavy chain 1	Retrograde motility of vesicles and organelles along microtubules	Cytoskeleton

GCN1	eIF-2-alpha kinase activator homologue	Chaperones tRNAs to ribosomes	Cytosol
HUWE1	HECT, UBA and WWE domain containing 1	E3 ubiquitin protein ligase	Cytosol
IQGA1	IQ motif containing GTPase activating protein 1	Regulates dynamics and assembly of the actin cytoskeleton	Plasma membrane
PRKDC	Protein kinase, DNA-activated, catalytic subunit	Molecular sensor for DNA damage. Functions with the Ku70/80 protein in double strand break repair and recombination	Nuclear
SMCA2	SWI/SNF related, matrix associated, actin dependent regulator of chromatin, subfamily A, member 2	Chromatin remodeller	Nucleus, cytoskeleton
SON	SON DNA binding protein	Promotes pre-mRNA splicing, specifically many cell-cycle and DNA repair transcripts	Nuclear
SPTBN1	Spectrin beta, non-erythrocytic	Actin crosslinking protein	Golgi
TPR	Translocated promoter region	Component of the nuclear pore complex required for export of mRNA	Nucleus
UBR4	Ubiquitin protein ligase E3 component N-recognin 4	E3 ubiquitin ligase	Nucleus, cytosol

Enriched without UV only, in the top 500 by percentage of total spectrum

Protein	*Protein name*	*Brief description of function*	*Cellular localisation*
1433S	Stratifin	Cell cycle (G2/M) checkpoint protein	Cytosol
ADT2	Solute carrier family 25 member 5	Pore for exchange of cytoplasmic ADP with mitochondrial ATP across the inner mitochondrial membrane	Mitochondria
ATD2B	ATPase family, AAA domain containing 2B	Chromatin and lysine-acetylated histone binding	Nucleus
ATD3A	ATPase family, AAA domain containing 3A	Ubiquitously expressed mitochondrial membrane protein	Mitochondria
CAND1	Cullin associated and neddylation dissociated 1	Regulator of Cullin-RING ubiquitin ligases	Nucleus, golgi, cytosol

CKAP4	Cytoskeleton associated protein 4	Mediates the anchoring of the endoplasmic reticulum to microtubules	Endoplasmic reticulum, cytoskeleton
CNN2	Calponin 2	Implicated in the regulation and modulation of smooth muscle contraction	Cytoskeleton, extracellular
CYFP2	Cytoplasmic FMR1 interacting protein 2	Involved in T-cell adhesion and p53-dependent apoptosis	Cytosol, extracellular
DOCK8	Dedicator of cytokinesis 8	Guanine nucleotide exchange factor for CDC42	Plasma membrane
FAS	Fas cell surface death receptor	Regulator of programmed cell death	Extracellular
GEMI4	Gem nuclear organelle association protein 4	Role in the assembly of snRNPs	Nucleus, cytosol
HNRPM	Heterogeneous nucleus ribonucleoprotein	Influences pre-mRNA processing	Nucleus
HS90B	Heat shock protein HSP 90-beta	Molecular chaperone that aids protein folding	Cytosol
MUC7	Mucin 7	Though to facilitate clearance of bacteria in the mouth	Extracellular
NOC3L	Nucleolar complex protein 3 homologue	May be required for adipogenesis	Nucleus
NU155	Nucleoporin 155	Essential component of the nuclear pore complex	Nucleus
NUMA1	Nuclear mitotic apparatus protein 1	Structural component of the nuclear matrix with a role in forming the mitotic spindle	Nucleus
P66A	GATA Zinc finger domain containing 2A	Transcriptional repressor	Nucleus
PUR2	Phosphoribosylglycinamide Formyltransferase, Phosphoribosylglycinamide Synthetase, Phosphoribosylaminoimidazole Synthetase	Enzyme required for de novo purine biosynthesis	Nucleus, cytosol, mitochondria
PYR1	CAD trifunctional protein	Enzyme in the synthesis of pyrimidine nucleotides	Nucleus
RBBP4	Histone-binding protein RBBP4	Member of chromatin metabolism complexes eg CAF-1, HDAC, NuRD and NURF	Nucleus
SMCA5	SWI/SNF-related matrix-associated actin-dependent regulator of	Nucleosome remodeller that forms ordered arrays	Nucleus

	chromatin subfamily A member 5		
SMHD1	Structural maintenance of chromosomes flexible hinge domain containing 1	X inactivation maintenance	Nucleus
SYEP	Glutamyl-prolyl-tRNA synthetase	Part of a complex which attaches amino acids to their corresponding tRNA	Cytosol
SYFB	Phenylalanyl-tRNA synthetase subunit beta	Attaches l-phenylalanine to the terminal adenosine of the appropriate tRNA.	Cytosol
SYQ	Glutaminyl-tRNA synthetase	Catalyses the aminoacylation to tRNA	Cytosol
TCPQ	Chaperonin containing TCP1 subunit 8	Assists folding of proteins	Cytoskeleton, cytosol
UBA6	Ubiquitin like modifier activating enzyme 6	E1-like protein	Nucleus, cytosol
XRCC5	X-ray repair cross-complementing protein 5	Single-stranded DNA dependent ATP-dependent helicase that binds ends of double strand breaks	Nucleus

Appendix 4: ACE2 integrated clones

21 of 48 clones positive for FLAG (ACE2) and negative for IgG (correct integration, denoted by a red star)

R670=FLAG APC

Y/G585=IgG PE

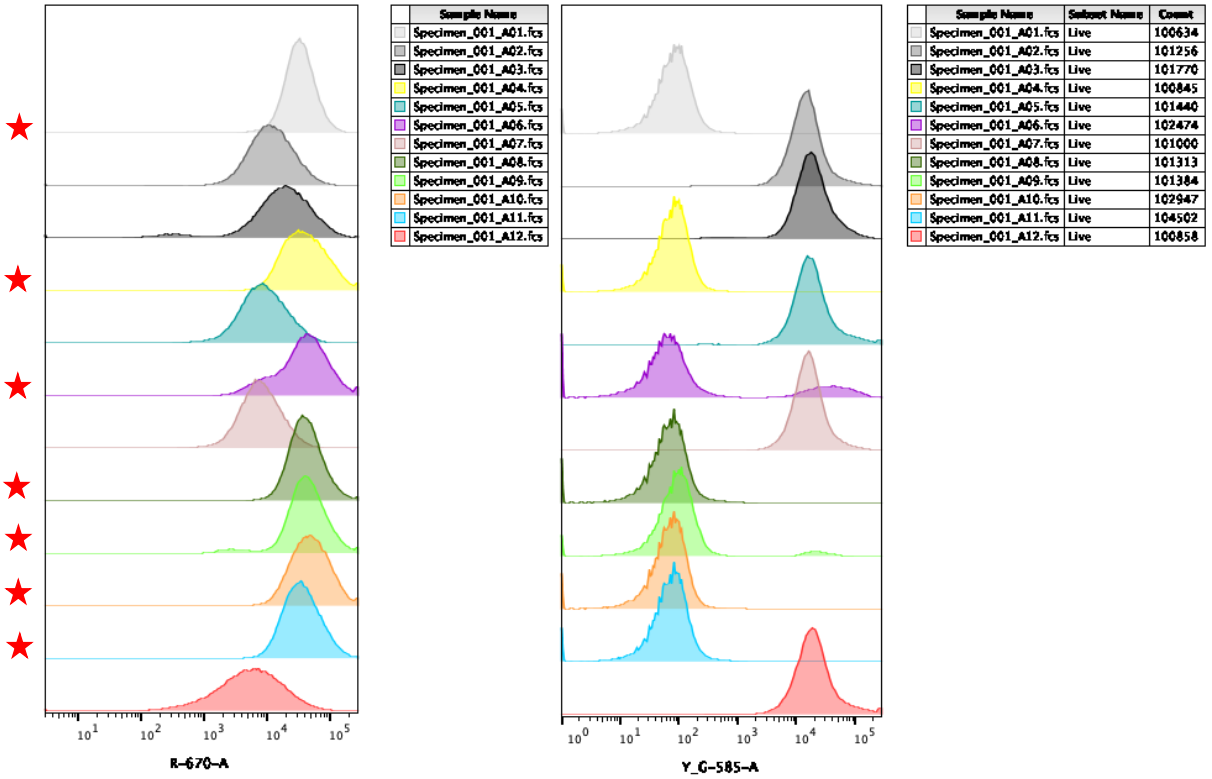

Sample Name	Subset Name	Count
Specimen_001_A01.fcs	Live	100634
Specimen_001_A02.fcs	Live	101256
Specimen_001_A03.fcs	Live	101770
Specimen_001_A04.fcs	Live	100845
Specimen_001_A05.fcs	Live	101440
Specimen_001_A06.fcs	Live	102474
Specimen_001_A07.fcs	Live	101000
Specimen_001_A08.fcs	Live	101313
Specimen_001_A09.fcs	Live	101384
Specimen_001_A10.fcs	Live	102947
Specimen_001_A11.fcs	Live	104502
Specimen_001_A12.fcs	Live	100858

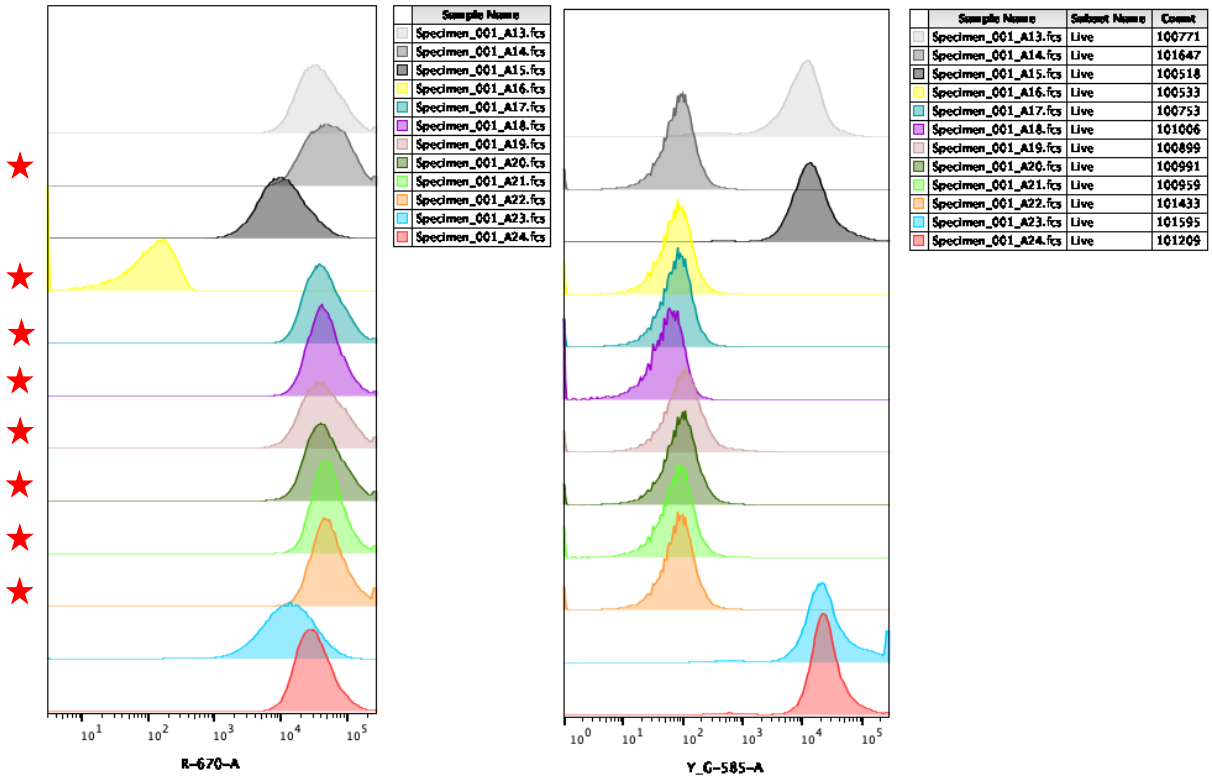

Sample Name	Subset Name	Count
Specimen_001_A13.fcs	Live	100771
Specimen_001_A14.fcs	Live	101647
Specimen_001_A15.fcs	Live	100518
Specimen_001_A16.fcs	Live	100533
Specimen_001_A17.fcs	Live	100753
Specimen_001_A18.fcs	Live	101006
Specimen_001_A19.fcs	Live	100899
Specimen_001_A20.fcs	Live	100991
Specimen_001_A21.fcs	Live	100959
Specimen_001_A22.fcs	Live	101433
Specimen_001_A23.fcs	Live	101595
Specimen_001_A24.fcs	Live	101209

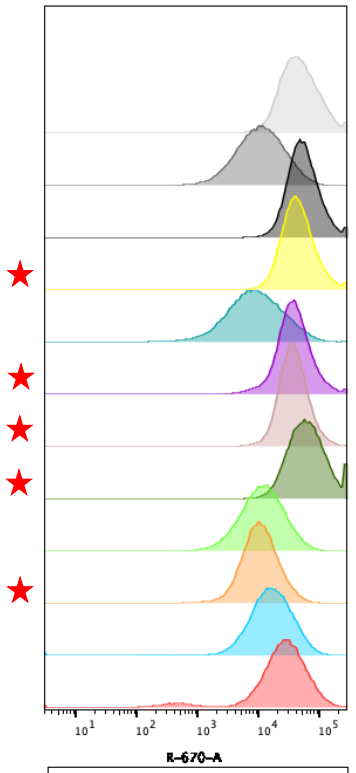

Sample Name
Specimen_001_B01.fcs
Specimen_001_B02.fcs
Specimen_001_B03.fcs
Specimen_001_B04.fcs
Specimen_001_B05.fcs
Specimen_001_B06.fcs
Specimen_001_B07.fcs
Specimen_001_B08.fcs
Specimen_001_B09.fcs
Specimen_001_B10.fcs
Specimen_001_B11.fcs
Specimen_001_B12.fcs

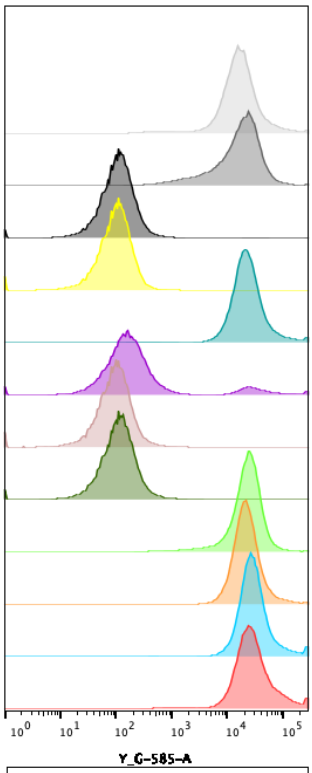

Sample Name	Subset Name	Count
Specimen_001_B01.fcs	Live	101296
Specimen_001_B02.fcs	Live	100121
Specimen_001_B03.fcs	Live	101291
Specimen_001_B04.fcs	Live	101033
Specimen_001_B05.fcs	Live	100820
Specimen_001_B06.fcs	Live	100693
Specimen_001_B07.fcs	Live	100726
Specimen_001_B08.fcs	Live	102628
Specimen_001_B09.fcs	Live	100178
Specimen_001_B10.fcs	Live	100438
Specimen_001_B11.fcs	Live	100934
Specimen_001_B12.fcs	Live	100750

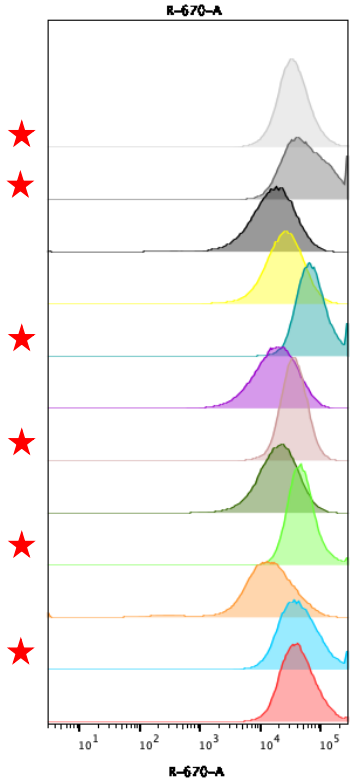

Sample Name
Specimen_001_B13.fcs
Specimen_001_B14.fcs
Specimen_001_B15.fcs
Specimen_001_B16.fcs
Specimen_001_B17.fcs
Specimen_001_B18.fcs
Specimen_001_B19.fcs
Specimen_001_B20.fcs
Specimen_001_B21.fcs
Specimen_001_B22.fcs
Specimen_001_B23.fcs
Specimen_001_B24.fcs

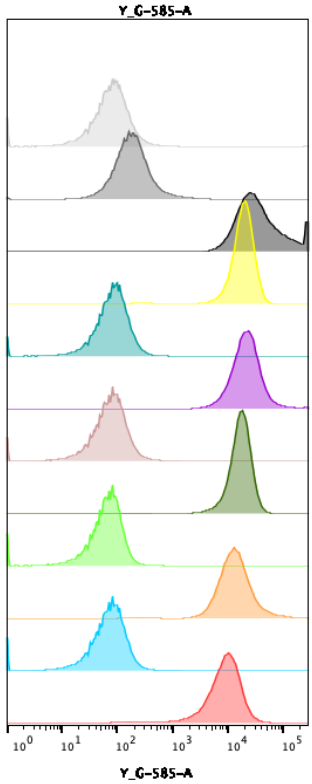

Sample Name	Subset Name	Count
Specimen_001_B13.fcs	Live	101832
Specimen_001_B14.fcs	Live	102108
Specimen_001_B15.fcs	Live	103625
Specimen_001_B16.fcs	Live	101160
Specimen_001_B17.fcs	Live	101894
Specimen_001_B18.fcs	Live	101827
Specimen_001_B19.fcs	Live	101177
Specimen_001_B20.fcs	Live	100807
Specimen_001_B21.fcs	Live	101001
Specimen_001_B22.fcs	Live	100644
Specimen_001_B23.fcs	Live	101846
Specimen_001_B24.fcs	Live	100843